Dynamics of physiological, structural and molecular responses to O stress in poplar leaves

Benjamin Turc

Ecole Doctorale SIReNa (Sciences et Ingénierie des Ressources Naturelles)
UMR 1434 Silva

Thèse

Présentée et soutenue publiquement pour l'obtention du titre de

DOCTEUR DE l'UNIVERSITE DE LORRAINE

Mention : Biologie et écologie des forêts et des agrosystèmes

par **Benjamin TURC**

Sous la direction de Pr. Yves Jolivet

Dynamique des réponses physiologiques, structurales et moléculaires au stress O_3 dans les feuilles de peuplier

Soutenue publiquement le 10 décembre 2021

Membres du jury :

Directeur(s) de thèse	**M. Yves JOLIVET**	**Professeur, Université de Lorraine, Nancy**
Président de jury	**Mme Claire FOURREY**	**DR, INRAE, Centre INRAE Grand Est-Nancy**
Rapporteur	**Mme Anne REPELLIN**	**Professeure, Université Paris Est Créteil, Créteil**
Rapporteur	**Mr Vicent CATALAYUD**	**DR, Mediterranean Center for Environmental Studies, Valencia**
Examinateur	**Mme Claire FOURREY**	**DR, INRAE, Centre INRAE Grand Est-Nancy**
Examinateur	**Mr Luis LEITAO**	**MCF, Université Paris Est Créteil, Créteil**
Examinateur	**Mme Madeleine GUNTHARDT-GOERG**	**Dr, Institut fédéral de recherches sur la forêt, la neige et le paysage WSL**
Co-supervisor	**Mme Mireille CABANE**	**MCF, Université de Lorraine, Nancy**
Co-supervisor	**M. Pierre VOLLENWEIDER**	**DR, Institut fédéral de recherches sur la forêt, la neige et le paysage WSL**

Ecole Doctorale SIReNa (Sciences et Ingénierie des Ressources Naturelles)

UMR 1434 Silva

Thèse

Présentée et soutenue publiquement pour l'obtention du titre de

DOCTEUR DE l'UNIVERSITE DE LORRAINE

Mention : Biologie et écologie des forêts et des agrosystèmes

par **Benjamin TURC**

Sous la direction de Pr. Yves Jolivet

Dynamique des réponses physiologiques, structurales et moléculaires au stress O_3 dans les feuilles de peuplier

Soutenue publiquement le 10 décembre 2021

Membres du jury :

Directeur(s) de thèse	**M. Yves JOLIVET**	**Professeur, Université de Lorraine, Nancy**
Président de jury	**Mme Claire FOURREY**	**DR, INRAE, Centre INRAE Grand Est-Nancy**
Rapporteur	**Mme Anne REPELLIN**	**Professeure, Université Paris Est Créteil, Créteil**
Rapporteur	**Mr Vicent CATALAYUD**	**DR, Mediterranean Center for Environmental Studies, Valencia**
Examinateur	**Mme Claire FOURREY**	**DR, INRAE, Centre INRAE Grand Est-Nancy**
Examinateur	**Mr Luis LEITAO**	**MCF, Université Paris Est Créteil, Créteil**
Examinateur	**Mme Madeleine GUNTHARDT-GOERG**	**Dr, Institut fédéral de recherches sur la forêt, la neige et le paysage WSL**
Co-supervisor	**Mme Mireille CABANE**	**MCF, Université de Lorraine, Nancy**
Co-supervisor	**M. Pierre VOLLENWEIDER**	**DR, Institut fédéral de recherches sur la forêt, la neige et le paysage WSL**

Remerciements

Mes premiers remerciements vont à mes encadrants de thèse Yves Jolivet, Mireille Cabané et Pierre Vollenweider qui m'ont confié ce travail de recherche et qui m'ont très bien encadré. Ces 4 ans (et demi) de thèse ont été une merveilleuse expérience professionnelle mais aussi personnelle : ça a été l'occasion pour moi d'avoir mon premier logement, de découvrir une nouvelle ville, de rencontrer des gens formidables, de voyager et surtout de beaucoup apprendre. Merci pour votre disponibilité, votre patience, vos conseils … en fait merci pour tout !

Je remercie Vicent Catalayud et Anne Repellin d'avoir accepté d'être rapporteur de ma thèse. Et aussi, merci Anne de m'avoir envoyé vers Yves pour ce sujet de thèse, c'est aussi grâce à cela que j'avais postulé ! Merci également Claire Fourrey et Marcus Schaub pour leurs participations à mes comités de thèse. Je remercie aussi Madeleine Günthardt-Goerg et Luis Leitao d'avoir accepté d'être examinateur à mon jury de thèse, et encore une fois Claire Fourrey qui a accepté d'en être présidente.

D'une manière générale, merci à tous les membres du labo sans qui l'ambiance n'aurait pas été la même. Merci Marie-Noëlle pour les nombreuses rigolades en pauses café. Merci Pierrick pour les discussions que l'on a eu mais surtout pour la gestion du café (indispensable) et le pain au chocolat de la publi (je perpétuerai la « tradition »). Je remercie Joëlle pour son aide à la paillasse au début de ma thèse, surtout pour la mise au point de la coloration au bleu trypan. Un grand merci également à Anthony pour les discussions scientifiques, l'aide précieuse pour les mesures et l'analyse des échanges gazeux, les bons conseils, le soutien et heureusement que tu étais là au congrès à Chypre ! Merci beaucoup Audrey pour le soutien et l'aide en général, mais surtout pour les extractions d'ARN (la course Nanodrop !). Merci Stéphane pour la gestion des chambres phyto, et aussi pour les vidanges moto au verger ! Et merci Jean-Charles pour ton aide lors des expérimentations et les soirées à Ferrières, c'était trop bien ! Je n'oublie pas non plus les ATER / post doc : merci Maira pour les bons moments et pour t'être occupé de mon chat, et merci Adib et El aziz pour votre aide avec les statistiques !

Coté doctorant je tiens à remercier en premier Nicolas Dusart avec qui j'ai partagé mon bureau au début de ma thèse, qui aura su me faire profiter de son

expérience des débuts du doctorat, et grâce à qui je me suis mis à R (et heureusement !). Merci à Ricardo pour ta bonne humeur, et les délires qu'on a pu avoir et bon courage pour la fin. Enfin, merci à Nicolas Bras alias « l'évadé » pour les discussions, les délires et le soutien. Courage t'es bientôt à la fin aussi !!

Mention spéciale à mes voisins Gaëtan et Charlotte ! Je ne pouvais pas espérer mieux en termes de voisinage. Merci pour toutes ces soirées mémorables (ou pas, selon taux d'alcoolémie), et tous les gens que j'ai rencontré grâce à vous (Simo, Charline, Esther Marine, Antoine, les Manons et tous les autres), c'était vraiment génial.

Merci également à mes amis de Paris, avec qui j'ai pu décompresser lors de mes retours sur Paris, ou sur Discord en jouant à Destiny 2, RL, Osu! et autres ! Merci les gars, ça m'a vraiment aidé dans certains moments.

Un grand merci à ma maman et ma mamy pour leur soutient en général, mais surtout pour celui financier sans lequel la fin de ma thèse aurait été très compliquée. Merci beaucoup ! Continuant avec la famille, merci à mon frère Clément pour ces visites sur Nancy (on n'oubliera pas les Vosges à moto !), et ma sœur Maryon grâce à qui je suis parti en vacances un été.

Pour finir, je tiens à remercier Valérie Itier et Clarisse Balland Bolou-bi de l'Université de Créteil (UPEC). Merci à Valérie qui m'a recommandé à Clarisse, et sans qui je n'aurai pas eu de stage en 3ème année de licence. C'était peut-être anodin et pas grand-chose pour vous, mais de mon point de vue tout à commencer avec ce stage, et c'est grâce à vous. Enfin, merci à Clarisse avec qui j'ai fait mes 2 premiers stages en laboratoire de recherche. C'est avec ces stages que j'ai eu envie de poursuivre dans le monde de la recherche et d'aller jusqu'au doctorat. Encore merci à vous deux.

Liste des abréviations

ABA	Acide abscissique
ACC	1-Aminocyclopropane-1-carboxylate synthase
ACC oxydase	Aminocyclopropanecarboxylate oxydase
ACS	Accelerated Cell Senescence
ADN	Acide désoxyribonucléique
$AF_{st}Y$	Accumulated Flux through stomata over a threshold of X nmol m^{-2} s^{-1}
Anet	Assimilation nette de CO_2
AOT40	Accumulated Ozone Exposure Over A Threshold of 40 ppb
APX	Ascorbate peroxidase
ARN	Acide ribonucléique
ASA	Ascorbate
A_{sat}	Assimilation nette de CO_2 en lumière saturante
CAD	Cinnamyl alcool déshydrogénase
CF	Charcoal-filtered
CHS	Chalcone synthase
CL	Critical level
CUO	Cumulative O_3 Uptake
DEG	Differentially expressed genes
DFR	Dihydroflavonol 4 reductase
DHA	Déhydroascorbate
DHAR	Déhydrohascorbate réductase
ET	Ethylène
FACE	Free Air Concentration Enrichment
GIEC	Groupe d'experts intergouvernemental sur l'évolution du climat
GR	Glutathion reductase
GSH	Glutathion réduit
GSSG	Glutathion oxydé
GST	Glutathion synthase
g_w	Conductance stomatique à la vapeur d'eau
HR	Hypersensitive response
HR-like	Hypersensitive response-like
IAGOS	In-service aircraft for a global observing system
IFR	Isoflavonoïd reductase
JA	Acide jasmonique
MAPK	Mitogen-activated protein kinases
MDHA	Monodehydroascorbate
MDHAR	Monodehydroascorbate reductase
MYB	Facteur de transcription de la famille des myeloblastosis
NADP	Nicotinamide adénine dinucléotide (phosphate)
NADPH	Nicotinamide adénine dinucléotide (phosphate) réduit

NO_2	Dioxyde d'azote
NO_x	Oxydes d'azote
OTC	Open Top Chamber
PAL	Phénylalanine amonia-lyase
PCD	Programed Cell Death
PEPc	Phosphoenolpyruvate carboxylase
POD_y	Phytotoxic O_3 Dose above a threshold of Y nmol O^3 m^{-2} s^{-1}
ppb	Parties par billion
ppm	Parties par million
PR (protein)	Pathogenesis-Related (protein)
RCP	Representative Concentration Pathways
RNAseq	Ribonucleic acid sequencing
ROS	Reactive Oxygen Species
SA	Acide salicylique
SAG	Senescence-associated genes
WAK	Wall-associated kinase
WGCNA	Weighted gene co-expression network analysis

LISTE DES FIGURES

LISTE DES TABLEAUX

SOMMAIRE

Chapitre 1

INTRODUCTION

Chapitre 1 : Introduction

1. L'Ozone

L'ozone (O_3) est un gaz constitué de 3 atomes d'oxygène, naturellement présent dans l'atmosphère, et dont la caractérisation remonte au XIXème siècle. Il fut d'abord découvert en 1785 par le chimiste hollandais van Marum, avant d'être synthétisé et isolé en laboratoire en 1839 par le chimiste allemand Schönbein qui le nomma « ozone ». Par la suite, ses capacités d'absorption des UV (de 240 à 300 nm) seront montrées ce qui permettra de mettre en évidence la présence de la couche d'O_3. (Rubin, 2003; Muller, 2009).

1.1. L'O_3 stratosphérique

La majorité de l'O_3 atmosphérique, approximativement 90%, est situé dans la stratosphère à environ 20 à 40 km d'altitude (figure 1A). L'O_3 stratosphérique forme une couche, communément appelée « couche d'O_3 », capable d'absorber une partie du rayonnement UV émis par le soleil, protégeant ainsi le vivant de leurs effets nocifs. La formation d'O_3 dans la stratosphère est une conséquence directe du rayonnement solaire. En effet, sous l'effet d'une longueur d'onde inférieur à 300 nm, le dioxygène O_2 va être photo-dissocié en 2 atomes d'oxygène O. Les atomes d'oxygène vont ensuite réagir avec une molécule de O_2 pour former de l'O_3. Celui-ci va être à son tour photo-dissocié pour reformer une molécule d'O_2 et libérer un atome d'oxygène (Figure 1B). Ce cycle a été décrit la première fois par Chapman en 1930 (Staehelin et al., 2001; Rowland, 2009).

Dans les années 1960, un intérêt particulier est porté sur la recherche en chimie atmosphérique car il devenait évident que les émissions de gaz liées à l'activité humaine détruisaient la couche d'O_3, réduisant ses effets bénéfiques pour la biosphère. Ce sont notamment les composés organiques volatiles contenant du chlore, du fluor et du brome (comme les chlorofluorocarbures) qui vont participer à cette dégradation. En effet, en remontant jusqu'à la stratosphère, ces gaz deviennent sujets à de courtes longueurs d'onde (gamma < 230 nm) libérant des radicaux halogénés qui vont perturber la chimie de l'O_3. En conséquence, l'O_3 est plus

rapidement détruit que formé, ce qui conduit à une diminution de sa concentration. Cet effet a été le plus frappant en antarctique, où la diminution des concentrations d'O_3 amène à la disparition quasi-totale de la couche d'O_3 (Staehelin et al., 2001).

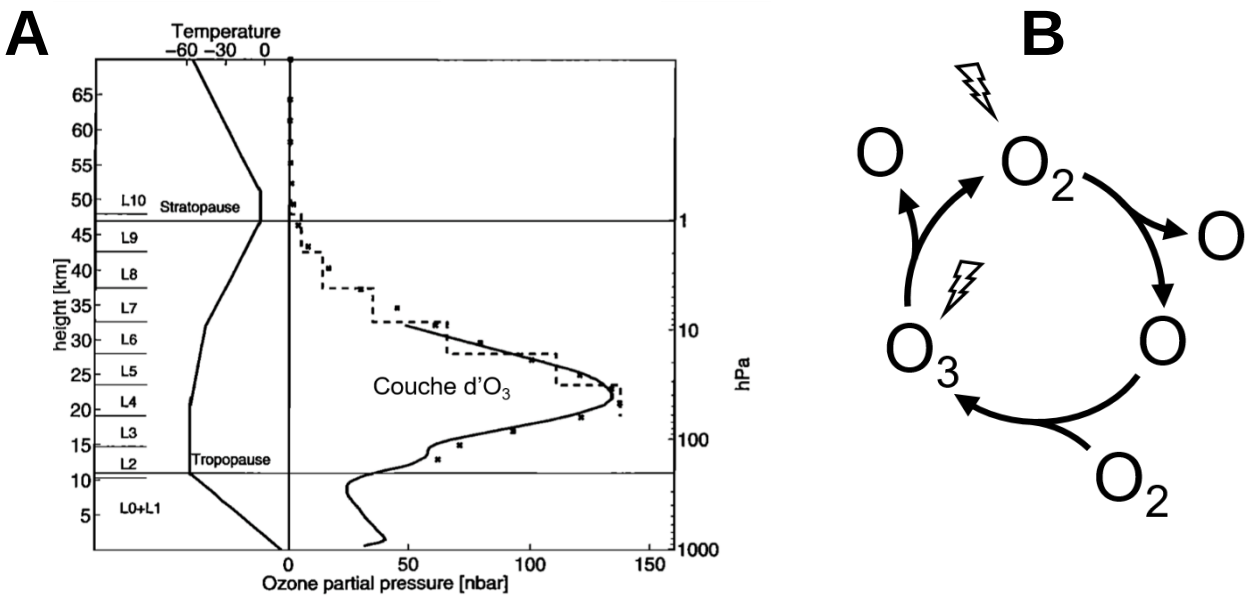

Figure 1. Répartition dans l'atmosphère (A) et cycle de formation (B) de l'O_3 dans la stratosphère d'après Chapman (Staehelin et al., 2001).

1.2. L'O_3 troposphérique

Tandis que l'O_3 présent dans la stratosphère peut être qualifié de « bon O_3 » car il protège la biosphère des radiations UV, celui présent dans la troposphère (10% de l'O_3 atmosphérique total) est un polluant atmosphérique toxique. Les variations des concentrations d'O_3 troposphérique au cours du temps et de l'espace dépendent de plusieurs facteurs, comme la proximité avec des sources importantes de précurseurs et les conditions météorologiques (Sicard et al., 2013; Gorai et al., 2017; Zhao et al., 2018).

1.2.1. Origine de l'O_3 dans la troposphère

L'O_3 troposphérique n'est pas directement émis mais produit photochimiquement dans l'atmosphère à partir de précurseurs. Le mécanisme est toutefois différent de celui intervenant dans la stratosphère, les radiations UV

responsables (γ < 300 nm) de la formation de l'O_3 à ces altitudes n'atteignant pas, ou très peu, la troposphère (Sillman, 1999).

La production d'O_3 troposphérique se fait par la combinaison d'un atome d'oxygène dans un état fondamental et d'une molécule de dioxygène (O_2) (Monks et al., 2015).

C'est la photodissociation par une longueur d'onde y comprise entre 300 et 400 nm du dioxyde d'azote (NO_2) en oxyde d'azote (NO) qui va produire l'atome d'oxygène :

$$NO_2 + \gamma_{(300 - 400\ nm)} \rightarrow NO + O \qquad (1)$$

L'atome d'oxygène ainsi libéré va réagir très vite avec une molécule de O_2 et former O_3 (M représente un troisième corps stabilisant la réaction) :

$$O + O_2 + M \rightarrow O_3 + M \qquad (2)$$

L'O_3 réagit ensuite rapidement avec une molécule de NO pour former une molécule de NO_2 et de O_2 :

$$NO + O_3 \rightarrow NO_2 + O_2 \qquad (3)$$

En conditions naturelles l'accumulation d'O_3 reste donc limitée. Il en va de même pour les zones urbaines riches en NO_x, ces derniers provenant de la combustion de combustibles fossiles, et particulièrement du transport routier (63% ; (Citepa, 2019). Cependant, en zone périurbaine et rurale, même si la concentration en NO_x n'est pas aussi élevée qu'en ville, la présence de composés organiques volatiles (COVs) émis par la végétation va perturber cette chaine de réactions en permettant la régénération du dioxyde d'azote NO_2 sans consommation d'O_3 (Chanin et al., 2015). Il faut aussi tenir compte du vent qui peut transporter les précurseurs ainsi que l'O_3 sur de grandes distances (Keating et al., 2010; Han et al., 2018).

1.2.2. Evolution des concentrations en O_3 troposphérique

Dues aux activités humaines, et notamment à l'utilisation de plus en plus intensive d'énergie fossile comme le pétrole, les émissions de précurseurs de l'O_3 troposphérique ont fortement augmenté fin XIXème et au cours du XXème siècle. En conséquence, les concentrations en O_3 ont fortement augmenté jusque dans les années 2000 (Maas and Grennfelt, 2016) Figure 2).

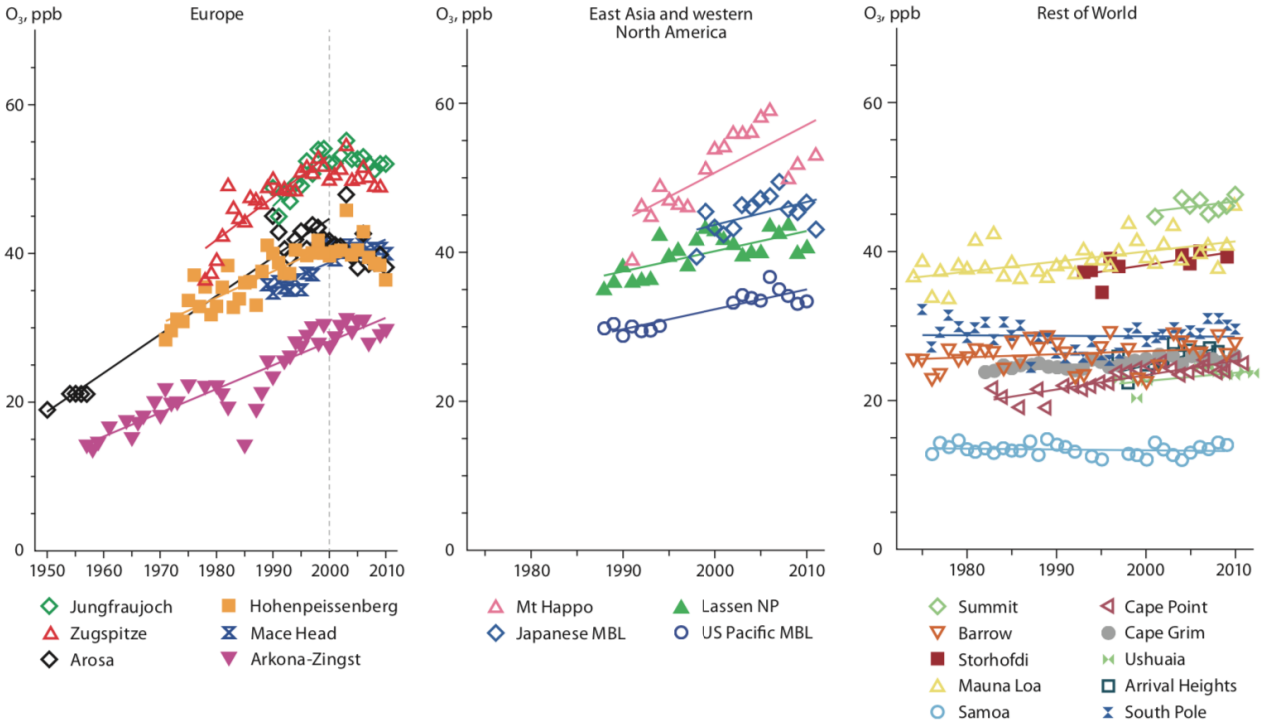

Figure 2. Concentrations moyennes annuelles d'O_3 sur plusieurs sites de surveillance régionale à travers le monde (Cooper et al., 2014).

Face à une telle augmentation, des décisions politiques et législatives sur la qualité de l'air ont permis de réduire les émissions de précurseurs (Monks et al., 2015; Simon et al., 2015; Jiang et al., 2020), limitant la formation de l'O_3 troposphérique. Des mesures réalisées par des sondes placées sur des avions commerciaux (IAGOS) ont pu confirmer que les concentrations en O_3 troposphérique étaient en légère diminution aux Etats-Unis, constantes en Europe mais en augmentation dans des zones très polluées de l'Asie de l'Est (Chang et al., 2017; Gaudel et al., 2018). En effet, même si les émissions de précurseurs ont stagné, voir diminué, dans les pays occidentaux, elles ont augmenté dans les pays asiatiques à cause de leur développement économique (Zhang et al., 2016).

Afin d'estimer les concentrations futures d'O_3, des modèles climatiques couplés à des modèles de chimie troposphérique ont été élaborés. Ces modèles prédictifs prennent en compte les concentrations passées et actuelles d'O_3, les émissions d'origine anthropique de précurseurs, ainsi que les scénarios de trajectoire du forçage radiatif (Representative Concentration Pathways, RCP) du GIEC. Ainsi, au début des années 2000, il était estimé que les concentrations d'O_3 continueraient d'augmenter jusqu'en 2100 pour atteindre 40 à 80 ppb au niveau mondiale (Vingarzan, 2004). Une étude plus récente de (Revell et al., 2015) utilisant un modèle chimie-climat intégrant le transport (modèle SOCOL) et suivant le scénario climatique RCP 6.0 (scénario relativement réaliste) va également dans ce sens. En effet, les concentrations d'O_3 estimées dans l'hémisphère Nord (30°- 60°) atteignent 80 ppb jusqu'en 2060, avant de décroitre à 60 ppb en 2100.

2. Conséquence pour les productions végétales : forêts et cultures

Une des conséquences d'une exposition de la végétation à l'O_3 se traduit par une réduction de croissance et de rendement, que ce soit pour les arbres (Wittig et al., 2009; Li et al., 2017) ou les espèces cultivées (Feng and Kobayashi, 2009). Dans ces méta-analyses, il a été pris en compte comme facteurs de variation le type de plante (tropicale vs tempérée, angiosperme vs gymnospermes), la méthode de fumigation (Open Top Chamber, FACE), la concentration d'O_3, la durée d'exposition et d'éventuels traitements additionnels (sécheresse, fort CO_2, ajout d'azote).

Les 2 méta-analyses réalisées sur les arbres (Wittig et al., 2009; Li et al., 2017) obtiennent des résultats similaires. Ainsi, sous une concentration élevée en O_3 (environ 100 ppb), la biomasse totale, la biomasse racinaire, et la taille des feuilles sont réduits de 15%, et le diamètre et la hauteur de 10% (figure 3). Des résultats similaires ont été obtenus avec des concentration d'O_3 plus faibles (entre 40 et 60 ppb) où la production primaire brute des forêts européennes est diminuée d'environ 10% à cause de l'O_3 (Proietti et al., 2016). De plus, selon une étude récente, la réduction de biomasse des forêts italiennes liée à l'O_3 engendrerait une perte économique de la filière bois allant de 30 à 60 millions d'euros par an (Sacchelli et al., 2021). Concernant

les espèces cultivées, les pertes de rendement sont estimées à 6% pour les pommes de terre, 10% pour le blé, l'orge et le soja, et jusqu'à 20% pour le riz et le haricot (figure 4)(Feng and Kobayashi, 2009). Des méta-analyses plus récentes confirment ces résultats, au moins pour le blé (Mills et al., 2018; Pleijel et al., 2018).

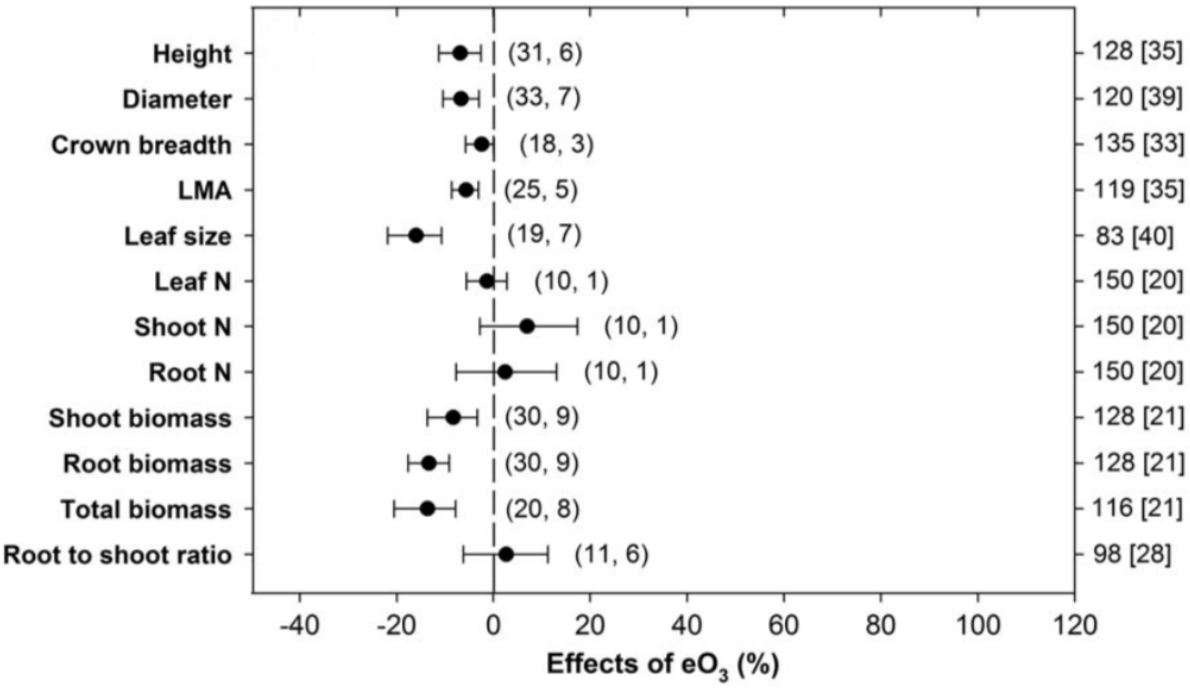

Figure 3. Effets de l'O_3 sur la croissance et la production de biomasse des arbres (Li et al., 2017). Les ronds pleins représentent les pourcentages de changements par rapport aux contrôles (les barres indiquent un intervalle de confiance à 95%). Le nombre d'articles et de mesures est présenté entre parenthèse et les concentrations moyennes d'O_3 sur l'axe des ordonnées à droite (la valeur entre crochet est la concentration moyenne des contrôles).

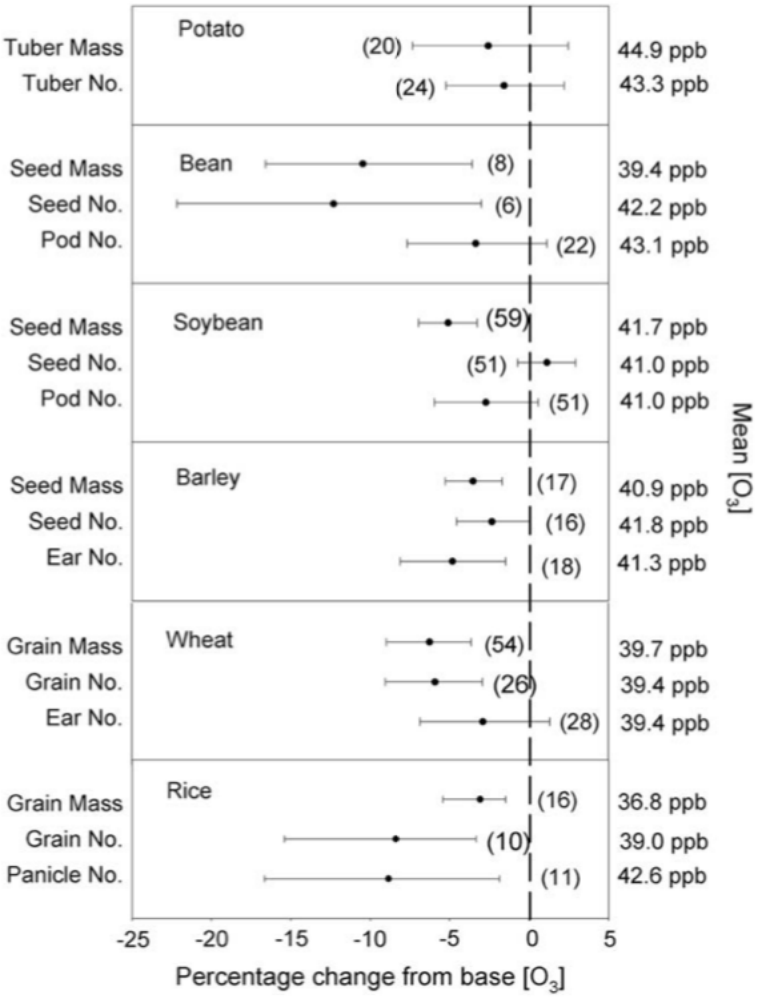

Figure 4. Effets de l'O_3 sur la production de grandes cultures (Feng and Kobayashi, 2009). Les symboles représentent les pourcentages de changements par rapport aux contrôles. Le nombre d'articles est présenté entre parenthèse et les concentrations moyennes d'O_3 sur l'axe des ordonnées à droite.

3. Seuils de risques à l'O_3

3.1. Basé sur la concentration atmosphérique d'O_3

Avec la mise en évidence des effets néfastes de l'O_3 sur les plantes, des indicateurs pour l'évaluation des risques pour la végétation ont été développés. Au cours des années 90, l'AOT40 a été le premier indicateur à être adopté en Europe. Il correspond à la somme des différences entre la concentration horaire d'O_3 et une valeur fixe de 40 ppb, pour les heures de la journée où l'ensoleillement est supérieur à 50 $W.m^2$ (Fuhrer et al., 1997).

L'intérêt de cet indice est sa facilité d'utilisation et de calcul à grande échelle, ainsi que son adaptabilité à de nombreux écosystèmes. Le niveau critique d'AOT40 pour les espèces agricoles est de 3 ppm.h et de 5 ppm.h pour les arbres, ce qui correspond à une diminution de biomasse de 5% respectivement (Mills G. et al., 2017).

Cependant, cet indice n'est basé que sur la concentration atmosphérique d'O_3, et ne prend pas en compte la quantité d'O_3 absorbée par la feuille. Considérant que l'O_3 affecte les plantes principalement en rentrant par les stomates, une même valeur d'AOT40 n'aura pas les mêmes effets sur 2 plantes ayant des conductances stomatiques différentes. De plus, une même valeur d'AOT40 n'aura pas non plus les mêmes effets sur 2 plantes n'ayant pas les mêmes capacités de détoxication et/ou de défense (Musselman et al., 2006). De ce fait, cet indice ne permet pas d'expliquer les relations de cause à effet de l'impact de l'O_3 sur la végétation, puisqu'il ne repose sur aucune base mécanistique.

3.2. Basé sur le flux d'O_3 cumulé dans la feuille

Avec la remise en cause de l'AOT40 au début des années 2000, un nouvel indice basé sur le flux d'O_3 cumulé entrant dans la feuille a été proposé (Karlsson et al., 2007; Mills et al., 2011). Ce nouvel indice, appelé au départ AF_{st} X (Accumulated Flux through stomata over a threshold of X nmol m^{-2} s^{-1}) ou encore CUO (Cumulative O_3 Uptake) correspond aujourd'hui au PODy (Phytotoxic O_3 Dose above a threshold of Y nmol O^3 m^{-2} s^{-1}). Le calcul de cet indice repose sur la somme cumulée de la différence entre les moyennes horaires de flux d'O_3 entrant dans la feuille et la valeur seuil Y. Cette valeur seuil vise à représenter les capacités de défense et/ou de détoxication de la plante, en somme le flux d'O_3 que la plante est capable de gérer sans apparition d'effets néfastes de l'O_3. Malgré un intérêt mécanistique et une pertinence biologique beaucoup plus élevé que l'AOT40, son calcul, et donc son application à grande échelle, restent très compliqués étant donné la prise en compte de la conductance stomatique. Cette dernière, lorsqu'elle n'est pas mesurée au niveau de la feuille, doit être estimée à partir des données climatiques disponibles (température, précipitations, intensité lumineuse, humidité relative, disponibilité en eau du sol) au travers de modèles comme celui de Jarvis (Emberson et al., 2000) ou de Ball-Woodward-Berry (Tuzet et al., 2011).

De nos jours, le seuil critique Y est officiellement défini pour une réduction de 4%, atteinte avec une dose de 5.2 mmol O_3 m^{-2}, de la biomasse totale pour les feuillus (hêtre et bouleau) et de 2%, atteinte avec une dose de 9.2 mmol O_3 m^{-2} pour les résineux (épicéa). Pour les plantes de grandes cultures, le seuil est défini pour un réduction de rendement de 5% et varie en fonction de l'espèce, allant de 1.5 mmol O_3 m^{-2} pour le blé, 2 mmol O_3 m^{-2} pour les tomates, et 3.8 mmol O_3 m^{-2} pour les pommes de terre (Mills G. et al., 2017), ce qui a du sens pour référer tout de suite à une perte économique.

Cependant, au vu des différences de conductance stomatique inter-espèces pouvant exister, le PODy se doit d'être spécifique à une espèce, complexifiant encore son application. De plus, pour idéalement compléter le PODy il faut déterminer la capacité de la plante à neutraliser l'O_3 entrant dans la feuille par les processus de défense/détoxication, or la quantification (absolue ou relative) de cette capacité est actuellement très difficile, du fait de la complexité des processus qu'elle implique (Büker et al., 2015).

De nombreuses études utilisent l'apparition de symptômes visibles foliaires comme indicateur d'une surcharge des processus de défense/détoxication pour définir un seuil critique Y (Gerosa et al., 2008; Marzuoli et al., 2009; Sicard et al., 2016; Sicard et al., 2021), en partant de l'idée que l'apparition de symptômes visibles foliaires entrainent *de facto* une réduction de biomasse. En fait suivant la stratégie de réponse adoptée par la plante face à l'O_3, une réduction de biomasse est envisageable sans apparition de symptômes visibles (Marzuoli et al., 2019).

Toutefois, la réduction de biomasse ou l'apparition de symptômes visibles sont des effets tardifs d'une exposition à l'O_3, dont les dynamiques résultent nécessairement de changements cellulaires induit en amont dans les feuilles. Il est donc nécessaire de comprendre ces mécanismes de défense/détoxication à l'échelle de la cellule, afin de pouvoir mieux estimer la part d'O_3 que la plante peut gérer avant l'apparition d'effet négatifs.

4. Impact de l'O_3 à l'échelle de la feuille

L'O_3 affecte la végétation par les feuilles, plus précisément en entrant dans celles-ci (figure 5). En conséquence, l'émergence de symptômes visibles résultants de changements microscopiques ainsi que des changements physiologiques et transcriptomiques ont pu être observés chez de nombreuses espèces.

4.1. Mécanisme d'entrée de l'O_3 dans la feuille

Le polluant va diffuser dans les tissus foliaires quasi-exclusivement par les stomates (Kerstiens and Lendzian, 1989; Laisk et al., 1989), son flux au travers de la cuticule étant négligeable car 10000 fois plus faible que par les stomates (Kerstiens and Lendzian, 1989).

Une fois dans le mésophylle, l'O_3 est immédiatement décomposé en *Reactive Oxygen Species* (ROS) comme le radical superoxyde (O_2^-), le radical hydroxyle (OH^-), et le peroxyde d'hydrogène (H_2O_2) (Castagna and Ranieri, 2009). Il est important de noter que les ROS sont naturellement présents et produits dans les plantes régulant de nombreux processus biologiques comme la différentiation et la prolifération cellulaire, le développement, ou encore la transmission de signal (Mittler, 2017).

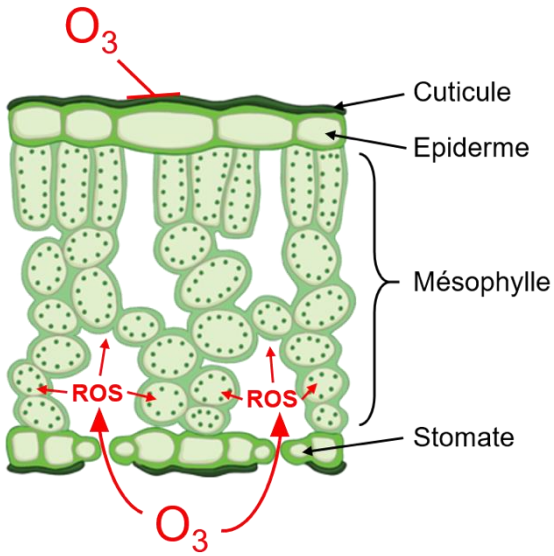

Figure 5. Diffusion de l'O_3 dans les tissus foliaires. L'O_3 passe par les stomates, puis est rapidement décomposés en ROS qui vont diffuser à travers le mésophylle. Le passe de l'O_3 par la cuticule est quasiment nul.

Les antioxydants vont constituer la première ligne de défense de la cellule contre les ROS. Dans l'apoplasme, l'ascorbate (ASA) peut réagir directement pour réduire l'H_2O_2 en H_2O, et former du monodehydroascorbate (MDHA), forme très instable et rapidement oxydée en déhydroascorbate (DHA). La régénération de la forme réduite ASA ne peut se faire dans l'apoplasme et nécessite l'import du DHA dans le cytosol où il sera réduit grâce à la déhydrohascorbate réductase (DHAR) en présence de glutathion. Le MDHA, qui peut être formé dans le cytosol par l'action d'une ascorbate peroxidase (APX) intracellulaire, peut être réduit grâce à la monodehydroascorbate reductase (MDHAR). Le glutathion oxydé (GSSG) sera à nouveau réduit par une glutathion reductase (GR) à partir de NADPH (figure 6) (Castagna and Ranieri, 2009). Tout cela suit un cycle appelé cycle Halliwell-Asada-Foyer, ou cycle glutathion-ascorbate (figure 4). La capacité de la cellule à pouvoir régénérer efficacement le GSH et l'ASA est donc un facteur pouvant expliquer la tolérance à l'O_3 (Dumont et al., 2014; Bellini and De Tullio, 2019). Cependant, une fois la capacité de detoxication de la feuille excédée, l'accumulation de ROS va oxyder toutes sortes de biomolécules (lipides membranaires, proteines, ADN, ARN) et déclencher un *oxidative burst* (Schraudner et al., 1998; Pasqualini et al., 2003) qui va induire de nombreux changements moléculaires, physiologiques, structuraux voire des symptômes visibles.

Les métabolites ascorbates et glutathion ne sont pas les seules molécules à pouvoir neutraliser ces ROS. En effet, la voie des phenylpropanoïdes est très souvent stimulée par l'O_3 et conduit à la production de composés phénoliques capable de réagir avec les ROS, limitant leurs dégâts dans la cellule (Castagna and Ranieri, 2009).

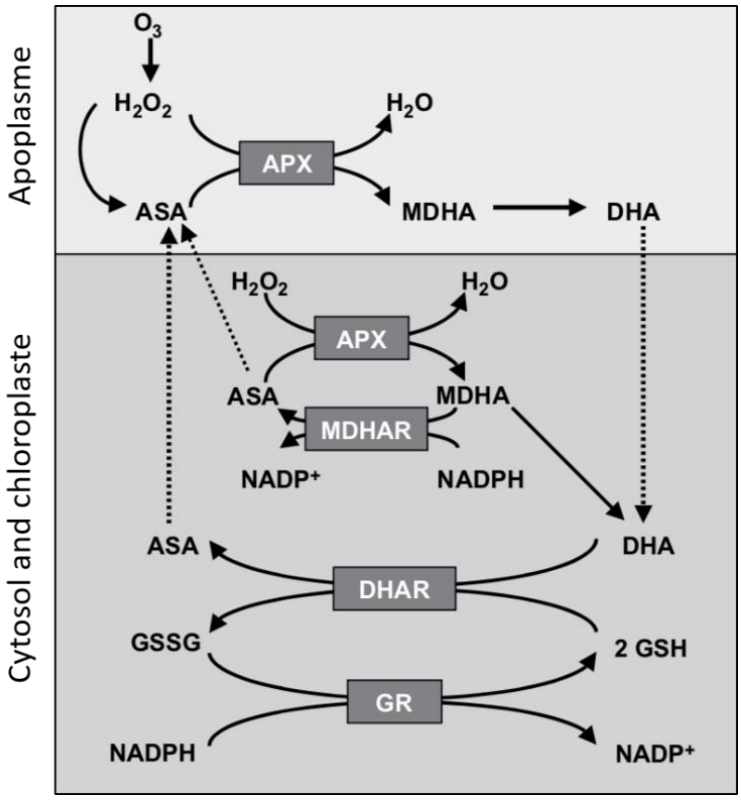

Figure 6. Cycle Halliwell-Asada-Foyer, d'après (Castagna and Ranieri, 2009). L'ascorbate (ASA) est utilisé par l'ascorbate peroxidase (APX) pour réduire l'H_2O_2 en H_2O. L'ascorbate oxydé (DHA) est régénéré dans la cellule à travers le cycle Ascorbate – Glutathion (cycle Halliwell-Asada-Foyer).

4.2. Emergence de symptômes visibles

La première étude à associer de fortes concentrations d'O_3 à l'apparition de symptômes visibles fut réalisée par (Heggestad and Middleton, 1959). Depuis, ils ont été observés dans de nombreuses études, que ce soit en chambres de fumigation, en *Open Top Chamber*, ou en pleine nature. Les symptômes visibles induits par l'O_3 sont multiples et peuvent apparaître comme un rougissement ou brunissement (bronzing) des feuilles, des lésions en pointillées (*stipples)* translucides/blanches ou brunes, des marbrures (*mottling)* accompagnées d'une décoloration (*bleaching*), et/ou des nécroses noires (figure 7).

4.2.1. Changement de pigmentation : rougissement, *bronzing*

Le rougissement et le brunissement (*bronzing*) (figure 7D-F) sont des changements de pigmentation survenant exclusivement dans la zone interveinale du limbe. Ces symptômes ont été observés sur différentes espèces d'arbre feuillu et

d’arbuste, comme le frêne, le robinier, le platane, le hêtre, la viorne ou la ronce (Gunthardt-Goerg et al., 2000; Vollenweider et al., 2002; Gerosa et al., 2008; Paoletti et al., 2009; Feng et al., 2016).

4.2.2. Stippling, mottling, *bleaching* et nécrose

Les *stipples* (pointillés) apparaissent comme pleins de petits points et peuvent être de 2 sortes différentes : blancs/translucides ou bruns (figure 7A-C). Comme le rougissement et le *bronzing*, les *stipples* sont présents uniquement dans la zone interveinale du limbe. Ce type de symptôme a été observé sur plusieurs espèces comme le frêne, l’érable, le tabac, le bouleau, l’ailante, l’*Astronium* ou le Croton (Günthardt-Goerg, 1996; Gunthardt-Goerg et al., 2000; Vollenweider et al., 2002; Paoletti et al., 2009; Moura et al., 2014; Feng et al., 2016). Le *mottling* (moucheture) (figure 7J) a été observé uniquement dans le cas de gymnosperme, plus particulièrement de pins (ponderosa, cembra, uncinata, arolla). Il s’agit de petites marbrures vertes claires développées autour des stomates au milieu du tissu des aiguilles et présentent sur les 2 faces des aiguilles. Ces marbrures s’élargissent et prennent une couleur marron dans les aiguilles plus âgées. Les spots de *mottling* sont souvent entourés d’un *bleaching* (i.e. une décoloration) du tissu. (Vollenweider et al., 2002; Sicard et al., 2011; Vollenweider et al., 2013; Kefauver et al., 2014).

Les nécroses (figure 7G) apparaissent comme des tâches noires et sont également localisées dans la partie interveinale de la feuille et ont été observé chez des arbres comme le peuplier (Vollenweider et al., 2002; Cabane et al., 2004; Bartoli et al., 2010; Sicard et al., 2011; Dghim et al., 2013; Guerrero et al., 2013; Vollenweider et al., 2013; Kefauver et al., 2014) ou le hêtre (Vollenweider et al., 2002) mais aussi sur des plantes comme le tabac (Heggestad and Middleton, 1959; Krupa et al., 2001) ou *Arabidopsis thalianna* (Overmyer et al., 2000).

Tous ces symptômes visibles sont la conséquence visible de changements structuraux microscopiques.

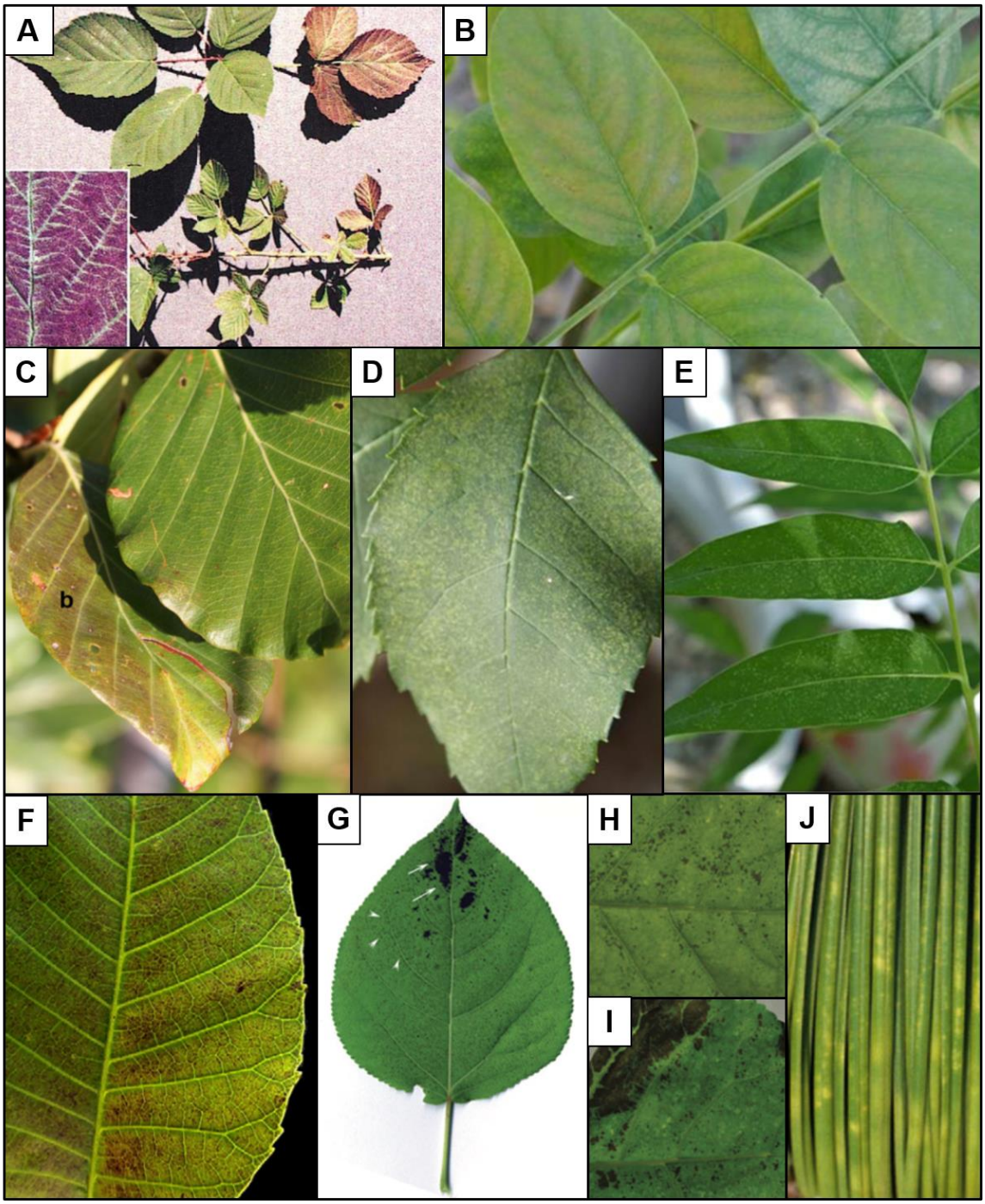

Figure 7. Symptômes visibles résultant d'une exposition à l'O_3. Rougissement de la feuille sur *Rubus fruticosus* (**A**) (Vollenweider et al., 2002) et *Robinia pseudoacacia* (**B**) (Feng et al., 2016) ; *Bronzing* (b) de la feuille sur *Fagus sylvatica* (**C**) (Vollenweider et al., 2019); *Stipples* blancs sur *Fraxinus chinensis* (**D**) et *Ailanthus altissima* (**E**) (Feng et al., 2016); *stipples* marrons sur *Astronium graveolens* (**F**) (Moura et al., 2018) ; Nécroses noires sur *Populus deltoides x maximowiczii* (**G**) (Bartoli et al., 2013), et peuplier euramericain (**H** et **I**) (Dghim et al., 2013); *Mottling* sur le pin ponderosa (**J**) (Vollenweider et al., 2013).

4.3. Changements microscopiques associés aux symptômes visibles

D'un point de vue microscopique, les tissus affectés en premiers sont les cellules du mésophylle, et plus précisément celles du parenchyme palissadique supérieur en raison du synergisme apparent entre stress oxydant et photooxydant. Au contraire, l'épiderme et les tissus vasculaires restent intacts (Vollenweider et al., 2002; Bartoli et al., 2010; Feng et al., 2016; Moura et al., 2018; Vollenweider et al., 2019).

4.3.1. Changements microscopiques sous-jacents au changement de pigmentation

Ces changements de pigmentation résultent de l'accumulation de métabolites secondaires oxydés, comme des anthocyanes, des isoflavonoïdes, des composés phénoliques (Vollenweider et al., 2002) ou des tannins (Feng et al., 2016), dans la vacuole (figure 8A). Une augmentation de la taille de la vacuole (figure 8B vs 8C) est également observée dans le cas de pigmentation suite à une exposition à l'O_3 (Paoletti et al., 2009; Vollenweider et al., 2019).

Un autre trait microscopique observé en réponse à l'O_3 est la réduction en taille des chloroplastes (figure 8B vs 8C) et une augmentation en taille et en nombre des plastoglobules dans les chloroplastes (figure 8D) (Mikkelsen and HeideJorgensen, 1996; Gunthardt-Goerg et al., 1997; Gunthardt-Goerg et al., 2000; Paoletti et al., 2009; Feng et al., 2016; Vollenweider et al., 2019). Les plastoglobules sont des gouttelettes lipidiques présentent dans le stroma des chloroplastes et associés aux thylakoïdes. Leur augmentation en nombre et taille a été observé dans le cas de nombreux stress abiotiques en plus de l'O_3, comme le stress hydrique, salin, lumineux, et métaux lourds (Brehelin et al., 2007), mais aussi au cours de la senescence (Lichtenthaler, 2013). Ils sont composés principalement de prenylquinones, dont de l'α-tocophérol jouant un rôle important dans le transport d'électrons photosynthétiques et dans la protection des lipides contre l'oxydation (van Wijk and Kessler, 2017).

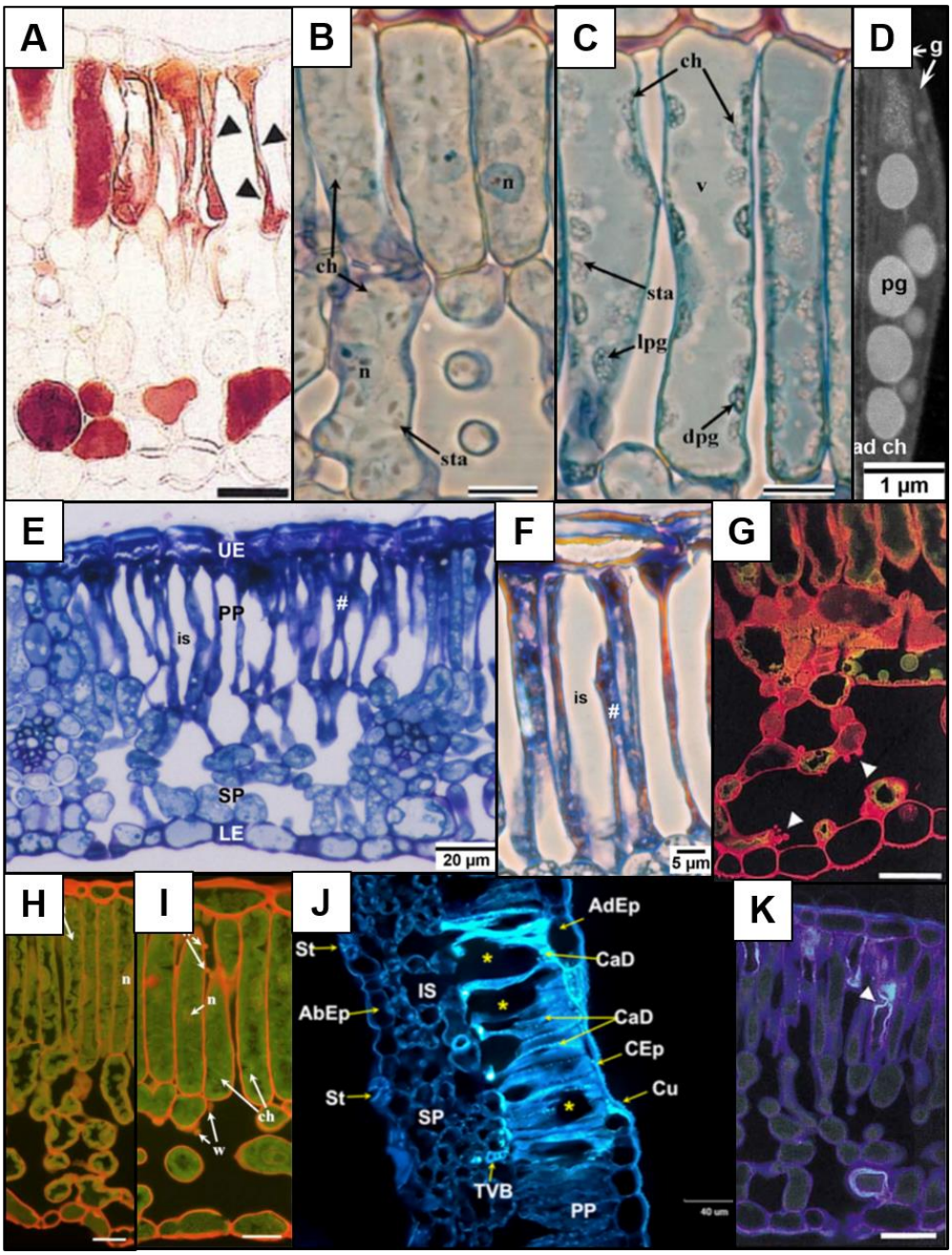

Figure 8. Changements structuraux et ultra-structuraux en réponse à l'O_3. **A** cellules collapsées dont la vacuole est pleine d'anthocyanes (*Robinia pseudoacacia*, bar : 25 µm (Vollenweider et al., 2002)) ; **B** (contrôle) vs **C** (symptomatique), réduction en taille et nombre des chloroplastes, et augmentation de la taille de la vacuole (*Fraxinus ornus*, bar : 10 µm, (Paoletti et al., 2009)) ; **D** Présence de plastoglobules (*pg*) dans un chloroplaste de la face adaxiale d'une feuille présentant du *bronzing* (*Fagus sylvatica*, (Vollenweider et al., 2019) ; **E** et **F** Groupe de cellules collapsée dans le parenchyme palissadique d'une feuille présentant des *stipples* (*Fagus sylvatica*, (Vollenweider et al., 2019)), **G** Protrusion pectinique (tête de flèches) dans l'apoplasme (*Fagus sylvatica*, bar : 25 µm, (Vollenweider et al., 2002)) ; **H** (contrôle) vs **I** (symptomatique), épaississement des parois et protrusion pectinique (w) (*Fraxinus ornus*, bar : 20 µm, (Paoletti et al., 2009)) ; **J** Déposition de callose (CaD), abréviations : AdEp : épiderme adaxial, AbEp : épiderme abaxial, IS :espace intercellulaire, SP : parenchyme spongieux, PP : parenchyme palissadique, St : stomate (*Ailanthus altissima*, (Feng et al., 2016)), **K** incurstation cellulosique conduisant à un épaississement des parois (Fagus sylvatica, bar :20 µm, (Vollenweider et al., 2002)).

Toutefois, durant la senescence, les plastoglobules se multiplient parallèlement au désassemblage des membranes des thylakoïdes et des complexes protéiques, ainsi qu'à la dégradation des pigments (caroténoïdes et chlorophylle). L'augmentation en taille et en nombre des plastoglobules dans une réponse à une exposition à l'O_3 reflète donc une augmentation du stress oxydant dans les chloroplastes et de la dégradation des membranes des thylakoïdes.

4.3.2. Changements microscopiques derrières les symptômes de type *stippling*, *mottling, bleaching* et nécroses

L'apparition de *stipples* et de *mottling* sur le limbe foliaire est la conséquence directe de cellules du parenchyme palissadique ayant collapsées (figure 8E, 8F) (Gunthardt-Goerg et al., 1997; Günthardt-Goerg and Vollenweider, 2007; Paoletti et al., 2009; Vollenweider et al., 2019). Les cellules collapsées sont le résultat d'une mort cellulaire rapide. Suite à une rupture du tonoplaste, le contenu de la vacuole et le matériel cellulaire se mélangent, conduisant à la décompartimentation de la cellule (Paoletti et al., 2009; Vollenweider et al., 2019). Les différents composants de la cellule (mitochondrie, chloroplaste, noyau etc…) deviennent ainsi la cible des protéases, hydrolases et lipases jusqu'à présent contenues dans la vacuole (Carter et al., 2004). La dégradation du matériel cellulaire se fait alors de manière anarchique et désorganisée, aboutissant à une dégradation incomplète des organelles (Vollenweider et al., 2002; Chaerle et al., 2007; Günthardt-Goerg and Vollenweider, 2007; Vollenweider et al., 2019). Le *bleaching* observé autour du mottling correspond à une dégradation de la chlorophylle dans des cellules du mésophylle entourant les cellules nécrotiques.

Dans les feuilles présentant des *stipples*, on peut également observer des modifications structurales des parois. Il a été fréquemment observé un épaississement des parois par déposition de callose, cellulose ou/et ou de pectine (figure 8G-K) (Günthardt-Goerg, 1996; Gunthardt-Goerg et al., 1997; Bussotti et al., 2005; Paoletti et al., 2009; Bartoli et al., 2013; Vollenweider et al., 2019). Ces dépositions se font généralement sur les cellules les plus proches du point d'entrée de l'O_3 dans la feuille, et serait un des premiers résultats de la cascade de réactions oxydatives provoquée par la génération de ROS dans l'apoplasme (Paoletti et al., 2009). En effet,

l'épaississement des parois permet de limiter la diffusion des ROS (et donc les dégâts qu'ils peuvent causer) dans la cellule.

Au final, selon Vollenweider et al. (2002) les changements structuraux et microscopiques peuvent être mis en relation avec 3 types de réponses : l'oxidative burst, la réponse hypersensible-like (HR-like) et la senescence accélérée de la cellule (ACS ; tableau 1). En effet, les changements microscopiques résultant d'une exposition à l'O_3 présentant des similitudes avec la réponse hypersensible induite lors d'un stress biotique ont été associé à la réponse HR-like (nommée ainsi pour cette raison) et ceux ressemblant à la senescence automnale ont été associé à l'ACS. Les changements microscopiques ne pouvant pas être associé directement à la HR-like ou l'ACS ont été associé à *l'oxidative burst*, processus induit pour le stress O_3.

Tableau 1. Association des changements microscopiques et structuraux observés en réponse à l'O_3 avec la réponse hypersensible-like, l'accélération de la senescence ou l'oxidative burst (Vollenweider et al., 2002).

Physiological responses	Observed cellular markers	References
Oxidative burst	a. wart-like and strand protrusion on cell walls	a. Günthardt-Goerg et al., 1997
	b. accumulation of antioxidants	b. Sandermann, 1996
	c. increased oxidation of cell content	c. Pellinen et al., 1999
Hypersensitive response-like	a. disruption of cell structure	a. Fett and Jones, 1995
	b. chromatin condensation and nucleus degeneration	a-c, e. Alvarez et al., 1998; Levine et al., 1996
	c. collapse of cell walls	
	d. incomplete degradation of cell organelles following rapid cell death	d. Fukuda, 2000
	e. condensation of cell remnants to apoptotic-like bodies	
Accelerated cell senescence	a. increase in vacuole and vacuome size	a. Pell et al., 1997
	b. slow degeneration of cell components as shown by moderate and progressive condensation of cell cytoplasm and nucleus	b. Fukuda 2000; Ruetze and Schmitt, 1988; Gahan, 1981
	c. accumulation of secondary compounds	c. Schraudner et al., 1997

4.4. L'O_3, éliciteur de la mort cellulaire programmée

Tous Les changements structuraux et microscopiques induits par l'O_3 et précédemment décrits peuvent être associés à la mort cellulaire programmée.

La mort cellulaire programmée (PCD) fait partie intégrante de la vie de la plante car elle est nécessaire pour la bonne formation de certains organes ou tissus, comme les éléments du xylème ou les aérenchymes (Jones, 2001; Rogers, 2005). En dehors de ces derniers évènements elle peut être impliquée dans deux processus survenant dans la vie de la plante: la sénescence et la réponse hypersensible (Locato and De Gara, 2018).

La sénescence est un processus au cours duquel la cellule met en œuvre des mécanismes qui conduisent à sa destruction organisée et contrôlée permettant la remobilisation de nutriments (Nooden et al., 1997). Elle est systématiquement induite quand la viabilité de la feuille ou sa capacité photosynthétique diminue, comme en automne quand la photopériode diminue (Bhalerao et al., 2003). La réponse hypersensible (HR) est un mécanisme de défense induit dans le cas de stress biotiques au cours duquel les cellules infectées et adjacentes sont tuées, afin de limiter la propagation d'un pathogène. Dans le cas de stress abiotique, une réponse similaire, appelée HR-like, est induite (Lam, 2004).

Dans le cas de l'O_3, ce sont les ROS générés dans l'apoplasme qui, en s'accumulant, vont participer à la mise en place de la PCD (ACS et/ou HR-like) (Bhattacharjee, 2005).

4.4.1. L'O_3 provoque une accélération de la senescence

Une exposition à l'O_3 peut engendrer une série de réponses physiologiques et structurales ressemblant fortement aux réactions mises en place pendant la senescence automnale. En effet, d'un point de vue physiologique, l'O_3 peut induire une diminution de la conductance stomatique, une dégradation des chlorophylles et une réduction de l'activité de la rubisco conduisant à une baisse de fixation et d'assimilation du CO_2 (Pell et al., 1992; Calatayud et al., 2004; Bagard et al., 2015; Dusart et al., 2019a). D'un point de vue structural, les changements observés lors de la sénescence regroupent une dégradation des chloroplastes, augmentation de la taille de la vacuole, une dégradation progressive du matériel cellulaire et une accumulation de métabolites secondaires (Mikkelsen and HeideJorgensen, 1996; Vollenweider et al., 2002; Moura

et al., 2018). Les mitochondries conservent leur intégrité jusqu'au dernier stade de la senescence et participent à la remobilisation des nutriments en assurant la synthèse de l'alpha-cétoglutarate et du glutamate, qui fournissent les squelettes carbonés pour la remobilisation de l'azote. Néanmoins, avec l'avancée de la senescence leur nombre se trouve réduit (Chrobok et al., 2016). Comme ces processus apparaissent avant l'automne aussi bien dans les feuilles jeunes que dans des feuilles âgées, ils ont été interprétés comme étant une accélération de la senescence, et donc qualifiés d'*Accelerated Cell Senescence* (ACS).

4.4.2. Une mort cellulaire rapide : la réponse hypersensible-like

Dans les feuilles, l'O_3 est capable d'induire des réponses et mécanismes de défense similaires à ceux observés dans le cas d'interaction plante/pathogènes. En effet, un « oxidative burst » (observé plusieurs heures après l'arrêt de l'O_3), une synthèse de protéines de type *Pathogenesis-Related* (PR ; comme des glucanase, des chitinase) ou encore de phytoalexines, sont induits en réponse au polluant (Sandermann et al., 1998; Pasqualini et al., 2003). Des marqueurs de défense comme un dépôt de callose et lignine, et une stimulation de la voie des phenylpropanoïdes en réponse aux pathogènes et à l'O_3 sont également observés (Sandermann et al., 1998; Pasqualini et al., 2003; Bussotti et al., 2005).

4.4.3. Rôles des phytohormones dans la PCD

La mort cellulaire programmée est contrôlée par les phytohormones, principalement par l'acide jasmonique (JA), l'acide salicylique (SA) et l'éthylène (ET) (figure 9).

L'éthylène (ET) est synthétisé par 2 enzymes, l'ACC synthase et l'ACC oxydase. L'induction de la biosynthèse de l'ET en réponse à l'O_3 est l'une des réponses les plus rapides survenant dans les quelques heures suivant l'exposition au gaz (Diara et al., 2005; Pellegrini et al., 2013). L'*oxidative burst* induit par les ROS générés par l'O_3, va activer une cascade de *Mitogen-activated protein kinases* (MAPKs) conduisant à l'activation de l'ACC synthase (Pellegrini et al., 2016), et donc à la synthèse d'ET qui va participer à la propagation de la mort cellulaire (Kangasjarvi et al., 2005).

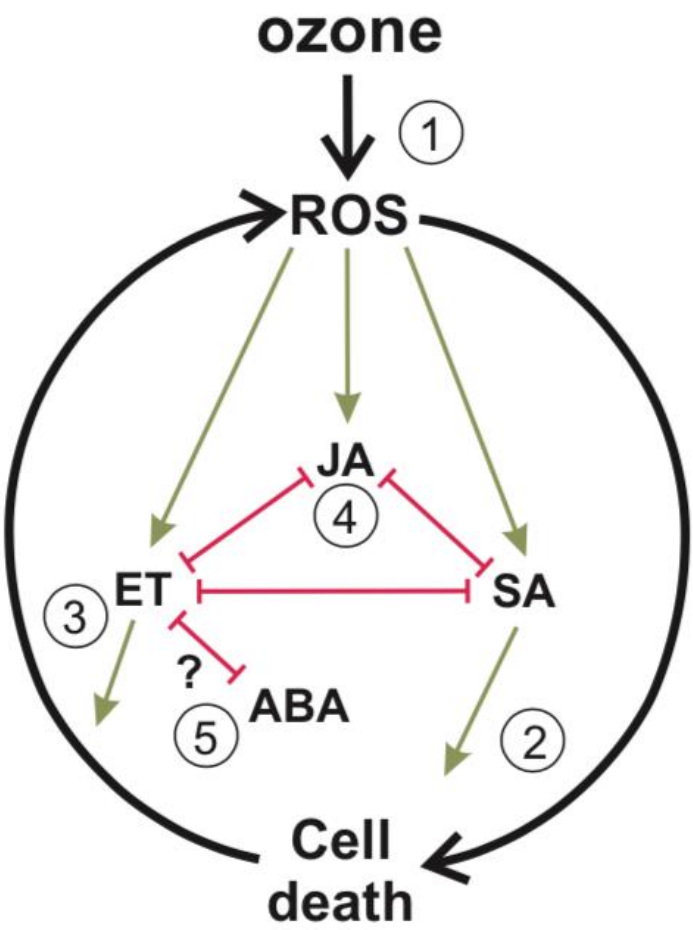

Figure 9. Interactions entre les ROS et les phytohormones en réponse à l'O_3 (Kangasjarvi et al., 2005). Les ROS induit par l'O_3 (1) vont induire une production d'acide salicylique (SA) et une mort cellulaire (2). La production d'éthylène (ET) va favoriser la propagation de la mort cellulaire (3) alors que l'acide jasmonique (JA) va agir de manière antagoniste à SA et ET (4). Le rôle de l'acide abscissique dans la limitation ou la propagation de la mort cellulaire n'est pas encore bien caractérisé (5).

L'acide salicylique (SA) peut être formé par 2 voies : une cytoplasmique faisant intervenir la phénylalanine amonia-lyase (PAL), et une chloroplastique faisant intervenir l'isochorismate synthase (Janda and Ruelland, 2015; Pellegrini et al., 2016). Sous une exposition aiguë d'O_3, l'augmentation de SA survient environ 7h après le début de l'exposition, soit un peu plus tardivement que celle de l'ET (Pasqualini et al., 2003; Kangasjarvi et al., 2005; Pellegrini et al., 2013). SA et l'ET vont agir de manière synergétique dans la propagation de la mort cellulaire (Kangasjarvi et al., 2005).

L'acide jasmonique (JA) est un dérivé d'acide gras synthétisé par la voie des lipoxygénases. Il a été montré que l'O_3 stimule la production de JA par réaction des ROS avec les lipides de la membrane (Rao et al., 2000) . L'augmentation de JA se fait

environ en même temps que celle de SA, et participe à limiter la propagation de la mort cellulaire (Overmyer et al., 2000; Kangasjarvi et al., 2005).

4.5. Impact de l'O_3 sur la physiologie

L'apparition de symptômes visibles et de changements structuraux s'accompagnent forcément d'une modification du métabolisme cellulaire

4.5.1. Réduction des processus photosynthétiques et des échanges gazeux

Une conséquence de l'exposition des plantes à l'O_3 est la réduction générale des processus photosynthétiques. Ces effets sont connus depuis longtemps puisqu'une réduction de la teneur en chlorophylles, de l'activité et de la quantité de rubisco ainsi qu'une réduction de l'assimilation nette de CO_2 ont été rapportées dès les années 80 et 90 (Reich, 1983; Pell et al., 1992).

Depuis, ces résultats ont été retrouvés pour de nombreuses espèces, dont des espèces ligneuses (Dizengremel, 2001) et ont fait l'objet de méta-analyses (Reich, 1983; Pell et al., 1992; Wittig et al., 2009; Li et al., 2017). Dans leur méta-analyse, (Wittig et al., 2009) ont déterminé que l'O_3 avait réduit l'assimilation nette de CO_2 en lumière saturante (A_{sat}) de 19%, les teneurs en chlorophylles totales de 10%, et de la teneur en rubisco de 8%, comparé aux contrôles et pour des concentrations d'O_3 de 81, 56 et 45 ppb respectivement. Ces réductions sont d'autant plus importantes que la concentration d'O_3 est élevée. En effet, dans la méta-analyse plus récente (Li et al., 2017), qui prend en compte des études ayant appliquées des concentrations plus fortes (115 ppb), les auteurs ont trouvé une diminution de A_{sat} de 28% et une réduction des teneurs en chlorophylles totales de 17% (figure 10). Bien que les quantités de rubisco ne soient pas rapportées, les auteurs ont déterminé la réduction de la vitesse maximale de carboxylation (-21%) et de la densité maximale du flux d'électron photosynthétiques (-23%), rendant compte de la diminution des capacités photosynthétiques sous O_3.

Unes des explications possibles pour cette diminution de l'assimilation du CO_2 est l'impact de l'O_3 sur les échanges gazeux. En effet, sous O_3, la conductance stomatique est réduite de 10% (Wittig et al., 2009) pour les plantes exposées à une concentration modérée (71 ppb) et de 20% (Li et al., 2017) pour celles exposées à une

concentration élevée (environ 100 ppb) (figure 10). Plusieurs mécanismes ont été proposés pour expliquer la fermeture des stomates : génération d'un *oxidative burst* directement dans les cellules de gardes des stomates ou une production d'acide abscissique (ABA) induite par les ROS, ou une émission d'éthylène (Kangasjarvi et al., 2005). Toutefois, une étude récente tendrait à confirmer l'hypothèse de la production d'ABA stimulée par les ROS qui induirait une fermeture des stomates (McAdam et al., 2017). Un autre effet de l'O_3 sur les stomates est la diminution de la vitesse d'ouverture et de fermeture des stomates : le *stomatal sluggishness* (Paoletti and Grulke, 2010; Dusart et al., 2019b).

Au final, la réduction des capacités photosynthétiques de la plante sous O_3, en plus de réduire la croissance et la productivité des arbres, va avoir un impact également sur la capacité de puit de carbone par les forêts (Sitch et al., 2007).

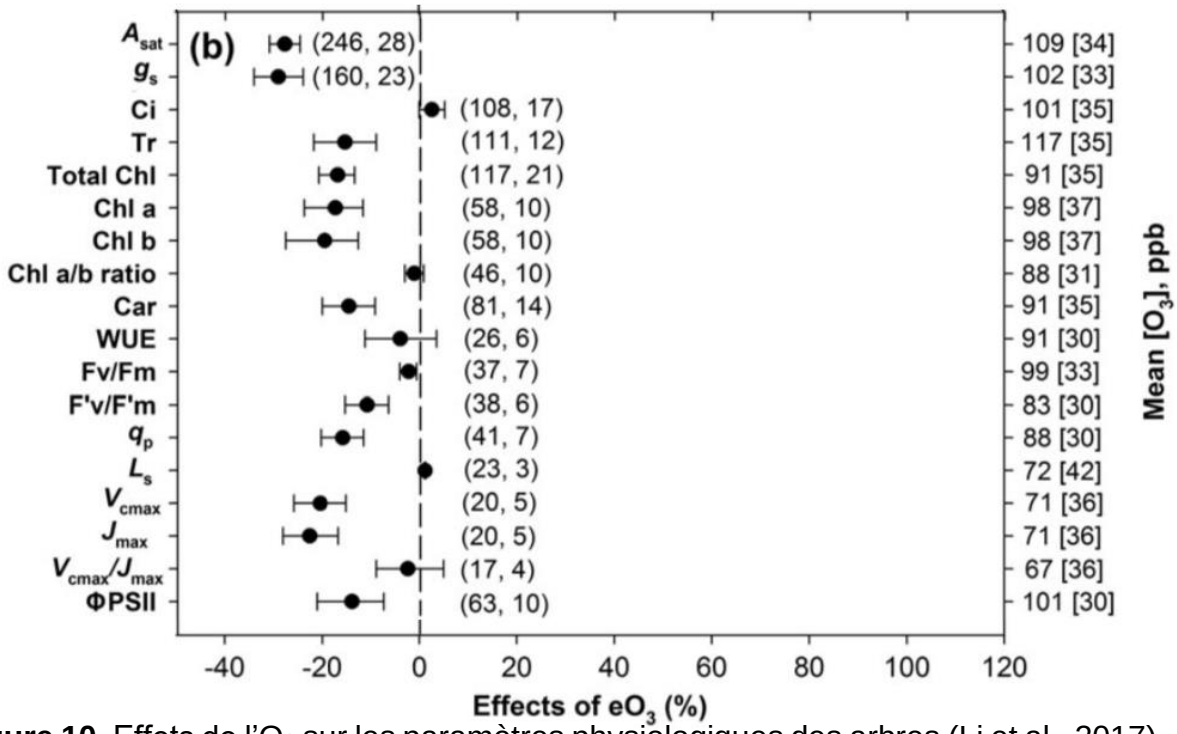

Figure 10. Effets de l'O_3 sur les paramètres physiologiques des arbres (Li et al., 2017). Les symboles représentent les pourcentages de changements par rapport aux contrôles. Le nombre d'articles et de mesures est présenté en parenthèse et les concentrations d'O_3 sur l'axe des ordonnées à droite (la valeur entre crochet est celle des contrôles).

4.5.2. Augmentation de la respiration et inhibition de la photorespiration

Une autre conséquence d'une exposition des plantes à l'O_3 est une augmentation de la respiration (Reich, 1983; Dizengremel, 2001; Paoletti et al., 2009; Yendrek et al., 2015) visant à une plus forte production d'énergie pour les mécanismes de réparation mais également afin de générer à certaines étapes du processus du pouvoir réducteur pour augmenter la tolérance au stress oxydant induit (Dizengremel et al., 2009; Dghim et al., 2013). En effet, l'augmentation de l''activité et de quantité de la phosphoenolpyruvate carboxylase (PEPc) (Fontaine et al., 1999; Dizengremel, 2001; Bagard et al., 2015) va conduire à une augmentation du malate cytosolique. Le malate va pouvoir être utilisé directement dans le cytosol par une enzyme malique à NADP. Dans ce cas, le malate sert à former du pyruvate et du NADPH. Il peut aussi être exporté dans la mitochondrie où, au travers le cycle de Krebs, il va être transformé en citrate puis exporté dans le cytosol sous forme d'isocitrate qui sera utilisé par une isocitrate déhydrogénase afin de former de l'oxoglutarate et du NADPH (figure 11). Le NADPH ainsi généré va servir aux enzymes impliquées dans la detoxication des ROS, comme par exemple la glutathione réductase (GR précédemment présentée) ou les glutarédoxines (enzymes liant du glutathion à une protéine pour empêcher son oxydation) (Dizengremel et al., 2008).

Une exposition à l'O_3 résulte aussi en une diminution des processus photorespiratoires, en concomitance avec la réduction des processus photosynthétiques (Dizengremel, 2001; Bagard et al., 2008). Le cycle photorespiratoire est perçu comme un processus permettant de consommer un excès d'énergie et de pouvoir réducteur et ainsi d'éviter les effets d'une photooxydation avec une fuite d'électrons et la formation d'espèces réactives de l'oxygène. Sous O_3, plusieurs travaux ont montré que la photorespiration était plutôt inhibée (Booker et al., 1997; Bagard et al., 2008). Une explication souvent avancée par ces auteurs est que la diminution concomitante de la photosynthèse et de la photorespiration, serait la conséquence d'une plus faible activité carboxylase et oxygénase, ainsi qu'une plus faible quantité de RubisCO.

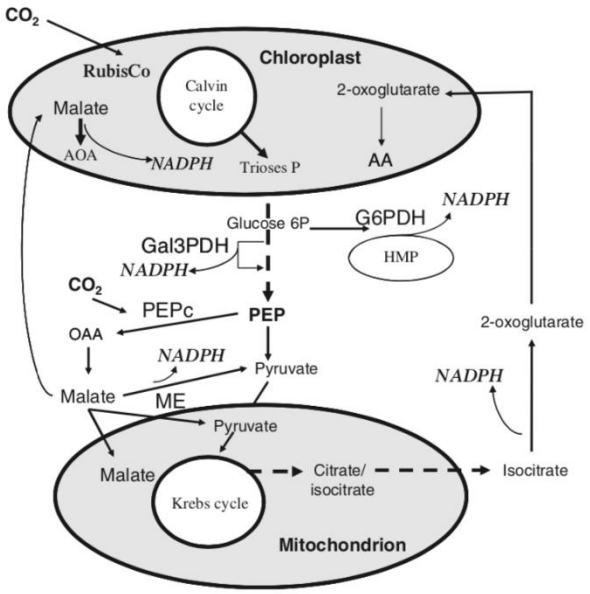

Figure 11. Enzymes et voies métaboliques contribuant à l'apport de NADPH dans une cellule foliaire (Dizengremel et al., 2009). AA : acide aminés, Gal3PDH : glyceraldéhyde-3-phosphate déshydrogénase, G6PDH : glucose-6-phosphate déshydrogénase, HMP : voie des hexoses monophosphates, IDH : isocitrate déshydrogénase, ME : enzyme malique, OAA : acide oxaloacétique, PEPc : phosphoénolpyruvate carboxylase.

4.6. Changements d'expression de gènes en réponse au stress O_3

La plupart des effets de l'O_3 décrit précédemment sont une conséquence d'un changement de l'expression du génome.

4.6.1. Baisse d'expression de gènes associés à la fixation de carbone

En accord avec les diminutions d'assimilation nette de CO_2, de photosynthèse et d'activité de RuBisCo, suite à une exposition à l'O_3 les gènes associés à la photochimie ou bien à la fixation/assimilation de carbone sont sous-exprimés. Cela a été observé aussi bien chez les herbacées (Conklin and Last, 1995; Papazian et al., 2016; Waldeck et al., 2017; Zhang et al., 2017) que chez les arbres (Gupta et al., 2005; Street et al., 2011b; Gottardini et al., 2016; Soltani et al., 2020). En effet, que ce soit pour les herbacées ou les arbres, l'O_3 induit la sous-expression de beaucoup de gènes codants pour des protéines impliquées dans les antennes collectrices (chlorophylle a/b binding), les photosystèmes I et II, la RuBisCo activase ainsi que la petite sous-unité

de la RuBisCo (Conklin and Last, 1995; Pelloux et al., 2001; Gupta et al., 2005; Waldeck et al., 2017; Soltani et al., 2020). A l'inverse et en accord avec l'augmentation de l'activité de la PEPc, les gènes codant pour la PEPc sont surexprimés en réponse à l'O_3 (Fontaine et al., 2003).

4.6.2. Stimulation de la voie des phénylpropanoïdes

La voie des phénylpropanoïdes aboutie à la synthèse de lignines, anthocyanes, tanins, flavonoïdes et composés phénoliques, impliqués dans la réponse au stress abiotique et biotique (Dixon et al., 2002; Sharma et al., 2019).

Dans le cas de l'O_3, plusieurs études ont rapporté une stimulation de l'expression de gènes et de l'activité pour la phénylalanine amonia-lyase (PAL ; (Koch et al., 1998; Richet et al., 2012; Yendrek et al., 2015)), ainsi que pour la cinnamyl alcool déshydrogénase (CAD ; (Cabane et al., 2004; Richet et al., 2012)). Cette stimulation conduit à une accumulation de lignines spécifiques, suggérant un rôle de défense contre les ROS induits par l'O_3 et augmentant la tolérance au stress (Cabane et al., 2004). On retrouve également une surexpression de gènes codant pour la DFR (dihydroflavonol 4 reductase), la IFR (isoflavonoïd reductase), et la CHS (chalcone synthase) (Yendrek et al., 2015), autres enzymes de la voie des phenylpropanoïdes menant à la synthèse d'anthocyanes et tanins condensés (DFR), et d'isoflavonoïdes (CHS et IFR). Ces composés ont des propriétés antioxydantes (Blokhina and Fagerstedt, 2006; Mierziak et al., 2014) et peuvent réagir avec les ROS pour limiter leurs dégâts.

4.6.3. Surexpression de gènes associés aux phytohormones et au système antioxydant

L'acide salicylique (SA), jasmonique (JA) et l'éthylène (ET) jouent un rôle important dans la réponse à l'O_3 puisqu'elles interviennent dans signalisation sous ozone (voir paragraphe 4.3.3). L'O_3 induit une stimulation de l'expression des gènes et de l'activité d'enzymes responsables de la biosynthèse de SA (Ogawa et al., 2007; Richet et al., 2012; Yendrek et al., 2015), à la biosynthèse du JA (Zhang et al., 2019) et à celle de l'ET (Tamaoki et al., 2003).

D'un point de vue moléculaire, concernant les antioxydants, l'O_3 induit surtout la synthèse et régénération du glutathion (Conklin and Last, 1995; Dumont et al., 2014;

Yendrek et al., 2015; Dusart et al., 2019a) avec une stimulation de la glutathion synthase (GST). Par ailleurs, le ou les gènes codant pour la glutathion réductase (GR) sont également fortement stimulées, témoignant de l'importance de la régénération du glutathion réduit dans les mécanismes antioxydants de la cellule sous O_3 (Dumont et al., 2014).

4.6.4. Expression de gènes relatifs à la mort cellulaire programmée

La senescence foliaire implique des changements d'expression de gènes particuliers. Parmi les gènes différentiellement exprimés pendant la senescence, ceux qui sont surexprimés sont appelés senescence-associated genes (SAGs). Les SAGs regroupent des gènes codants pour des enzymes de dégradation comme des RNases, des proteases, des lipases, des gènes codant pour des transporteurs de nutriments, et aussi des gènes codants pour l' ACC synthase (responsable de la synthèse de l'ET) (Zimmermann and Zentgraf, 2005).

En réponse à l'O_3, une partie de ces SAGs identifiés dans la senescence automnale ont été surexprimés chez *Arabidopsis thalianna* (Miller et al., 1999; D'Haese et al., 2006) et chez le peuplier (Gupta et al., 2005). Ces résultats indiquent une dégradation et une remobilisation des nutriments, en relation avec la senescence accélérée provoquée par l'O_3. De par leur similitude de structure et d'activités avec ces caspases, les cystéines protéases présentent dans le monde végétal ont été appelé « métacaspase » (Rocha, 2017). Les métacaspases sont à l'origine de la mort cellulaire induite lors de la réponse hypersensible en cas d'attaque de pathogènes. C'est l'*oxidative burst* déclenché par une production de ROS lors de l'attaque qui va engendrer la transcription et l'activation des métacaspases (He et al., 2008; Fagundes et al., 2015). Au cours d'une étude, du maïs exposé à des concentration chronique d'O_3 a montré une très forte stimulation de l'activité et de l'expression d'un gène codant pour une métacaspase (Ahmad et al., 2012), rapprochant la réponse à l'O_3 à celle des pathogènes.

4.6.5 Etudes transcriptomiques globales : le RNAseq

Depuis quelques années des études d'expression de l'ensemble du génome (RNAseq), ont permis d'étudier la réponse globale du transcriptome de la plante au

stress O_3. Ces études ont été menées sur des arbres, comme le peuplier (Street et al., 2011a; Zhang et al., 2019) ou le chêne (Natali et al., 2018; Soltani et al., 2020) ou sur des herbacées, comme *Salvia officinalis* (Marchica et al., 2019), le soja (Cho et al., 2013; Whaley et al., 2015; Waldeck et al., 2017) ou le haricot (Yendrek et al., 2015), exposés à des concentrations chroniques d'O_3, et plus rarement à des concentrations très élevées (acute) sur *Arabidopsis thaliana* (Xu et al., 2015). Quelle que soit la plante (arbre ou herbacée), la réponse transcriptomique commune comprend la surexpression de gènes liés au métabolisme secondaire, à la réponse au stress (biotique et abiotique), aux phytohormones, à la signalisation (MAPK) et aux facteurs de transcription (WRKY, MYB) (Street et al., 2011a; Cho et al., 2013; Whaley et al., 2015; Xu et al., 2015; Yendrek et al., 2015; Waldeck et al., 2017; Natali et al., 2018; Marchica et al., 2019; Soltani et al., 2020). En revanche, les gènes liés au métabolisme primaire, à la photosynthèse, au métabolisme des glucides et à la croissance sont couramment sous-exprimés en réponse à l'O_3 (Whaley et al., 2015; Waldeck et al., 2017; Natali et al., 2018; Soltani et al., 2020). Cependant, la plupart de ces études se sont concentrées sur la différence de réponse induite par l'O_3 entre un génotype tolérant et un génotype sensible, sans aucune investigation sur la relation entre la dynamique de ces changements transcriptomiques.

5. Objectif du travail de thèse

5.1. Présentation des équipes rattachées au projet EFFECTO3-Flux

Mon projet de thèse s'inscrit dans le projet EFFECTO3-Flux, fruit d'une collaboration entre les unités de recherche Dynamique Forestière du WSL (Birmensdorf, Suisse) et Silva de l'Université de Lorraine (Nancy, France).

L'unité Dynamique Forestière regroupe des équipes travaillant sur la croissance des forêts, l'écologie des perturbations, l'écophysiologie et les dendrosciences. L'équipe Ecophysiologie se concentre sur l'étude des mécanismes de réponse des arbres aux contraintes abiotiques dues aux facteurs climatiques et édaphiques, du niveau de la cellule à celui de l'écosystème, à travers un diagnostic des stress et des modélisations mécanistiques. Depuis les années 90, une partie des recherches de cette équipe étudie les changements structuraux en réponse à divers stress

abiotiques, y compris l'O_3 (Günthardt-Goerg, 1996; Gunthardt-Goerg et al., 1997; Gunthardt-Goerg et al., 2000; Vollenweider et al., 2002; Günthardt-Goerg and Vollenweider, 2007; Vollenweider et al., 2013; Vollenweider et al., 2016; Vollenweider et al., 2019). Au travers de ces études, les changements microscopiques résultant d'une exposition à l'O_3 ont été (i) caractérisés aussi bien en milieu naturel qu'en conditions contrôlées, (ii) reliés à l'émergence des symptômes visibles et (iii) associés à des réponses cellulaires de mort programmée.

L'unité Silva regroupe 3 équipes réparties à la faculté des Sciences et Technologies de l'Université de Lorraine (Nancy), à l'INRAE (Institut National de Recherche Agronomique ; Champenoux) et AgroParisTech (Nancy).

Parmi les équipes qui la composent, l'équipe PHARE (Physiologie de l'Arbre en REponse au stress) a pour objectif principal la compréhension des mécanismes d'acclimatation et d'adaptation des arbres à un environnement changeant, les facteurs environnementaux étudiés étant la sécheresse, les fortes températures et la pollution atmosphérique, notamment l'O_3. Ainsi, depuis le début des années 2000, les travaux de cette équipe ont montré bon nombre d'altération des processus cellulaires en réponse à l'O_3, premièrement chez le pin d'Alep et plus récemment chez le peuplier (Pelloux et al., 2001; Cabane et al., 2004; Bagard et al., 2008; Richet et al., 2012; Dghim et al., 2013; Dumont et al., 2013; Bagard et al., 2015; Dusart et al., 2019a).

5.2. Contexte scientifique global

Malgré des efforts pour réduire les émissions de ses précurseurs, l'O_3 troposphérique reste problématique vis à vis de la végétation. En effet, les concentrations de fond d'O_3 troposphérique ont atteint des niveaux phytotoxiques impactant négativement aussi bien les espèces cultivées que la végétation naturelle (Wittig et al., 2009; Proietti et al., 2016; Li et al., 2017). De plus, il est prévu que cet impact se poursuive au cours des prochaines décennies (Karlsson et al., 2017).

Pour mieux évaluer les risques et les pertes économiques que peut entrainer l'O_3, des seuils critiques d'exposition ont été calculés à travers différents indicateurs, notamment le POD_Y qui met en relation le flux d'O_3 entrant dans la feuille (calculé à partir de la modélisation de la conductance stomatique) et la réponse de la plante. L'introduction d'un seuil Y représentant la fraction du flux stomatique d'O_3 que la plante parvient à détoxifier conduit à définir la dose d'O_3 effective (i.e. la fraction du flux

stomatique d'O_3 pour laquelle les effets négatifs apparaissent). Dans tous les cas, que ce soit la perte de biomasse ou l'apparition de symptômes visible, ce sont des effets négatifs tardifs de l'O_3 résultant forcément d'une modification des processus cellulaires. Cependant, peu de choses sont connues sur la dynamique des effets précoces de l'O_3 (changements microscopique, physiologique et transcriptomique) en fonction de la dose d'O_3 effective. Il est donc important d'approfondir les connaissances scientifiques sur ces aspects pour mieux comprendre les mécanismes de réponse à l'O_3 en fonction de la dose d'O_3 effective.

Ma thèse s'inscrit dans la continuité des thématiques de recherches des 2 unités rattachées au projet EFFECTO3-Flux, et a pour objectif général de **relier le développement spatio-temporel des changements structurels avec les réponses cellulaires en relation avec la dose d'O_3 effective** dans le but de mieux comprendre la dynamique des effets précoces de l'O_3 amenant aux marqueurs utilisés pour définir les seuils de risques. Cela permettra de mieux évaluer les capacités de défense/detoxication des plantes, et ainsi améliorer la détermination du seuil Y appliqué au POD.

Les objectifs spécifiques de ce travail sont donc de :

(i) Caractériser la dynamique des réponses foliaire précoces en fonction de la dose d'O_3 cumulée et du stade de développement de la feuille. Les réponses foliaires comprennent les paramètres physiologiques en lien avec les échanges gazeux, les variations relatives en chlorophylles totales et la dynamique du développement des lésions microscopiques et macroscopiques

(ii) Suivre et décrire la dynamique des changements structuraux et ultra-structuraux en fonction de la dose d'O_3 cumulée et du stade de développement de la feuille.

(iii) Etablir la dynamique de changements d'expression de gènes sous O_3 et établir les éventuelles relations en lien avec les changements structuraux et ultra-structuraux en fonction de la dose d'O_3 cumulée et du stade de développement de la feuille

Pour atteindre ces objectifs, des peupliers hybrides (*Populus tremula x alba*) ont été exposés à l'O_3 en phytotron (conditions contrôlées) à des concentrations de 80 et 100 ppb d'O_3. Le choix de ces doses d'exposition sera abordé dans le premier chapitre. Outre son utilisation depuis environ 20 ans au sein du laboratoire Silva, cet hybride a été choisi car il présente des avantages non négligeables : l'obtention de clone par micro-bouturage, une croissance rapide et simple, des feuilles larges (figures 12A,B)

et un génome entièrement séquencé et annoté. Enfin, la fumigation en conditions contrôlées (figure 12C) permet, dans le cas d'analyse de changements métaboliques ou d'expression de gènes, d'obtenir uniquement l'effet de l'O_3 en limitant celui d'autres stress pouvant interagir avec la réponse des arbres en milieu naturel (comme par exemple un stress biotique ou des carences en nutriments).

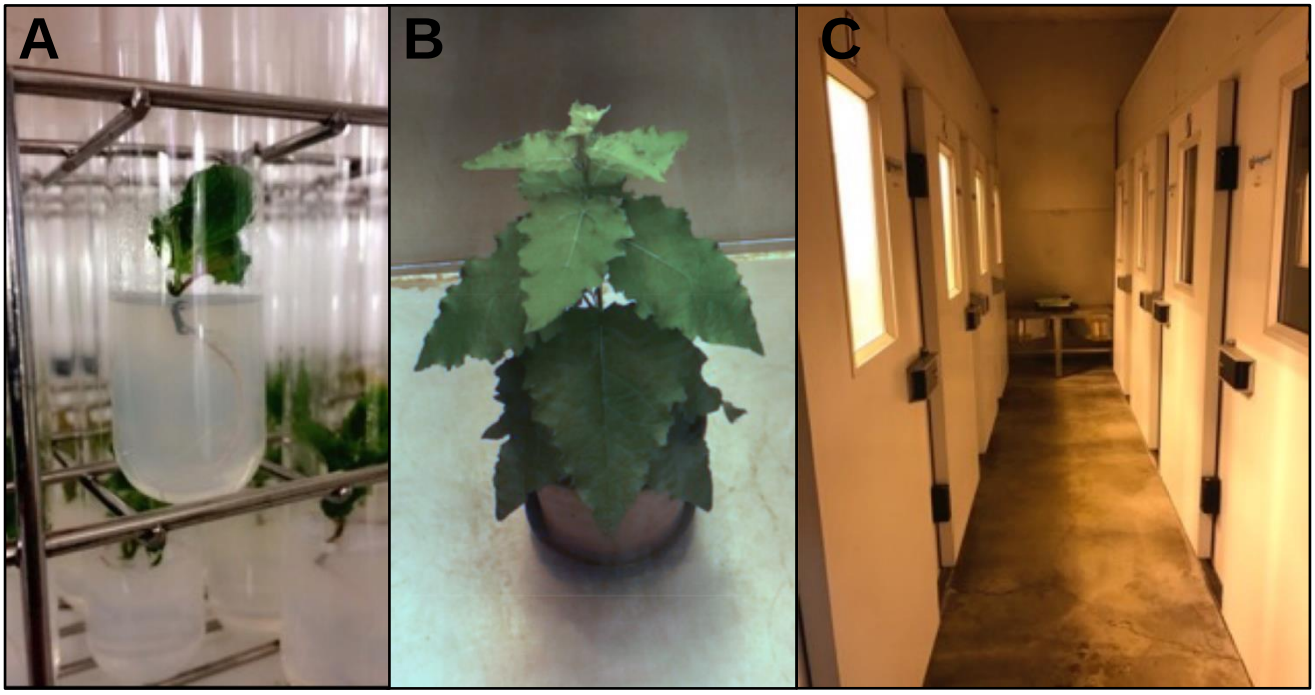

Figure 12. Peupliers (A,B) et dispositif expérimental (C) utilisés lors des expérimentations. Les peupliers (*Populus tremula x alba*) utilisés lors des expérimentations ont été obtenus par microbouturage (A), puis transplantés en pot de 10L pour atteindre 30 cm au début de l'expérimentation (B). Les peupliers ont été exposés à l'O_3 dans des chambres phytotroniques aux conditions environnementales entièrement contrôlées (C).

Chapitre 2

DYNAMIQUE DES REPONSES FOLIAIRES EN FONCTION DE LA DOSE D'O_3 PHYTOTOXIQUE CUMULEE

Chapitre 2 : Dynamique des réponses foliaires chez le peuplier en fonction de la dose d'O_3 phytotoxique

Préface

Les concentrations de fond ayant atteint des niveaux phytotoxiques au cours du siècle dernier, l'ozone troposphérique (O_3) est devenu un agent clé du changement climatique, contrecarrant le piégeage du carbone par les écosystèmes forestiers. L'une des principales lacunes dans les connaissances pour la mise en œuvre des récents niveaux critiques (CL) basés sur les flux d'O_3 concerne l'évaluation de la dose effective d'O_3 entraînant des effets néfastes sur les plantes. Dans cette étude, nous examinons la dynamique des réponses physiologiques liées à l'assimilation carbonée ainsi que la dynamique des lésions microscopiques et des lésions visibles induites par deux niveaux d'exposition à l'O_3 (80 et 100 ppb) dans le feuillage du peuplier hybride, en fonction de la dose d'O_3 phytotoxique (POD_0) et du stade de développement foliaire.

Au cours d'une précédente expérimentation, les jeunes peupliers ont été exposés à 5 concentrations d'O_3 : 60, 100, 120, et 150 ppb dans le but de trouver une concentration optimale pour induire les deux types de réponses foliaire ACS et HR-like. Avec des concentrations de 120 et 150 ppb, la défoliation était trop rapide pour l'étude de la cinétique des réponses foliaires. Au contraire, avec une concentration de 60 ppb, les réponses n'étaient pas suffisamment induites. Nous avons donc retenu la concentration de 100 ppb d'O_3, et ajouté celle de 80 ppb en intermédiaire entre 100 et 60 ppb O_3.

Les jeunes peupliers ont été soumis à l'O_3 en condition totalement contrôlées. Le suivi de la dynamique des échanges gazeux a permis d'estimer la quantité d'O_3 cumulée absorbée par les feuilles pendant l'expérimentation. Le développement de la senescence cellulaire accélérée (ACS) a été suivie via la dégradation des chlorophylles mesurée au moyen d'un Dualex (méthode non-destructive). Au niveau des lésions microscopiques, la réponse hypersensible-like (HR-like) a été suivie via la coloration au bleu trypan, ultérieurement quantifiée par analyse d'image assistée par

ordinateur. Les cellules colorées par le bleu trypan ont été précédemment caractérisée comme résultant d'une réaction HR-like.

Après une période de latence liée au développement ontologique du feuillage, il ressort de cette étude que les échanges gazeux et la teneur en chlorophylle diminuent de façon monotonique avec l'augmentation du POD_0. Des lésions HR-like sont apparues très tôt au cours de l'exposition quel que soit le traitement O_3 (80 ou 100 ppb) et ont montré une dynamique de type sigmoïde, variant selon l'âge de la feuille. Malgré les réactions susmentionnées et les lésions initiales visibles sur le feuillage, les peupliers traités n'ont pas montré de réduction de croissance ou de biomasse alors que le niveau critique défini par le $PODY_{\_SPE}$ était atteint. Ainsi, cette étude démontre que le développement des réponses cellulaires ACS et HR-like montre des dynamiques de réponse étroitement déterminée par le stade ontologique du feuillage et les conditions environnementales.

Ces résultats ont été publié dans la revue *Frontiers in Plant Science* :

Dynamics of foliar responses to O_3 stress as a function of phytotoxic O_3 dose in hybrid poplar

Benjamin Turc[1,2], Pierre Vollenweider[2], Didier Le Thiec[1], Anthony Gandin[1], Marcus Schaub[2], Mireille Cabané[1], Yves Jolivet[1], 2021, *Dynamics of foliar responses to O3 stress as a function of phytotoxic O_3 dose in hybrid poplar.*

(1) University of Lorraine, AgroParisTech, INRAE, SILVA, F-54000 Nancy, France

(2) Section Forest Dynamics, Swiss Federal Institute for Forest, Snow and Landscape Research WSL, Zucherstrasse 111, CH-8903 Birmensdorf, Switzerland

DOI: 10.3389/fpls.2021.679852

Keywords: ozone, POD_x, hybrid poplar, dynamics of foliar responses, hypersensitive response-like, accelerated cell senescence

Abstract

With background concentrations having reached phytotoxic levels during the last century, tropospheric ozone (O_3) has become a key climate change agent, counteracting carbon sequestration by forest ecosystems. One of the main knowledge gaps for implementing the recent O_3 flux-based critical levels (CL) concerns the assessment of effective O_3 dose leading to adverse effects in plants. In this study, we investigate the dynamics of physiological, structural and morphological responses induced by two levels of O_3 exposure (80 and 100 ppb) in foliage of hybrid poplar, as a function of phytotoxic O_3 dose (POD_0) and foliar developmental stage. After a latency period driven by foliar ontological development, the gas exchanges and chlorophyll content decreased with higher POD_0 monotonically. Hypersensitive response-like lesions appeared early during exposure and showed sigmoidal-like dynamics, varying according to leaf age. At current POD_{1_SPEC} CL, notwithstanding the aforementioned reactions and initial visible injury to foliage, the treated poplars had still not shown any growth or biomass reduction. Hence, this study demonstrates the development of a complex syndrome of early reactions below the flux-based CL, with response dynamics closely determined by the foliar ontological stage and environmental conditions. General agreement with patterns observed in the field appear indicative of early O_3 impacts on processes relevant for *e.g.* biodiversity ecosystem services prior to those of economic significance – *i.e.* wood production, as targeted by flux-based CL.

Introduction

The ground-level concentrations of ozone (O_3) have increased during the past century (Maas and Grennfelt, 2016), and are predicted to remain stable or increase during the 21st century (Revell et al., 2015; Fu and Tian, 2019). They have already reached levels negatively affecting crop plants and the natural vegetation (Wittig et al., 2009; Jolivet et al., 2016; Proietti et al., 2016; Li et al., 2017), and steady or increasing impacts are expected over the course of next decades (Karlsson et al., 2017).

Once entering the leaf through stomata, O_3 degradation causes the formation of Reactive Oxygen Species (ROS), the accumulation of which triggers rapid oxidative bursts (Schraudner et al., 1998; Pasqualini et al., 2003; Moura et al., 2018). ROS can also act as elicitors of programed cell death (PCD) reminiscent of plant responses

during defensive plant/pathogen interactions which are subsequently designated as Hypersensitive Response-like (HR-like) (Vollenweider et al., 2002; Bhattacharjee, 2005; Günthardt-Goerg and Vollenweider, 2007; Moura et al., 2018). In parallel, an Acceleration of Cell Senescence (ACS), with distinct apparent mechanisms, can be observed (Pell et al., 1999; Günthardt-Goerg and Vollenweider, 2007; Vollenweider et al., 2019). The characteristic symptoms thus include marked degenerative injuries in chloroplasts, in apparent relation to an increase in the constitutive ROS load resulting from the daily photosynthetic activity. As a consequence, these latter organelles are particularly sensitive to O_3 stress (Joo et al., 2005; Kangasjarvi et al., 2005). However, the sequence of plant reactions in response to O_3 stress remains unclear, especially given the driving – but still partially understood – effects of interacting environmental conditions and ontological development. In field *versus* climate chamber conditions for example, the high *versus* low intensity illumination can lead to contrasted symptom expression, with clear synergies between photooxidative and O_3 stress in the former case only (Günthardt-Goerg and Vollenweider, 2007; Paoletti et al., 2009; Moura et al., 2018; Vollenweider et al., 2019). Hence, the dynamics of responses to O_3 stress as a function of environmental conditions needs further research.

Although the effects of O_3 stress have been observed in both mature and developing foliage, their intensity is strongly related to the leaf ontology, the mature leaves being more sensitive than those still in expansion. However, the younger *versus* older leaves can show higher rates of stomatal conductance and O_3 uptake (Reich, 1983; Strohm et al., 1999; Bagard et al., 2008; Zhang et al., 2010; Guerrero et al., 2013), suggesting an enhanced detoxification capacity (Bellini and De Tullio, 2019). Still, the mechanisms underlying the apparently higher O_3 tolerance in developing foliage remain largely obscure (Strohm et al., 2002) and the differences in response dynamics as a function of leaf ontogenetic development require further investigations.

To assess and prevent O_3 injury on vegetation and forest trees, a concentration-based index, namely the Accumulated O_3 exposure Threshold over 40 ppb (AOT40), was initially proposed (Fuhrer et al., 1997). Given the dependency of O_3 phytotoxicity on stomatal conductance, the biologically (Karlsson et al., 2007; Mills et al., 2011) and environmentally (Musselman et al., 2006; Dizengremel et al., 2013; Büker et al., 2015) more relevant flux-based approach has been increasingly implemented. Nowadays, the O_3 Critical Level (CL) are defined for given vegetation types or plant species and

calculated as the Phytotoxic O_3 Dose over an Y threshold for a specific species or group of species (POD_{Y_SPEC};(Mills G. et al., 2017). Based on empirical evidence from risk assessment studies - linking POD_{Y_SPEC} values to tree biomass loss or foliar injury - the current CL typically target 4% maximum *i.e.* growth reductions by oxidative stress. However, such markers represent some late O_3 stress effects, at least partly resulting from earlier processes in foliage (*i.e.* reduced physiological activity/extensive cellular injury) which dynamics primarily depends on detoxification processes (Dghim et al., 2013; Dumont et al., 2014; Dusart et al., 2019a). With a view to the larger implementation and acceptance of flux-based approach, there is then an important knowledge gap regarding the dynamics and effective POD_x of first effective O_3 stress effects, prior to the appearance of current risk assessment markers.

In this study, our main objective was to characterize the dynamics of early physiological and structural responses to O_3 stress in poplar trees as a function of flux-based O_3 dose and prior to *e.g.* growth reduction and extensive foliar injury, the primary markers of O_3 stress for defining O_3 CL (Sanz and Catalayud, 2011; Mills G. et al., 2017). The tested hypotheses (H) included: H1) the development of injury and growth response to O_3 stress, as well as physiological and structural changes, proceeds in a sequential order, with each response showing specific dynamics; H2a) O_3 elicits different injury responses within the foliage of trees H2b) with ACS occurring before the development of HR-like lesions (Vollenweider et al., 2019); H3a) at comparable O_3 dose and irrespective of the applied O_3 concentration, leaves show similar responses and, (H3b) response dynamics; H4) the dynamics of responses depends on the leaf developmental stage (Moura et al., 2018). Therefore, rooted cuttings of hybrid poplar (*Populus tremula x alba*) were exposed to three O_3 concentrations in fully-controlled conditions for a month. The leaf physiology, development of ACS and HR-like lesions and appearance of visible injuries were monitored over the course of 29 days. The interaction between foliar response dynamics and leaf ontological development was evaluated by assessing the responses to treatments at two distinct leaf positions.

Materials and methods

Plant material and controlled O_3 exposure

Young trees from a hybrid *Populus tremula x alba* clone (INRAE 717-1b4) were cultivated similarly to Cabane et al. (2004). Prior to the experimental exposure, micropropagated cuttings were grown for two weeks in 0.5 L pots containing compost (Gramoflor Universel) and perlite [1:1, (v/v)], and placed in containers covered with transparent acrylic hoods inside a growth chamber. The environmental conditions were set at 22°C/18°C day/night temperature, 350 µmol m^{-2} s^{-1} photosynthetic active radiation (PAR, 1 m below lamps) during a 14-h photoperiod (Philips Son-T Agro 400 W lamps), 75%/85% relative humidity (day/night). The young trees were then transplanted into 10 L pots filled with compost (Gramoflor Universel) and fertilized with 3 g l^{-1} of slow-release Nutricot T 100 granules (13:13:13:2 N:P:K:MgO, Fertil, Boulogne-Billancourt, France). They were further cultivated for one month in the same growth chamber and watered to field capacity every day. The trees retained (n = 48), with a view to the forthcoming O_3 exposure experiments, were 29.5 ± 0.2 cm high, with 13.1 ± 0.1 leaves. During experiments. all foliar assessments were repeated at the 3rd and 10th leaf position from the tree base, thus selecting the youngest fully expanded leaf and that still in expansion at tree top by the start of exposure.

Prior to exposure, the selected trees were randomly distributed among six ventilated phytotron chambers (1 air change min^{-1}; 120 x 117 cm and 204 cm high) within the O_3-exposure facility of PEPLor platform (Faculty of Sciences and Technologies, University of Lorraine). Within each chamber (N = 8 trees), the plant position was randomized by each assessment. The transferred poplars were then left to acclimate for one week, with environmental conditions similar to those in the growth chamber. The O_3 exposure experiment included three treatments [charcoal-filtered (CF) air; CF + 80 ppb O_3; CF + 100 ppb O_3] replicated in two chambers each and performed for 30 days (N = 16 trees per treatment). O_3 was generated from pure oxygen using an O_3 generator (Innovatec II, Rheinbach, Germany), and provided to the chambers during the daytime period in the form of a 13h square wave, starting 1h after the light was switched on. The O_3 concentrations within each phytotron chamber were monitored twice an hour using a computer-assisted automatic O_3 analyzer (O341M, Environment SA, Paris).

Dynamics of leaf physiology responses and estimation of phytotoxic O_3 dose

The effect of treatments on the dynamics of leaf gas exchanges were assessed by measuring the net CO_2 assimilation rates (A_{net})) and stomatal conductance to water vapor (g_w) every two days, 3 h after starting the O_3 exposure. Selecting six trees per treatment, the measurements were performed using a Li-6400XT portable photosynthesis system (LiCor, Inc., Lincoln, NE, USA), with cuvette temperature set at 22 °C, light intensity (PAR) at 300 and 320 µmol m^{-2} s^{-1} for measurements at the 3rd and 10th leaf position respectively, air flow at 300 µmol s^{-1}, CO_2 concentration at 400 ppm, and leaf vapor pressure deficit (VPD_{leaf}) < 1 kPa. The values were recorded once g_w and A_{net} remained stable for 30 s.

The g_w estimates (mol H_2O m^{-2} s^{-1}) were used to calculate the instantaneous O_3 uptake into the leaf under environmental stable conditions (F_{O_3}), according to Bagard et al. (2015):

$$F_{O_3} = [O_3]_{atm} * g_{O_3}$$

with F_{O_3} as the O_3 flux (nmol O_3 m^{-2} s^{-1}), $[O_3]_{atm}$ as the O_3 concentration (ppb) in the phytotron chamber, and g_{O_3} (O_3 m^{-2} s^{-1}) as the stomatal conductance to O_3, according to (Lamaud et al., 2009):

$$g_{O_3} = \frac{D_{O_3}}{D_{H_2O}} * g_w$$

with D_{O_3} and D_{H_2O} as the O_3 and water molecular diffusivity (cm^{-2} s^{-1}) respectively (Massman, 1998). The hourly O_3 uptake (mmol O_3 m^{-2} h^{-1}) was calculated by integrating F_{O_3} over an hour and the POD_0 (mmol O_3 m^{-2}), by cumulating the hourly O_3 uptake since the beginning of experiment. Missing g_w measurements were estimated based on values from flanking days (Bagard et al., 2008).

The effect of treatments on the dynamics of leaf chlorophyll content were assessed by measuring estimates of surface-based concentrations of chlorophylls (total chlorophyll index) every days, 1 h after switching the light on and before the start of O_3 treatment. Selecting six trees per treatment, the estimates were obtained

averaging ten measurements per leaf performed with a leaf clamp sensor device (Dualex Force-A, Orsay, France).

Dynamics of microscopic and visible leaf injury

The development of HR-like lesions within the mesophyll and that of O_3 symptoms throughout foliage was monitored by means of completing microscopic assessments and visible injury observations. For microscopic assessments, two discs (diameter = 6 mm) per leaf position in two trees per chamber were sampled every two days, until HR-like lesions were detected in the 100 ppb O_3 treatment at both leaf positions; the sampling interval was then extended (three to six-days). The harvested discs were processed immediately after sampling.

Necrotic cells within mesophyll as a consequence of HR-like lesions were evidenced using the Trypan blue assay (Pasqualini et al., 2003; Joo et al., 2005; Faoro and Iriti, 2009). Briefly, the leaf discs were stained for 3 min in a hot lactophenol Trypan blue mixture (60 mL staining solution: 10 g phenol,10 mg Trypan blue, 30 mL ethanol, 10 mL glycerol, 10 mL lactic acid and 10 mL distilled water) and the necrotic cells contrasted for 20 min against a clear background using 2.5 g mL^{-1} hot chloral hydrate, prior to mounting in 60% glycerol (Pasqualini et al., 2003). The preparations were then transferred to WSL where all microscopy assessments were performed. The disk's central part, free of staining artefacts, was observed using the 5x objective of a Leica microscope (Leitz DM/RB). Given the disk thickness (> 200 µm) and with a view to creating high contrast pictures, the preparations were imaged after inserting the 10x condenser and removing most filters and diaphragms, using the INFINITY 2-1R camera and Lumenera Infinity Analyze (release 6.4) software (Lumenera Corp., Ottawa, Canada). The center of each disk preparation was photographed, creating composite images made of nine tiles each. The percentage area, particle size and shape properties of HR-like lesions inside of stitched images were quantified by means of computer-assisted color image analysis (software WinCELL™ 2004, Regent Instruments Inc., Canada). Briefly, the software attributed the whole lesion or part of it to one of two color classes (non-oxidized: violet hue; oxidized: dark blue hue) made of ten shades each, defined on the basis of a representative batch of images and contrasting with the background color class (grayish hue, on the basis of ten white to

gray shades). The quantified parameters characterized the size and shape properties of total and individual lesion particles.

The HR-like lesions and oxidation diagnosis were verified on the basis of hand, and semi-thin sections from samples collected in all treatments at the two leaf positions during the whole study, and subsequently processed and observed as described previously (Moura et al., 2018). Briefly, supplementary leaf discs were infiltrated upon sampling with EM-grade 2.5% glutaraldehyde buffered at pH 7.0 with 0.067 M Soerensen phosphate buffer, renewed after vacuum infiltration. Sections (60 µm) obtained using a custom-made hand microtome and kept unstained were used for visualizing chlorophylls and the oxidation of HR-like lesions. Technovit-embedded 1.5 µm sections, obtained using a Supercut Reichert 2050 microtome and stained with Toluidine blue (Vollenweider et al., 2016), were used to identify HR-like markers within necrotic mesophyll cells, after observation with phase contrast illumination in bright field microscopy using the 5-100 x objectives of the Leica microscope and imaged using the Infinity camera, as mentioned above.

The development of O_3 injury in response to treatments was surveyed in the morning, before the start of O_3 exposure, on a daily basis. Upon appearance, the development of visible injury was monitored with pictures of symptomatic leaves. The percentage area of necrosis per leaf within the latter material was quantified by means of color image analysis, using the Color Segmentation plugin in Fiji freeware (ver. 2.0.0; (Schindelin et al., 2012)).

Morphological assessments

After 30 days of exposure, all trees were harvested and biometric assessments conducted. Tree height was recorded and stem diameter 1.5 cm above root collar was measured, using a hand caliper. The number of leaves per tree, shed or still attached, was recorded prior to harvest. Leaf and stem material was oven dried to constant weight, prior to determining the dry mass of each fraction.

Statistical analysis

The dynamics of physiological and structural responses to treatments in foliage, and the differences in whole-tree morphology and biomass between groups by the end of experiment were analyzed by means of linear mixed-effects models (lmem). The

fixed-effect factors included the O_3 treatment, leaf position, time or POD_0 and interactions, whereas the tree nested in chamber (leaf data; with the leaf position as the statistical unit) or the chamber (morphology/biomass data; with the tree as the statistical unit) were introduced in models as random terms. Homoscedasticity and normality of residuals were verified graphically, and the dependent variables were log- or square-transformed to meet the model assumptions, as needed. The differences between treatments at given assessment dates were tested by means of post-hoc tests (TukeyHSD). All statistical analyses were performed using R statistical software, version 3.5.0 (R Development Core Team, 2017), with the packages lme4 (Bates et al., 2015) for linear mixed-effects models, and emmeans (Lenth, 2016) for post-hoc testing.

Results

Morphological responses

After 30 days of exposure, no change in tree height, stem diameter or foliar dry mass in response to O_3 exposure were observed (Table 1). However, the stem biomass (P = 0.014), amount of leaves (P = 0.003) and leaf shedding (P = 1.2 x10^{-6}) were increased, with significant differences between the 80 and 100 ppb O_3 treatments in the case of leaf shedding.

Table 1. Morphological responses to O_3 treatments in hybrid poplar (*Populus tremula x alba*) at the end of the experiment (model: lmer(variable ~ O_3 treatment + (1 | chamber)); *** p ≤ 0.001; ** p ≤ 0.01; * p ≤ 0.05; ns not significantly different). Values represent means ± SE, n = 16. Different letters indicate significant differences between treatments by the end of experiment (post-hoc TukeyHSD, p ≤ 0.05).

Treatment	Tree height (cm)	Stem diameter (mm)	Foliage biomass (g)	Stem dry mass (g)	Leaf shedding (%)	Leaf number
Charcoal-filtered	100.31 ±0.95	9.93 ±0.18	30.09 ±0.86	15.72 ±0.53 a	1.59 ±0.81 a	33.31±0.54
80 ppb ozone	104.38 ±1.66	10.16 ±0.33	31.54 ±1.50	17.51 ±0.91 b	7.41 ±1.99 b	35.00±0.61
100 ppb ozone	101.75 ±0.81	10.23 ±0.12	28.83 ±0.61	16.50 ±0.39 ab	16.94 ±2.21 c	35.44±0.39
Treatment	ns	ns	ns	*	***	**

At both leaf positions, the 100 and 80 ppb O_3 treatments significantly reduced g_w (Fig. 1A; O_3 treatment: P < 0.001) and accelerated its leaf ontology-driven decrease (O_3 treatment*Time: P < 0.001). This reduction was delayed at the 10th *versus* 3rd leaf position (O_3 treatment*Leaf position, O_3 treatment*Time*Leaf position: P < 0.001), with

a 50% decrease in g_w reached in 15 *versus* 6 days respectively in the 100 ppb O_3 treatment. As indicated by increasing g_w in maturing leaves (10th leaf position) during the first ten days of exposure irrespective of O_3 exposure (Leaf position: $P < 0.001$), the O_3 treatment affected g_w only once the ontological development had been achieved (latency phase, fig 1A). By the end of experiment and only at the 10th leaf position, the differences in g_w between the 100 and 80 ppb treatments were significant.

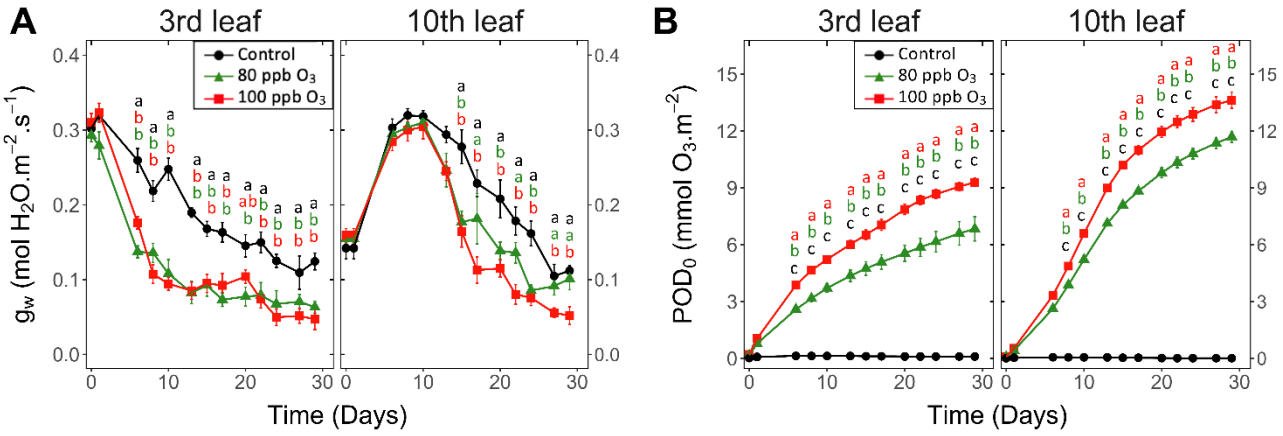

	g_w		POD$_0$
O_3 treatment	***	O_3 treatment	***
Leaf Position	***	Leaf Position	***
Time	***	Time	***
O_3 treatment:Time	***	O_3 treatment:Time	***
O_3 treatment:Leaf Position	***	O_3 treatment:Leaf Position	***
Leaf Position:Time	***	Leaf Position:Time	***
O_3 treatment:Time:Leaf Position	***	O_3 treatment:Time:Leaf Position	***

Figure 1. Dynamics of changes in the (**A**) stomatal conductance to water (g_w) and (**B**) phytotoxic O_3 dose (POD$_0$) of hybrid poplar leaves (*Populus tremula x alba*), as a function of O_3 treatment (charcoal-filtered air ●, 80 ppb O_3 ▲, 100 ppb O_3 ■), leaf position, time of assessment and interactions (model: lmer(sqrt(variable) ~ O_3 treatment * leaf position * time + (1 | tree / chamber)); *** p ≤ 0.001). Values represent means ± SE, n = 6. Different letters indicate significant differences between treatments for a given assessment date (post-hoc TukeyHSD, p ≤ 0.05).

By the end of experiment, trees in the 100 *versus* 80 ppb O_3 treatment showed a larger POD$_0$, as a consequence of their higher O_3 concentrations and mostly similar g_w (Fig. 1B; O_3 treatment, O_3 treatment*Time: $P < 0.001$). After 30 days of exposure, the POD$_0$ at the 3rd and 10th leaf position was thus 1.4 and 1.2 times higher in the 100 *versus* 80 ppb O_3 treatments. The POD$_0$ was also higher in leaves at the 10th *versus* 3rd leaf position (Leaf position: $P < 0.001$), as a consequence of the delayed leaf ontogeny and higher g_w (O_3 treatment*Leaf position: $P < 0.001$). After ten days of exposure, the POD$_0$ levels in younger foliage thus exceeded those in older material by

approximately 25% and outpaced them by 40% by the end of exposure (O_3 treatment*Time*Leaf position: $P < 0.001$).

Dynamics of leaf physiology responses

Irrespective of the leaf position, A_{net} showed responses to treatments and response dynamics similar to g_w (Fig. 2A *versus* 1A). After 30 days of exposure, A_{net} in the 100 ppb O_3 *versus* CF treatment was decreased by 70% and 35% at the 3rd and 10th leaf position respectively. Once the leaf ontogenetic differentiation achieved, A_{net} decreased with POD_0 in a basically constant and monotonic manner (Fig. 2B; POD: $P < 0.001$), regardless of the treatment or leaf position. The significant effects of O_3 treatment and O_3 treatment*POD factors ($P < 0.001$) could then be related to the less affected A_{net} values in the 80 *versus* 100 ppb treatment at highest POD_0 reached by the end of exposure. The observed reduction in A_{net} as a function of POD_0 was stronger at the 3rd *versus* 10th leaf position (Fig. 2B; Leaf position $P < 0.001$) but the dynamics at both leaf positions was similar (Leaf position*POD: ns). Hence, at POD_0 of 5 mmol O_3 m^{-2}, A_{net} at the 10th leaf position did not show any reduction relative to CF treatment yet, *versus* 50% A_{net} loss in older leaves, irrespective of the O_3 treatment. The response differences between the two leaf positions were further observed at higher POD_0. With POD_0 above 9 mmol O_3 m^{-2}, as recorded in younger leaves only, and also as a consequence of the aforementioned latency effect (Fig. 1B), A_{net} never dropped to levels observed at the 3rd leaf position for lower POD_0. Consequently, the photosynthetic activity in younger *versus* older foliage appeared less sensitive to the absorbed O_3 dose.

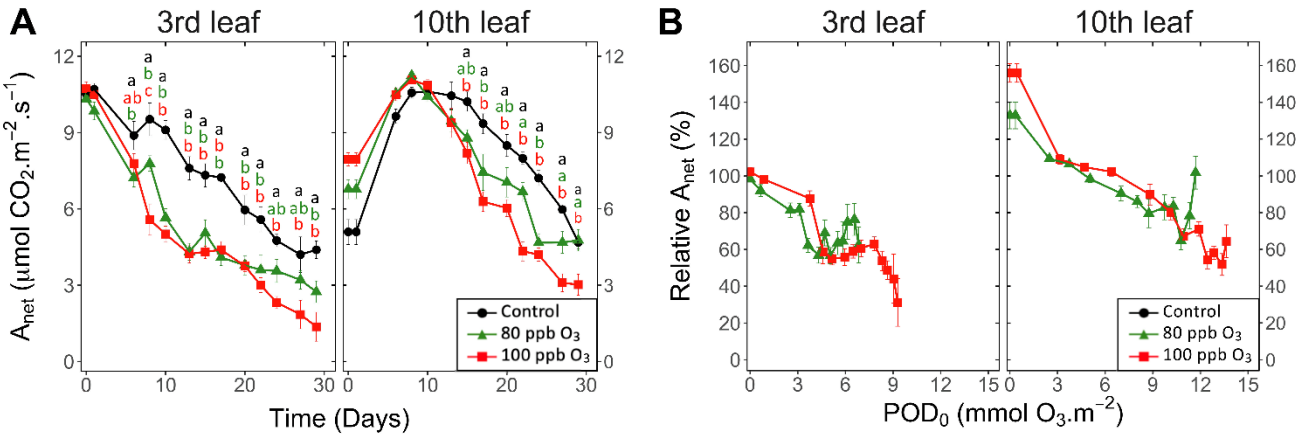

	A_{net}
O_3 treatment	***
Leaf Position	***
Time	***
O_3 treatment:Time	***
O_3 treatment:Leaf Position	***
Leaf Position:Time	***
O_3 treatment:Time:Leaf Position	***

	A_{net}
O_3 treatment	***
Leaf Position	***
POD_0	***
O_3 treatment:POD_0	***
O_3 treatment:Leaf Position	ns
Leaf Position:POD_0	ns
O_3 treatment:POD_0:Leaf Position	ns

Figure 2. Dynamics of changes in the net CO_2 assimilation (A_{net}) of hybrid poplar leaves (*Populus tremula x alba*), as a function of assessment time (**A**), phytotoxic O_3 dose (POD_0; **B**), O_3 treatment (charcoal-filtered air ●, 80 ppb O_3 ▲, 100 ppb O_3 ■), leaf position and interactions (model: lmer(variable) ~ O_3 treatment * leaf position * time + (1 | tree / chamber)); *** $p \leq 0.001$; ns not significantly different). Values represent means ± SE, n = 6. Different letters indicate significant differences between treatments at a given assessment date (post-hoc TukeyHSD, $p \leq 0.05$).

An O_3 impact on the chlorophyll content index of leaves was detected after 24 days of the experiment. The impact was restricted to the 3rd leaf position (Fig. 3A; O_3 treatment: ns; O_3 treatment*Time, O_3 treatment*Leaf position: $P < 0.001$), showing a decrease of 30% for the total chlorophyll index in the 100 ppb O_3 *versus* CF treatment. These findings primarily related to latency effects due to leaf ontological maturation, which were observed at the 3rd as well as the 10th leaf position in the case of this parameter, lasting 7 and 17 days, respectively. Accordingly, a larger latency peak was observed in younger than older foliage. The total chlorophyll index decreased with higher POD_0 (Fig. 3B; POD: $P < 0.05$), irrespective of the O_3 treatment (O_3 treatment: ns, O_3 treatment*POD: ns). At low POD_0, the decline was rather monotonic, but accelerated with values exceeding 8 mmol m^{-2} at the 3rd leaf position, thus contrasting with the nearly linear drop observed in younger leaves. Confirming a higher O_3 tolerance, leaves at the 10th leaf position showed smaller (Leaf position: $P < 0.05$) and slower (Leaf position*POD_0 $P < 0.001$) drops with higher POD_0.

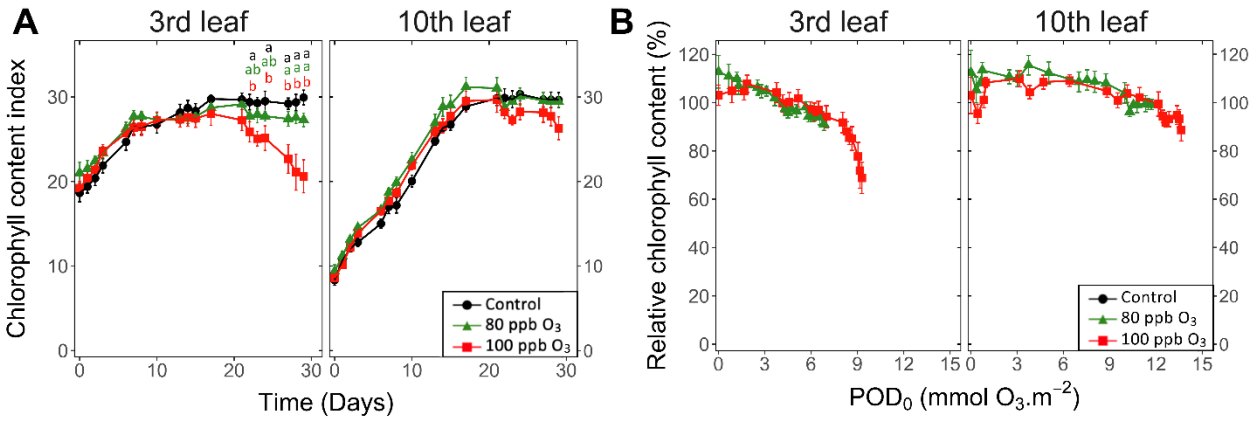

	Chlorophyll Content Index		Chlorophyll Content Index
O_3 treatment	ns	O_3 treatment	ns
Leaf Position	***	Leaf Position	*
Time	***	POD_0	***
O_3 treatment:Time	***	O_3 treatment:POD_0	ns
O_3 treatment:Leaf Position	***	O_3 treatment:Leaf Position	*
Leaf Position:Time	***	Leaf Position:POD_0	***
O_3 treatment:Time:Leaf Position	***	O_3 treatment:POD_0:Leaf Position	ns

Figure 3. Dynamics of changes in the surface-based concentration of chlorophylls (total chlorophyll content index of Dualex) within hybrid poplar leaves (*Populus tremula x alba*), as a function of assessment time (**A**), phytotoxic O_3 dose (POD_0; **B**), O_3 treatment (charcoal-filtered air ●, 80 ppb O_3 ▲, 100 ppb O_3 ■), leaf position and interactions (model: lmer(variable) ~ O_3 treatment * leaf position * time + (1 | tree / chamber)); *** $p \leq 0.001$, * $p \leq 0.05$, ns not significantly different). Values represent means ± SE, n = 6. Different letters indicate significant differences between treatments at a given assessment date (post-hoc TukeyHSD, $p \leq 0.05$).

Dynamics of HR-like lesion spread and development

The microscopic necrosis observed in mesophyll using the Trypan blue assay were diagnosed as being caused by HR-like processes (Fig. 4A-D), based on several typical O_3-stress markers (Paoletti et al., 2009; Vollenweider et al., 2019). They included 1) the characteristic intercostal distribution of lesions (Fig. 4E), 2) the development of injury first in older leaves (Fig. 5A) or 3) the multiple HR-like events restricted to cells or small groups of cells within mesophyll (Fig. 4E-G, I-L).

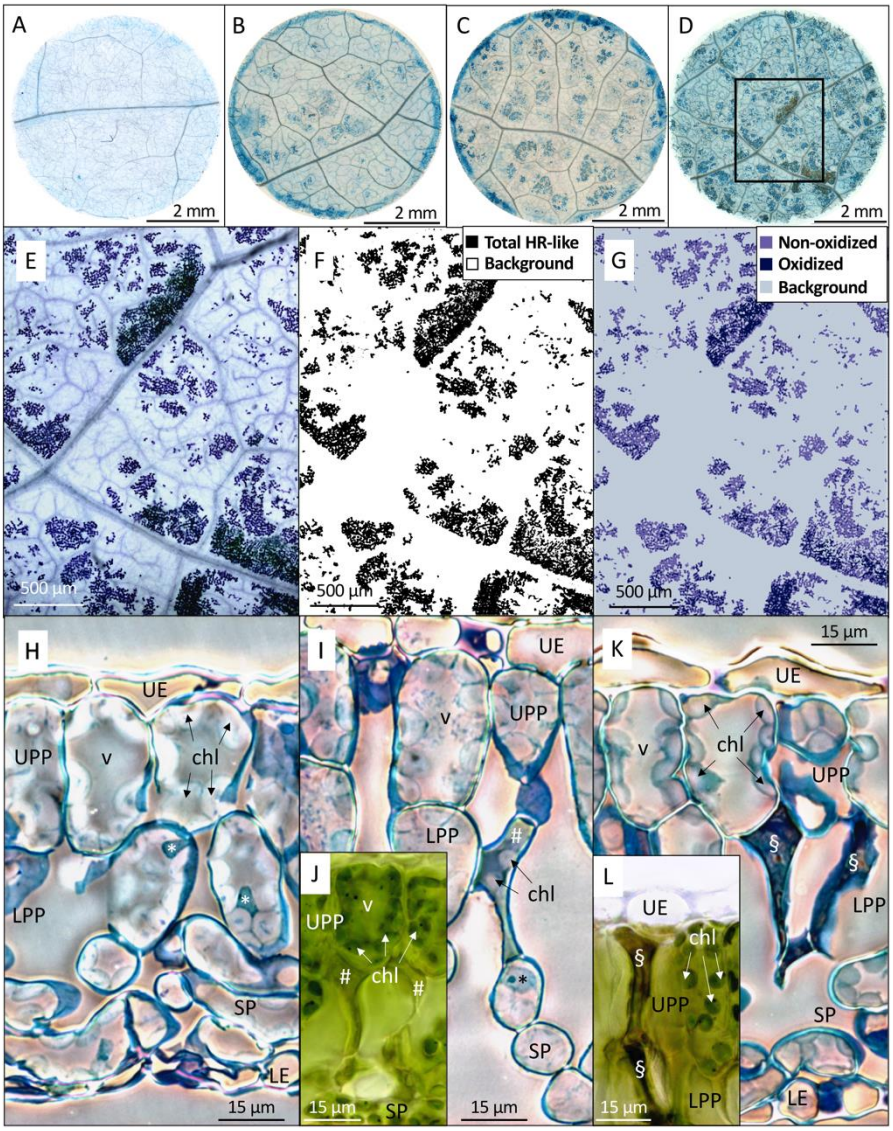

Figure. 4. Distribution, morphology and structural properties of HR-like lesions within hybrid poplar leaves (*Populus tremula x alba*). **A**-**D** Foliar discs excised at low leaf position (3rd) from leaves exposed to 100 ppb O_3 during 2 (**A**), 8 (**B**), 13 (**C**) and 27 (**D**) days. **A**: central area within each disk was photographed each time (frame in **D**). **E**-**G**: Image analysis of HR-like lesion after 27 days of treatment, as framed in **D**. **E**: Synthetic digital image, made of 9 stitched micrographs (5x magnification). The lesions are separated by veinlets and non-symptomatic tissues. **F**: binary image of total HR-like lesion *versus* background (white). **G**: classification of HR-like injuries into oxidized and non-oxidized lesion groups, based on color classes. **H**-**L**: changes in the mesophyll tissue and cell structure underlying the HR-like lesions. **H**: asymptomatic leaf tissues in a leaf sample from the filtered air treatment. **I**-**L**: necrotic cells within the upper (UPP) and lower (LPP) palisade parenchyma underlying the HR-like-lesions. **I**-**J**: within mesophyll cells having recently undergone HR-like necrosis (#), the chloroplasts (chl) were still visible and had retained their green color (**J**). **K**-**L**: at a later stage, the HR-like lesions (§) showed cell-content disruption and oxidation (**L**). Other structures: UE: upper epidermis, SP: spongy parenchyma, LE: lower epidermis, v: vacuole, *: nucleus. Technical specifications: staining with Trypan blue (**A**-**E**) and Toluidine blue (**H**, **I**, **K**); observations in bright field microscopy (**A**-**E**, **H**-**L**) using phase-contrast (**H**, **I**, **K**); **J**, **L** fresh, unfixed and unstained leaf sample preparations.

Collapsed dead cells were mainly observed in the lower palisade parenchyma (Fig. 4I-L *versus* 4H). Non-oxidized lesions (Fig. 4G) showed up first (Fig. 5A, 5C, 6C), with, for instance, still green chloroplasts visible within collapsed dead cells (Fig. 4I-J). The dark hues of oxidized lesions (Fig. 4L) were enhanced by staining with Trypan blue (Fig. 4E, G). Oxidized cells showed sharp wall angles indicative of breaks and disrupted cell content (Fig. 4K, L). All these typical HR-like traits showed little variation, regardless of the O_3 treatment or leaf position.

The first HR-like lesions at the 3rd and 10th leaf position were observed after 6 and 13 days of exposure, respectively. This was much earlier than reductions in the chlorophyll content index (Fig. 5A). Despite large response variability among trees, the effect of O_3 treatment was significant (Fig. 5A; O_3 treatment: $P < 0.05$; O_3 treatment*Time: $P < 0.001$). A larger leaf percentage area showing HR-like lesions was observed for the 100 *versus* 80 ppb O_3 treatment, with differences between the two treatments at the 3rd leaf position becoming significant after 20 days of exposure (O_3*Time; $P < 0.001$). After 27 days of treatment, the percentage area of lesions in the 100 *versus* 80 ppb O_3 treatment was two and five times higher at the 3rd and 10th leaf position, respectively. However, each leaf position showed specific response dynamics (O_3 treatment*Leaf position: $P < 0.01$, O_3 treatment*Time*Leaf position: $P < 0.05$), rather sigmoidal-like *versus* linear - once lesions appeared - in older *versus* younger foliage (Fig. 5A). Moreover, the HR-like lesions in response to the two O_3 concentrations showed up simultaneously at the 3rd leaf position whereas a seven-day delay was observed at the 10th leaf position (Fig. 5A).

When expressed as a function of POD_0, the differences between the two O_3 treatments in the leaf percentage area showing HR-like lesions were leveled out, especially at the 3rd leaf position (Fig. 5B; O_3 treatment: ns). However, the dependency on POD_0 was lessened at the 10th *versus* 3rd leaf position (Leaf position*POD: $P < 0.001$), and distinctly higher lesion percentage areas in response to similar POD_0 were observed in the 100 *versus* 80 ppb O_3 treatment in younger leaves (O_3 treatment*POD*Leaf position: $P < 0.05$).

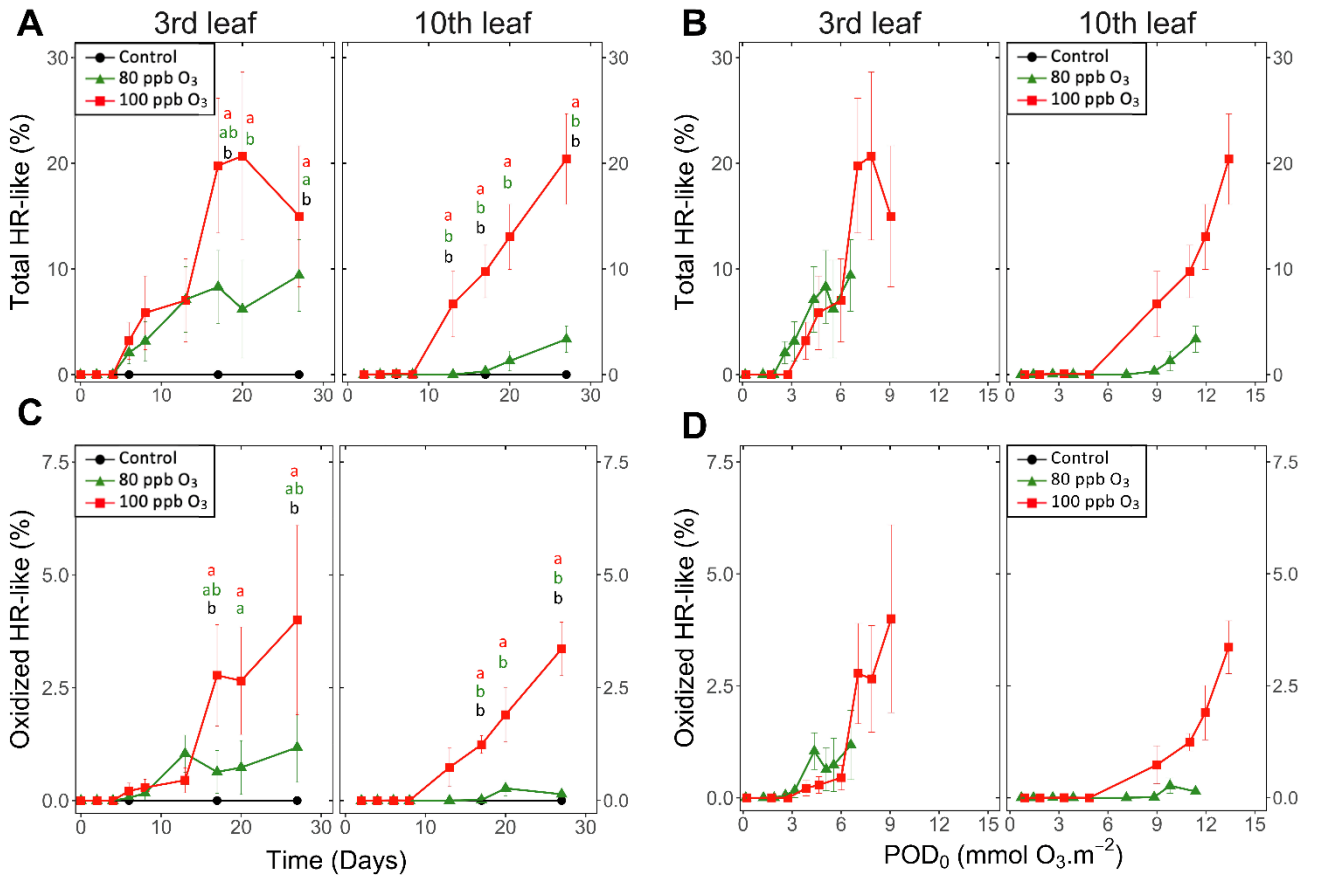

	Total HR-like	Oxidized HR-like
O_3 treatment	*	ns
Leaf Position	ns	ns
Time	***	***
O_3 treatment:Time	***	***
O_3 treatment:Leaf Position	**	ns
Leaf Position:Time	*	ns
O_3 treatment:Time:Leaf Position	*	ns

	Total HR-like	Oxidized HR-like
O_3 treatment	ns	ns
Leaf Position	ns	ns
POD_0	***	***
O_3 treatment:POD_0	**	***
O_3 treatment:Leaf Position	ns	ns
Leaf Position:POD_0	***	***
O_3 treatment:POD_0:Leaf Position	*	ns

Figure. 5. Development dynamics of HR-like lesions (**A**, **B**) and lesion oxidation (**C**, **D**) in hybrid poplar leaves (*Populus tremula x alba*), as a function of the assessment time (**A**, **C**), phytotoxic O_3 dose (POD_0; **B**, **D**), O_3 treatment (charcoal-filtered air ●, 80 ppb O_3 ▲, 100 ppb O_3 ■), leaf position and interactions (model: lmer(sqrt(variable) ~ O_3 treatment * leaf position * time + (1 | tree / chamber)); *** $p \leq 0.001$, ** $p \leq 0.01$, * $p \leq 0.05$, ns not significantly different). Values represent means ± SE of percentage area of leaf discs showing microscopic injury, n = 4. Different letters indicate significant differences between treatments at a given assessment date (post-hoc TukeyHSD, $p \leq 0.05$).

Hence, not only the O_3 dose but also the O_3 absorption rate then determined the lesion severity. The oxidized HR-like lesions, expressed as a function of time or POD_0, showed responses and response dynamics basically similar to HR-like lesions taken globally (Fig. 5C, D *versus* A, B). The main differences included a smaller percentage of injured area and weaker symptom dynamics. At the 10th leaf position, oxidized HR-like lesions in the 80 ppb O_3 treatment were observed only occasionally.

Analyzing single HR-like injuries, the shape (data not shown) and size of lesions remained stable over time or with increasing POD_0. Furthermore, they did not respond to the O_3 treatment, leaf position or interaction factors (Fig. 6A-B; all factors: ns). The only change observed was an increasing oxidation with longer exposures and at higher POD_0 (Fig. 6C-D; Time, POD: $P < 0.05$). Hence, the observed increases in the percentage area of HR-like lesions with time, or higher POD_0 and in response to the O_3 treatment (Fig. 5A-B) resulted as a consequence of the multiplication of single HR-like reactions and higher lesion density, rather than from increased growth of already developed injuries. However, both the higher lesion density and the growing oxidation of individual HR-like lesions could contribute to the observed increase in the leaf percentage area showing oxidation (Fig. 5C-D).

Emergence of visible symptoms

The first visible symptoms in leaves exposed to the O_3 treatments appeared by the end of experiment, that is, 23 days after the start of exposure. The first HR-like lesions had been detected more than two weeks earlier, whereas the observed drops in foliar chlorophyll content index were rather synchronous (fig 7A *versus* 5A, 3A). These visible symptoms consisted of intercostal necrotic dark spots spread in the leaf blade, as previously observed in poplar (Fig 7A; (Cabane et al., 2004; Giacomo et al., 2010; Dghim et al., 2013). By the end of exposure, only low levels of injury could develop (O_3 treatment: ns; O_3 treatment*Time $P < 0.001$), with significantly higher percentages in the 100 *versus* 80 ppb O_3 treatment at the 3rd leaf position only. In younger leaves, visible injury appeared 4 days later than at the 3rd leaf position and differences between treatments throughout the experiment remained non-significant (Leaf position, O_3 treatment*Time*Leaf position: $P < 0.05$; O_3 treatment*Leaf position: $P < 0.01$).

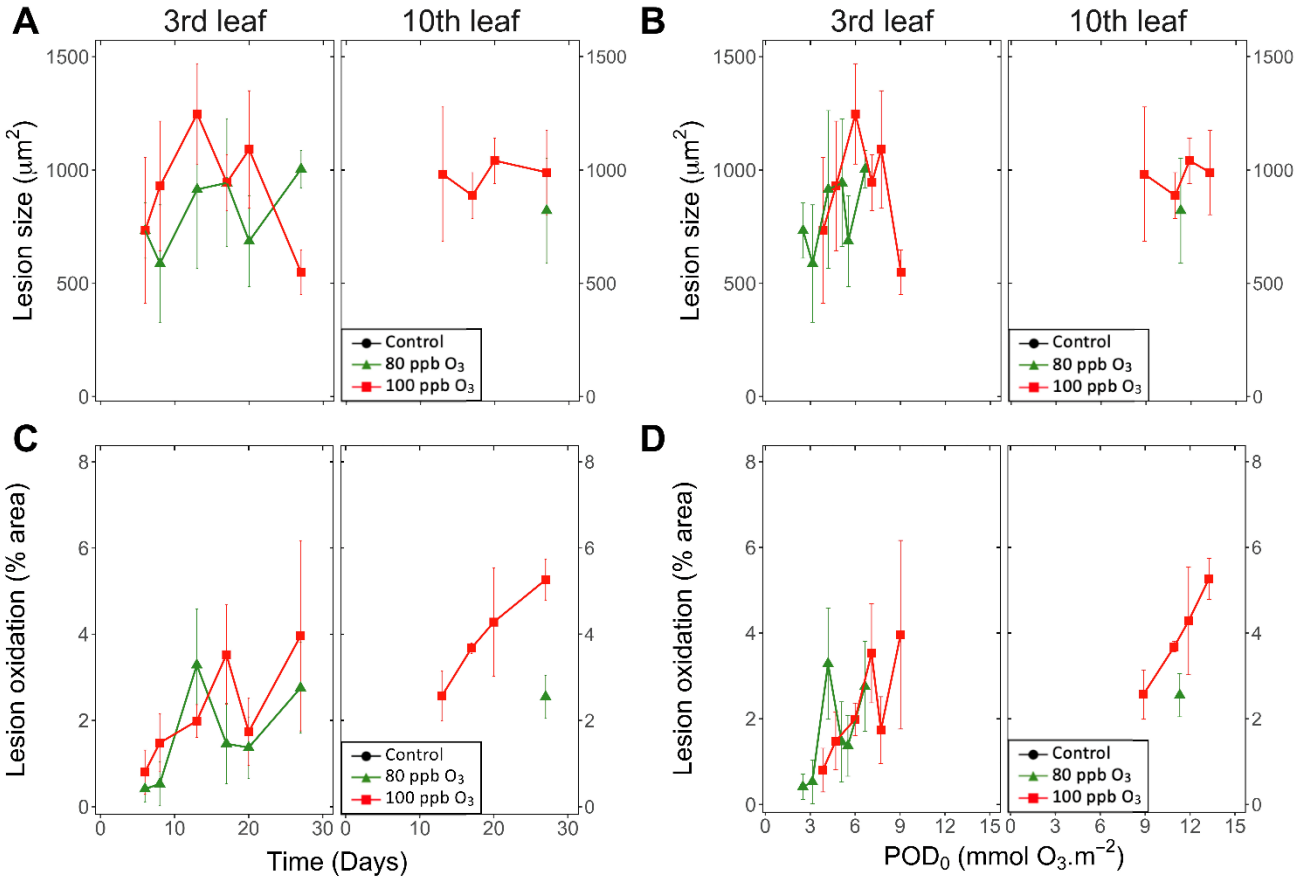

	Lesion size	Lesion oxidation		Lesion size	Lesion oxidation
O_3 treatment	ns	ns	O_3 treatment	ns	ns
Leaf Position	ns	ns	Leaf Position	ns	ns
Time	ns	*	POD_0	ns	*
O_3 treatment:Time	ns	ns	O_3 treatment:POD_0	ns	ns
O_3 treatment:Leaf Position	ns	ns	O_3 treatment:Leaf Position	ns	ns
Leaf Position:Time	ns	ns	Leaf Position:POD_0	ns	ns
O_3 treatment:Time:Leaf Position	ns	ns	O_3 treatment:POD_0:Leaf Position	ns	ns

Figure. 6. Dynamics of changes in the size (**A**, **B**) and degree of oxidation (**C**, **D**) of single HR-like lesions in hybrid poplar leaves (*Populus tremula x alba*), as a function of the assessment time (**A**, **C**), phytotoxic O_3 dose (POD_0; **B**, **D**), O_3 treatment (charcoal-filtered air ●, 80 ppb O_3 ▲, 100 ppb O_3 ■), leaf position and interactions (model: lmer(variable) ~ O_3 treatment * leaf position * time + (1 | tree / chamber)); * $p \leq 0.05$, ns not significantly different, na not tested). A, B: the size of HR-like lesions did not respond to the experimental factors and interactions. Values represent means ± SE of distinct lesion size (**A**, **B**) and percentage area showing oxidation (**C**, **D**), n = 4.

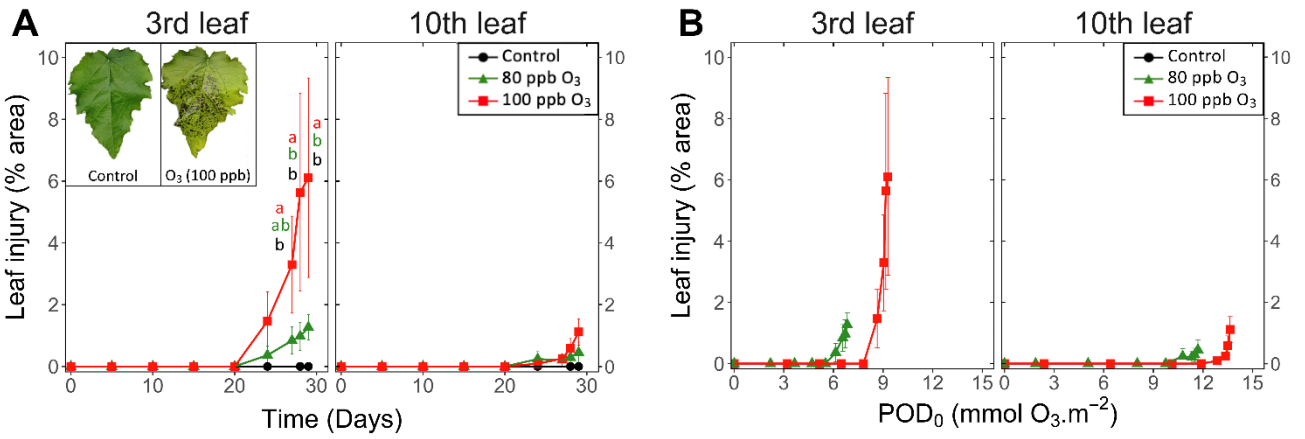

	Leaf injury
O_3 treatment	ns
Leaf Position	*
Time	***
O_3 treatment:Time	***
O_3 treatment:Leaf Position	**
Leaf Position:Time	**
O_3 treatment:Time:Leaf Position	*

	Leaf injury
O_3 treatment	ns
Leaf Position	ns
POD_0	***
O_3 treatment:POD_0	*
O_3 treatment:Leaf Position	ns
Leaf Position:POD_0	***
O_3 treatment:POD_0:Leaf Position	*

Figure 7. Development dynamics of visible O_3 injury in hybrid poplar leaves (*Populus tremula x alba*), as a function of the assessment time (**A**), phytotoxic O_3 dose (POD_0; **B**), O_3 treatment (charcoal-filtered air ●, 80 ppb O_3 ▲, 100 ppb O_3 ■), leaf position and interactions (lmer(log(variable) ~ O_3 treatment * leaf position * time + (1 | tree / chamber)); *** $p \leq 0.001$, ** $p \leq 0.01$, * $p \leq 0.05$, ns not significantly different). The insert in A shows typical O_3 symptoms, in the form of intercostal necrotic dark spots, within a leaf at 3rd leaf position exposed for 30 days (POD_0 = 9.3 mmol O_3 m^{-2}, 100 ppb O_3 treatment) *versus* an asymptomatic leaf from the CF treatment, sampled at the same leaf position and at the end of treatment. Values represent means ± SE of leaf percentage area showing visible injury, n = 6. Letters indicate significant differences between treatments at a given assessment date (post-hoc TukeyHSD, $p \leq 0.05$).

When expressed as a function of POD_0, the visible injuries appeared at a lower O_3 threshold at the 3rd than 10th leaf position (9 and 12 mmol O_3 m^{-2} in the case of 100 ppb treatment; Fig. 7B). With only the beginning of injury development assessed in a 30-day experiment, the O_3 treatment effects could not reach any significance, and only preliminary information on the dynamics of visible symptom development was thus obtained. The simultaneous detection of early injury in the two O_3 treatments (Fig. 7A) thereby resulted in higher injury values for similar POD_0 in the 80 *versus* 100 ppb O_3 treatment (Fig. 7B; O_3 treatment*POD: $P < 0.05$). Similarly, differences between younger and older leaves were detected as a trend only, with still very low injury values recorded at the 10th leaf position and for the higher POD_0 values only (Leaf position: ns; Leaf position*POD: $P < 0.001$).

Discussion

Dynamics of physiological and structural responses to O_3 stress

The physiological and structural responses detected during 30 days of O_3 exposure developed mostly before and in some cases at the same time as the initial visible injury and first leaf shedding, whereas no O_3 effect on the gross morphology of trees was observed. The two O_3 treatments accelerated the ontological decline of leaf gas exchange at the two leaf positions, once leaf physiology had reached maturity. O_3-induced reductions in the stomatal conductance and net CO_2 assimilation are well-documented in the case of various species, including poplars (Pell et al., 1992; Bagard et al., 2015; Dusart et al., 2019a) but more rarely with a leaf ontogenetic perspective. The decrease in net CO_2 assimilation could result from a smaller stomatal aperture, limiting CO_2 availability. Indeed, the O_3 effects on stomata are well-established (Kangasjarvi et al., 2005), including slower movements of cell guard cells upon exposure referred to as stomatal sluggishness, as observed in different species but with higher measurement frequency than in our case (Paoletti and Grulke, 2010; Dumont et al., 2013; Dusart et al., 2019b). Lower mesophyll conductance could also contribute to the observed acceleration of A_{net} reduction, as compared with the ontogenetic decrease observed in CF trees (Xu et al., 2019). Although not significant in older foliage, the drop in A_{net} tended to be more expressed in the 100 *versus* 80 ppb treatment after 20 days, suggesting additional reduction in carboxylation efficiency and rate of electron transport (Bagard et al., 2008; Shang et al., 2017). A possible cause could be the starting degradation of photosynthetic machinery, as suggested by the concomitant reduction in the chlorophyll content index.

The reduction in leaf chlorophyll content is another well-documented leaf physiological response to elevated O_3 (Reich, 1983; Bagard et al., 2015; Dusart et al., 2019b), indicative of ACS, together with other markers of chloroplast degeneration (Mikkelsen and HeideJorgensen, 1996; Günthardt-Goerg and Vollenweider, 2007; Moura et al., 2018). Also typical of ACS and degenerative processes was the progressive and mostly monotonic reductions observed in the case of all physiology parameters (g_w, A_{net}, chlorophyll index). This contrasted with abrupt responses upon exceedance of a threshold, as observed in the case of HR-like reactions. In the field,

the ontogeny-driven ACS latency observed in both younger and older foliage (total chlorophyll index) may also contribute to delaying the onset of degenerative events in response to O_3-stress, as suggested by the development of ACS traits and visible injury rarely occurring before summer, once foliage has fully matured (Vollenweider et al., 2019).

The new cell necrosis assay, by means of computer-assisted color image analysis, allowed us to monitor the emergence and development of validated HR-like reactions for the first time. It provided unprecedented capacity for quantitative assessments of cell death reactions in experimental conditions, overcoming limitations and uncertainties regarding the observation of visible injury only. Typical HR-like markers were detected in the lesions (Paoletti et al., 2009; Vollenweider et al., 2013; Feng et al., 2016; Vollenweider et al., 2019). However, there were marked differences in classical traits as well, including the mid- rather than upper-mesophyll location of HR-like lesions or a missing intra- and intercellular gradient of injury. Such features indicated low levels of photo-oxidative stress (Foyer et al., 1994; Günthardt-Goerg and Vollenweider, 2007; Guerrero et al., 2013). Given maximum PAR above 2000 *versus* 350 µmol m^{-2} s^{-1} with high (Ritchie, 2010; Poorter et al., 2019) *versus* low light conditions, HR-like reaction peculiarities – together with the late onset of ACS - can be attributed to specifics in the environmental conditions, especially regarding PAR supply. This finding thus provides a further confirmation of the close dependency relating the O_3 symptom expression in foliage and precise experimental and exposure conditions of tested material (Moura et al., 2018; Paoletti et al., 2009; Vollenweider et al., 2019).

The rather sigmoidal-like injury dynamics observed in older foliage was in good agreement with already existing molecular and trait evidence on HR-like processes. The 6 days/ 3 mmol O_3 m-2 s-1 delay between the start of exposure and occurrence of first lesions was thus indicative of the O_3 dose-dependent onset of genetically-controlled PCD (Rao et al., 2000; Overmyer et al., 2005). The steep increase in injury percentage area reflected the rapid cell death completion once PCD started (Overmyer et al., 2005; Günthardt-Goerg and Vollenweider, 2007). Finally, the plateau reached was indicative of lesion containment, blocking its further spread (Overmyer et al., 2003; Kangasjarvi et al., 2005; Marchica et al., 2019). In younger foliage, the experiment was terminated before a plateau could be reached, with values of lesion percentage area

which would probably have been sizably higher than at the 3rd leaf position. Further suggesting the genetic control of PCD, in older foliage, the first HR-like reactions occurred 17 days/ at 5.3 mmol O_3 m-2 s-1 before any evidence of biochemical limitation and chloroplast injury, as indicated by low levels of chlorophyll content indexes. The early HR-like responses, and their antecedence with respect to ACS and first visible injury, contrasted with field evidence (Vollenweider et al., 2019), further outlining how important the environmental conditions can be regarding response order and dynamics.

Image analysis in WinCELL based on three color classes allowed us to quantify the structurally contrasted non-oxidized and oxidized lesions, based on constitutive and stained-color characteristics. REDOX changes during oxidative stress and cell death form an important cell physiology process (Foyer and Noctor, 2005) that is well-documented in the case of O_3 stress (Ranieri et al., 2000; Baier et al., 2005; Chen and Gallie, 2005; Bellini and De Tullio, 2019), detectable with different structural and ultra-structural markers (Moura et al., 2018; Vollenweider et al., 2019) and underlying changes in visible symptom expression. Expressed as leaf area percentages, the oxidized and total HR-like lesions showed similar dynamics and responses to increasing POD_0 (same results for non-oxidized lesions, data not shown). The main differences in oxidized *versus* non-oxidized lesions included their 1) lower percentage area, 2) delay in development and 3) higher severity (*i.e.,* cell wall breaks, cell content disruption). Non-oxidized and oxidized lesions may thus correspond to two types or two stages of HR-like reactions. However, the first hypothesis appears unlikely, given lacking molecular evidence for alleged PCD severity variation. In favor of the second, oxidized *versus* non-oxidized lesions appeared later, and the oxidation degree of a lesion increased with time. However, it implies the further evolution of HR-like lesions after cell collapse and death, which needs further structural and ultrastructural confirmation.

Visible injury was detected only once 2-5% of the leaf percentage area showed oxidized lesions, thus with a detection delay and a POD_0 gap compared to the onset of HR-like reactions amounting to 18 days and 4.9 mmol O_3 m^{-2} s^{-1}. Similarly, risk assessment studies using visible injury markers rather target the late and final structural evolution of responses to O_3 stress in foliage, with possible interspecific variation, instead of the injury appearance in foliage.

Leaf position dependency of responses to O_3 stress

Reductions in leaf gas exchanges or the development of HR-like lesions and visible symptoms at the 10th *versus* 3rd leaf position occurred later and for larger POD_0. Given the higher stomatal conductance and POD_0 in younger leaves, their greater physiological activity and lower levels of injury suggest higher O_3 tolerance, whilst a contribution by enhanced stomatal closure can be excluded. This finding is confirmed by similar reports on enhanced O_3 tolerance in maturing leaves (Reich, 1983; Paakkonen et al., 1996; Strohm et al., 2002; Bagard et al., 2008; Zhang et al., 2010; Guerrero et al., 2013). This may be related to sink functional properties and larger resource availability for defense and repair (Coleman, 1986). Resource availability in young leaves could be increased by the supply of nutrients (such as nitrogen, potassium and phosphorus) coming from senescent leaves (Maillard et al., 2015; Have et al., 2017). Hence, the concentration of phenolics with antioxidant properties and other antioxidative capacities decline during sink-to-source transition in maturing foliage, thus increasing leaf susceptibility to oxidative stress (Coleman, 1986; Strohm et al., 2002; Blokhina and Fagerstedt, 2006; Bellini and De Tullio, 2019). However, and in contrast to older foliage, the development of HR-like lesions as a function of POD_0 at the 10th leaf position depended on the O_3 treatment, with a higher O_3 tolerance in the 80 ppb O_3 treatment. Given the high O_3 dose in maturing leaves, this finding highlights the importance of O_3 absorption rate in view of the saturation of the antioxidative system. The higher O_3 tolerance in younger *versus* older foliage was further confirmed by their still comparable leaf percentage areas showing HR-like lesions in the 100 ppb O_3 treatment despite 1.8 times higher POD_0 at the 10th leaf position.

Reaction gradient in foliage in relation to critical O_3 levels

In our experiment, the current CL (POD_{Y_SPEC} for beech and birch = 5.2 mmol O_3 m^{-2}; Mills et al., 2017) was equivalent to a POD_0 of 5.7 mmol O_3 m^{-2}. By the end of exposure, this CL had thus been exceeded by 1.54 and 2.35 times at the 3rd and 10th leaf position, respectively. If any impairment of tree morphology and biomass was still lacking, reductions in leaf gas exchange, development of structural injury and emergence of visible symptoms at the 3rd leaf position had already been observed for O_3 dose, amounting to 0.82, 0.69 and 1.46 times the current CL, respectively. At the

10th leaf position, these responses were detected for POD_{Y_SPEC} 1.83, 1.18 and 2.32 times above CL. These findings highlight the high dependency of sensitivity evaluations on the selected parameters and scale of observation. They also outline the within-tree gradient of sensitivity to O_3 stress, given the large size of such organisms, which, as a result, complicates O_3 risk assessment. They finally indicate that below CL, significant effects in the foliage of trees, such as in the impairment of leaf physiology and development of microscopic necrosis in extended parts of mesophyll, can be expected. These responses may already contribute to reduced carbon uptake and storage in foliage and other tree organs before reaching CL thresholds.

Conclusion

In this study, we characterized the dynamics of physiological, structural and morphological responses to two levels of O_3 exposure and as a function of time, POD_0 and leaf position, in fully controlled conditions. We observed contrasting dynamics, monotonic or sigmoidal-like, as a function of plant responses but irrespective of leaf position, prior to any visible symptoms and effects on the gross morphology of trees. The first microscopic necrosis developed weeks before the appearance of visible symptoms and at half the O_3 dose. With regard to experimental hypotheses (H), the sequential development and distinct dynamics of physiological, structural, and morphological responses to O_3 stress was confirmed (confirmation of H1); both HR-like and ACS responses were elicited, the former occurring first (confirmation of H2a, rejection of H2b). When expressed as a function of POD_0, leaf responses did not depend on the O_3 treatment (confirmation of H3a), except for the development of structural injury that depended on the O_3 absorption rates in younger foliage (partial rejection of H3b). Finally, response dynamics were strongly related to leaf age as a function of time or POD_0, showing delay in younger foliage (confirmation of H4). This study thus sheds light on the syndrome of early reactions to O_3 stress and disentangles the specific dynamics of distinct but co-occurring plant responses, prior to CL exceedance. The resulting variety of symptoms, as observed by the end of experiment, provides an exemplary experimental demonstration for integrative injury display, as found in the field late in summer. Given ACS and HR-like timing inversion, compared to field conditions, the ontogenetical and environmental drivers also appear to have a prevailing effect over the sensitivity of affected markers, regarding the timing and

dynamics of each cellular response. Whatever the exact sequence order of early reactions to O_3 stress below CL - in field or controlled conditions, they will modify key foliage properties. Such impacts can be relevant for some *e.g.* biodiversity ecosystem services prior to those of economic significance – *i.e.* wood production, as targeted by flux-based CL.

Acknowledgements

The research was funded by grants from the French National Research Agency (ANR, "Investissements d'Avenir" from the program Lab of Excellence ARBRE: ANR-11-LABX-0002-01), Grand-Est region, France, and WSL (201701N1428). Technical support by Terry Menard (microscopy), Christophe Robin (leaf physiology) as well as Jean-Charles Olry et Stéphane Martin (members of the experimental phytotrons platform of Lorraine PEPLor, University of Lorraine, France) is also gratefully acknowledged.

The authors have no conflict of interest to declare.

REFERENCES

Bagard, M., Jolivet, Y., Hasenfratz-Sauder, M.P., Gerard, J., Dizengremel, P., and Le Thiec, D. (2015). Ozone exposure and flux-based response functions for photosynthetic traits in wheat, maize and poplar. *Environ Pollut* 206**,** 411-420.

Bagard, M., Le Thiec, D., Delacote, E., Hasenfratz-Sauder, M.P., Banvoy, J., Gerard, J., Dizengremel, P., and Jolivet, Y. (2008). Ozone-induced changes in photosynthesis and photorespiration of hybrid poplar in relation to the developmental stage of the leaves. *Physiol Plant* 134**,** 559-574.

Baier, M., Kandlbinder, A., Golldack, D., and Dietz, K.J. (2005). Oxidative stress and ozone: perception, signalling and response. *Plant Cell & Environ.* 28**,** 1012-1020.

Bates, D., Machler, M., Bolker, B.M., and Walker, S.C. (2015). Fitting linear mixed-effects models using lme4. *J. Stat. Softw.* 67**,** 1-48.

Bellini, E., and De Tullio, M.C. (2019). Ascorbic acid and ozone: Novel perspectives to explain an elusive relationship. *Plants* 8.

Bhattacharjee, S. (2005). Reactive oxygen species and oxidative burst: Roles in stress, senescence and signal transduction in plants. *Curr. Sci.* 89**,** 1113-1121.

Blokhina, O., and Fagerstedt, K. (2006). "Oxidative Stress and Antioxidant Defenses in Plants," in *Oxidative Stress, Disease and Cancer*. (Covent Garden: Imperial Coll Press), 151-199.

Büker, P., Feng, Z., Uddling, J., Briolat, A., Alonso, R., Braun, S., Elvira, S., Gerosa, G., Karlsson, P.E., Le Thiec, D., Marzuoli, R., Mills, G., Oksanen, E., Wieser, G., Wilkinson, M., and Emberson, L.D. (2015). New flux based dose-response

relationships for ozone for European forest tree species. *Environ Pollut* 206**,** 163-174.
Cabane, M., Pireaux, J.C., Leger, E., Weber, E., Dizengremel, P., Pollet, B., and Lapierre, C. (2004). Condensed lignins are synthesized in poplar leaves exposed to ozone. *Plant Physiol.* 134**,** 586-594.
Chen, Z., and Gallie, D.R. (2005). Increasing tolerance to ozone by elevating foliar ascorbic acid confers greater protection against ozone than increasing avoidance. *Plant Physiol.* 138**,** 1673-1689.
Coleman, J.S. (1986). Leaf development and leaf stress: increased susceptibility associated with sink-source transition. *Tree Physiol.* 2**,** 289-299.
Dghim, A.A., Dumont, J., Hasenfratz-Sauder, M.P., Dizengremel, P., Le Thiec, D., and Jolivet, Y. (2013). Capacity for NADPH regeneration in the leaves of two poplar genotypes differing in ozone sensitivity. *Physiol Plant* 148**,** 36-50.
Dizengremel, P., Jolivet, Y., Tuzet, A., Ranieri, A., and Le Thiec, D. (2013). "Integrative leaf-level phytotoxic ozone dose assessment for forest risk modelling," in *Climate Change, Air Pollution and Global Challenges: Understanding and Perspectives from Forest Research,* eds. R. Matyssek, N. Clarke, P. Cudlin, T.N. Mikkelsen, J.P. Tuovinen, G. Wieser & E. Paoletti. (Netherlands: Elsevier), 267-288.
Dumont, J., Keski-Saari, S., Keinanen, M., Cohen, D., Ningre, N., Kontunen-Soppela, S., Baldet, P., Gibon, Y., Dizengremel, P., Vaultier, M.N., Jolivet, Y., Oksanen, E., and Le Thiec, D. (2014). Ozone affects ascorbate and glutathione biosynthesis as well as amino acid contents in three Euramerican poplar genotypes. *Tree Physiol* 34**,** 253-266.
Dumont, J., Spicher, F., Montpied, P., Dizengremel, P., Jolivet, Y., and Le Thiec, D. (2013). Effects of ozone on stomatal responses to environmental parameters (blue light, red light, CO2 and vapour pressure deficit) in three *Populus deltoides* x *Populus nigra* genotypes. *Environ Pollut* 173**,** 85-96.
Dusart, N., Gerard, J., Le Thiec, D., Collignon, C., Jolivet, Y., and Vaultier, M.N. (2019a). Integrated analysis of the detoxification responses of two Euramerican poplar genotypes exposed to ozone and water deficit: Focus on the ascorbate-glutathione cycle. *Sci Total Environ* 651**,** 2365-2379.
Dusart, N., Vaultier, M.N., Olry, J.C., Bure, C., Gerard, J., Jolivet, Y., and Le Thiec, D. (2019b). Altered stomatal dynamics of two Euramerican poplar genotypes submitted to successive ozone exposure and water deficit. *Environ Pollut* 252**,** 1687-1697.
Faoro, F., and Iriti, M. (2009). Plant cell death and cellular alterations induced by ozone: key studies in Mediterranean conditions. *Environ Pollut* 157**,** 1470-1477.
Feng, G., Calatayud, V., García-Breijo, F., Reig-Armiñana, J., and Feng, Z. (2016). Effects of elevated ozone on physiological, anatomical and ultrastructural characteristics of four common urban tree species in China. *Ecol. Indic.* 67**,** 367-379.
Foyer, C.H., Lelandais, M., and Kunert, K.J. (1994). Photooxidative stress in plants. *Physiol Plant* 92**,** 696-717.
Foyer, C.H., and Noctor, G. (2005). Redox homeostasis and antioxidant signaling: A metabolic interface between stress perception and physiological responses. *Plant Cell* 17**,** 1866-1875.
Fu, T.M., and Tian, H. (2019). Climate change penalty to ozone air quality: Review of current understandings and knowledge gaps. *Curr. Pollut. Rep.* 5**,** 159-171.

Fuhrer, J., Skarby, L., and Ashmore, M.R. (1997). Critical levels for ozone effects on vegetation in Europe. *Environ Pollut* 97**,** 91-106.
Giacomo, B., Forino, L.M.C., Tagliasacchi, A.M., Bernardi, R., and Durante, M. (2010). Ozone damage and tolerance in leaves of two poplar genotypes. *Caryologia* 63**,** 422-434.
Guerrero, C.C., Gunthardt-Goerg, M.S., and Vollenweider, P. (2013). Foliar symptoms triggered by ozone stress in irrigated holm oaks from the city of madrid, spain. *Plos One* 8.
Günthardt-Goerg, M.S., and Vollenweider, P. (2007). Linking stress with macroscopic and microscopic leaf response in trees: new diagnostic perspectives. *Environ Pollut* 147**,** 467-488.
Have, M., Marmagne, A., Chardon, F., and Masclaux-Daubresse, C. (2017). Nitrogen remobilization during leaf senescence: lessons from *Arabidopsis* to crops. *J. Exp. Bot.* 68**,** 2513-2529.
Jolivet, Y., Bagard, M., Cabane, M., Vaultier, M.N., Gandin, A., Afif, D., Dizengremel, P., and Le Thiec, D. (2016). Deciphering the ozone-induced changes in cellular processes: a prerequisite for ozone risk assessment at the tree and forest levels. *Ann. For. Sci.* 73**,** 923-943.
Joo, J.H., Wang, S.Y., Chen, J.G., Jones, A.M., and Fedoroff, N.V. (2005). Different signaling and cell death roles of heterotrimeric G protein alpha and beta subunits in the *Arabidopsis* oxidative stress response to ozone. *Plant Cell* 17**,** 957-970.
Kangasjarvi, J., Jaspers, P., and Kollist, H. (2005). Signalling and cell death in ozone-exposed plants. *Plant Cell & Environ.* 28**,** 1021-1036.
Karlsson, P., Braun, S., Broadmeadow, M., Elvira, S., Emberson, L., Gimeno, B.S., Le Thiec, D., Novak, K., Oksanen, E., Schaub, M., Uddling, J., and Wilkinson, M. (2007). Risk assessments for forest trees: The performance of the ozone flux versus the AOT concepts. *Environ Pollut* 146**,** 608-616.
Karlsson, P.E., Klingberg, J., Engardt, M., Andersson, C., Langner, J., Karlsson, G.P., and Pleijel, H. (2017). Past, present and future concentrations of ground-level ozone and potential impacts on ecosystems and human health in northern Europe. *Sci Total Environ* 576**,** 22-35.
Lamaud, E., Loubet, B., Irvine, M., Stella, P., Personne, E., and Cellier, P. (2009). Partitioning of ozone deposition over a developed maize crop between stomatal and non-stomatal uptakes, using eddy-covariance flux measurements and modelling. *Agric. For. Meteorol.* 149**,** 1385-1396.
Lenth, R.V. (2016). Least-Squares Means: The R Package lsmeans. *J. Stat. Softw.* 69**,** 1-33.
Li, P., Feng, Z.Z., Catalayud, V., Yuan, X.Y., Xu, Y.S., and Paoletti, E. (2017). A meta-analysis on growth, physiological, and biochemical responses of woody species to ground-level ozone highlights the role of plant functional types. *Plant Cell & Environ.* 40**,** 2369-2380.
Maas, R., and Grennfelt, P. (2016). Towards cleaner air. Scientific assessment report. Emep steering body and working group on effects of the convention on long-range transboundary air pollution, Oslo. 12-16.
Maillard, A., Diquelou, S., Billard, V., Laine, P., Garnica, M., Prudent, M., Garcia-Mina, J.M., Yvin, J.C., and Ourry, A. (2015). Leaf mineral nutrient remobilization during leaf senescence and modulation by nutrient deficiency. *Front. Plant Sci.* 6.

Marchica, A., Lorenzini, G., Papini, R., Bernardi, R., Nali, C., and Pellegrini, E. (2019). Signalling molecules responsive to ozone-induced oxidative stress in *Salvia officinalis*. *Sci Total Environ* 657**,** 568-576.

Massman, W.J. (1998). A review of the molecular diffusivities of H2O, CO2, CH4, CO, O-3, SO2, NH3, N2O, NO, AND NO2 in air, O-2 AND N-2 near STP. *Atmos. Environ.* 32**,** 1111-1127.

Mikkelsen, T.N., and Heidejorgensen, H.S. (1996). Acceleration of leaf senescence in *Fagus sylvatica* L by low levels of tropospheric ozone demonstrated by leaf colour, chlorophyll fluorescence and chloroplast ultrastructure. *Trees-Struct Funct.* 10**,** 145-156.

Mills, G., Pleijel, H., Braun, S., Buker, P., Bermejo, V., Calvo, E., Danielsson, H., Emberson, L., Fernandez, I.G., Grunhage, L., Harmens, H., Hayes, F., Karlsson, P.E., and Simpson, D. (2011). New stomatal flux-based critical levels for ozone effects on vegetation. *Atmos. Environ.* 45**,** 5064-5068.

Mills G., Harmens H., Hayes F., Pleijel H., Buker P., and I., G. (2017). Mapping critical levels for vegetation. Manual on methodologies and criteria for Modelling and mapping critical loads and levels and air pollution effects, Risks and Trends. *International Cooperative Programme on Effects of Air Pollution on Natural Vegetation and Crops***,** 1-66.

Moura, B.B., Alves, E.S., Marabesi, M.A., De Souza, S.R., Schaub, M., and Vollenweider, P. (2018). Ozone affects leaf physiology and causes injury to foliage of native tree species from the tropical Atlantic Forest of southern Brazil. *Sci Total Environ* 610**,** 912-925.

Musselman, R.C., Lefohn, A.S., Massman, W.J., and Heath, R.L. (2006). A critical review and analysis of the use of exposure- and flux-based ozone indices for predicting vegetation effects. *Atmos. Environ.* 40**,** 1869-1888.

Overmyer, K., Brosche, M., and Kangasjarvi, J. (2003). Reactive oxygen species and hormonal control of cell death. *Trends Plant Sci* 8**,** 335-342.

Overmyer, K., Brosche, M., Pellinen, R., Kuittinen, T., Tuominen, H., Ahlfors, R., Keinanen, M., Saarma, M., Scheel, D., and Kangasjarvi, J. (2005). Ozone-induced programmed cell death in the *Arabidopsis* radical-induced cell death1 mutant. *Plant Physiol* 137**,** 1092-1104.

Paakkonen, E., Metsarinne, S., Holopainen, T., and Karenlampi, L. (1996). The ozone sensitivity of birch (*Betula pendula*) in relation to the developmental stage of leaves. *New Phytol.* 132**,** 145-154.

Paoletti, E., Contran, N., Bernasconi, P., Gunthardt-Goerg, M.S., and Vollenweider, P. (2009). Structural and physiological responses to ozone in Manna ash (*Fraxinus ornus* L.) leaves of seedlings and mature trees under controlled and ambient conditions. *Sci Total Environ* 407**,** 1631-1643.

Paoletti, E., and Grulke, N.E. (2010). Ozone exposure and stomatal sluggishness in different plant physiognomic classes. *Environ Pollut* 158**,** 2664-2671.

Pasqualini, S., Piccioni, C., Reale, L., Ederli, L., Della Torre, G., and Ferranti, F. (2003). Ozone-induced cell death in tobacco cultivar Bel W3 plants. The role of programmed cell death in lesion formation. *Plant Physiol* 133**,** 1122-1134.

Pell, E.J., Eckardt, N., and Enyedi, A.J. (1992). Timing of ozone stress and resulting status of ribulose bisphosphate carboxylase oxygenase and associated net photosynthesis. *New Phytol* 120**,** 397-405.

Pell, E.J., Sinn, J.P., Brendley, B.W., Samuelson, L., Vinten-Johansen, C., Tien, M., and Skillman, J. (1999). Differential response of four tree species to ozone-induced acceleration of foliar senescence. *Plant Cell & Environ.* 22**,** 779-790.

Poorter, H., Niinemets, U., Ntagkas, N., Siebenkas, A., Maenpaa, M., Matsubara, S., and Pons, T. (2019). A meta-analysis of plant responses to light intensity for 70 traits ranging from molecules to whole plant performance. *New Phytol* 223**,** 1073-1105.

Proietti, C., Anav, A., De Marco, A., Sicard, P., and Vitale, M. (2016). A multi-sites analysis on the ozone effects on gross primary production of european forests. *Sci Total Environ* 556**,** 1-11.

R Development Core Team (2017). "R: A language and environment for statistical computing". (Vienna, Austria: R Foundation for Statistical Computing).

Ranieri, A., Petacco, F., Castagna, A., and Soldatini, G.F. (2000). Redox state and peroxidase system in sunflower plants exposed to ozone. *Plant Science* 159**,** 159-167.

Rao, M.V., Lee, H., Creelman, R.A., Mullet, J.E., and Davis, K.R. (2000). Jasmonic acid signaling modulates ozone-induced hypersensitive cell death. *Plant Cell* 12**,** 1633-1646.

Reich, P.B. (1983). Effects of low concentrations of O3 on net photosynthesis, dark respiration, and chlorophyll contents in aging hybrid poplar leaves. *Plant Physiol* 73**,** 291-296.

Revell, L.E., Tummon, F., Stenke, A., Sukhodolov, T., Coulon, A., Rozanov, E., Garny, H., Grewe, V., and Peter, T. (2015). Drivers of the tropospheric ozone budget throughout the 21st century under the medium-high climate scenario RCP 6.0. *Atmospheric Chem. Phys.* 15**,** 5887-5902.

Ritchie, R.J. (2010). Modelling photosynthetic photon flux density and maximum potential gross photosynthesis. *Photosynthetica* 48**,** 596-609.

Sanz, M., and Catalayud, V. (2011). *Ozone injury in European forest species* [Online]. Available: http://www.ozoneinjury.org/ [Accessed December 12, 2020].

Schindelin, J., Arganda-Carreras, I., Frise, E., Kaynig, V., Longair, M., Pietzsch, T., Preibisch, S., Rueden, C., Saalfeld, S., Schmid, B., Tinevez, J.Y., White, D.J., Hartenstein, V., Eliceiri, K., Tomancak, P., and Cardona, A. (2012). Fiji: an open-source platform for biological-image analysis. *Nat. Methods* 9**,** 676-682.

Schraudner, M., Moeder, W., Wiese, C., Van Camp, W., Inze, D., Langebartels, C., and Sandermann, H. (1998). Ozone-induced oxidative burst in the ozone biomonitor plant, tobacco Bel W3. *Plant Journal* 16**,** 235-245.

Shang, B., Feng, Z.Z., Li, P., Yuan, X.Y., Xu, Y.S., and Calatayud, V. (2017). Ozone exposure- and flux-based response relationships with photosynthesis, leaf morphology and biomass in two poplar clones. *Sci Total Environ* 603**,** 185-195.

Strohm, M., Eiblmeier, M., Langebartels, C., Jouanin, L., Polle, A., Sandermann, H., and Rennenberg, H. (1999). Responses of transgenic poplar (*Populus tremula* x *P-alba*) overexpressing glutathione synthetase or glutathione reductase to acute ozone stress: visible injury and leaf gas exchange. *J Exp Bot* 50**,** 365-374.

Strohm, M., Eiblmeier, M., Langebartels, C., Jouanin, L., Polle, A., Sandermann, H., and Rennenberg, H. (2002). Responses of antioxidative systems to acute ozone stress in transgenic poplar (*Populus tremula* x *P-alba*) over-expressing glutathione synthetase or glutathione reductase. *Trees-Struct Funct.* 16**,** 262-273.

Vollenweider, P., Fenn, M.E., Menard, T., Günthardt-Goerg, M., and Bytnerowicz, A. (2013). Structural injury underlying mottling in ponderosa pine needles

exposed to ambient ozone concentrations in the San Bernardino Mountains near Los Angeles, California. *Trees* 27**,** 895-911.
Vollenweider, P., Günthardt-Goerg, M.S., Menard, T., Baumgarten, M., Matyssek, R., and Schaub, M. (2019). Macro- and microscopic leaf injury triggered by ozone stress in beech foliage (*Fagus sylvatica* L.). *Ann. For. Sci.* 76**,** 71.
Vollenweider, P., Menard, T., Arend, M., Kuster, T.M., and Gunthardt-Goerg, M.S. (2016). Structural changes associated with drought stress symptoms in foliage of Central European oaks. *Trees-Struct Funct.* 30**,** 883-900.
Vollenweider, P., Ottiger, M., and Günthardt-Goerg, M.S. (2002). Validation of leaf ozone symptoms in natural vegetation using microscopical methods. *Environ Pollut* 124**,** 101-118.
Wittig, V.E., Ainsworth, E.A., Naidu, S.L., Karnosky, D.F., and Long, S.P. (2009). Quantifying the impact of current and future tropospheric ozone on tree biomass, growth, physiology and biochemistry: a quantitative meta-analysis. *Glob. Change Biol.* 15**,** 396-424.
Xu, Y.S., Feng, Z.Z., Shang, B., Dai, L.L., Uddling, J., and Tarvainen, L. (2019). Mesophyll conductance limitation of photosynthesis in poplar under elevated ozone. *Sci Total Environ* 657**,** 136-145.
Zhang, J., Schaub, M., Ferdinand, J.A., Skelly, J.M., Steiner, K.C., and Savage, J.E. (2010). Leaf age affects the responses of foliar injury and gas exchange to tropospheric ozone in *Prunus serotina* seedlings. *Environ Pollut* 158**,** 2627-2634.

Chapitre 3

DYNAMIQUE DES CHANGEMENTS STRUCTURAUX ET ULTRASTRUCTURAUX

Chapitre 3 : Dynamique des changements structuraux et ultrastructuraux induits par l'O_3 dans les feuilles de peupliers

Préface

L'O_3 est connu pour induire de nombreux changements structuraux et ultrastructuraux pour lesquels la dynamique est loin d'être connue. Dans l'étude qui fait l'objet de ce deuxième chapitre nous avons étudié la dynamique de ces changements en lien avec le développement de la réponse hypersensible (HR-like) et de la sénescence cellulaire accélérée (ACS). Pour suivre cette dynamique, le *design* expérimental est le même que celui décrit dans le premier chapitre avec deux niveaux de traitement par O_3 (80 et 100 ppb), et la prise en considération de deux stades de développement foliaire avec la feuille 3 et la feuille 10. Les changements structuraux et ultra-structuraux sont appréciés au moyen de la microscopie photonique et électronique. Comme tous les prélèvements ne pouvaient pas être observé, le choix s'est porté sur les prélèvements après :

- 8 et 23 jours d'exposition pour les contrôles (CF) afin d'observer l'évolution structurale des feuilles en lien avec leur ontogenèse,

- 8, 13 et 23 jours d'exposition à 100 ppb O_3 pour appréhender les changements sous contrainte O_3, changements qui seront comparés à ceux survenant après 13 jours pour une exposition à 80 ppb O_3

Dans ce chapitre rédigé sous la forme d'une publication, il est montré que la dynamique des HR-like dépendait du traitement O_3, de la position de la feuille et du POD_0 mais pas la dynamique cellulaire résultant de l'évolution chimique post-mortem du contenu cellulaire. En revanche, la dynamique de l'ACS et des changements microscopiques associés dépendaient des traitements O_3, de la position de la feuille et du POD_0. Nos résultats suggèrent donc que les dynamiques et mécanismes distincts de la HR-like et de l'ACS pourraient résulter d'une accumulation spatiale distincte des ROS induits par l'O_3. Cette étude démontre également que les symptômes visibles résultant d'une réaction de type HR sous-estiment largement les

dommages structuraux, et que la dynamique des changements ultra-structuraux des chloroplastes peuvent être une indication de la dose d'O_3 absorbée par la feuille dans les échantillons symptomatiques en milieu naturel.

Abstract

By reaching phytotoxic levels during the last century, tropospheric ozone (O_3) pollution will remain a lasting concern in next decades. O_3 is known to induced numerous structural and ultrastructural changes, related either to the hypersensitive response-like (HR-like) or to the accelerated cell senescence (ACS), but the characterization of their respective dynamics is still missing. In this study, we have investigated the dynamics of HR-like lesion and ACS-related changes occurring in response to two levels of O_3 treatment (80 and 100 ppb) in the foliage of hybrid poplar, as a function of time, phytotoxic O_3 dose (POD_0) and foliar developmental stage. Dynamics of HR-like was depending on O_3 treatment, leaf position and POD_0 but not the cellular dynamic resulting from chemical post-mortem evolution of cellular content. By contrast, both dynamics of ACS and related microscopic changes were depending on O_3 treatments, leaf position and POD_0. Hence, our results suggest that distinct dynamics and mechanisms of the HR-like and ACS could result from distinct spatial accumulation of O_3-induced ROS. This study also demonstrates that the visible symptoms resulting from an HR-like reaction greatly underestimates structural damages, and chloroplast-related changes can be a structural indication of the O_3 uptake by leaf in symptomatic samples from field.

Introduction

Tropospheric ozone (O_3) concentrations have increased during past decades (Maas and Grennfelt, 2016) as a consequence of the increase in use of fossil fuels. Despite efforts to reduce O_3 precursors emissions, background levels of tropospheric O_3 are expected to remain stable or increase during the next century (Revell et al., 2015; Fu and Tian, 2019). This air pollutant is considered as one of the most impacting natural vegetation and crops as adverse effects have already been observed (Wittig et al., 2009; Jolivet et al., 2016; Proietti et al., 2016), and are predicted to increase or remain unchanged over the course of next decades (Karlsson et al., 2007). Effects of O_3 are mediated through stomata aperture, thus critical level (CL) of O_3 is calculated as the Phytotoxic Ozone Dose over a threshold of Y for a specific species or group of species ($POD_{Y\_SPEC;}$ (Mills G. et al., 2017)) and correspond to the cumulative O_3 uptake by leaf.

After reaching apoplast, O_3 is decomposed into reactive oxygen species (ROS) inducing an oxidative burst (Schraudner et al., 1998; Pasqualini et al., 2003; Moura et al., 2018), leading to the hypersensitive response-like (HR-like) comparable to responses induced in case of incompatible plant/pathogen interactions (Vollenweider et al., 2002; Bhattacharjee, 2005; Günthardt-Goerg and Vollenweider, 2007; Moura et al., 2018). Moreover, O_3 generates an early initiation of autumnal senescence, defined as accelerated cell senescence (ACS; (Pell et al., 1999; Günthardt-Goerg and Vollenweider, 2007; Vollenweider et al., 2019)). HR-like and ACS were shown to have distinct dynamics (sigmoidal-like vs monotonic, respectively (Turc et al., 2021) which depend on both leaf ontology and cumulated O_3 dose.

Visible injury in foliage is one of the most obvious indications of O_3 stress and have been used for O_3 monitoring and bioindication (Sanz and Catalayud, 2011), although a microscopic validation is needed to ascertain O_3 injury (Günthardt-Goerg and Vollenweider, 2007). Microscopic changes resulting from an O_3 stress are widely documented (Vollenweider et al., 2002; Paoletti et al., 2009; Moura et al., 2018; Vollenweider et al., 2019) including disruptive and degenerative traits within cell. They were linked to either HR-like or ACS by mechanistic understanding of their cause and development (Moura et al., 2018; Vollenweider et al., 2019). In most of the studies, microscopic changes are investigated at the end of the growing season on symptomatic samples from field conditions, thus once O_3 responses are well established and partially overlapping, making difficult to relate their dynamics with O_3 uptake. Nevertheless, the concomitant observation of degenerative and disruptive trait within the same cell strongly suggested a succession of O_3 responses, with ACS progressing until a threshold is reached and subsequent triggering of HR-like. However, this sequence is strongly dependent on environmental factors and particularly photooxidative stress (Moura et al., 2018; Vollenweider et al., 2019; Turc et al., 2021). Hence, characterization of the dynamics of structural and ultrastructural changes in response to O_3 as a function of environmental factors and O_3 uptake is still missing to fully understand response processes in foliage.

Higher tolerance of young vs old foliage to O_3 stress has been observed in several cases and species. However, mechanism underlying this higher tolerance is still obscure as a lower O_3 uptake by young vs old foliage can be excluded (Strohm et al., 1999; Bagard et al., 2008; Zhang et al., 2010; Turc et al., 2021). Given the high

rearrangement of cell wall involving ROS during cell expansion (Knox, 2008) in young vs old foliage, investigation of structural and ultrastructural dynamics of O_3 responses as a function of leaf ontology can provide insight on O_3 tolerance.

In this study, our main objective was to characterize dynamics of structural and ultrastructural responses to O_3 stress in hybrid poplar leaves as a function of O_3 uptake. The tested hypothesis (H) included: (H1) structural and ultrastructural changes occurring in response to O_3 stress follow the previously described dynamic of HR-like and ACS, (H2) structural difference between young vs old foliage participate to the higher tolerance of young foliage, and (H3) structural changes related to ACS or HR-like can be linked to POD_0.

Materials & Methods

Plant material and O_3 fumigation

Young hybrid poplar trees (*Populus tremula x alba*; clone INRAe 717-1B4) were cultivated as previously described (Turc et al., 2021). Micro propagated poplars were transplanted into pots filled with compost (Gramoflor Universel) and perlite (1:1, [v/v]). Pots were put for two weeks into a growth chamber set at 22°C/18°C temperature (day/night) with a 14 h photoperiod (Philips Son-T Agro 400 W lamps, PAR= 350 µmol m^{-2} s^{-1}) and 75%/85% relative humidity (day/night). Young poplars were then transplanted into 10 L containing compost (Gamoflor) fertilized with Nutricot T 100 granules (3 g l^{-1}; 13:13:13:2 N/P/K/MgO, Fertil, Boulogne-Billancourt, France). After one month, a set of 48 trees was randomly distributed in six identical phytotron chambers (PEPLor platform, Faculty of Sciences and Technologies, University of Lorraine) set at similar environmental conditions to those in the growth chambers. All foliar assessments were repeated at the third and tenth leaf position from the tree base, respectively the youngest fully expanded and that still in expansion at treetop by the start of exposure.

After one week of acclimation, two chambers (n = 16 trees) were maintained in charcoal-filtered (CF) air, two chambers were exposed to CF + 80 ppb O_3 and two chambers were exposed to CF + 100 ppb O_3 for 23 days. O_3 was generated from pure oxygen using an O_3 generator (Innovatec II, Rheinbach, Germany), and provided to chambers in the form of a 13 h square wave during the light period. The O_3

concentrations were recorded twice an hour using an O_3 UV analyzer (O341M, Environment SA, Paris).

Leaf physiology analysis

The impact of O_3 treatment on the dynamics of stomatal conductance to water vapor (g_w) was measured using a LI-6400 portable photosynthesis system (LiCor, Inc, Lincoln, NE, United States), with inner chamber temperature maintained at 22°C, light intensity (PAR) at 300 and 320 µmol m^{-2} s^{-1} for measurements at the third and tenth leaf position respectively, airflow at 300 µmol s^{-1}, CO_2 concentration at 400 ppm, and leaf vapor pressure deficit (VPD_{leaf}) < 1kPa. G_w was recorded once it remained stable for 30 s. Measurements were performed on 4 trees per treatment and inside the fumigation chamber, 3 h after starting O_3 exposure. In order to disturb the O_3 treatment as less as possible, and based on previous results (Turc et al., 2021), g_w assessment was restricted to 5, 7, 12, 16, 21 days of exposure. Measurments fo g_w was used to estimates cumulated O_3 uptake (POD_0) as previously described (Bagard et al., 2015; Turc et al., 2021).

The impact of O_3 on dynamics of the leaf chlorophyll content was assessed by spectrophotometric measurement of total chlorophylls content using a spectrophotometer (SAFAS UVmc1 spectrophotometer). Leaves were sampled on four trees per treatment after 2, 8, 13, 23 days of exposure and immediately frozen in liquid nitrogen. Frozen leaves were further ground in mortar chilled with liquid nitrogen. An aliquot of the resulting powder (about 100 mg) was mixed with 1 mL of acetone (100%) and incubated 10 min in the dark. Samples were then centrifuged (10 000 rpm / 10 min / 4°C) and 0.8 mL of supernatant was mixed with 0.2 mL of distilled water for spectrophotometric assessment.

The total chlorophyll content (chl_{tot}; mg.g^{-1} of FM) was determined according to (Lichtenthaler, 1987):

$$Chl_{tot} = 7.15 * A_{663.2} + 18.71 * A_{646.8}$$

with chl_{tot} as the total chlorophyll content, $A_{663.2}$ and $A_{646.8}$ as the optical absorbance at 663.2 nm and 646.8 nm respectively.

Structural and cytological analysis

Structural assessments were performed on two discs per leaf position in four trees per treatment sampled after 2, 8, 13 and 23 days of exposure. HR-like lesions were quantified using trypan blue coloration followed by computer-assisted color analysis, as previously described (Turc et al., 2021). Supplementary leaf discs were fixed with EM-grade 2.5% glutaraldehyde buffered at pH 7.0 with 0.067 M Soerensen phosphate buffer, renewed after vacuum infiltration and stored at 4°C until further processing. For structural investigations using either diascopic and episcopic (fluorescence) light illumination, 1.5 µm semi-thin sections were obtained using a Supercut Reichert 2050 microtome from Technovit-embedded dehydrating samples. Sections were further stained with Aniline blue (Callose detection) and Toluidine blue (Vollenweider et al., 2016). All sections were observed under a Leica microscope (Leitz DM/RB) with 5x to 100x objectives. Micrographs were taken using the INFINITY 2-1R camera and Lumenera Infinity Analyze (release 6.4) software (Lumenera Corp., Ottawa, ON, Canada).

Given the several ultrastructural changes occurring in response to O_3 exposure which are not observable under light microscopy (Moura et al., 2018; Vollenweider et al., 2019), transmitted electron microscopy was used in complement. Therefore, EM-grade fixed samples were post-fixed in buffered 2% OsO_4, dehydrated by successive baths of graded ethanol, infiltrated by series of graded propylene oxide/Epon 812 mixture (with DDSA, NMA, DMP hardener) and embedded in Epon (Moura et al., 2018). Ultra-thin sections were obtained using a Reichert UltraCut S ultra-microtome, mounted on gold grids and contrasted using saturated uranyl acetate in 50% ethanol and lead citrate. Sections were observed using a Philipps CM12 transmission electron microscope (Center for Microscopy and Image Analysis, University of Zurich).

The observed ultrastructural changes of chloroplast in response to O_3 exposure were quantified from TEM pictures using ImageJ (ver. 2.0.0; (Schindelin et al., 2012)). Measurements were repeated on ten chloroplasts distributed in 3 to 4 cells from the upper and lower palisade parenchyma (respectively UPP and LPP). They included chloroplast area (A_{chloro}) and perimeter (A_{chloro}), chloroplast major and minor axis (R_1 and R_2 respectively), and plastoglobuli and starch area.

First, chloroplast shape was estimated by calculating chloroplast circularity (Cir_{chloro}), following the formula:

$$Cir_{chloro} = \frac{A_{chloro} * 4\pi}{P_{chloro}}$$

with Cir_{chloro} as the chloroplast circularity (no units), A_{chloro} as chloroplast area (µm^2), and P_{chloro} as chloroplast perimeter (µm). The average size and shape of chloroplast was modelled through an ellipse using R_1 and R_2 respectively as major and minor radius respectively in which total plastoglobuli and grain starch area were represented as red and blue circle respectively. Elliptical representations of chloroplast were drawn using R software, version 3.5.0 (R Development Core Team, 2017) with the package Plotrix (J., 2006). Total chlorophyll content was reported to color chloroplast according to a scale from senescent leaf green to healthy mature leaf green:

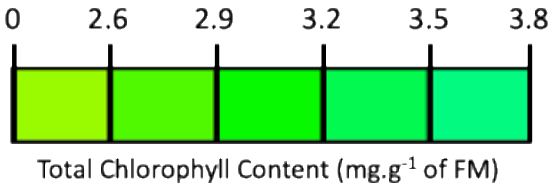

Statistical analysis

Dynamics of leaf responses (HR-like lesion and total chlorophyll content) and micromorphological changes of chloroplast in response to O_3 treatments were analyzed using linear-mixed effects model (lmem). Time or POD_0, O_3 treatment, leaf position, mesophyll layer (chloroplast micromorphological data only) and interactions were introduced in the model as fixed-effect factors. Tree nested in the chamber (leaf data; leaf position as the statistical unit), and cell nested in the tree (chloroplast micromorphological data; chloroplast as the statistical unit) were introduced in the model as random-effect factors. Statistical analysis was performed using R statistical software, version 3.5.0 (R Development Core Team, 2017), with the packages lme4 (Bates et al., 2015) for linear mixed-effects models, and emmeans (Lenth, 2016) for post- hoc testing.

Results

Dynamics of leaf responses

HR-like dynamics (Figure 1) were quite similar to the previously described at those leaf positions in this poplar (Turc et al., 2021). Indeed, at the third leaf position, a higher leaf percentage area showing non-oxidized HR-like lesion was observed in the 100 vs 80 ppb O_3 treatment, with differences becoming significant after 13 days of exposure (figure 1 and S1; O_3 treatment & O_3 treatment*Time: $P > 0.001$). Similar results were observed by comparing leaf percentage area of HR-like lesion in the 100 vs 80 ppb O_3 treatment at the tenth leaf position, although dynamic was leaf specific (figure S1; O_3 treatment*Leaf position: $P < 0.05$, O_3 treatment*Time*Leaf position: $P < 0.001$). Nevertheless, in both leaves and for the two O_3 treatment, a larger leaf percentage area showing non-oxidized vs oxidized HR-like lesion was observed (figure 1 and S1; Oxidation State: $P <0.001$; Oxidation State*Time: $P <0.001$).

Likewise, total chlorophyll content dynamics were also similar to the previously described at those leaf positions in this poplar (Turc et al., 2021). Total chlorophyll content was more reduced in the 100 vs 80 ppb O_3 treatment (figure 2A; O_3 treatment: $P < 0.001$, O_3 treatment*Time: $P < 0.001$) and this decrease occurred earlier at the third vs the tenth leaf position (figure 2A; O_3 treatment*Leaf position: $P < 0.05$). However, effect of O_3 on total chlorophyll content was observed 10 days earlier than in Turc et al. (2021), mainly due to the use of a different quantification technique (biochemical *vs.* spectral assessment).

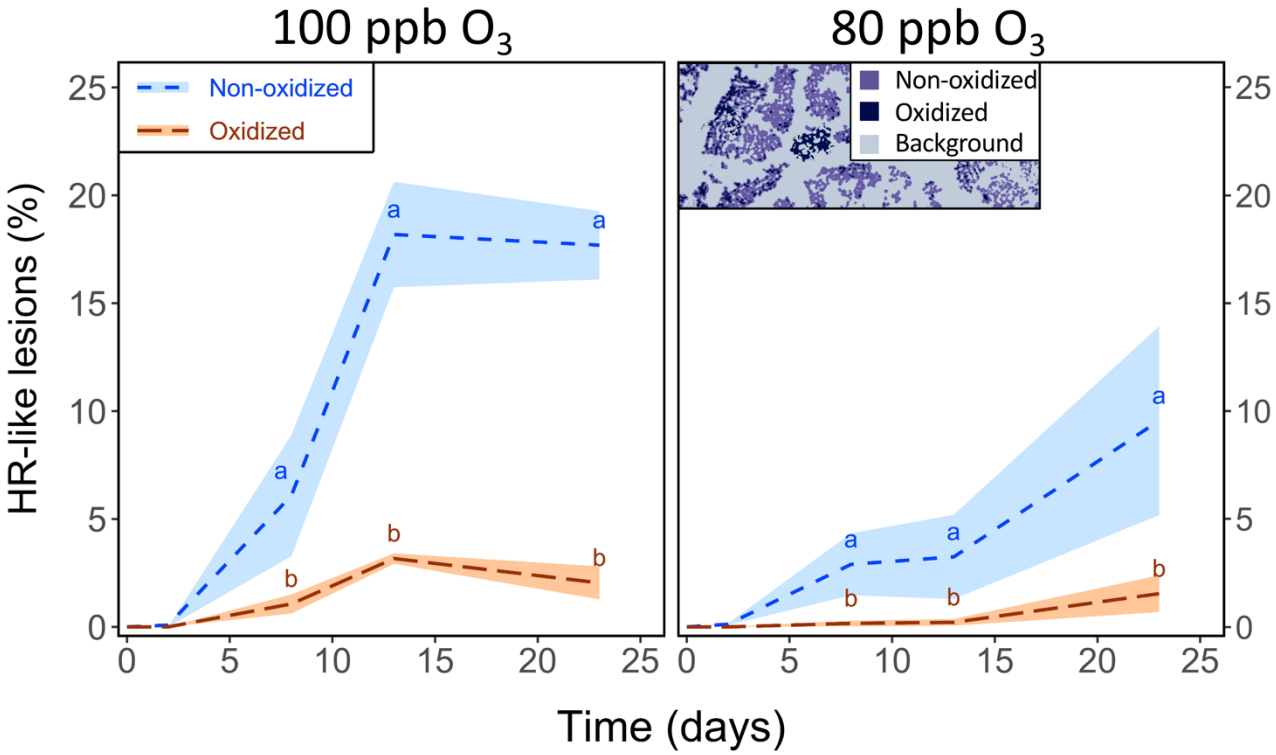

	HR-like lesions
O_3 treatment	***
Leaf Position	***
Time	***
Oxidation	***
O_3 treatment:Time	***
O_3 treatment:Leaf Position	*
O_3 treatment:Oxidation	***
Leaf Position:Time	***
Oxidation:Time	***
Oxidation:Leaf	***
O_3 treatment:Time:Leaf Position	***

Figure 1. Development dynamic of non -oxidized and oxidized HR-like lesion at the third leaf position in hybrid poplar (*Populus tremula x alba*), as a function of O_3 treatment, time of assessment and interactions {model: lmer[log(variable+1) ~ leaf position * Oxidation * Time * O_3 treatment + (1|pot)]; *** $p \leq 0.001$; * $p \leq 0.05$}. The insert shows synthetic image of HR-like injuries classification into non-oxidized and oxidized lesion groups, based on color classes. Values represent means ± SE of percentage area of leaf discs showing microscopic injury, n = 4. Different letters indicate significant differences between treatments at a given assessment date (post-hoc Tukey's honest significant difference, $p \leq 0.05$).

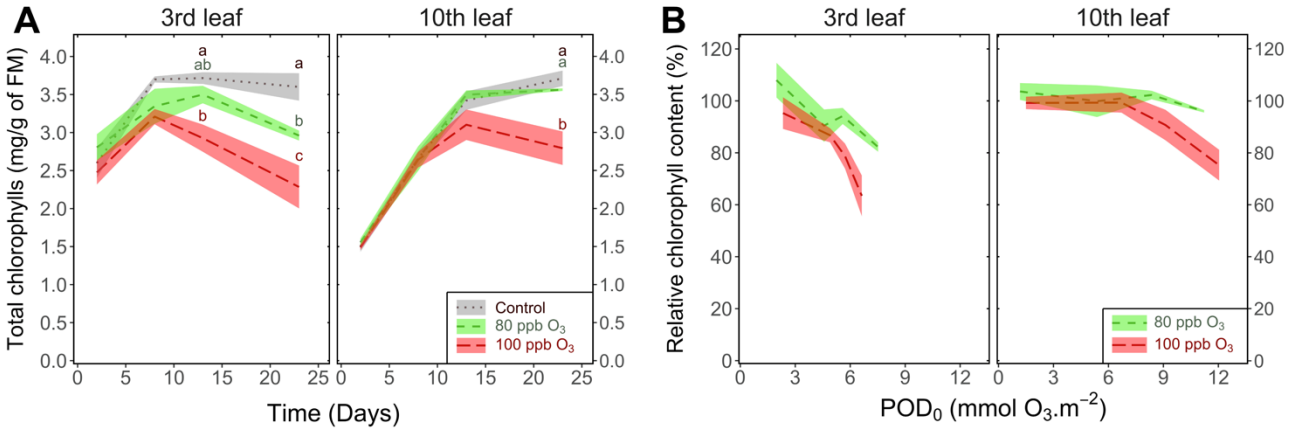

	Total chlorophyll		Relative chlorophyll content
O_3 treatment	***	O_3 treatment	ns
Leaf Position	***	Leaf Position	ns
Time	***	POD_0	***
O_3 treatment:Time	***	O_3 treatment:POD_0	ns
O_3 treatment:Leaf Position	*	O_3 treatment:Leaf Position	ns
Leaf Position:Time	***	Leaf Position:POD_0	***
O_3 treatment:Time:Leaf Position	***	O_3 treatment:POD_0:Leaf Position	ns

Figure 2. Dynamic of changes in the total chlorophyll content (mg g^{-1} of fresh matter) within hybrid poplar leaves (*Populus tremula x alba*), as a function of assessment time (**A**) and phytotoxic O_3 dose (POD_0; **B**), O_3 treatment (dotted line: charcoal-filtered air, dashed line: 80 ppb O_3, long dash line: 100 ppb O_3), leaf position and interactions (model: lmer(variable) ~ O_3 treatment * leaf position * time + (1 | tree / chamber)); *** $p \leq 0.001$, * $p \leq 0.05$, ns not significantly different). Values represent means ± SE, n = 4. Different letters indicate significant differences between treatments at a given assessment date (post-hoc TukeyHSD, $p \leq 0.05$).

Measurements of g_w allowed for POD_0 estimation. POD_0 was higher at the tenth vs third leaf position, mainly explained by a higher stomatal conductance at the tenth leaf position. However, given the lower g_w in the 100 vs 80 ppb O_3 treatment (figure S2A), POD_0 was very similar between O_3 treatment (figure S2B) at both leaf positions. Relative total chlorophyll content decreased with increasing POD_0 (Figure 2B; POD_0: P <0.001), and irrespective of the O_3 treatment (O_3 treatment: ns). The decline remained smaller and slower at the 10th leaf position, despite higher POD_0 (Leaf Position*POD_0: P < 0.001).

Based on these results, structural and ultra-structural changes related to O_3 stress were investigated in samples from the 100 ppb O_3 treatment after 8, 13 and 23 days of exposure. Evolution of structural leaf features without O_3 treatment were observed in samples from CF treatment after 8 and 23 days of exposure. Samples from the 80 ppb O_3 treatment were observed after 13 days of exposure, as an intermediate between the 100 ppb O_3 and CF treatment.

Structural ontology of HR-like lesion was not related to O_3 exposure or leaf position

HR-like lesions were observed earlier and mainly in the lower palisade parenchyma, probably as a consequence of missing photooxidative stress and a larger influx of the pollutant through the lower epidermis. Event sequence of ultra-structural changes related to HR-like lesion was the same under the both exposition dose (100 or 80 ppb) or relative to the leaf position (the third or tenth). This sequence started with cell death as indicated by vacuole segmentation and shrinkage, and by tonoplast and plasmalemma rupture before the observation of structural changes in organelles (figures 3E-F; Table 1). Cell content continued to evolve despite cell death. In a later ontological stage, cellular material disruption was indicated by incomplete degradation of organelles (figures 3G, G'; Table 1). Mitochondrial matrix and membrane were degraded, and sometimes associated with a membrane rupture (figures 3H; Table 1), nucleus was deformed and condensed (figure 3I; Table 1), and chloroplast thylakoid were disassembled (figure 3J; Table 1). Degraded cellular material leaking into apoplast through cell wall rupture was observed (figures 3K,K'; Table 1). The final ontological evolution of cell content disruption was indicated by the complete degradation of cellular material (figures 3L-N; Table 1). The remnant cellular content was dense, homogenous, completely fused and only starch grain remained visible (figures 3M,N). Healthy adjacent cells showed local cell wall thickening by callose deposition between plasma membrane and cell wall at the contact point with dead cells (figures 3O,P; Table 1).

Table 1. Structural and ultrastructural markers of O_3 stress observed within the leaf mesophyll of hybrid poplar leaves (*Populus x tremula alba*) during the O_3 exposure.

Compartment	Structural marker	Physiological process	Experimental factors								Observation (Fig.)
		Treatment	*100 ppb O_3*						*80 ppb O_3*		
		Leaf position	*3rd*			*10th*			*3rd*	*10th*	
		Exposure (days)	*8*	*13*	*23*	*8*	*13*	*23*	*13*	*13*	
Leaf blade	Leakage of cellular material into apoplast	HR-like	+	-	-	-	+	-	-	-	3M
Cell	Cytorrhisis	HR-like	-	+	+	-	+	+	+	-	3G,N
	Rupture of cell wall	HR-like	-	+	+	-	+	+	-	-	3M'
Disruption of cell content											
	Rupture of membrane (plasmalemma and tonoplast)	HR-like	-	+	+	-	+	+	+	-	3E-F
	Disruption of organelles	HR-like	-	+	+	-	+	+	-	-	3H-L
	Condensation of cellular debris	HR-like	-	+	+	-	+	+	+	-	3O,P
Cell wall thickening											
	Wart-like protrusion	Oxidative stress	-	-	+	-	-	+	-	-	Not shown
	Discharge of autophagic vacuoles	ACS	-	-	+	-	-	-	-	-	5F
	Cell wall synthesis	Leaf ontology	-	+	+	+	+	+	-	-	5A-D, 5G-J
	Callose deposition	HR-like	-	+	+	-	-	+	-	-	3Q,R
Cytoplasm	Autophagy	ACS	-	-	+	-	-	-	-	-	5E,F,K
	Condensation	ACS	-	+	+	-	+	+	-	-	4P
Vacuole	Size increase	ACS	-	+	+	-		+	+	-	4Q vs 4G
	Collapse	HR-like	-	+	+	-	+	+	+	-	3E,E'
	Accumulation of secondary product in the vacuole	Oxidative stress and ACS	-	+	+	-	-	+	-	-	4P
Nucleus	Picnosis	HR-like	-	+	-	-	-	-	-	-	3K
	Condensation	ACS		-	+	-	-	+	-	-	Not Shown
Chloroplast	Size decrease	ACS	-	+	+	-	-	+	-	-	6
	Increase in size and density of plastoglobuli	ACS	-	+	+	-	+	+	+	-	4S vs 4H
	Higher circularity	ACS	-	-	+	-	-	+	-	-	6
	Disruption	HR-like	-	+	+	-	+	+	+	-	4T
Mitochondria	Disruption	Oxidative stress	-	+	+	-	+	+	+	+	3K

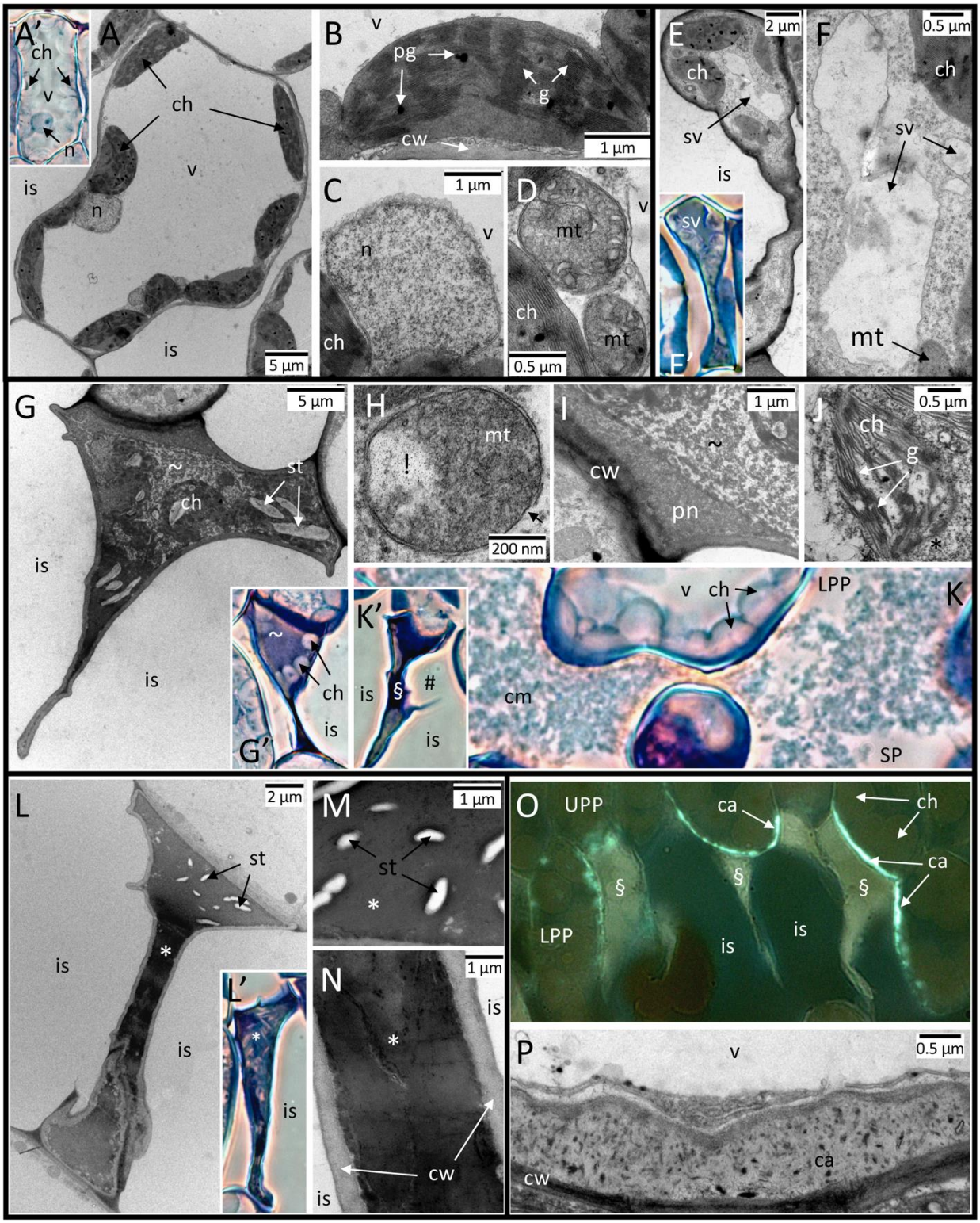

Figure 3. Evolution of structural and ultrastructural traits in HR-like lesions, as observed in hybrid poplar leaves (*Populus tremula x alba*) from the two O_3 treatments (80 and 100 ppb O_3). Asymptomatic samples from CF treatment (**A**-**D**). First stage of HR-like lesion (**E**-**F**): vacuole was shrunken (sv) but chloroplast (ch) and mitochondria (mt) were not affected. Intermediate stage of HR-like lesion (**G**-**K'**): cell was cytorrhyzed and partially decompartimented (~, **G**,**G'**) with disruption of cell content, as indicated by degradation of mitochondrial matrix (!, **H**) and membrane (arrow, **H**), pynotic nucleus (pn, **I**), and chloroplast (ch) degradation (**J**). Some cellular material leaked into apoplast (cm, **K**) through rupture of cell wall (#, **K'**). Final stage of HR-like lesion (**L**-**N**): cellular content was completely fused, extremely dense (*) and only

starch grain (st) were visible. **O**-**P** Local thickening of cell wall (cw) by callose deposition (ca) was observed in healthy cell adjacent to collapsed cell (§). Other structures: g: grana, is: intercellular space, LPP: lower palisade parenchyma, n: nucleus, UPP: upper palisade parenchyma, v: vacuole. Technical specifications: postfixation using OsO4, contrasting using uranyl acetate and lead citrate, observation in TEM (A, B-E, F-H, I-L, N, O, P, R); staining with Toluidine blue and observation under phase contrast in bright field microscopy (E', H', M', N'); staining with Aniline blue and observation in fluorescence microscopy (Q).

Dynamic of structural and ultra-structural changes related to ACS

Structural and ultra-structural markers of senescence were observed in response to O_3 treatment (80 and 100 ppb) at both leaf position (third and tenth). They included an increase of the vacuole size (figures 4A,B vs 4F,G and figures 4K,L vs 4P-Q; Table 1), a decrease of nuclei activity indicated by nucleoli loss (figures 4D,I vs 4N,S), an accumulation of secondary metabolism products in vacuole (figure 4P vs F; Table 1) and a disruption of chloroplast grana (figure 4J vs 4T; Table 1) in relation to an apparent increase in number and size of plastoglobuli (figure 4D vs 4J and figure 4M vs figure 4R; Table 1).

Despite a majority of similar structural and ultrastructural changes, some differences were noticed between leaf position. Cell wall reinforcement activity was observed mainly at the tenth vs third leaf position, as indicated by an accumulation of mitochondria, dictyosome with secreted vesicles trafficking to RER toward cell wall and apparent microfibers of cellulose between cell wall and membrane (figures 5A-E; Table 1). By contrast, autophagic activity was observed mostly at the third leaf position in the 100 ppb O_3 treatment (Table 1). Vesicular bodies, full of degraded cellular material, were discharged in the periplasm by exocytosis (figure 5F,G; Table 1).

Moreover, the dynamics of senescence markers differed according both O_3 treatment and leaf position. They appeared earlier in the 100 vs 80 ppb O_3 treatment and at the third vs tenth leaf position, concomitantly with total chlorophyll content decrease (Table 1).

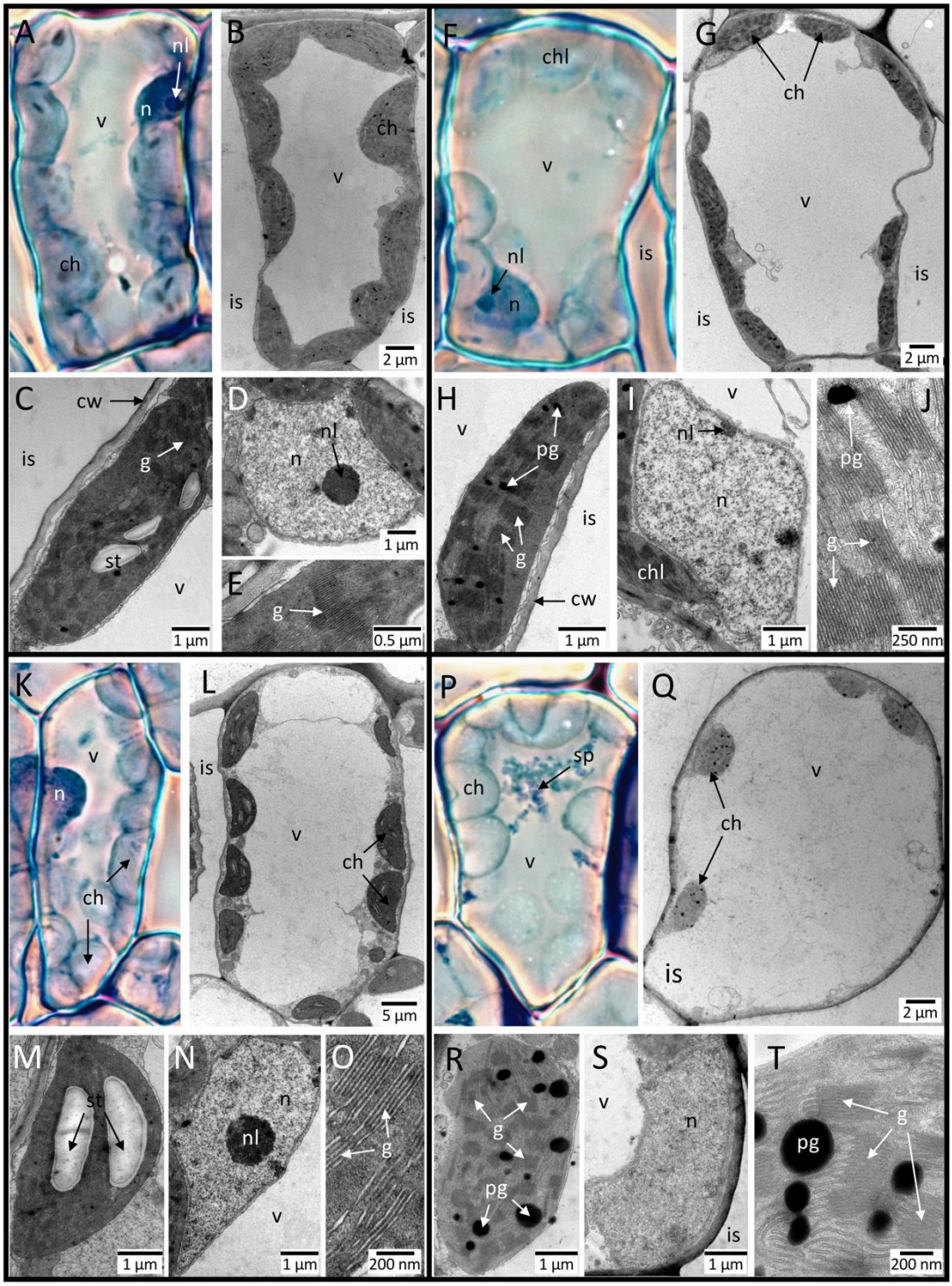

Figure 4. Degenerative structural and ultrastructural traits observed in the mesophyll of leaves at the third position from hybrid poplar trees (*Populus tremula x alba*) in the 100 ppb O_3 treatment, with increasing exposure duration. Asymptomatic samples from CF treatment after 8 (**A**-**E**) and 23 days (**F**-**J**) vs. O_3-exposed leaves after 8 (**K**-**O**) and 23 days (**P**-**T**). At cellular level, senescence was indicated by an increase in vacuole (v) size, reduction in chloroplast (ch) number and accumulation of secondary product (sp) in vacuole (**F**,**G** vs. **P,Q**). At subcellular level, chloroplast were disrupted as indicated by poor resolution of grana (g) and larger plastoglobuli (**H**,**J** vs. **R**,**T**). Decrease in nucleus (n) activity was indicated by the loss of nucleoli (nl) (**N** vs **S** and **D** vs **I**). Other structure: cw: cell wall, is: intercellular space; st: starch grain. Technical specifications: postfixation using OsO_4, contrasting using uranyl acetate and lead citrate, observation in TEM (**B**, **C**-**E**, **G**-**J**, **L**-**O**, **Q**-**T**); staining with Toluidine blue, observation under phase contrast in bright field microscopy (**A**, **F**, **K**, **P**).

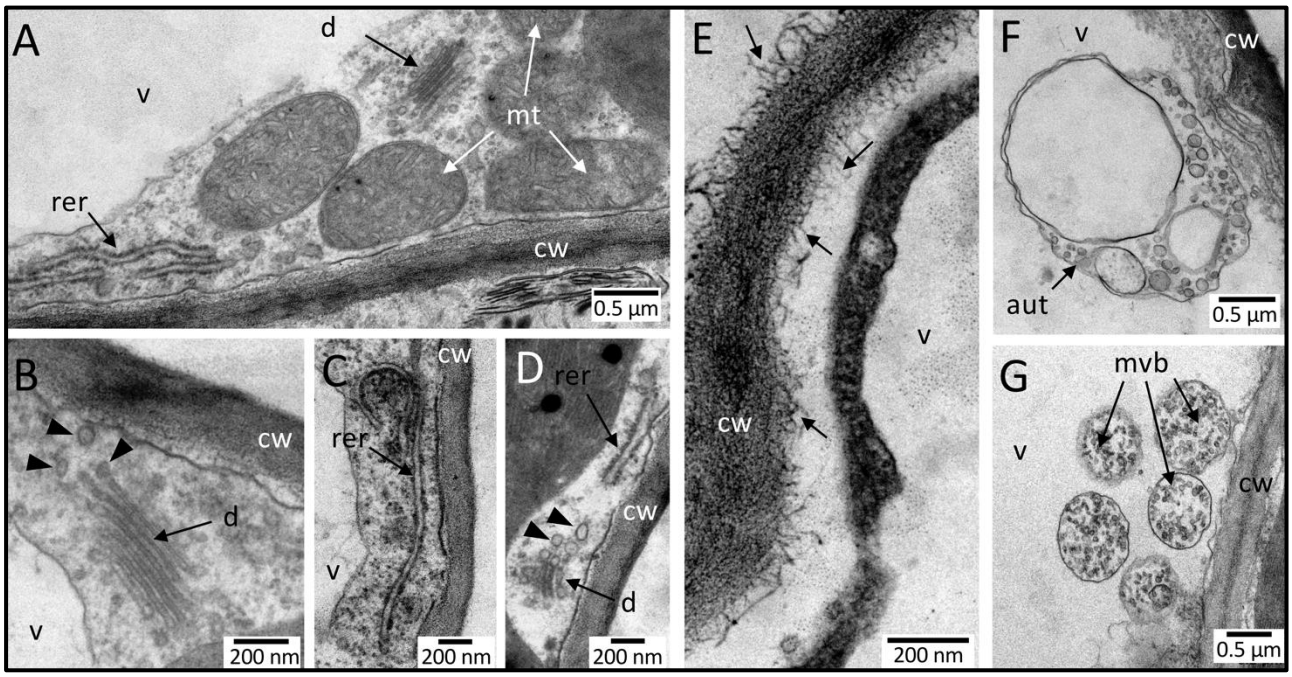

Figure 5. Ultrastructural trait differences observed in hybrid poplar leaves (*Populus tremula x alba*) at the tenth (**A**-**E**) and third position (**F**,**G**) from the 100 ppb O_3 treatment. (**A**-**E**) Enhanced cell wall reinforcement activity at the tenth vs third leaf position was indicated by a higher accumulation of mitochondria (mt), dictyosome (d) secreting vesicles (arrow head, **B,D**), and rough endoplasmic reticulum (rer, **C**) toward cell wall (cw). (**E**) Cellulose microfibiers (arrow) were observed in periplasm. (**F**,**G**) Larger and more numerous autophagic vesicles (aut) were observed at the third leaf position. The resulting multivesicular bodies (mvb, **G**) were observed only at the third leaf position, and excreted by exocytosis (**G**). Other structure: is: intercellular space, v: vacuole. Technical specifications: postfixation using OsO_4, contrasting using uranyl acetate and lead citrate, observation in TEM.

Close dependency between dynamics of structural chloroplast-related changes and both O_3 treatment and leaf position was shown by quantitative analysis of chloroplast features. Chloroplast features were measured after 8, 13 and 23 days of exposure in the 100 ppb O_3 treatment, after 8 and 23 days in the CF treatment (figure 6), and after 13 days in the 80 ppb O_3 treatment (figure S2). Chloroplast size, chloroplast circularity, grain starch and total plastoglobuli area were all affected by O_3 exposure. Chloroplast size and starch grain area were impacted early by O_3 treatment, as significant effect was observed after 13 (figure S3; O_3 treatment: $P < 0.001$), but not after 23 days of O_3 treatment, indicative of an acceleration of ontological-related changes. By contrast, chloroplast circularity and total plastoglobuli area increased in response to O_3 exposure (figure 6 and S3; O_3 treatment: $P < 0.001$). By the end of

exposure, plastoglobuli area was 10-fold higher, and chloroplast circularity was increased by 40%, in the 100 ppb O_3 vs CF treatment at both leaf position (figure 6, O_3 treatment*Time: $P < 0.001$, Table S1A). Dynamics of O_3 impact on chloroplast were depending on leaf ontology (figure 6 and S3, Leaf Position: $P < 0.01$), with earlier effect observed at the third vs tenth leaf position (Table S1A). Finally, dynamic of chloroplast-related changes in response to O_3 exposure were also depending on the mesophyll layer as O_3 treatment seemed to impact more the lower vs upper palisade parenchyma (figure 6 and S3, Mesophyll Layer: $P < 0.05$), indicative the absence of photooxidative stress.

Only relative plastoglobuli area and chloroplast circularity were related to POD_0, and both increased with POD_0 (figure 6, POD_0: $P < 0.001$), although plastoglobuli area increased for a lower POD_0 (figure S3, POD_0: $P < 0.001$) than chloroplast circularity (figure S3, POD_0: ns). Nevertheless, relative plastoglobuli area and chloroplast circularity increased at a lower O_3 threshold at the third vs the tenth leaf position (figure 6; Leaf Position:POD_0: $P < 0.001$).

Discussion

Contrast between HR-like and ACS

The structural and ultrastructural changes of HR-like and ACS resulting of O_3 exposure showed contrasted dynamic. Typical HR-like markers were detected in the lesions and included cytorrhysis, disruption of organelles, complete and incomplete degradation of cellular material (Table 1, (Feng et al., 2016; Moura et al., 2018; Vollenweider et al., 2019)). Similar to (Turc et al., 2021), HR-like lesion showed sigmoidal-like dynamic in older foliage, and were detected in two oxidation states (i.e. non-oxidized and oxidized). Structural and ultrastructural investigation showed post-mortem evolution of cellular content, confirming that non-oxidized and oxidized lesions correspond to two stages of HR-like reactions, as previously suggested (Turc et al., 2021). The smaller area of oxidized vs non-oxidized HR-like lesion, as well as the final state of cellular material (homogenous and dense) supports this idea. The post-mortem evolution of cell content suggests that this process was not under biological control. Moreover, opposite to HR-like lesions, ACS-related changes occurred much prior to cell death.

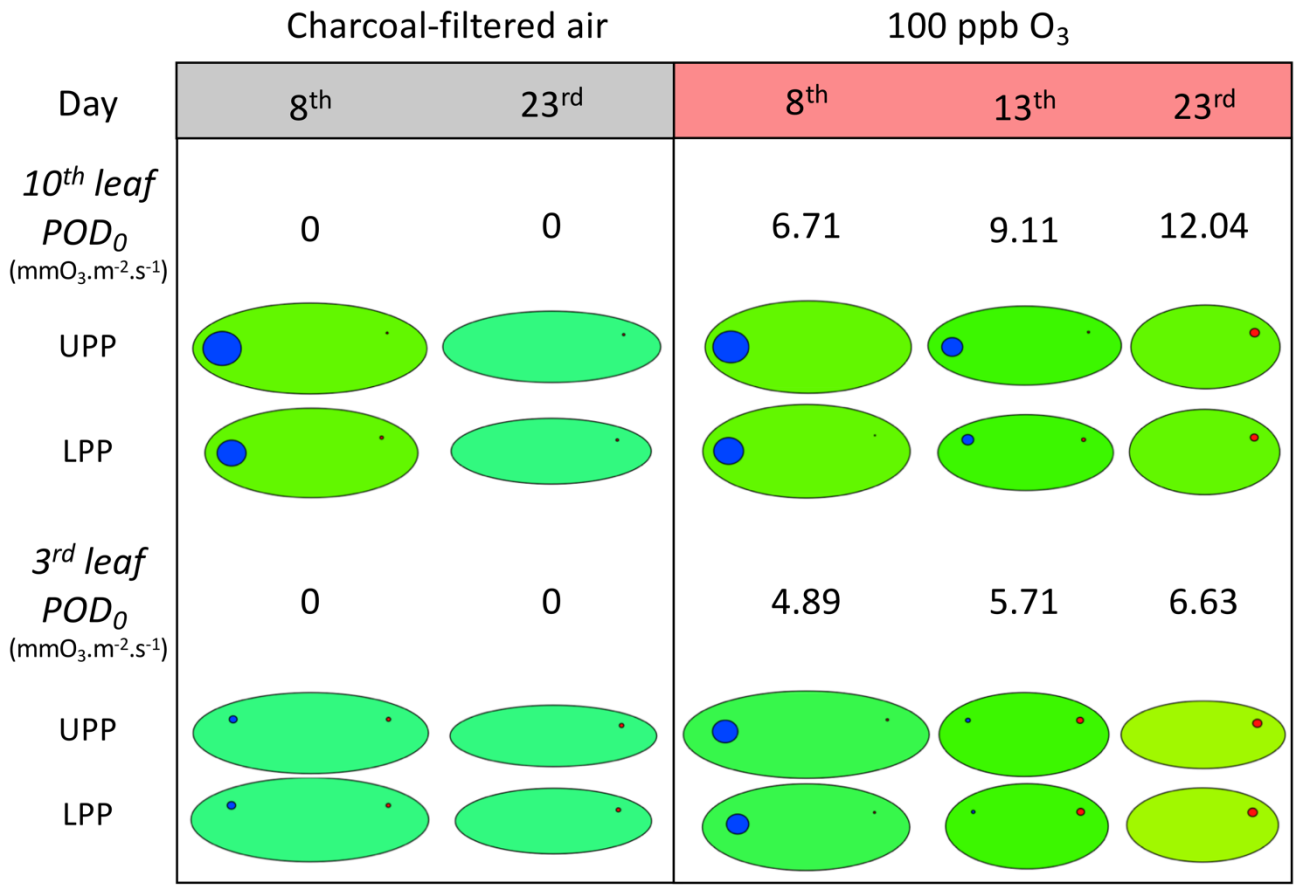

	Chloroplast Size	Chloroplast Circularity	Starch Grain Area	Total Plastoglobuli Area
O_3 treatment	ns	***	ns	***
Leaf Position	ns	***	***	***
Time	***	ns	***	***
Mesophyll Layer	ns	***	***	ns
O_3 treatment:Time	ns	***	ns	***
O_3 treatment:Leaf position	ns	*	ns	***
Leaf Position:Time	ns	ns	**	ns
Leaf position:Mesophyll Layer	ns	**	***	ns
Mesophyll Layer:Time	ns	ns	***	ns

	Relative Chloroplast Size	Relative Chloroplast Circularity	Relative Grain Starch Area	Relative Total Plastoglobuli Area
O_3 treatment	ns	***	ns	***
Leaf Position	ns	**	ns	ns
POD_0	ns	***	ns	***
Mesophyll Layer	ns	ns	ns	ns
O_3 treatment:POD_0	ns	ns	ns	ns
O_3 treatment:Leaf Position	ns	ns	ns	ns
Leaf Position:POD_0	ns	**	ns	**
Mesophyll Layer:Leaf Position	ns	ns	ns	ns
Mesophyll Layer:POD_0	ns	ns	ns	ns

Figure 6. Dynamics of size and shape changes for chloroplast traits as a function of O_3 treatment, leaf position, assessment time or POD_0, mesophyll layer and interactions, as observed in the leaf mesophyll of hybrid poplar trees (*Populus tremula x alba*; model: lmer(variable ~ O_3 treatment * leaf position * time + (1 | cell /tree)); *** $p \leq 0.001$, * $p \leq 0.05$, ns not significantly different). Green ellipse: chloroplast relative size and shape, blue circle: total starch grain area, red circle: total plastoglobuli area. Changes in the chloroplast green shade are graded according to decrease in the total chlorophyll content ($mg.g^{-1}$ of FM).

Reduction of total chlorophyll content is a well-known O_3 effect on leaf physiology (Reich, 1983; Bagard et al., 2015; Dusart et al., 2019) indicative of ACS, together with other degenerative markers including increase in vacuole size and chloroplast-related changes (Table 1; (Mikkelsen and HeideJorgensen, 1996; Moura et al., 2018). Consistent with the previously described ACS dynamic as monotonic, relative loss of chlorophyll content and intensity of ACS-related changes were both progressively higher with increasing exposure time and POD_0. Quantification of chloroplast features showed close relation with O_3 treatment, leaf position and POD_0, especially changes in shape likely explained by thylakoid breakdown, indicated by apparent increase in size and number of plastoglobuli (Lichtenthaler, 2013).

During biotic stress, a first apoplastic ROS accumulation mediated by NADPH oxidase following pathogen recognition induced hypersensitive response (HR) in cell (Jwa and Hwang, 2017). Given the close similarities already observed between HR and HR-like (Vollenweider et al., 2002; Bhattacharjee, 2005; Günthardt-Goerg and Vollenweider, 2007; Moura et al., 2018), our results may suggest that apoplastic accumulation of O_3-induced ROS could mimic the one induced by NADPH oxidase and trigger HR-like reaction. Supporting this idea, callose deposition between plasma membrane and cell wall was observed in healthy cell adjacent to HR-like lesion, as commonly observed in case of pathogen intrusion (Wang et al., 2021). In this case, callose deposition have several roles including strengthening of the cell wall and restrict the ingression of pathogen-secreted cell wall-degrading enzymes, in order to limit spread of pathogen-induced damage. Callose deposition following O_3 exposure have been widely documented (Vollenweider et al., 2002; Paoletti et al., 2009; Feng et al., 2016), however, according to our knowledge, this is the first time callose deposition was clearly observed between the plasma membrane and cell wall of healthy adjacent cell in case of O_3 treatment. It is well known that salicylic acid (SA) and jasmonic acid (JA) respectively promotes and limits cell death (Kangasjarvi et al., 2005). Since callose deposition is enhanced by SA and suppressed by JA in case of biotic stress (Yi et al., 2014), our results suggest that callose deposition under O_3 treatment would be a consequence of SA, and JA could limit callose deposition around necrotic sites.

During autumnal senescence, the chloroplast has a central place since a decrease in its antioxidant capacity leads to an increase of photosynthesis-induced ROS which triggers the senescence process (Mayta et al., 2019). Therefore, O_3-

induced ROS may contribute to accelerate cell senescence by increasing oxidant stress in chloroplast and thus triggering senescence processes. The earlier observation of ACS vs HR-like reaction in field and high illumination condition (Vollenweider et al., 2019) linked to a synergism between photooxidant and oxidant stress supports this idea as photooxidant stress was missing under our experimental conditions of O_3 exposure.

Hence, a distinct spatial accumulation of ROS (apoplastic vs. chloroplastic) could explain the distinct dynamics and mechanisms of the HR-like and ACS reactions in response to O_3 exposure.

Leaf differences

Reduction in total chlorophyll content, emergence of HR-like lesion and ACS-related microscopic changes occurred later and for a larger POD_0 at the tenth vs third leaf position. This is consistent with higher tolerance of maturing leaves previously reported (Paakkonen et al., 1996; Strohm et al., 2002; Turc et al., 2021), and structural contrast were observed in young vs old foliage. Although observed at both leaf position, cell wall thickening activity was higher at the tenth vs third leaf position, mainly explained by leaf ontology differences. Indeed, during leaf expansion and cell growth of young foliage, cell wall is tightly modeled by cell wall protein to allow cell expansion and may contribute to adaptation of their changing environment (Knox, 2008). Moreover, cell expansion implied tight transcriptional regulation of ROS homeostasis (Mangano et al., 2016; Schmidt et al., 2016) thus helping to cope with accumulation of O_3-induced ROS, at least during cell growth.

Sink-to-source transition is accompanied by an increase in stress susceptibility (Coleman, 1986) and was previously proposed as an explanation of the higher O_3 tolerance of young vs old foliage (Turc et al., 2021). Supporting this idea, ACS-related microscopic changes were observed in maturing foliage once sink-to-source transition was achieved (indicated by total chlorophyll content and stomatal conductance). Therefore, our results strongly suggest that ACS was trigger by O_3-induced ROS once photosynthetic apparatus was fully developed and functional, thus increasing photosynthesis-derived ROS and subsequent oxidative stress in chloroplast.

Dynamics of HR-like and ACS microscopic changes in relation to O_3 uptake

Microscopic investigations of O_3 stress markers in forest can be useful to ascertain adverse effect of O_3 in foliage, and can relate on the experienced O_3 dose (Vollenweider et al., 2019). In our study, HR-like lesions were detected in two different oxidations states (non-oxidized vs oxidized) and this change in oxidation sate contribute to visible injury appearance. Indeed, they emerge when oxidized lesions are sufficiently frequent to be detected at the leaf scale with naked eye as non-oxidized lesions (even in large group) are invisible at leaf scale (Turc et al., 2021). Therefore, survey of visible injury resulting from HR-like reaction in order to assess O_3 stress in forest is good because specific to O_3 response, however, it obviously lacks of sensibility which consequently lead to an underestimation of adverse effect of O_3 in foliage.

Although typical of O_3 stress, ACS related changes are not used in risk assessment, mainly due to their lack of specificity to O_3 response, making it more complicated to use in semi-natural vegetation. However, in our study dynamics of ACS-related changes was closely related to POD_0, with decrease in chloroplast size occurring before the increase in plastoglobuli and subsequent shape changing. Therefore, assessment of O_3 stress using microscopic validation can consider chloroplast-related changes as an indication of O_3 uptake by the leaf, by comparison with asymptomatic material. Nevertheless, giving the synergism between photooxidant and oxidant stress, particular attention should be paid to illumination condition of foliage.

Supplemental material

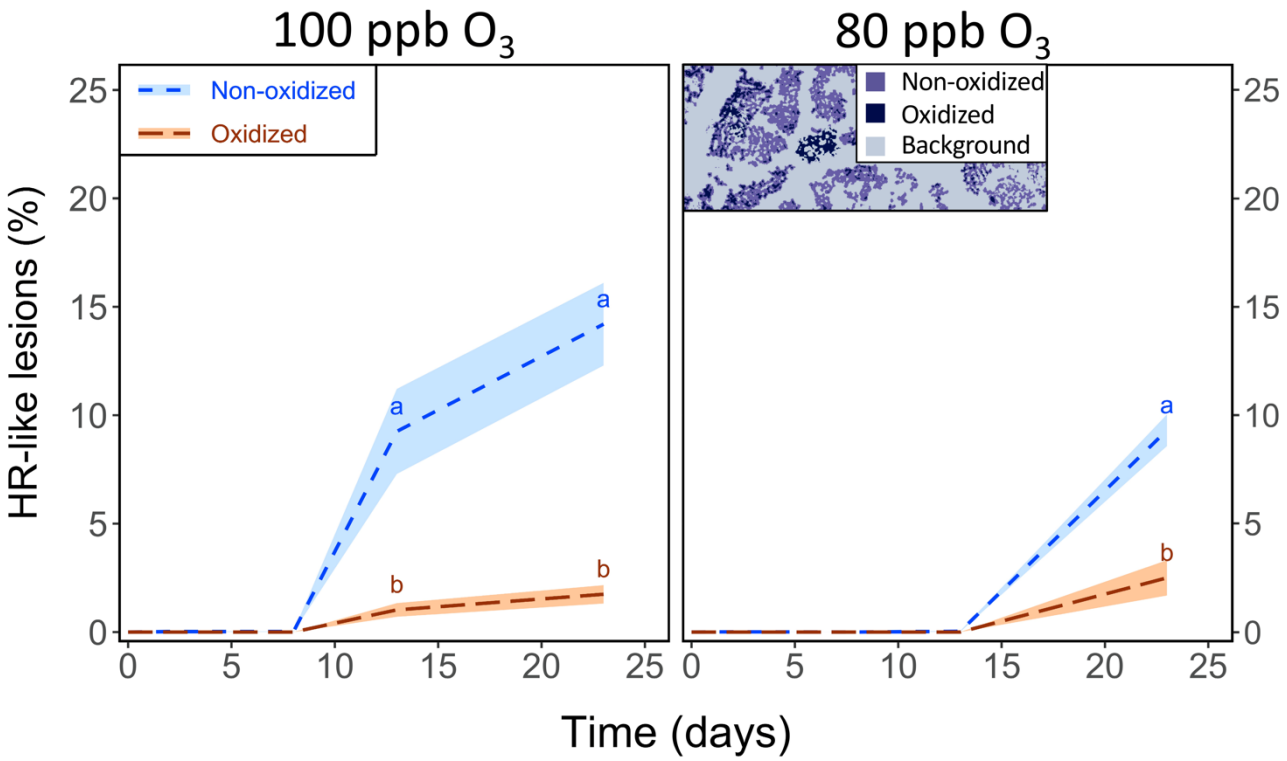

	HR-like lesions
O_3 treatment	***
Leaf Position	***
Time	***
Oxidation	***
O_3 treatment:Time	***
O_3 treatment:Leaf Position	*
O_3 treatment:Oxidation	***
Leaf Position:Time	***
Oxidation:Time	***
Oxidation:Leaf	***
O_3 treatment:Time:Leaf Position	***

Figure S1. Development dynamic of non -oxidized and oxidized HR-like lesion at the tenth leaf position in hybrid poplar (*Populus tremula x alba*), as a function of O_3 treatment and time of assessment and interactions {model: lmer[log(variable+1) ~ leaf position * Oxidation * Time * O_3 treatment + (1|pot)]; *** $p \leq 0.001$; * $p \leq 0.05$}.}. The insert shows synthetic image of HR-like injuries classification into non-oxidized and oxidized lesion groups, based on color classes. Values represent means ± SE of percentage area of leaf discs showing microscopic injury, n = 4. Different letters indicate significant differences between treatments at a given assessment date (Tukey's post-hoc test, $p \leq 0.05$).

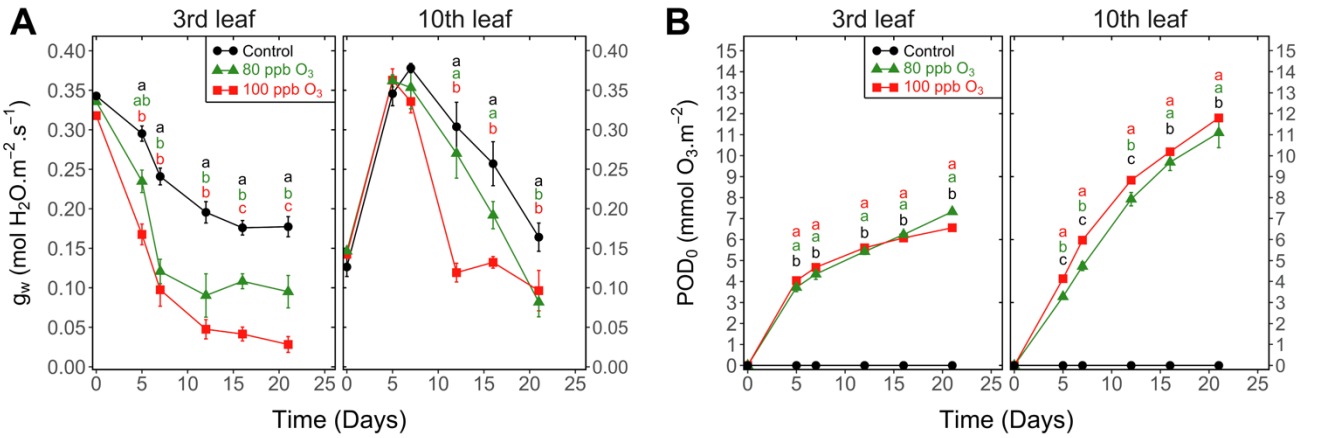

	G_w		POD_0
O_3 treatment	***	O_3 treatment	***
Leaf Position	***	Leaf Position	***
Time	***	Time	***
O_3 treatment:Time	***	O_3 treatment:Time	***
Leaf Position:Time	***	Leaf Position:Time	****
O_3 treatment:Leaf Position	***	O_3 treatment:Leaf Position	***
O_3 treatment:Leaf Position:Time	***	O_3 treatment:Leaf Position:Time	***

Figure S2. Dynamics of changes in the (**A**) stomatal conductance to water (g_w) and (**B**) phytotoxic O_3 dose (POD_0) of hybrid poplar leaves (*Populus tremula x alba*), as a function of O_3 treatment (charcoal-filtered air ●, 80 ppb O_3 ▲, 100 ppb O_3 ■), leaf position, time of assessment and interactions {model: lmer[sqrt(variable)] ~ O_3 treatment ∗ leaf position ∗ time + (1 | tree / chamber); *** $p \leq 0.001$}. Values represent means ± SE, n = 4. Different letters indicate significant differences between treatments for a given assessment date (Tukey's post-hoc test, $p \leq 0.05$).

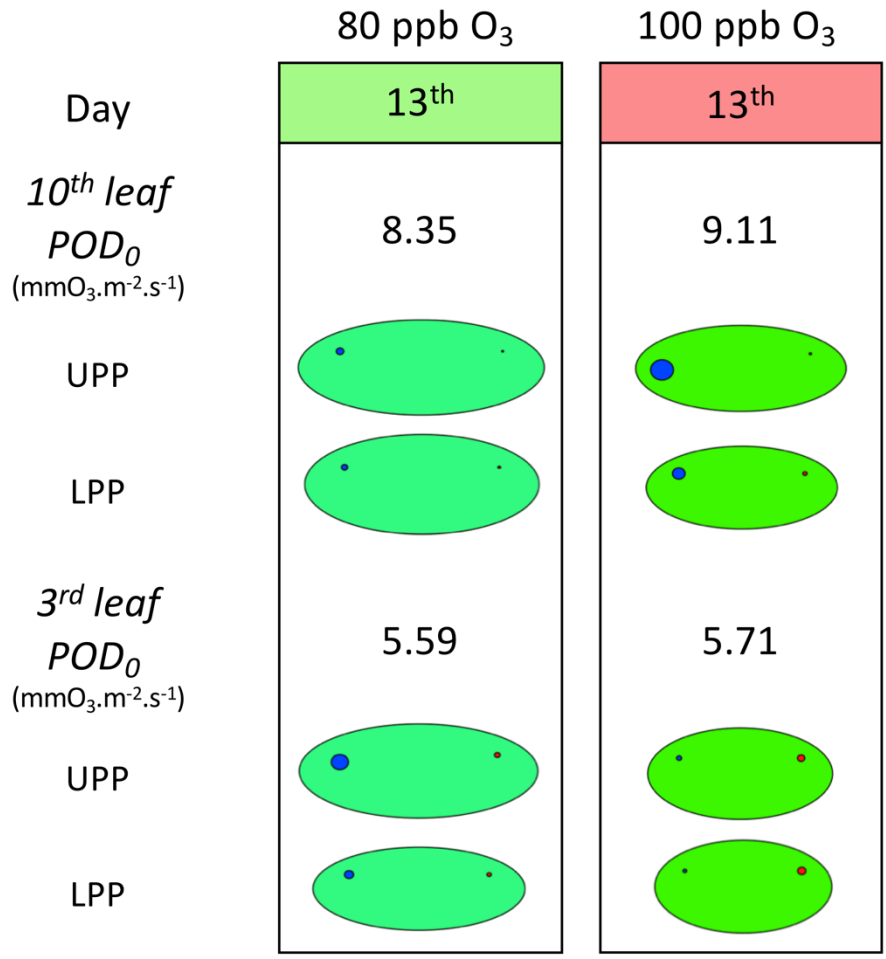

	Chloroplast Size	Chloroplast Circularity	Grain Starch Area	Total Plastoglobuli Area
O_3 treatment	***	ns	***	***
Leaf Position	**	ns	***	ns
POD_0	ns	ns	***	***
Mesophyll Layer	*	ns	***	ns
Leaf Position:POD_0	ns	ns	ns	ns
Leaf Position:Mesophyll Layer:	ns	ns	***	ns
O_3 treatment:Mesophyll Layer	ns	ns	***	ns
POD_0:Mesophyll Layer:	ns	ns	***	ns

Figure S3. Dynamics of size and shape changes for chloroplast traits as a function of O_3 treatment, leaf position, POD_0, mesophyll layer and interactions, as observed in the leaf mesophyll of hybrid poplar trees (*Populus tremula x alba*; model: lmer(variable ~ O_3 treatment * leaf position * POD_0 + (1 | cell /tree)); *** $p \leq 0.001$, * $p \leq 0.05$, ns not significantly different). Green ellipse: chloroplast, blue circle: total starch grain area, red circle: total plastoglobuli area. Green shade represent total chlorophyll content ($mg.g^{-1}$ of FM).

Table S1. Micromorphological changes observed in chloroplasts from the leaf mesophyll of hybrid poplar leaves (*Populus tremula x alba*), in response to O_3 treatment and as a function of the leaf position, assessment time or POD_0 and mesophyll layer. A, B Trait values in the 100 ppb O_3 and charcoal-filtered air (**A**), 80 and 100 ppb O_3 (B), treatment 8, 13 and 23 (A) or 13 (**B**) days after starting the exposure. Model: lmer(variable ~ O_3 treatment * leaf position * time + (1 | cell /tree)); *** $p \leq 0.001$, * $p \leq 0.05$, ns not significantly different). Values represent mean ± SE, $n = 4$. Different letters indicate significant differences between treatments for a given assessment date (Tukey- s post-hoc test, $p \leq 0.05$).

A

Leaf Position	*Mesophyll Layer*	***Chloroplast area (µm²)***					***Chloroplast circularity (µm²)***				
		Charcoal-filtered air		100 ppb O_3			Charcoal-filtered air		100 ppb O_3		
		8 days	*23 days*	*8 days*	*13 days*	*23 days*	*8 days*	*23 days*	*8 days*	*13 days*	*23 days*
10th leaf	UPP	14.67 ±0.86 a	10.78 ±0.72 a	13.86 ±0.68 a	10.70 ±0.63 a	9.04 ±0.61 a	0.62 ±0.01 abc	0.57 ±0.01 ab	0.69 ±0.02 c	0.73 ±0.02 ab	0.77 ±0.02 cd
	LPP	12.97 ±0.61 a	8.75 ±0.47 a	13.74 ±0.53 a	9.30 ±0.71 a	9.35 ±0.60 a	0.63 ±0.02 abc	0.54 ±0.02 ab	0.71 ±0.02 c	0.72 ±0.03 ab	0.79 ±0.02 cd
3rd leaf	UPP	12.71 ±0.88 a	8.84 ±0.51 a	14.07 ±1.11 a	10.18 ±0.53 a	8.07 ±0.63 a	0.55 ±0.02 ab	0.53 ±0.02 a	0.54 ±0.04 a	0.65 ±0.03 ab	0.68 ±0.02 bc
	LPP	13.54 ±0.81 a	8.97 ±0.39 a	11.91 ±0.55 a	9.93 ±0.73 a	8.11 ±0.43 a	0.60 ±0.03 abc	0.57 ±0.02 ab	0.63 ±0.03 bc	0.64 ±0.02 ab	0.73 ±0.02 d

Leaf Position	*Mesophyll Layer*	***Starch grain area (µm²)***					***Total plastoglobuli area (µm²)***				
		Charcoal-filtered air		100 ppb O_3			Charcoal-filtered air		100 ppb O_3		
		8 days	*23 days*	*8 days*	*13 days*	*23 days*	*8 days*	*23 days*	*8 days*	*13 days*	*23 days*
10th leaf	UPP	3.84 ±0.39 bd	0.00 ±0 a	3.39 ±0.31 cd	1.16 ±0.17 cd	0.00 ±0 a	0.01 ±0.004 ab	0.02 ±0.004 a	0.00 ±0.0007 a	0.01 ±0.004 abc	0.23 ±0.03 b
	LPP	2.21 ±0.29 ac	0.00 ±0 a	2.36 ±0.33 ab	0.35 ±0.09 ab	0.00 ±0 a	0.03 ±0.005 abc	0.02 ±0.005 a	0.00 ±0.002 ab	0.04 ±0.005 def	0.16 ±0.02 b
3rd leaf	UPP	0.16 ±0.06 a	0.00 ±0 a	1.70 ±0.47 abcd	0.06 ±0.04 abcd	0.00 ±0 a	0.05 ±0.007 bc	0.05 ±0.008 a	0.02 ±0.01 ab	0.12 ±0.015 def	0.22 ±0.04 b
	LPP	0.19 ±0.07 a	0.00 ±0 a	1.32 ±0.3 ab	0.03 ±0.03 abcd	0.00 ±0 a	0.05 ±0.01 c	0.05 ±0.007 a	0.01 ±0.004 ab	0.15 ±0.016 ghi	0.23 ±0.02 b

B

Leaf Position	*Mesophyll Layer*	***Chloroplast area (µm²)***		***Chloroplast circularity (µm²)***		***Starch grain area (µm²)***		***Total plastoglobuli area (µm²)***		***Starch grain area (µm²)***		***Total plastoglobuli area (µm²)***	
		80 ppb O_3	100 ppb O_3	80 ppb O_3	100 ppb O_3	80 ppb O_3	100 ppb O_3	80 ppb O_3	100 ppb O_3	80 ppb O3	100 ppb O3	80 ppb O3	100 ppb O3
		13 days	*13 days*	*13 days*	*13 days*	*13 days*	*13 days*	*13 days*	*13 days*	*13 days*	*13 days*	*13 days*	*13 days*
10th leaf	UPP	13.55 ±0.84 d	10.70 ±0.63 abcd	0.63 ±0.02 a	0.73 ±0.02 ab	0.12 ±0.04 a	1.16 ±0.17 c	0.01 ±0.003 a	0.01 ±0.004 a	0.12 ±0.04 a	1.16 ±0.17 c	0.01 ±0.003 a	0.01 ±0.004 a
	LPP	13.25 ±0.74 cd	9.30 ±0.71 a	0.61 ±0.02 ab	0.72 ±0.03 ab	0.09 ±0.04 a	0.35 ±0.09 ab	0.02 ±0.005 ab	0.04 ±0.005 bc	0.09 ±0.04 a	0.35 ±0.09 ab	0.02 ±0.005 ab	0.04 ±0.005 bc
3rd leaf	UPP	12.92 ±0.70 bcd	10.18 ±0.53 abcd	0.63 ±0.02 ab	0.65 ±0.03 b	0.65 ±0.15 bc	0.06 ±0.04 a	0.07 ±0.01 c	0.12 ±0.015 d	0.65 ±0.15 bc	0.06 ±0.04 a	0.07 ±0.01 c	0.12 ±0.015 d
	LPP	10.23 ±0.61 abc	9.93 ±0.73 ab	0.63 ±0.02 ab	0.64 ±0.02 b	0.18 ±0.06 a	0.03 ±0.03 a	0.04 ±0.006 c	0.15 ±0.016 d	0.18 ±0.06 a	0.03 ±0.03 a	0.04 ±0.006 c	0.15 ±0.016 d

REFERENCES

Bagard, M., Jolivet, Y., Hasenfratz-Sauder, M.P., Gerard, J., Dizengremel, P., and Le Thiec, D. (2015). Ozone exposure and flux-based response functions for photosynthetic traits in wheat, maize and poplar. *Environ Pollut* 206**,** 411-420.

Bagard, M., Le Thiec, D., Delacote, E., Hasenfratz-Sauder, M.P., Banvoy, J., Gerard, J., Dizengremel, P., and Jolivet, Y. (2008). Ozone-induced changes in photosynthesis and photorespiration of hybrid poplar in relation to the developmental stage of the leaves. *Physiol Plant* 134**,** 559-574.

Bates, D., Machler, M., Bolker, B.M., and Walker, S.C. (2015). Fitting linear mixed-effects models using lme4. *J. Stat. Softw.* 67**,** 1-48.

Bhattacharjee, S. (2005). Reactive oxygen species and oxidative burst: Roles in stress, senescence and signal transduction in plants. *Curr. Sci.* 89**,** 1113-1121.

Coleman, J.S. (1986). Leaf development and leaf stress: increased susceptibility associated with sink-source transition. *Tree Physiol.* 2**,** 289-299.

Dusart, N., Vaultier, M.N., Olry, J.C., Bure, C., Gerard, J., Jolivet, Y., and Le Thiec, D. (2019). Altered stomatal dynamics of two Euramerican poplar genotypes submitted to successive ozone exposure and water deficit. *Environ Pollut* 252**,** 1687-1697.

Feng, G., Calatayud, V., García-Breijo, F., Reig-Armiñana, J., and Feng, Z. (2016). Effects of elevated ozone on physiological, anatomical and ultrastructural characteristics of four common urban tree species in China. *Ecol. Indic.* 67**,** 367-379.

Fu, T.M., and Tian, H. (2019). Climate change penalty to ozone air quality: Review of current understandings and knowledge gaps. *Curr. Pollut. Rep.* 5**,** 159-171.

Günthardt-Goerg, M.S., and Vollenweider, P. (2007). Linking stress with macroscopic and microscopic leaf response in trees: new diagnostic perspectives. *Environ Pollut* 147**,** 467-488.

J., L. (2006). Plotrix: a package in the red light district of R. *R-News* 6**,** 8-12.

Jolivet, Y., Bagard, M., Cabane, M., Vaultier, M.N., Gandin, A., Afif, D., Dizengremel, P., and Le Thiec, D. (2016). Deciphering the ozone-induced changes in cellular processes: a prerequisite for ozone risk assessment at the tree and forest levels. *Ann. For. Sci.* 73**,** 923-943.

Jwa, N.S., and Hwang, B.K. (2017). Convergent Evolution of Pathogen Effectors toward Reactive Oxygen Species Signaling Networks in Plants. *Frontiers in Plant Science* 8.

Kangasjarvi, J., Jaspers, P., and Kollist, H. (2005). Signalling and cell death in ozone-exposed plants. *Plant Cell & Environ.* 28**,** 1021-1036.

Karlsson, P., Braun, S., Broadmeadow, M., Elvira, S., Emberson, L., Gimeno, B.S., Le Thiec, D., Novak, K., Oksanen, E., Schaub, M., Uddling, J., and Wilkinson, M. (2007). Risk assessments for forest trees: The performance of the ozone flux versus the AOT concepts. *Environ Pollut* 146**,** 608-616.

Knox, J.P. (2008). Revealing the structural and functional diversity of plant cell walls. *Current Opinion in Plant Biology* 11**,** 308-313.

Lenth, R.V. (2016). Least-Squares Means: The R Package lsmeans. *J. Stat. Softw.* 69**,** 1-33.

Lichtenthaler (1987). ChlorolShylls and Carotenoids: Pigments of Photosynthetic Biomembranes. *METHODS IN ENZYMOLOGY* 148.

Lichtenthaler, H. (2013). "Plastoglobuli, Thylakoids, Chloroplast Structure and Development of Plastids," in *Plastid Development in Leaves during Growth and Senescence,* eds. B. Biswal, K. Krupinska & U. Biswal. Springer), 337-361.

Maas, R., and Grennfelt, P. (2016). Towards cleaner air. Scientific assessment report. Emep steering body and working group on effects of the convention on long-range transboundary air pollution, Oslo. 12-16.

Mangano, S., Juarez, S.P.D., and Estevez, J.M. (2016). ROS Regulation of Polar Growth in Plant Cells. *Plant Physiology* 171**,** 1593-1605.

Mayta, M.L., Hajirezaei, M.R., Carrillo, N., and Lodeyro, A.F. (2019). Leaf Senescence: The Chloroplast Connection Comes of Age. *Plants-Basel* 8.

Mikkelsen, T.N., and Heidejorgensen, H.S. (1996). Acceleration of leaf senescence in *Fagus sylvatica* L by low levels of tropospheric ozone demonstrated by leaf colour, chlorophyll fluorescence and chloroplast ultrastructure. *Trees-Struct Funct.* 10**,** 145-156.

Mills G., Harmens H., Hayes F., Pleijel H., Buker P., and I., G. (2017). Mapping critical levels for vegetation. Manual on methodologies and criteria for Modelling and mapping critical loads and levels and air pollution effects, Risks and Trends. *International Cooperative Programme on Effects of Air Pollution on Natural Vegetation and Crops***,** 1-66.

Moura, B.B., Alves, E.S., Marabesi, M.A., De Souza, S.R., Schaub, M., and Vollenweider, P. (2018). Ozone affects leaf physiology and causes injury to foliage of native tree species from the tropical Atlantic Forest of southern Brazil. *Sci Total Environ* 610**,** 912-925.

Paakkonen, E., Metsarinne, S., Holopainen, T., and Karenlampi, L. (1996). The ozone sensitivity of birch (*Betula pendula*) in relation to the developmental stage of leaves. *New Phytol.* 132**,** 145-154.

Paoletti, E., Contran, N., Bernasconi, P., Gunthardt-Goerg, M.S., and Vollenweider, P. (2009). Structural and physiological responses to ozone in Manna ash (Fraxinus ornus L.) leaves of seedlings and mature trees under controlled and ambient conditions. *Science of the Total Environment* 407**,** 1631-1643.

Pasqualini, S., Piccioni, C., Reale, L., Ederli, L., Della Torre, G., and Ferranti, F. (2003). Ozone-induced cell death in tobacco cultivar Bel W3 plants. The role of programmed cell death in lesion formation. *Plant Physiol* 133**,** 1122-1134.

Pell, E.J., Sinn, J.P., Brendley, B.W., Samuelson, L., Vinten-Johansen, C., Tien, M., and Skillman, J. (1999). Differential response of four tree species to ozone-induced acceleration of foliar senescence. *Plant Cell & Environ.* 22**,** 779-790.

Proietti, C., Anav, A., De Marco, A., Sicard, P., and Vitale, M. (2016). A multi-sites analysis on the ozone effects on gross primary production of european forests. *Sci Total Environ* 556**,** 1-11.

R Development Core Team (2017). "R: A language and environment for statistical computing". (Vienna, Austria: R Foundation for Statistical Computing).

Reich, P.B. (1983). Effects of low concentrations of O3 on net photosynthesis, dark respiration, and chlorophyll contents in aging hybrid poplar leaves. *Plant Physiol* 73**,** 291-296.

Revell, L.E., Tummon, F., Stenke, A., Sukhodolov, T., Coulon, A., Rozanov, E., Garny, H., Grewe, V., and Peter, T. (2015). Drivers of the tropospheric ozone budget throughout the 21st century under the medium-high climate scenario RCP 6.0. *Atmospheric Chem. Phys.* 15**,** 5887-5902.

Sanz, M., and Catalayud, V. (2011). *Ozone injury in European forest species* [Online]. Available: http://www.ozoneinjury.org/ [Accessed December 12, 2020].

Schindelin, J., Arganda-Carreras, I., Frise, E., Kaynig, V., Longair, M., Pietzsch, T., Preibisch, S., Rueden, C., Saalfeld, S., Schmid, B., Tinevez, J.Y., White, D.J., Hartenstein, V., Eliceiri, K., Tomancak, P., and Cardona, A. (2012). Fiji: an open-source platform for biological-image analysis. *Nat. Methods* 9**,** 676-682.

Schmidt, R., Kunkowska, A.B., and Schippers, J.H.M. (2016). Role of Reactive Oxygen Species during Cell Expansion in Leaves. *Plant Physiology* 172**,** 2098-2106.

Schraudner, M., Moeder, W., Wiese, C., Van Camp, W., Inze, D., Langebartels, C., and Sandermann, H. (1998). Ozone-induced oxidative burst in the ozone biomonitor plant, tobacco Bel W3. *Plant Journal* 16**,** 235-245.

Strohm, M., Eiblmeier, M., Langebartels, C., Jouanin, L., Polle, A., Sandermann, H., and Rennenberg, H. (1999). Responses of transgenic poplar (*Populus tremula* x *P-alba*) overexpressing glutathione synthetase or glutathione reductase to acute ozone stress: visible injury and leaf gas exchange. *J Exp Bot* 50**,** 365-374.

Strohm, M., Eiblmeier, M., Langebartels, C., Jouanin, L., Polle, A., Sandermann, H., and Rennenberg, H. (2002). Responses of antioxidative systems to acute ozone stress in transgenic poplar (*Populus tremula* x *P-alba*) over-expressing glutathione synthetase or glutathione reductase. *Trees-Struct Funct.* 16**,** 262-273.

Turc, B., Vollenweider, P., Le Thiec, D., Gandin, A., Schaub, M., Cabane, M., and Jolivet, Y. (2021). Dynamics of Foliar Responses to O-3 Stress as a Function of Phytotoxic O-3 Dose in Hybrid Poplar. *Frontiers in Plant Science* 12.

Vollenweider, P., Günthardt-Goerg, M.S., Menard, T., Baumgarten, M., Matyssek, R., and Schaub, M. (2019). Macro- and microscopic leaf injury triggered by ozone stress in beech foliage (*Fagus sylvatica* L.). *Ann. For. Sci.* 76**,** 71.

Vollenweider, P., Menard, T., Arend, M., Kuster, T.M., and Gunthardt-Goerg, M.S. (2016). Structural changes associated with drought stress symptoms in foliage of Central European oaks. *Trees-Struct Funct.* 30**,** 883-900.

Vollenweider, P., Ottiger, M., and Günthardt-Goerg, M.S. (2002). Validation of leaf ozone symptoms in natural vegetation using microscopical methods. *Environ Pollut* 124**,** 101-118.

Wang, Y., Li, X.F., Fan, B.F., Zhu, C., and Chen, Z.X. (2021). Regulation and Function of Defense-Related Callose Deposition in Plants. *International Journal of Molecular Sciences* 22.

Wittig, V.E., Ainsworth, E.A., Naidu, S.L., Karnosky, D.F., and Long, S.P. (2009). Quantifying the impact of current and future tropospheric ozone on tree biomass, growth, physiology and biochemistry: a quantitative meta-analysis. *Glob. Change Biol.* 15**,** 396-424.

Yi, S.Y., Shirasu, K., Moon, J.S., Lee, S.G., and Kwon, S.Y. (2014). The Activated SA and JA Signaling Pathways Have an Influence on flg22-Triggered Oxidative Burst and Callose Deposition. *Plos One* 9.

Zhang, J., Schaub, M., Ferdinand, J.A., Skelly, J.M., Steiner, K.C., and Savage, J.E. (2010). Leaf age affects the responses of foliar injury and gas exchange to tropospheric ozone in *Prunus serotina* seedlings. *Environ Pollut* 158**,** 2627-2634.

Chapitre 4

DYNAMIQUE DES CHANGEMENTS TRANSCRIPTOMIQUES

Chapitre 4 : Sensibilité de la feuille de peuplier à l'O_3 en fonction de l'âge : dynamique des changements transcriptomiques

Préface

L'ozone troposphérique (O_3) est connu pour avoir un impact négatif sur la végétation en réduisant la biomasse des arbres et le rendement des cultures. L'une des principales lacunes dans l'évaluation des risques basée sur l'absorption de l'O_3 est la quantification de la capacité de la plante à neutraliser une partie de l'O_3 entrant dans la feuille. Par conséquent, une meilleure compréhension des mécanismes de réponse cellulaire est nécessaire. De nombreuses études ont examiné la réponse transcriptomique des plantes à l'O_3, mais elles se sont concentrées sur la différence entre les génotypes sensibles et tolérants sans tenir compte du flux d'O_3 entrant dans la feuille. Dans cette étude constituant ce troisième chapitre, nous avons étudié la dynamique des changements transcriptomiques en réponse au traitement à l'O_3 (80 et 100 ppb) en fonction de l'âge des feuilles et de la dose cumulée d'O_3 (POD_0), en ce qui concerne les réponses de type HR et ACS. Les changements transcriptomiques ont été appréhendé par RNAseq, une technique jusqu'alors jamais utilisé par le laboratoire et permettant d'obtenir l'expression de tous les gènes et ainsi d'avoir une approche exploratoire sur le transcriptome. Une des forces de cette technique est la corrélation possible entre l'expression des gènes et des données phénotypiques, ici plus particulièrement la HR-like et l'ACS, grâce à la méthode du Weighted Gene Co-expression Network Analysis (WGCNA). Pour cette étude transcriptomique, les échantillons foliaires proviennent de la même expérimentation que celle du deuxième chapitre, permettant une corrélation d'autant plus forte entre le transcriptome et les observations microscopiques. Le coût de cette technique étant très élevé, tous les échantillons ne pouvaient pas être analysés, le choix s'est porté sur les prélèvements suivants :

- 2 jours d'exposition, quand aucune lésion structural (HR-like) ou dégradation de la chlorophylle n'a été observée bien que la dose d'O3 cumulée (POD_0) était supérieure à 0,

- 8 jours d’exposition, quand des lésions structurales (HR-like) ont été observées dans les feuilles matures mais pas dans les jeunes, malgré un POD_0 similaire,

- 13 jours d’exposition, quand des lésions structurales et/ou une dégradation de la chlorophylle ont été observées dans toutes les conditions sauf dans la feuille jeune exposée à 80 ppb O_3.

Dans ce chapitre rédigé sous la forme d’un article scientifique, il est montré que la dynamique des changements transcriptomiques est étroitement liée à l'âge des feuilles, et que le nombre de gènes exprimés de manière différentielle augmente de manière concomitante avec les réponses HR-like et ACS. Les gènes liés à la sénescence ont été régulés tôt pendant l'exposition à l'O_3. D’une manière générale, la dose cumulée d'O_3 n’est pas suffisante pour expliquer la dynamique des changements transcriptomiques. Nous avons donc proposé une liste de gènes fortement corrélés avec HR-like comme marqueurs moléculaires potentiels du stress dû à l'O_3. Enfin, cette étude suggère que l'expression des gènes impliqués dans le développement pendant l'expansion des feuilles pourrait conférer une plus grande tolérance au stress O_3.

Abstract

Tropospheric ozone (O_3) is known to negatively impact vegetation by reducing tree biomass and crop yield. One of the main gap in risk assessment based on O_3 uptake is the quantification of a plant capacity to neutralize a portion of the O_3 entering the leaf. Therefore, a better understanding of cellular response mechanisms is required. Numerous studies have investigated the transcriptomic response of plants to O_3, but focused on the difference between sensitive and tolerant genotypes without considering the cumulative ozone dose. In this study, we investigated the dynamics of transcriptomic changes in response to O_3 treatment (80 and 100 ppb) as a function of leaf age and cumulated O_3 dose (POD_0), with regards to HR-like and ACS responses. The dynamics of transcriptomic changes was closely related to leaf age and number of differentially expressed genes increased concomitantly with HR-like and ACS. Senescence-related genes were regulated early during O_3 exposure. However, cumulated-O_3 dose was not sufficient to explain the dynamics of transcriptomic changes, therefore we proposed a list of genes highly correlated with HR-like as potential molecular markers of O_3 stress. Finally, this study suggested that expression of genes involved in development during leaf expansion could confer a higher tolerance to O_3 stress.

Introduction

Because of human activities, tropospheric ozone (O_3) concentrations have increased during past decades (Maas and Grennfelt, 2016) and are expected to remain stable or increase during the next century (Revell et al., 2015; Fu and Tian, 2019). Adverse effects of O_3 on natural vegetation and crops have already been observed (Wittig et al., 2009; Jolivet et al., 2016; Proietti et al., 2016), and are predicted to increase or remain unchanged over the course of next decades (Karlsson et al., 2007).

Effect of O_3 on plant mainly depends on its uptake through stomata, therefore a cumulated flux-based approach, namely the Phytotoxic Ozone Dose over a threshold of Y (POD_Y), has been developed to assess the critical level for vegetation (Mills et al., 2011; Dizengremel et al., 2013; Büker et al., 2015). The threshold Y represents the amount of O_3 neutralized within the leaf. This threshold which is empirically determined primarily depends on complex defense/detoxification processes (Büker et al., 2015).

Understanding of the cellular response to O_3 is therefore necessary to improve the determination of the threshold Y.

After entry into the leaf through stomata, O_3 is degraded into reactive oxygen species (ROS), triggering a rapid oxidative burst (Schraudner et al., 1998; Pasqualini et al., 2003; Moura et al., 2018). ROS have also signaling function and can elicit programed cell death (PCD) with (i) hypersensitive response-like (HR-like) comparable to responses induced in case of incompatible plant/pathogen interactions (Vollenweider et al., 2002; Bhattacharjee, 2005; Günthardt-Goerg and Vollenweider, 2007; Moura et al., 2018) and (ii) an early initiation of autumnal senescence, defined as accelerated cell senescence (ACS; (Pell et al., 1999; Günthardt-Goerg and Vollenweider, 2007; Vollenweider et al., 2019)).

To decipher molecular mechanism underlying O_3 responses in leaves, transcriptomic studies were conducted either on trees like poplar (Zhang et al., 2019) or oak (Natali et al., 2018; Soltani et al., 2020), or on herbaceous like *Arabidopsis thaliana* (Xu et al., 2015), *Salvia officinalis* (Marchica et al., 2019), soybean (Cho et al., 2013; Whaley et al., 2015; Waldeck et al., 2017) or bean (Yendrek et al., 2015), providing knowledge about differentially expressed genes under elevated O_3 stress. Whatever the plant (herbaceous or trees), common transcriptomic response includes up-regulation of genes related to secondary metabolism, response to stress (biotic and abiotic), phytohormones, signaling (MAPK) and transcription factor (WRKY, MYB) (Street et al., 2011; Cho et al., 2013; Whaley et al., 2015; Xu et al., 2015; Yendrek et al., 2015; Waldeck et al., 2017; Natali et al., 2018; Marchica et al., 2019; Soltani et al., 2020). By contrast, genes related to primary metabolism, photosynthesis, carbohydrate process and growth are commonly down-regulated in response to O_3 exposure (Whaley et al., 2015; Waldeck et al., 2017; Natali et al., 2018; Soltani et al., 2020). However, most of those studies were focused on difference of O_3-induced response between a tolerant and a sensitive genotype, without any investigations on the relation between dynamics of transcriptomic changes and HR-like or ACS response. Furthermore, higher tolerance of young vs old foliage to O_3 stress has been observed in several cases and species (Reich, 1983; Strohm et al., 1999; Bagard et al., 2008; Zhang et al., 2010; Turc et al., 2021), and only one study investigated transcriptomic response to O_3 in different leaf stages (Waldeck et al., 2017). However, mechanism underlying this higher tolerance is still obscure as a lower O_3 uptake by

young vs old foliage can be exclude (Strohm et al., 1999; Bagard et al., 2008; Zhang et al., 2010; Turc et al., 2021). Therefore, dynamics of transcriptomic changes in an old *vs* young foliage is also matter of investigation.

In this study, our main objective was to relate dynamics of transcriptomic changes with HR-like and ACS dynamics, as a function of cumulated O_3 dose and leaf age, to better understand the cellular dynamics of response to O_3. In a previous study (Turc et al., 2021), we showed that dynamics of HR-like and ACS were quite different and depend on both leaf age and cumulated O_3 dose. Moreover, in young foliage dynamics of HR-like was also depending on atmospheric O_3 concentration (Turc et al., 2021). Therefore, young poplars were exposed to two different concentration of O_3 in fully control conditions, giving four different modalities differing by leaf response intensity as a function of cumulated O_3 dose.

Material and methods

Plant material and growth conditions

Micropropagated poplars (*Populus tremula x alba*, clone INRAE 717-1B4) were acclimated and cultivated into 10-L pots filled with compost (Gramoflor) and fertilized with 30 g of Nutricot T 100 granules (13:13:13:2 N/P/K/MgO, Fertil, Boulogne-Billancourt, France). Young trees were grown in controlled chamber set at 22°C/18°C temperature (day/night) with a 14 h photoperiod (Philips Son-T Agro 400 W lamps, PAR= 350 µmol m^{-2} s^{-1}) and 75%/85% relative humidity (day/night).

Young poplars (2.5-month-old) were exposed to O_3 into phytotronic chambers of the PEPLor platform (Faculty of Sciences and Technologies, University of Lorraine, France) with environmental conditions similar to those in the growth chamber. The experimental O_3 exposure included three treatments: charcoal-filtered air (CF), CF + 80 ppb O_3, and CF + 100 ppb O_3. O_3 was generated using an O_3 generator (Innovatec II, Rheinbach, Germany) and provided to the chambers during 13h of the daytime period. O_3 was continuously monitored using a computer assisted automatic O_3 analyzer (O341M, Environment SA, Paris).

Experiment sampling

At each time point (2, 8, 13 and 23 days of treatment), leaves were harvested on 4 biological replicates. On each tree, the third leaf and tenth leaf (numbered from the bottom) were collected and further analyzed for leaf visible injury, HR-like lesion, total chlorophyll content, LMA. RNAseq was carried out on the same samples except for the time point 23 days. Gas exchange measurements were performed on the same trees, one day before harvest and also at 5 and 16 days of treatment.

Leaf visible injury

Leaf visible injury was monitored by taking a picture of leaves. The leaf percentage area showing necrosis was quantified by means of color image analysis, using the Color Segmentation plugin in Fiji freeware (ver. 2.0.0; (Schindelin et al., 2012)).

HR-like lesion

Necrotic cells resulting from HR-like reaction were evidenced using trypan blue coloration (Pasqualini et al., 2003; Joo et al., 2005; Faoro and Iriti, 2009) and quantified as previously described (Turc et al., 2021). Sample were harvested and processed immediately.

Total chlorophyll content and LMA

For biochemical assessments of total chlorophyll content, leaves were sampled and immediately frozen in liquid nitrogen. Frozen leaves were further ground in mortar chilled with liquid nitrogen. About 100 mg of the resulting powder was mixed with 1 mL of pure acetone (100%), incubated 10 min in the dark and centrifuged (10 000 rpm / 10 min / 4°C). Then, 0.8 mL of supernatant was mixed with 0.2 mL of distilled water and optical absorbance at 663.2 nm and 646.8 nm were measured using a spectrophotometer (SAFAS UVmc1 spectrophotometer). Extraction steps were repeated three times per pellet sample to ensure total extraction chlorophyll.

The total chlorophyll content (chl_{tot}) was determined according to Lichtenthaler (1987):

$$Chl_{tot} = 7.15 * A_{663.2} + 18.71 * A_{646.8}$$

with chl_{tot} as the total chlorophyll content, $A_{663.2}$ and $A_{646.8}$ as the optical absorbance at 663.2 nm and 646.8 nm respectively.

Leaf mass per area was calculated as LMA = Leaf area (cm^2) / Leaf mass (g). Leaves were weighted and leaf area was quantified using Fiji freeware (ver. 2.0.0; (Schindelin et al., 2012)) .

Leaf gas exchange and estimation of POD_0

Stomatal conductance to water vapour (g_w) and net CO_2 assimilation (A_{net}) were measured inside the fumigation chamber, 3h after O_3 exposure started. To disturb the O_3 exposure as less as possible, and based on previous results (Turc et al., 2021), leaf gas exchange assessments were restricted to 1, 5, 7, 12, 16, 21 days of exposure. Leaf gas exchange were recorded using a LI-6400 portable photosynthesis system (LiCor Inc, Lincoln, NE, United States), with inner chamber temperature maintained at 22°C, light intensity (PAR) at 300 and 320 µmol m^{-2} s^{-1} for measurements at the third and tenth leaf position respectively, airflow at 300 µmol s^{-1}, CO_2 concentration at 400 ppm, and leaf vapor pressure deficit (VPD_{leaf}) < 1kPa. G_w was recorded once it remained stable for 30 s. POD_0 was estimated from g_w values, as previously described (Bagard et al., 2015; Turc et al., 2021).

RNA-extraction and sequencing

Total RNA was extracted using TRIzol (Invitrogen) as described in Richet et al. (2012). Quantity and integrity of RNA were examined using a Bioanalyzer 2000 (Agilent Technologies) before RNAseq library construction and sequencing at GEnoToul (Toulouse). The libraries were sequenced on an illumina Novaseq instrument with all samples in one lane and pair end 150bp runs.

RNA-sequencing data processing

Raw reads were filtered and trimmed based on their sequence quality using erne-filter command (Erne v2.1.1, default parameters except --min-size=70; (Del

Fabbro et al., 2013)). The resulting high-quality reads were aligned to the *Populus trichocarpa* genome sequence v4.1 (Phytozome v13, (Tuskan et al., 2006; Goodstein et al., 2012)) using TopHat2 v2.12 (Trapnell et al., 2009; Kim et al., 2013). TopHat2 default parameters were applied except for the following options: -r 35 --mate-std-dev 20 --read-mismatche 15 --read-gap-length 15 --read-edit-dist 30 -I 20000 -i 20 --read-realign-edit-dist 10 --max-insertion-length 19 --max-deletion-length 19 -g 10 --segment-mismatches 3 --segment-length 25 --min-segment-intron 20 --max-segment-intron 20000 --b2-very-sensitive. Reads that mapped once were extracted from "Alignment-Map" files (accepted_hits.bam, TopHat2 output) using the NH:i:1 tag as described by Loraine et al. (2013). Raw read counts were summarized per genes using the 'featureCounts' command (Subread package v1.6.1, (Liao et al., 2014)) with the following parameters: -O –s2 -p -P -d20 -D55000, and implemented with the "Ptrichocarpa_533_v4.1.gene_exons.gff3" file as map of genomic features. Alignment statistics are given in Table S1. Only e loci for which at least 10 reads were counted for each replicate of a given modality were further analysed.

Identification of differentially expressed genes

R software, version 3.5.0 (R Development Core Team, 2017) and DESeq2 package v1.24.0 (Love et al., 2014) were used for read counts normalization and for computing differential gene expression. Differentially expressed genes (DEGs) were defined as having a *P*-value ≤ 0.05 (Wald test *P*-values corrected for multiple testing by applying false discovery rate).

Gene ontology analysis

Gene Ontology (GO) annotation, GO-Slim summarization, and enrichment analysis were performed as described in Royer et al., 2016 using Blast2GO (v5.2; (Conesa et al., 2005)). Briefly, the 34,699 *P. trichocarpa* protein sequences were blasted against *A. thaliana* database ('blastp', default parameters, except *e-value* threshold=0.001). The best hit was imported in Blast2GO allowing to assign poplar gene models to the GO annotation of their closest *Arabidopsis* orthologs. GO was summarized as plant GO-Slim terms. Detection of enriched GO terms relied on a Fisher's exact test combined with an FDR correction for multiple testing. A corrected P-value cutoff of 0.05 was used to identify significant enrichments.

Weighted gene co-expression network analysis

Co-expression network analysis was performed using the R package WGCNA v1.70 (weighted correlation network analysis, (Langfelder and Horvath, 2008). The expression matrix was Log2 (normalized count+1)-transformed. Scale-free topology was obtained by applying a soft power of 18 which was provided by the network topology analysis function 'pickSoftThreshold' (with default parameters, "signed" network type and biweight midcorrelation "bicor"). The network was constructed using the "blockwiseModules" function (parameter: signed network type, bicor, power= 18, maxBlockSize = 15,000, minModuleSize = 50, reassignThreshold = 1e-6, mergeCutHeight = 0.25, maxPOutliers = 0.05 and deepSplit = 3). WGCNA identifies clusters of highly correlated loci and summarizes clusters using module eigengene (ME), which is the first component of each module and represents the gene expression profile in the module. Module-based biological significance (Langfelder and Horvath, 2008) was computed as the value of the Pearson correlation between module eigengenes and quantitative traits (leaf percentage area with HR-like lesion, g_w, A_{net}, total chlorophyll content, POD_0 and relative loss of chlorophyll content).

Results

Dynamics of structural injury and relative loss of chlorophyll content

HR-like lesion, loss of chlorophyll content and leaf visible injury were followed at two different leaf levels in response to O_3 treatment (80 ppb or 100 ppb) (Figure 1). At the beginning of fumigation, the 10th leaf is a young expanding leaf and the 3rd leaf is a fully expanded leaf. The10th leaf is approximately 10 days younger than the 3rd leaf.

The dynamics of structural injury (HR-like) and chlorophyll degradation depended on leaf position at both O_3 concentrations. The tenth leaf was less affected by O_3 than the third leaf. HR-like lesion and relative loss of chlorophyll content were observed later at the tenth vs third leaf position (Figure 1A,B). The better O_3 tolerance of the tenth leaf compared to the third leaf was also noticed as a function of cumulative

O_3 flux entering the leaf (POD_0) (Figure 1C,D). At a given leaf level, the response was dependent on O_3 concentration. HR-like lesion and chlorophyll degradation appeared earlier and/or were significantly more intense in the 100 vs 80 ppb O_3 treatment (Figure 1A,B, Table S2). By the end of O_3 exposure, leaf percentage area showing HR-like lesion and relative loss of chlorophyll content in the 100 vs 80 ppb O_3 treatment were respectively 1.8 and 2.2 times higher at the third leaf position, and respectively 1.5 and 6 times higher at the tenth leaf position. This difference in response intensity was also observed for a similar POD_0 (Figure 1C,D), given the similar time-course of POD_0 between the 100 and 80 ppb O_3 treatment (Fig S1). HR-like lesion and loss of chlorophyll occurred long before any leaf visible injuries which were observed only at the end of the experiment, and mainly at the third leaf position exposed to 100 ppb O_3 treatment.

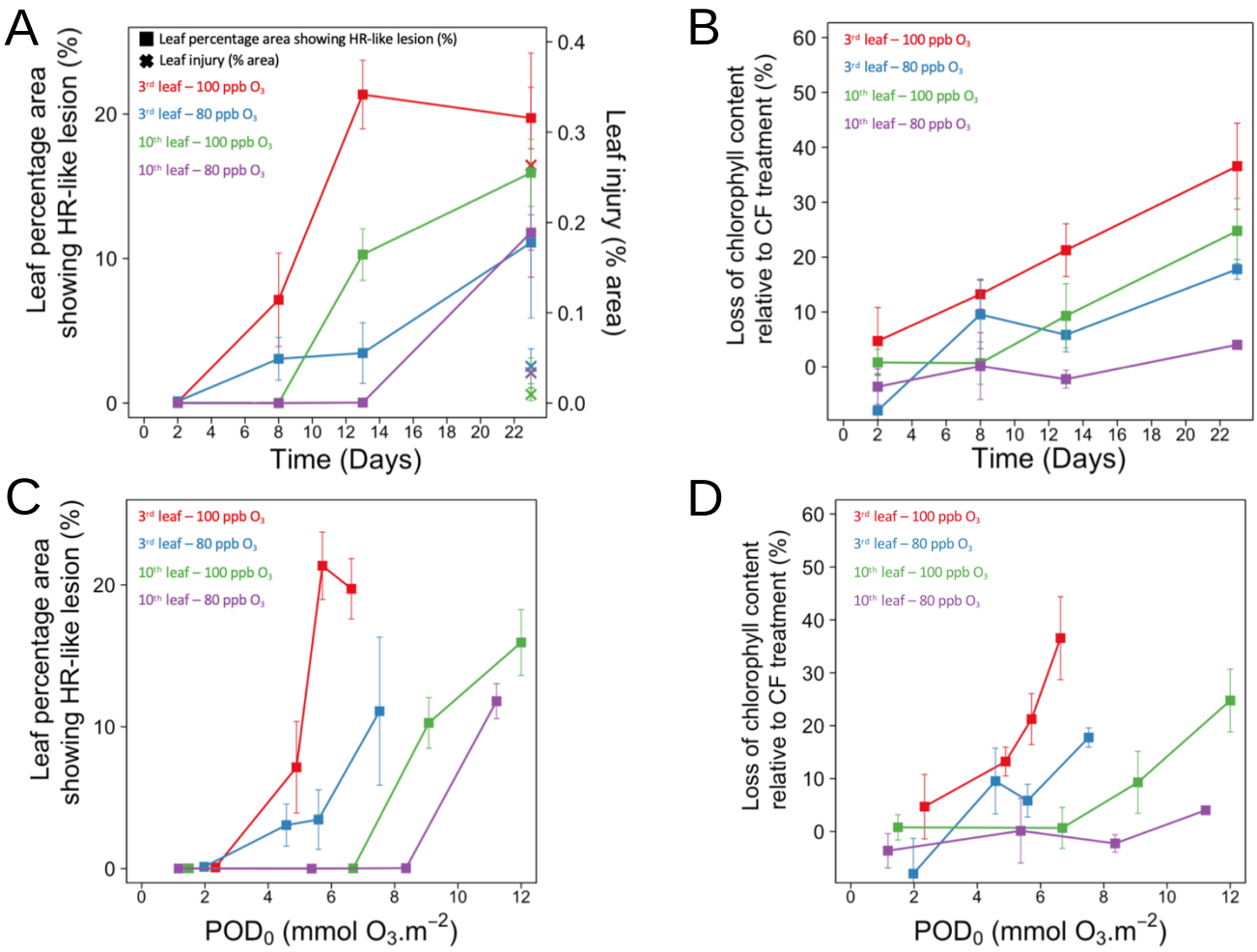

Figure 1. Dynamics of HR-like lesion and visible injury (**A**,**C**), and relative loss of chlorophyll content (**B**,**D**) as a function of time (**A**,**B**) and POD_0 (**C**,**D**) at the third and tenth leaf position. Values represent means ± SE, n = 4.

Based on these results, leaves sampled at 2, 8 and 13 days of treatment were selected for RNA-sequencing analysis, given the following reasons: (i) after 2 days of exposure no structural injury (HR-like) or chlorophyll degradation were observed although POD_0 was over 1 mmol $O_3.m^{-2}$, (ii) after 8 days of exposure structural injury was observed at the third but not at the tenth leaf position despite a similar POD_0, and (iii) after 13 days of exposure structural injury or chlorophyll degradation were observed in all conditions except at the tenth leaf position in the 80 ppb O_3 treatment.

Differential gene expression and GO enrichment

A total of 72 cDNA libraries with 4 biological replicates per condition (timepoint, leaf and treatment) were sequenced with the novaseq system from illumina resulting in approximately 27 million pair end reads of 150bp per library. After quality filtering, reads were mapped onto the *P.trichocarpa* genome (95% mapped reads).

Differentially expressed genes (DEG) between O_3 and control condition were analyzed from normalized expression data (mean of 4 biological replicates). Similar to the dynamics of structural injury and chlorophyll degradation, the number of identified DEGs was higher in the 100 vs 80 ppb O_3 treatment and at the third vs tenth leaf position (figure 2). The number of DEGs ranged from 0 after 2 and 8 days at the tenth leaf position in the 80 ppb O_3 exposure, to 12’012 (6’238 up-, 5’774 downregulated) after 13 days at the third leaf position in the 100 ppb O_3. Most of DEGs were found after 13 days of O_3 exposure, except at third leaf position in the 100 ppb O_3 treatment. In this condition, the number of DEGs was already high after 2 days of exposure (1’947 up-, 1’198 downregulated) and kept increasing after 8 days of exposure (3’865 up-, 2’535 downregulated) and 13 days of exposure (6’238 up-, 5’574 downregulated). Among these DEGs, 15% (20% up-, 9% downregulated) were common to 2 and 8 days and 28% (32% up-, 24% downregulated) were common to 8 and 13 days of exposure.

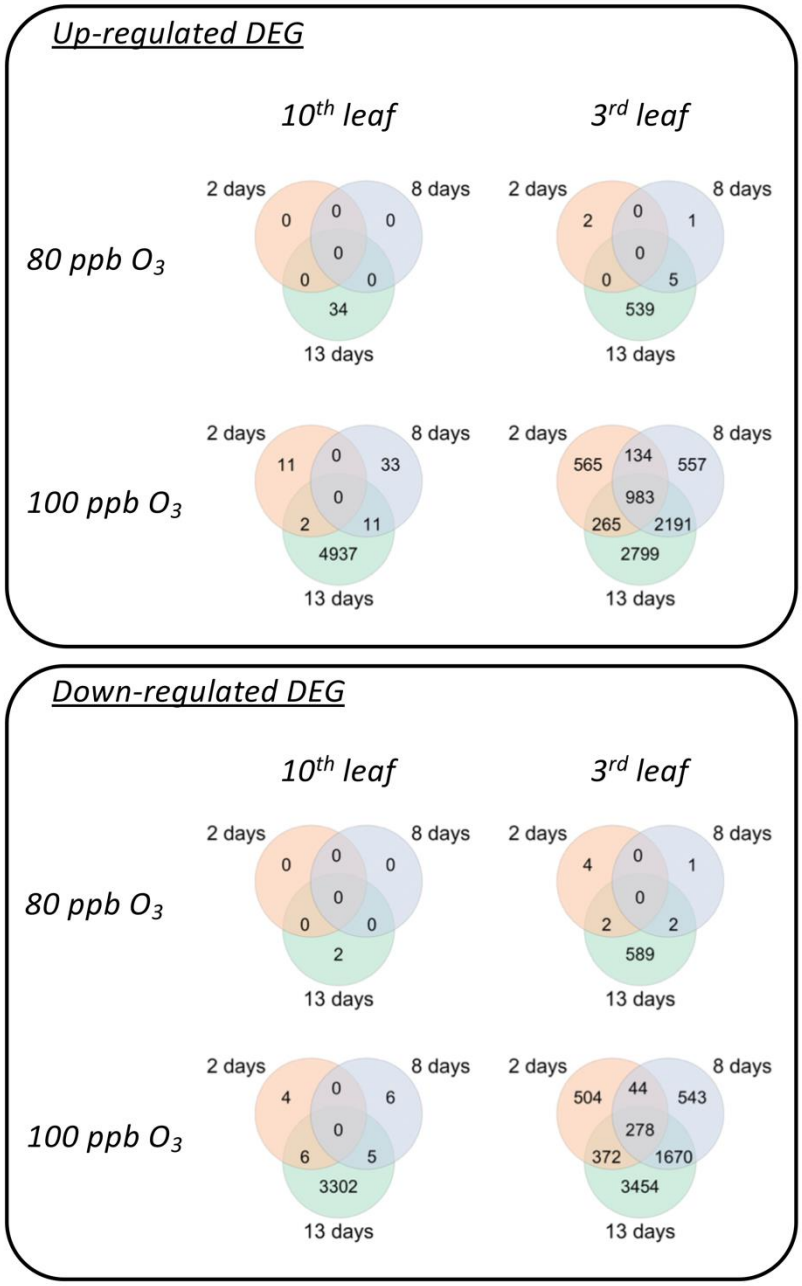

Figure 2. Venn diagrams showing number of up- and down-regulated DEGs from third and tenth leaf position of hybrid poplars exposed to O_3 treatments (80 and 100 ppb) over time. Time of sampling (2, 8 and 13 days) are represented by 2 days, 8 days and 13 days respectively, and O_3 treatments by 80 ppb O_3 and 100 ppb O_3.

To characterize the biological function of large set of DEGs, GO enrichment was conducted separately for each O_3 treatment (100 and 80 ppb O_3) and leaf position (the third and the tenth). Analysis of GO enrichment of large set of DEGs revealed significant functional enrichment common to the five conditions (figure 3). The most significantly enriched GOs of up-regulated DEGs were shared by all large set of DEGs. They were more significantly enriched in the 100 vs 80 ppb O_3 treatment, and were

more significantly enriched earlier at the third vs tenth leaf position (figure 3A). These GOs include genes involved in stress and stimulus responses (“response to biotic stimulus”, “response to stress” and “response to external stimulus”), synthesis and modification of protein ("cellular protein modification process”, “golgi apparatus”, “endoplasmic reticulum”, “nucleotide binding”), cell communication (“signal transduction”, “kinase activity”) and cell death (“cell death”, “hydrolase activity”, “vacuole”). By contrast, the most significantly enriched GOs of downregulated DEGs were mainly found in the 100 ppb O_3 treatment after 8 and 13 days of exposure at the third leaf position, and after 13 days of exposure at the tenth leaf position (figure 3B). These GOs gathered genes involved in photosynthesis (“photosynthesis”, “response to light stimulus”, “thylakoid”, “chloroplast”, “carbohydrate metabolic process”) and cellular organization (“cellular component organization”, “cytoskeleton”).

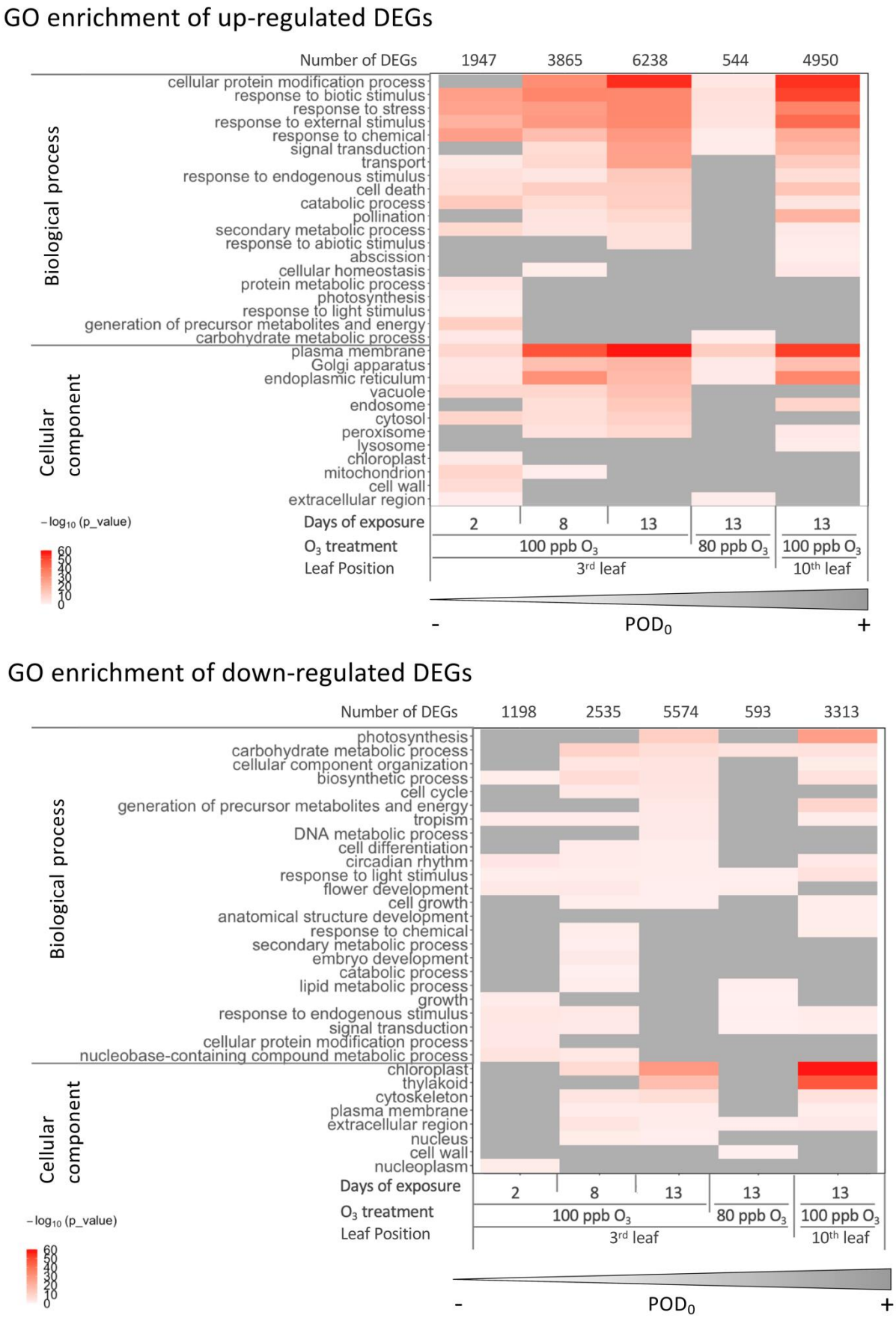

Figure 3. GO enrichments of large set of DEGs (>100) of the third and tenth leaf position of hybrid poplars as a function of O_3 treatment, leaf position and POD_0. Values are $-\log_{10}(p\_value)$ of the enrichment (grey: ns).

Weighted Gene Co-expression Network Analysis (WGCNA)

To identify co-regulation of gene clusters over the whole experiment, weighted gene co-expression network analysis (WGCNA) was carried out using all samples. The total of 34'709 genes of *Populus trichocarpa* were grouped in 13 clusters, with a range of 54 (module 12) to 9'043 (module 1) genes per module. A module is a subset of highly co-expressed genes, and for each one a module eigengene (ME), representing an average expression of all the genes in the module, was calculated. ME was used to calculate Pearson correlation coefficient (P_{coef}) with phenotypic data (HR-like lesion, relative loss of chlorophyll content, relative net CO_2 assimilation, POD_0, LMA, total chlorophyll content, net CO_2 assimilation and stomatal conductance).

We identified five modules (1, 2, 4, 7, 11) for which O_3 treatment and leaf position significantly impacted gene expression (figure 4A-F and S3), with at least one significant difference for a given assessment date observed at both leaf position. For each of these modules, O_3 effect on gene expression was greater in the 100 vs 80 ppb O_3 treatment, and occurred earlier at the third vs tenth leaf position.

Module 1 (9'043 genes) and 7 (743 genes) were found to be positively correlated with both leaf percentage area showing HR-like lesion (figure 4G; P_{coef} = 0.63 and 0.65 respectively), relative loss of chlorophyll content (figure 4G; P_{coef} = 0.43 and 0.49 respectively) and relative loss of net CO_2 assimilation (figure 4G; P_{coef} = 0.6 and 0.43 respectively).

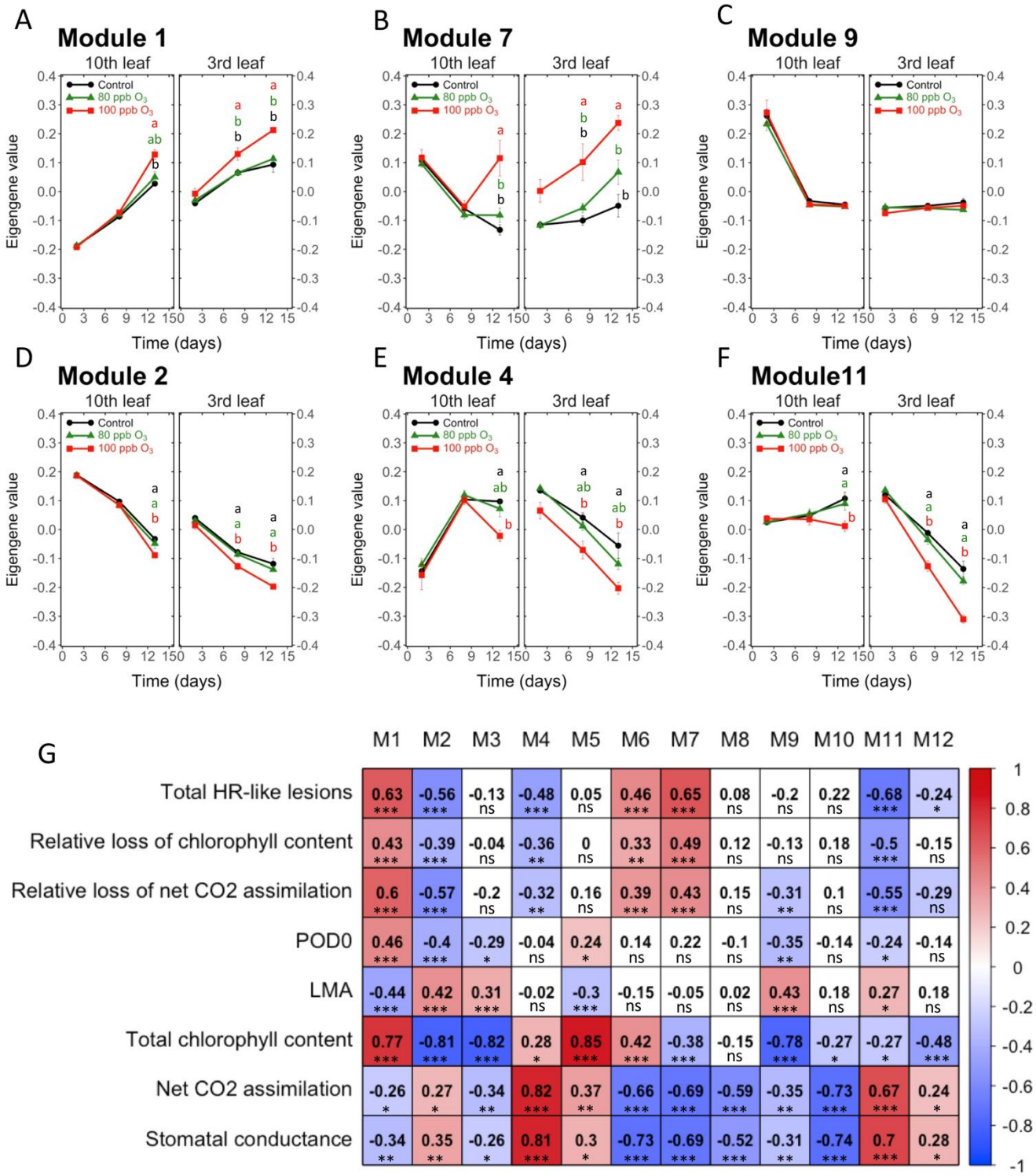

Figure 4. WGCNA module profile as a function of O_3 treatment, leaf position and time (A-F), and correlation table between phenotypic data and WGCNA modules (G). Values represent means ± SE, *n* = 4. Different letters indicate significant differences between treatments at a given assessment date (Tukey's post-hoc test, $p \leq 0.05$). Individual module is indicated on X-axis and phenotypic data on the Y-axis. In each box Pearson correlation coefficient and its *p_value* are indicated (*** $p \leq 0.001$; * $p \leq 0.05$).

Expression of genes of module 1 increased with leaf age. This increase was enhanced only in the 100 ppb O_3 treatment and earlier at the third vs tenth leaf position (figure 4A). GO enrichment analysis revealed that genes of this module were involved in response to stress, cell death, modification and degradation of proteins, and cell communication (Table S3). Core genes of this module (Table S4) encode for a secretory carrier-associated membrane protein (secretory carrier 3, *Potri.004G036600*) involved in membrane trafficking and host defense against pathogens, two ring finger domain proteins (*Potri.003G129900* and *Potri.012G011500*), a transcription factor (WRKY47; *Potri.014G111900*), a NAC domain containing protein (*Potri.014G041300*) and an exocyst subunit complex (*Potri.015G058200*) involved in exocytosis.

By contrast, expression of genes of module 7 decreased with leaf age and was stimulated with O_3 (figure 4B). Genes of this module were more up-regulated in the 100 vs 80 ppb O_3 treatment, and much earlier at the third vs tenth leaf position. Note that the higher level of expression of these genes at the tenth vs third leaf position after 2 days of exposure in CF treatment. Genes of modules 7 (Table S4) are involved in protein metabolism (“protein metabolic process”, “endoplasmic reticulum”, “golgi apparatus”) and cell wall (“cell wall”) (Table S3). Core genes of this module include a COBRA-like protein precursor (*Potri.004G117100*) involved in cellulose deposition, a geranylgeranyl reductase (*Potri.009G139600*) implied in isoprenoid biosynthesis, a O-fucosyltransferase family protein (*Potri.016G109700*) known to participate to autumnal senescence, a ribonuclease inhibitor (*Potri.011G169700*), a Serine incorporator-domain containing serine (Potri.003G174200) know to incorporate serine into membranes and facilitates the synthesis of two serine-derived lipids, phosphatidylserine and sphingolipids, and a regulator of transcription (LJRHL1-like 1; *Potri.006G186600*). Module 1 and 7 contained most of the up-regulated DEGs (Fig 5).

Module 2 (7’639 genes), 4 (2’217 genes), and 11 (94 genes) were negatively correlated with leaf percentage area showing HR-like lesion (figure 4G; P_{coef} = -0.56, -0.48, -0.66 respectively), relative loss of chlorophyll content (figure 4G; P_{coef} = -0.39, -0.36, -0.50 respectively) and relative loss of net CO^2 assimilation (figure 4G; P_{coef} = -0.57, -0.32 and -0.55 respectively). Expression of genes of module 2 and 4 were the reverse of those from module 1 and 7 respectively.

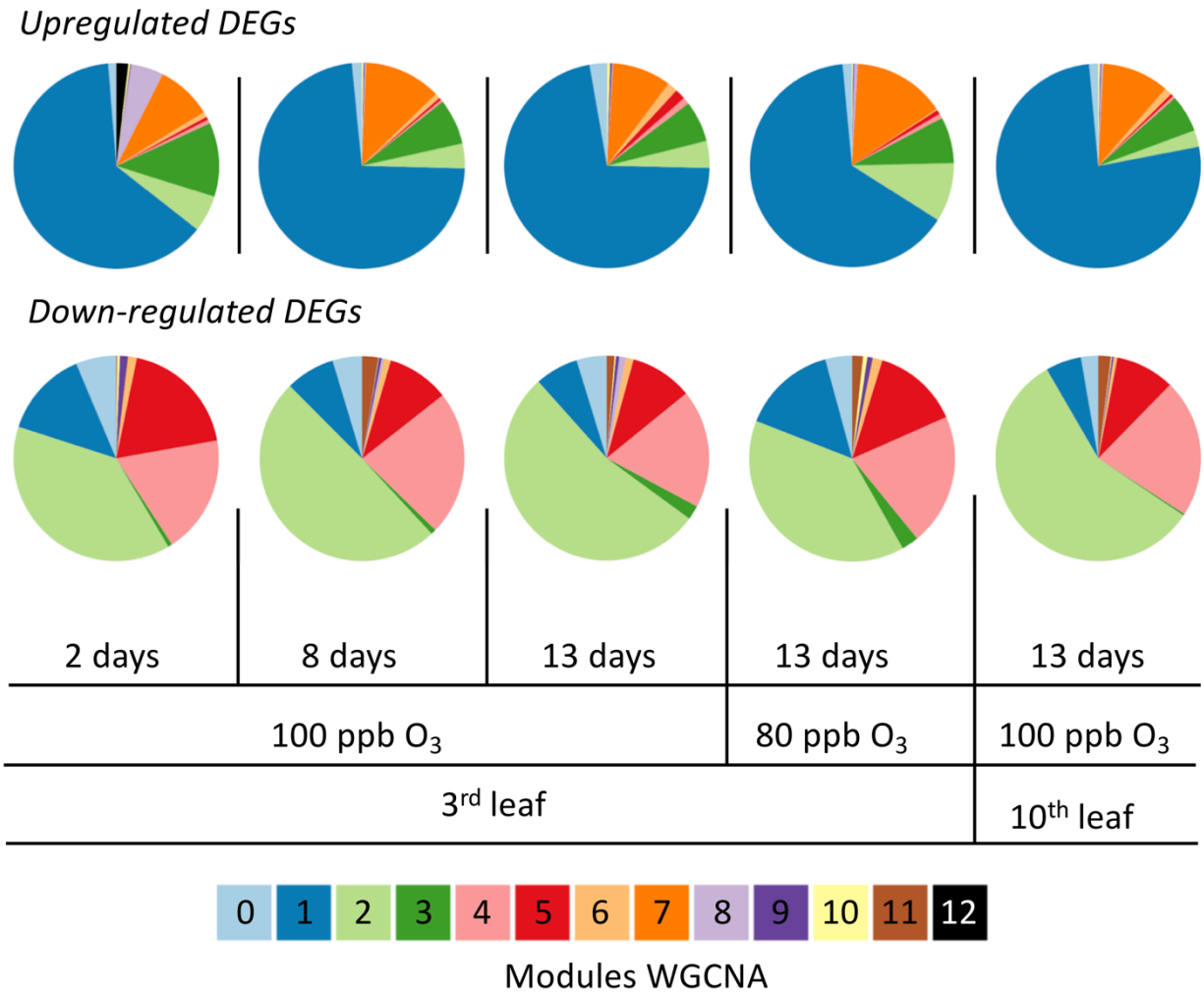

Figure 5. Distribution of up- and down-regulated DEGs among WGCNA modules of the tenth and third leaf position of hybrid poplar in response to O_3.

Expression of genes of module 2 decreased with leaf age, but this decrease was accelerated only in the 100 ppb O_3 treatment, and earlier at the third vs tenth leaf position (figure 4D). Genes of module 2 were involved in cell growth and organization ("cell growth", "cell differentiation", "cytoskeleton", "motor activity", "cell cycle", "cellular component organization") and photosynthesis ("photosynthesis", "carbohydrate metabolic process", "chloroplast", "thylakoid") (Table S3). Core genes of this module (Table S4) encode for two ribosomal protein (*Potri.002G154600* and *Potri.006G221100*), a thylakoid rhodanese-like protein (*Potri.014G096500*) and a ribose 5-phosphate isomerase (*Potri.005G052000*).

On the contrary, expression of genes of module 4 increased before decreasing with leaf age, but the decrease was faster in the 100 vs 80 ppb of O_3 treatment, and occurred much earlier at the third vs tenth leaf position (figure 4E). Genes of module 4 (Table S4) were involved only in photosynthesis ("photosynthesis", "carbohydrate

metabolic process", "chloroplast", "thylakoid"; Table S3), and core genes of this module include a photosynthetic electron transport in photosystem I (PGR5-LIKE A; *Potri.003G119200*), a photosynthetic electron transfer C (*Potri.013G148900*) and a light harvesting complex of photosystem II (*Potri.016G115200*).

Expression of genes of module 11 also decreased once leaf expansion was achieved, what was accelerated only in the 100 ppb O_3 treatment, and earlier at the third vs tenth leaf position (figure 4F). This module encompassed genes involved in cellular organization ("cellular component organization", "cytoskeleton") and carbohydrate metabolic process (Table S3). This module is mainly structured by genes encoding for three laccase (*Potri.011G120200*, *Potri.009G042500* and *Potri.011G120300*) potentially involved lignin polymerization, a IQ-domain (*Potri.011G096500*) that may be involved in recruiting calmodulins or calmodulins-like protein to microtubules, and a tubulin alpha chain (*Potri.002G111900*) implied in microtubule synthesis (Table S4). Modules 2, 4, and 11 contained most of the down regulated DEGs (Fig 5).

Module 9 (528 genes) was positively correlated with LMA (figure 4G; P_{coef} = 0.43). This module gathers genes whose expression was not impacted by O_3 treatment (figure 4C). These genes are implied in cell differentiation during development ("DNA metabolic process", "cell cycle", "cell differentiation", "nucleus", "DNA binding"; Table S3). Therefore, leaf development was clearly indicated by this module, and young foliage finished expanding after 8 days of exposure, as also indicated by stomatal conductance dynamics (fig. S1)

DEG shared with autumnal senescence and autophagy in poplar

To relate genes identified in this study to genes previously characterized in autumnal senescence process in poplar, DEGs were compared to 14415 genes reported by (Lu et al., 2020). Up- and down regulated genes during autumnal senescence in poplar leaves (*Populus trichocarpa*) were classified into three transition phases by (Lu et al., 2020): (i) growth to senescence initiation, (ii) senescence initiation to reorganization and (iii) reorganization to termination. Shared DEGs between O_3-treated leaves and senescence transition phases were found in all large set of DEGs (Figure 6). More common DEGs were found in the 100 vs 80 ppb O_3 treatment, and at

the 3rd vs 10th leaf position (figure S3 and S4). Furthermore, in each condition, number of common DEGs was higher in the first and second vs the third transition phase (growth to senescence initiation, and reorganization to termination), except at the 3rd leaf position in the 100 ppb O_3 treatment after 13 days of exposure. In this condition, number of shared DEGs was similar for the three transition phases (Figure S3 and S4).

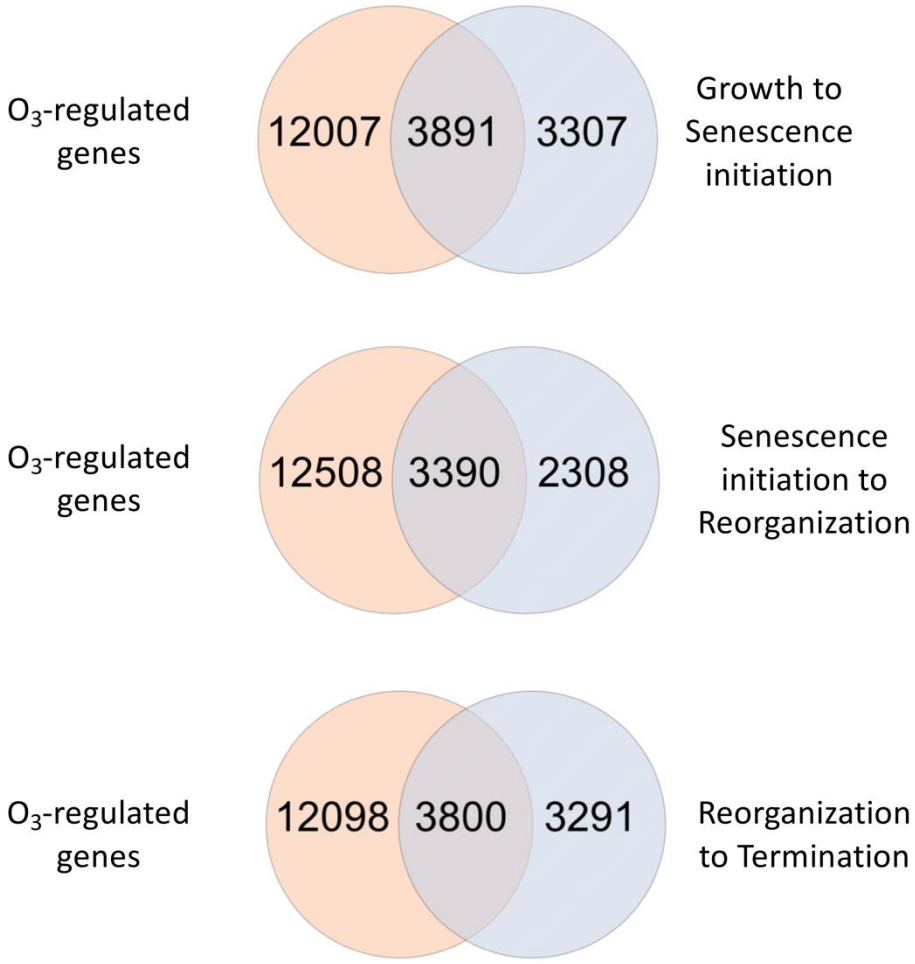

Figure 6. Venn diagrams showing number DEGs (up- and down-regulated) from third and tenth leaf position of hybrid poplars exposed to O_3 treatments (80 and 100 ppb) and DEGs in relation to three phases of senescence transition according to Lu et al. (2020).

To investigate transcriptomic changes related to autophagy in response to O_3 exposure, DEGs were compared to the list of homologous autophagy genes in yeast and Arabidopsis thaliana reviewed by (Han et al., 2011). Most of autophagy genes were found to be up-regulated only at the 3rd leaf position exposed to 100 ppb O_3

treatment (fig S5). The most up-regulated gene was encoding for ATG8 (*Potri.010G153400*), a ubiquitin-like protein required for the formation of autophagosomal membranes.

Correlation between gene expression and HR-like lesion

Genes correlated with HR-like lesion were identified using R^2 coefficient between gene expression level and leaf percentage area showing HR-like lesion. Genes with a R^2 coefficient higher than 0.7, and for which the slope of the regression line was higher than 30 were selected and are presented in table S4. The five most correlated genes (Table S4) with HR-like lesion found were encoding for two glutamate receptors 2.7 (*Potri.001G374600* and *Potri.001G374700*) that may be involved in calcium homeostasis, a S-locus lectin protein kinase (*Potri.004G027400*) which belongs to receptor-like kinase family involved in both abiotic and biotic stress response, a UDP-glycosyltransferase (*Potri.001G302400*) and a NB-ARC domain-containing disease resistance protein (*Potri.003G099000*) involved in pathogens recognition and subsequent activation of plant defense responses.

Discussion

Dynamics of transcriptomic changes in response to O_3 stress

In this study, the number of differentially expressed genes in the hybrid poplar leaves increased as both a function of time and O_3 concentrations. This have been already observed in several studies using RNA-seq to investigate the impact of O_3 stress on gene expression patterns in herbaceous like soybean (Whaley et al., 2015; Waldeck et al., 2017) or woody species like poplar (Zhang et al., 2019) or oak (Natali et al., 2018; Soltani et al., 2020). However, number of differentially expressed genes in our study was much higher than those obtained in study on woody species. This can be explained by (i) the daily O_3 exposure time which was longer in our study, (ii) environmental conditions of exposure (Open Top Chamber vs. fully controlled conditions) and (iii) the use of a single clone.

Number of differentially expressed genes increased concomitantly with HR-like and ACS, quantified by total HR-like lesions and relative loss of chlorophyll content

respectively. Functional enrichment of differentially expressed genes revealed common biological responses across assessment time and O_3 treatments, including stimulation of various stress responses (biotic and abiotic) and repression of photosynthesis and carbohydrate processes, as already observed in several study (Cho et al., 2013; Whaley et al., 2015; Waldeck et al., 2017; Natali et al., 2018; Soltani et al., 2020). However, our results showed that O_3 treatments, exposure time and leaf position did not affect the nature of transcriptomic changes but their dynamics. Differentially expressed genes involved in these biological pathways were also co-expressed in response to O_3 as they were assigned to co-expression modules: M1 and M7 for up-regulated genes, and M2, M4 and M11 for down-regulated genes. All five modules were highly (positively or negatively) correlated to total HR-like lesion and relative loss of chlorophyll content (thus to HR-like and ACS respectively) but showed distinct patterns. Modules 1 and 2 clearly showed ACS-related profiles as O_3 accelerated the developmental regulation of genes belonging to these modules. Furthermore, the differentially expressed genes common to the O_3 response and autumnal senescence were in module 1 (upregulated genes) and 2 (down-regulated genes). Finally, the linear increase in the number of these genes over time was indicative of a gradual establishment of senescence as the cumulated O_3 dose increased. Moreover, investigation of microscopic changes occurring in these poplar leaves under the same experimental conditions (Chapter 2) showed a later emergence of ACS-related microscopic changes than transcriptomic regulation. Hence, ACS-related changes might be a consequence of transcriptomic changes induced by O_3-generated ROS.

Much more differentially expressed genes were detected once HR-like lesions were observed, likely explained by the regulation of cell death involving several pathways with overlapping mechanisms (Kangasjarvi et al., 2005; Xu et al., 2015). Despite high correlation with HR-like lesion, no module showed a similar profile to the sigmoidal-like dynamics of HR-like previously observed in poplar leaves (Turc et al., 2021). However, the sharp increase in number of differentially expressed gene observed in parallel to HR-like lesion emergence suggests a regulation of genes related to HR-like reaction once O_3-induced ROS exceeded a threshold, as observed for the HR-like dynamic. Given the close relationship of ACS and HR-like with ROS, the opposite dynamic of transcriptomic changes of the 2 processes are likely the

consequence of different signaling which might be induced by a distinct spatial accumulation of ROS. Indeed, the accumulation of ROS initiating the autumnal senescence is of chloroplast origin. In fact, the decrease in chloroplast antioxidant capacity leads to an accumulation of ROS initiating senescence (Mayta et al., 2019). On the contrary, hypersensitive response (HR) is induced by an accumulation of apoplastic ROS triggered by the activation of NAPDH oxidase following the recognition of a pathogen (Jwa and Hwang, 2017). Given the similarities already observed between HR and HR-like (Vollenweider et al., 2002; Bhattacharjee, 2005; Günthardt-Goerg and Vollenweider, 2007; Moura et al., 2018), we can hypothesize that HR-like is the consequence of an apoplastic accumulation of O_3-induced ROS triggering biotic stress response.

Leaf age and O_3

Transcriptomic changes occurred later (and for a larger POD_0) at the tenth vs the third leaf position. Given the mostly similar functional enrichment of differentially expressed genes at both leaf position, regulation of a specific pathway explaining leaf differences can be excluded. Co-expression modules encompassing differentially expressed genes (M1, M2, M7, M4 and M11) showed profiles strongly depending on leaf age, and the effect of O_3 on transcriptomic changes occurred once leaf expansion was achieved, as previously observed at least for soybean (Waldeck et al., 2017). However, by contrast to modules 1 and 2, the genes in modules 4, 7, 11 showed a different regulation of their expression once the leaf was fully expanded. Module 4 contained genes related to photosynthesis, and the high correlation between its profile and net CO_2 assimilation suggests an O_3 impact on CO_2 fixation once photosynthetic apparatus is fully functional. Module 11 encompassed genes related to cell wall and structure during expansion, and their expression during cell growth may help to delay negative effects of O_3 on cell structure, allowing a longer integrity preservation and viability. Module 7 was of particular interest because expression of its genes decreased with leaf development, then increased again in response to O_3 exposure. Those genes are implied in protein metabolic process partly localized in cell wall. During cell growth, cell wall is constantly re-arranged by cell wall protein to allow cell expansion and to contribute to the adaptation of their changing environment (Knox, 2008), thus high expression level of genes encoding such protein could confer tolerance to O_3-induced ROS. This is consistent with the high cell wall reinforcement activity observed in young

vs old foliage under same exposure conditions (Chapter 2). Furthermore, core gene of this module encoded for a COBRA-like protein precursor involved in cellulose deposition, frequently observed in response to O_3 stress ((Vollenweider et al., 2002; Paoletti et al., 2009; Feng et al., 2016); chapter 2).

The effect of O_3 observed once cell expansion was achieved is consistent with previous results (Turc et al., 2021), and with the general increase in leaf stress susceptibility after the sink-to-source transition (Coleman, 1986). However, the better tolerance of young poplar leaves is more likely due to a more active cell wall remodeling (M7), an integrity that is easier to maintain (M11), and a less sensitive photosynthetic apparatus because it is not yet fully functional (M4) than an increased phenolic compound content or antioxidant activity as previously proposed (Strohm et al., 2002; Bellini and De Tullio, 2019; Turc et al., 2021).

Identification of molecular markers for O_3 stress diagnosis

In our experiment, cumulated O_3 dose in leaves (POD_0) was not sufficient to explain transcriptomic changes in response to O_3 exposure as much more differentially expressed genes were detected in the 100 vs 80 ppb O_3 treatment although similar POD_0 levels. Therefore, we proposed a list of highly expressed and correlated genes with HR-like lesion in response to O_3 (Table S5), which can be an initial list to determine molecular O_3 markers for forest health diagnosis, as recently proposed by (Nosenko et al., 2021) in case of pathogen.

Among the most five correlated genes with HR-like lesion, four encoded for genes involved in response to biotic and/or abiotic stress and include two glutamate receptors (GLR), a S-locus lectin protein kinase and a NB-ARC domain-containing disease resistance protein. In plant, glutamate (Glu) was recently found to have signaling properties involved in many physiological processes including growth, germination, root architecture, pathogen resistance and abiotic stress response (Qiu et al., 2020). Glu exerts its signaling function by glutamate receptor (GLR), which partially mediated the cytosolic increase in Ca^{2+} inducing defense-related gene expression following pathogen infection (Li et al., 2013; Manzoor et al., 2013). Lectin receptor kinase are involved in pathogen recognition and subsequent activation of defense-related genes (Singh and Zimmerli, 2013) and NB-ARC domain containing protein is implied in pathogen defense (Takken et al., 2006).

Therefore, the higher tolerance of young leaves can be attributed to the expression of genes involved in development, rather than expression of particular genes stimulated only in young leaves. The genes correlated with HR-like have functions in biotic stress bringing insights on the molecular mechanism of HR-like, making it closer to HR. Nevertheless, this list of genes constitutes a set of early molecular markers of O_3 stress that needs to be validated in further experiments and under a wide range of conditions.

Supplemental material

Table S1. Number of sequenced and single-mapped reads in the 72 libraries

		Number of reads					
	Librairies	sequenced	after quality filtering and trimming	mapped	single-mapping reads	overlapping reads per locus	single-mapping reads (% of the mapped reads)
2d_CTL_F3_1	**BP01**	86949182	86173220	83258197	81467013	80786376	97.8
2d_CTL_F3_2	**BP02**	73382104	72650876	69975895	68417610	67793499	97.8
2d_CTL_F3_3	**BP03**	88289690	87440029	84473782	82469368	81796982	97.6
2d_CTL_F3_4	**BP04**	100419746	98231416	94342691	92292616	91445650	97.8
2d_O80_F3_1	**BP05**	86520168	85195107	81476064	79764067	78875882	97.9
2d_O80_F3_2	**BP06**	79592482	78662109	75877023	74183948	73604054	97.8
2d_O80_F3_3	**BP07**	90859052	83508805	80026696	78223406	77505028	97.7
2d_O80_F3_4	**BP08**	86738448	85521678	82208228	80378659	79713923	97.8
2d_O100_F3_1	**BP09**	89443710	88386984	85227506	83275488	82549037	97.7
2d_O100_F3_2	**BP10**	91612184	90165763	86883953	84918670	84235296	97.7
2d_O100_F3_3	**BP11**	107568564	106731702	103175256	100776564	100065473	97.7
2d_O100_F3_4	**BP12**	78880646	64790786	62188891	60511070	59937556	97.3
2d_CTL_F10_1	**BP13**	78642946	77468292	74762058	72922128	72318618	97.5
2d_CTL_F10_2	**BP14**	81408884	80143401	77716354	75740543	75133995	97.5
2d_CTL_F10_3	**BP15**	69199210	67962782	65372516	63630960	63102055	97.3
2d_CTL_F10_4	**BP16**	80887492	78176363	75329798	73424768	72819795	97.5
2d_O80_F10_1	**BP17**	90337842	86987693	84045699	81903110	81179867	97.5
2d_O80_F10_2	**BP18**	59416398	58501358	56428214	55013409	54569613	97.5
2d_O80_F10_3	**BP19**	66575718	65930618	64016500	62472504	61973603	97.6
2d_O80_F10_4	**BP20**	80385272	77463622	75234288	73393085	72804150	97.6
2d_O100_F10_1	**BP21**	114093820	109087249	105841676	103158019	102316827	97.5
2d_O100_F10_2	**BP22**	66925678	66041557	63839580	62208021	61604656	97.4
2d_O100_F10_3	**BP23**	83878614	81889500	78828869	77186925	76392651	97.9
2d_O100_F10_4	**BP24**	66738300	65617606	63439224	62125673	61540105	97.9
8d_CTL_F3_1	**BP25**	94164554	93371122	89348260	87236324	86293835	97.6
8d_CTL_F3_2	**BP26**	73314756	72546800	69097597	67430978	66655154	97.6
8d_CTL_F3_3	**BP27**	113750398	112534582	107146415	104453618	103145335	97.5
8d_CTL_F3_4	**BP28**	101287910	100470148	95790268	93156608	92147651	97.3
8d_O80_F3_1	**BP29**	76183626	75595003	72298311	70528643	69768714	97.6
8d_O80_F3_2	**BP30**	82211270	81399784	77719339	75766304	74941471	97.5
8d_O80_F3_3	**BP31**	67387204	66712679	63953730	62381947	61715196	97.5
8d_O80_F3_4	**BP32**	65698658	64189484	61290438	59808053	59149993	97.6
8d_O100_F3_1	**BP33**	75073568	74211468	70935201	69015637	68187752	97.3
8d_O100_F3_2	**BP34**	62632622	61810542	58857814	57462401	56768779	97.6
8d_O100_F3_3	**BP35**	101649164	100390850	96000810	93643283	92613143	97.5
8d_O100_F3_4	**BP36**	67656568	65881922	62737596	60986843	60258194	97.2
8d_CTL_F10_1	**BP37**	69141120	68436181	66341465	64863745	64385503	97.8
8d_CTL_F10_2	**BP38**	72642142	71953968	69511602	68008786	67455389	97.8
8d_CTL_F10_3	**BP39**	77489446	76439678	73868457	72213073	71631772	97.8
8d_CTL_F10_4	**BP40**	70743604	70197314	67986264	66446705	65950371	97.7
8d_O80_F10_1	**BP41**	71640528	70573501	67783230	66318202	65797844	97.8
8d_O80_F10_2	**BP42**	66876106	65426466	62951061	61555261	61143936	97.8
8d_O80_F10_3	**BP43**	95213022	94165379	90872506	88886898	88133396	97.8
8d_O80_F10_4	**BP44**	99914888	98976415	95389418	93266037	92465336	97.8
8d_O100_F10_1	**BP45**	93847110	82478634	79743719	77747659	77064698	97.5
8d_O100_F10_2	**BP46**	83433672	79601569	76892349	74848602	74263000	97.3
8d_O100_F10_3	**BP47**	71092090	69974436	67323094	65692530	65090735	97.6
8d_O100_F10_4	**BP48**	77225248	69864367	67705857	66011985	65492568	97.5
13d_CTL_F3_1	**BP49**	88578782	87105601	83198474	81082517	80160042	97.5
13d_CTL_F3_2	**BP50**	80986562	80177987	75788846	73667615	72607609	97.2
13d_CTL_F3_3	**BP51**	84543874	83722812	79955157	77553826	76629958	97.0
13d_CTL_F3_4	**BP52**	89065826	88028837	83344579	80750843	79748138	96.9
13d_O80_F3_1	**BP53**	91421876	87425276	83415096	81030808	79970412	97.1
13d_O80_F3_2	**BP54**	85424862	84349814	80294992	77963660	76973677	97.1
13d_O80_F3_3	**BP55**	**48785588**	48166521	46024295	44696380	44168085	97.1
13d_O80_F3_4	**BP56**	95293574	94554728	90119911	87984745	86875491	97.6
13d_O100_F3_1	**BP57**	112383350	111027344	105658266	102654191	101402472	97.2
13d_O100_F3_2	**BP58**	88088370	87396139	83114629	80682795	79656183	97.1
13d_O100_F3_3	**BP59**	80682698	75833390	72473190	70457470	69626564	97.2
13d_O100_F3_4	**BP60**	88983930	88334042	84278120	82044812	81059297	97.4
13d_CTL_F10_1	**BP61**	78384828	77377573	74294611	72581769	71776647	97.7
13d_CTL_F10_2	**BP62**	90703234	89315513	86113052	83901254	83214322	97.4
13d_CTL_F10_3	**BP63**	88271508	87540884	84179516	82151881	81377983	97.6
13d_CTL_F10_4	**BP64**	78676070	77933817	74680096	72994970	72305624	97.7
13d_O80_F10_1	**BP65**	90754838	89543337	84943603	82909040	81956783	97.6
13d_O80_F10_2	**BP66**	81533182	80705560	77419805	75548184	74845498	97.6
13d_O80_F10_3	**BP67**	72344882	71831277	68748070	67103053	66363886	97.6
13d_O80_F10_4	**BP68**	95848762	94939996	91356092	89213182	88441261	97.7
13d_O100_F10_1	**BP69**	84973034	83809934	80015893	77945623	77065601	97.4
13d_O100_F10_2	**BP70**	81110582	80099775	76430906	74267505	73439424	97.2
13d_O100_F10_3	**BP71**	98765896	97740354	93349325	90627553	89619236	97.1
13d_O100_F10_4	**BP72**	85026754	83692665	79447739	77347581	76519869	97.4

Table S2. Dynamics of leaf percentage area showing HR-like lesion, loss of chlorophyll content relative to control treatment and leaf visible injury observed in hybrid poplar leaves (*Populus tremula x alba*), in response to O_3 treatment and as a function of the leaf position and assessment time. Model: lmer(variable ~ O_3 treatment * leaf position * time + (1 | pot)); *** $p \leq 0.001$, * $p \leq 0.05$, ns not significantly different). Values represent mean ± SE, n = 4. Different letters indicate significant differences between treatments for a given assessment date (Tukey- s post-hoc test, $p \leq 0.05$).

Leaf position	Time (days)	Total HR-like (leaf %)			Relative loss of chlorophyll content (%)		Visible injury (leaf %)		
		Control	*80 ppb O_3*	*100 ppb O_3*	*80 ppb O_3*	*100 ppb O_3*	*Control*	*80 ppb O_3*	*100 ppb O_3*
10th	2	0 ±0.00 *a*	0.01 ±0.01 *a*	0.02 ±0.02 *a*	-3.62 ±3.24 *a*	0.80 ±2.39 *a*	0.00 ±0.00 *a*	0.00 ±0.00 *a*	0.00 ±0.00 *a*
	8	0 ±0.00 *a*	0.00 ±0.00 *a*	0.02 ±0.01 *a*	0.14 ±6.08 *a*	0.68 ±3.86 *a*	0.00 ±0.00 *a*	0.00 ±0.00 *a*	0.00 ±0.00 *a*
	13	0 ±0.00 *a*	0.03 ±0.02 *a*	10.28 ±1.79 *c*	-2.25 ±1.65 *a*	9.30 ±5.86 *ab*	0.00 ±0.00 *a*	0.00 ±0.00 *a*	0.00 ±0.00 *a*
	23	0 ±0.00 *a*	11.81 ±1.23 *bc*	15.94 ±2.32 *bc*	4.03 ±0.46 *a*	24.76 ±5.93 *b*	0.00 ±0.00 *a*	0.03 ±0.02 *a*	0.01 ±0.01 *a*
3rd	2	0 ±0.00 *a*	0.12 ±0.04 *a*	0.08 ±0.07 *a*	-7.96 ±6.67 *a*	4.71 ±6.1 *a*	0.00 ±0.00 *a*	0.00 ±0.00 *a*	0.00 ±0.00 *a*
	8	0 ±0.00 *a*	3.07 ±1.48 *b*	7.15 ±3.23 *a*	9.54 ±6.22 *b*	13.23 ±2.72 *a*	0.00 ±0.00 *a*	0.00 ±0.00 *a*	0.00 ±0.00 *a*
	13	0 ±0.00 *a*	3.46 ±2.10 *b*	21.35 ±2.37 *c*	5.84 ±3.09 *ab*	21.25 ±4.81 *b*	0.00 ±0.00 *a*	0.00 ±0.00 *a*	0.00 ±0.00 *a*
	23	0 ±0.00 *a*	11.10 ±5.21 *b*	19.73 ±2.12 *c*	17.78 ±1.8 *ab*	36.55 ±7.84 *b*	0.00 ±0.00 *a*	0.04 ±0.02 *a*	0.26 ±0.12 *b*

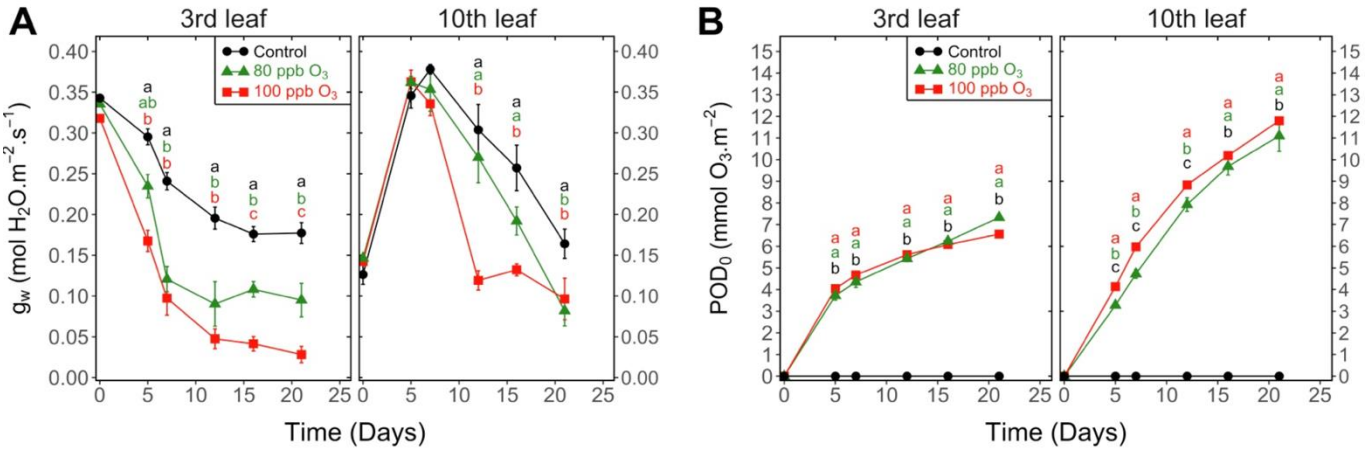

Figure S2. Dynamics of changes in the (**A**) stomatal conductance to water (g_w) and (**B**) phytotoxic O_3 dose (POD_0) of hybrid poplar leaves (*Populus tremula x alba*), as a function of O_3 treatment (charcoal-filtered air ●, 80 ppb O_3 ▲, 100 ppb O_3 ■), leaf position, time of assessment and interactions {model: lmer[sqrt(variable)] ~ O_3 treatment ∗ leaf position ∗ time + (1 | tree / chamber); ∗∗∗ $p \leq 0.001$}. Values represent means ± SE, n = 4. Different letters indicate significant differences between treatments for a given assessment date (Tukey's post-hoc test, $p \leq 0.05$).

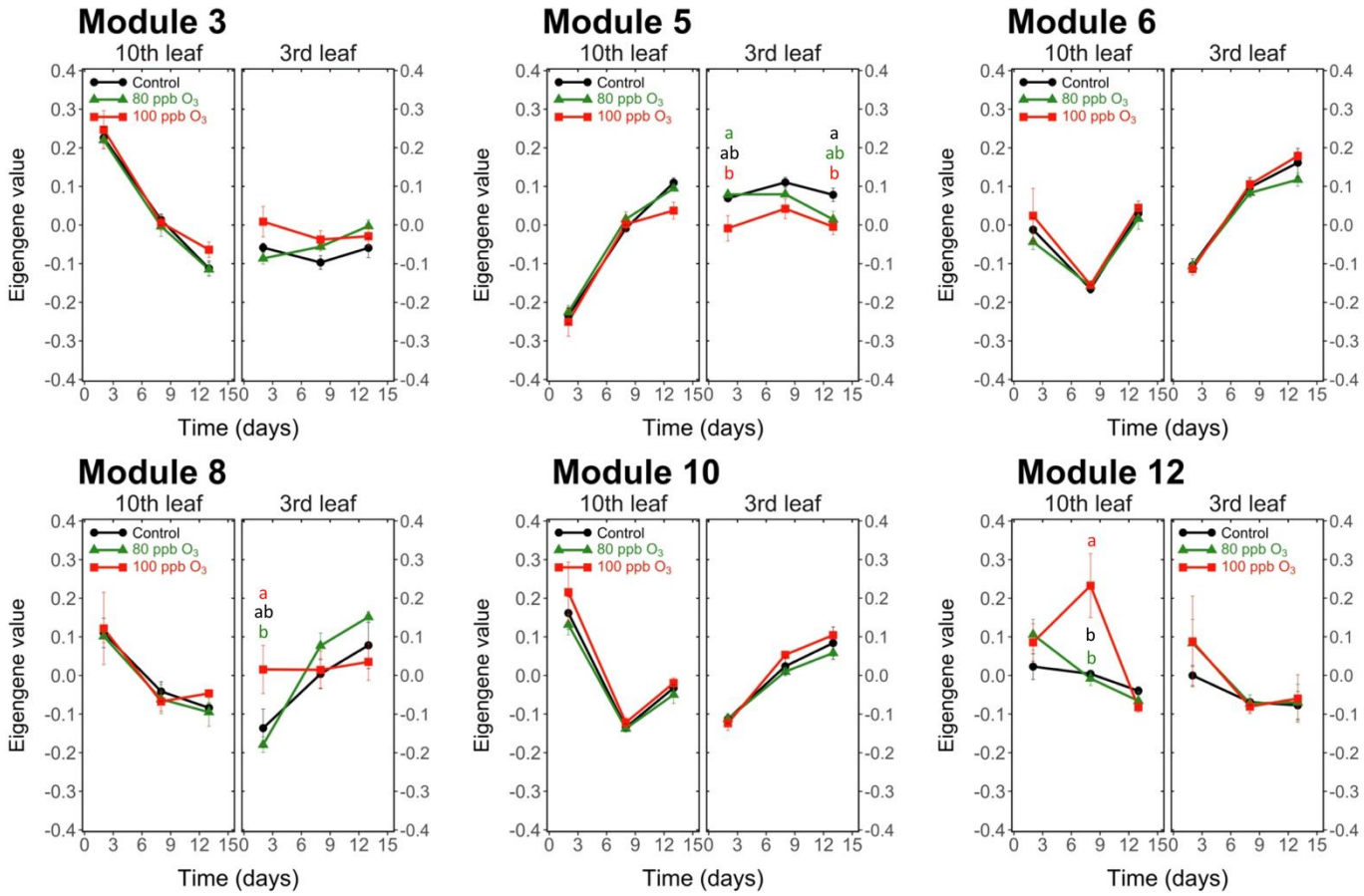

Figure S2. WGCNA module profile as a function of O_3 treatment, leaf position and time. Values represent means ± SE, *n* = 4. Different letters indicate significant differences between treatments at a given assessment date (Tukey's post-hoc test, $p \leq 0.05$).

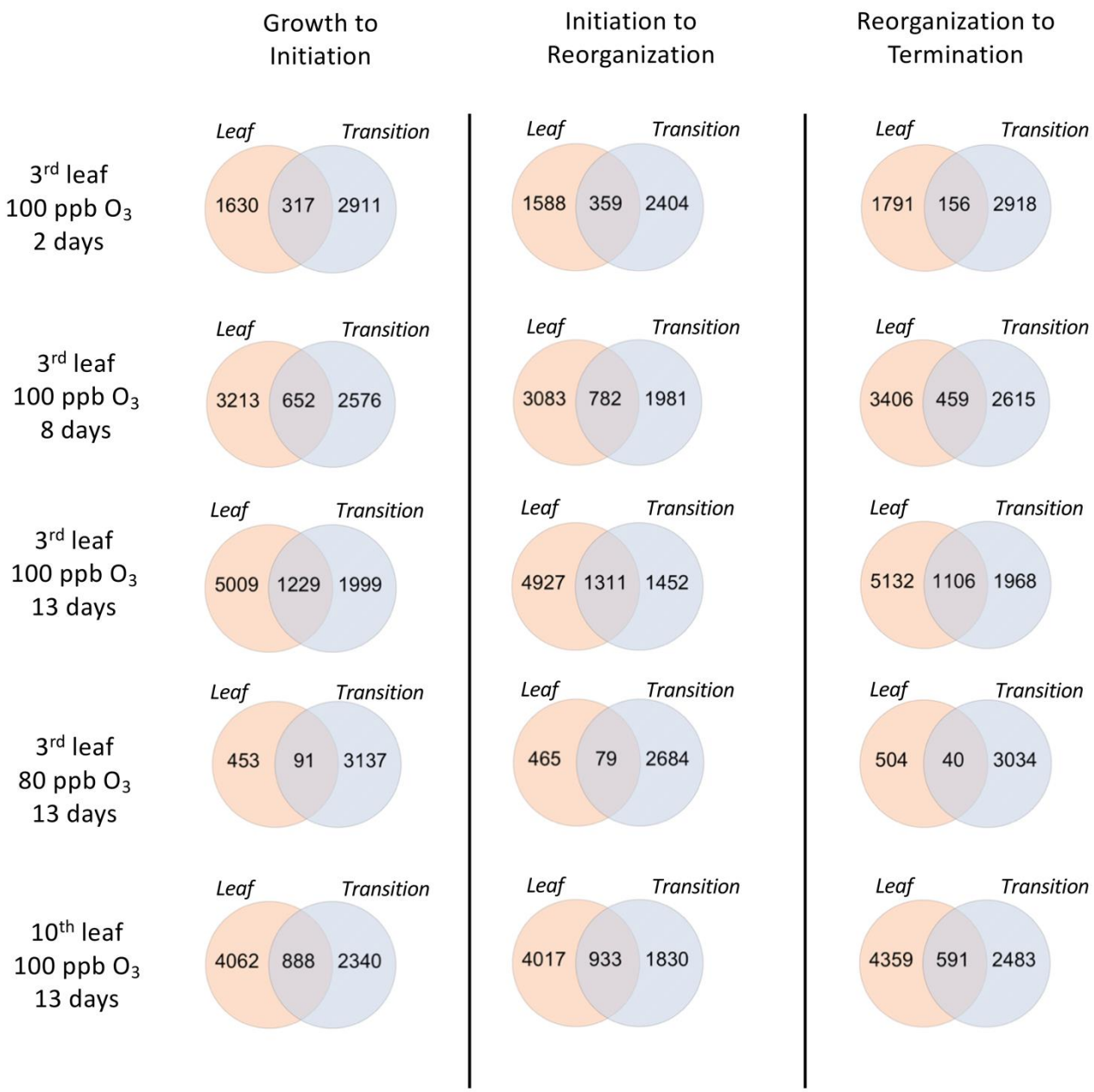

Figure S3. Venn diagrams showing number of upregulated DEGs from third and tenth leaf position of hybrid poplars exposed to O_3 treatments (80 and 100 ppb) and DEGs in relation to three phases of senescence transition according to Lu et al. (2020).

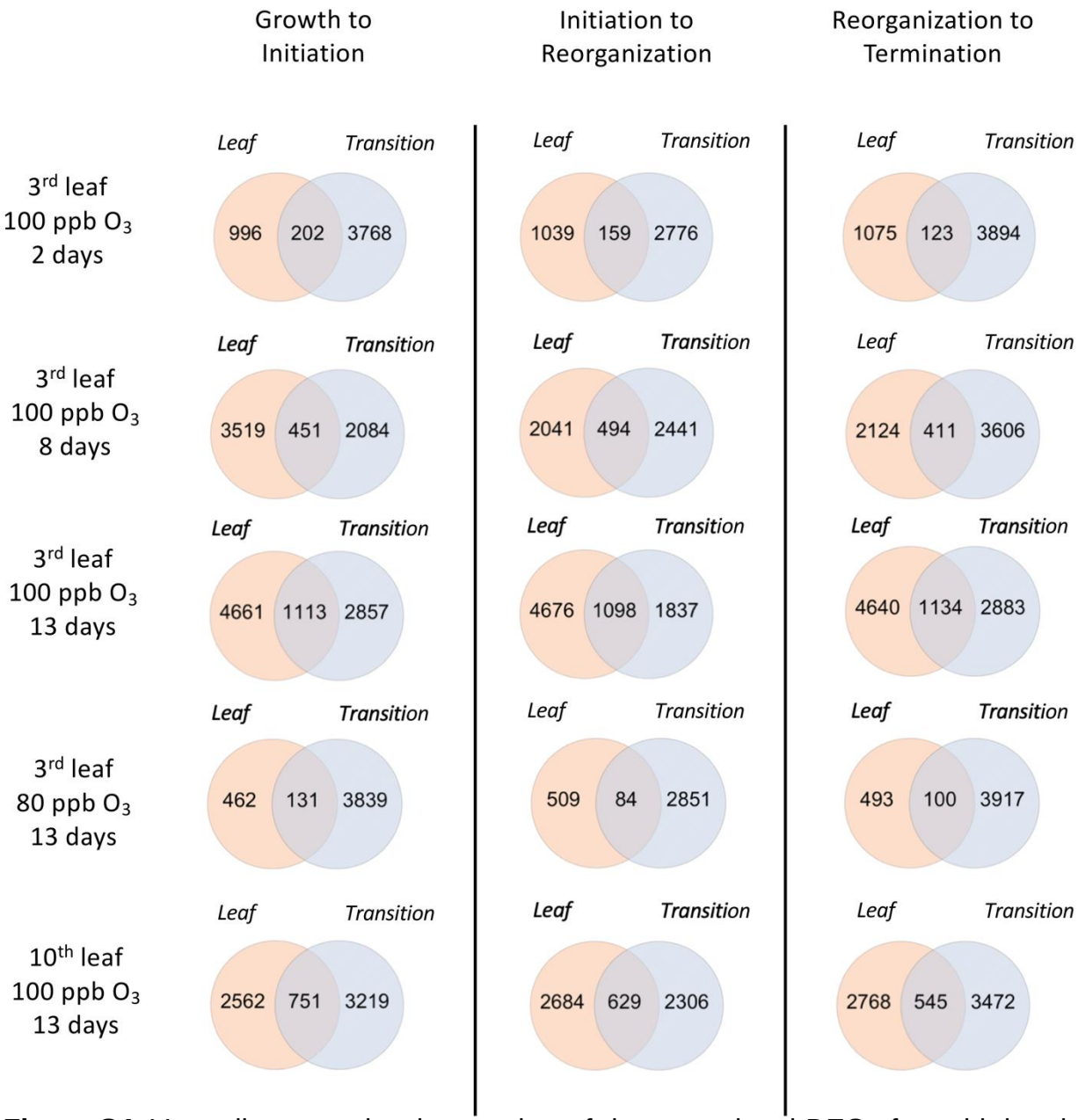

Figure S4. Venn diagrams showing number of down-regulated DEGs from third and tenth leaf position of hybrid poplars exposed to O_3 treatments (80 and 100 ppb) and DEGs in relation to three phases of senescence transition according to Lu et al. (2020).

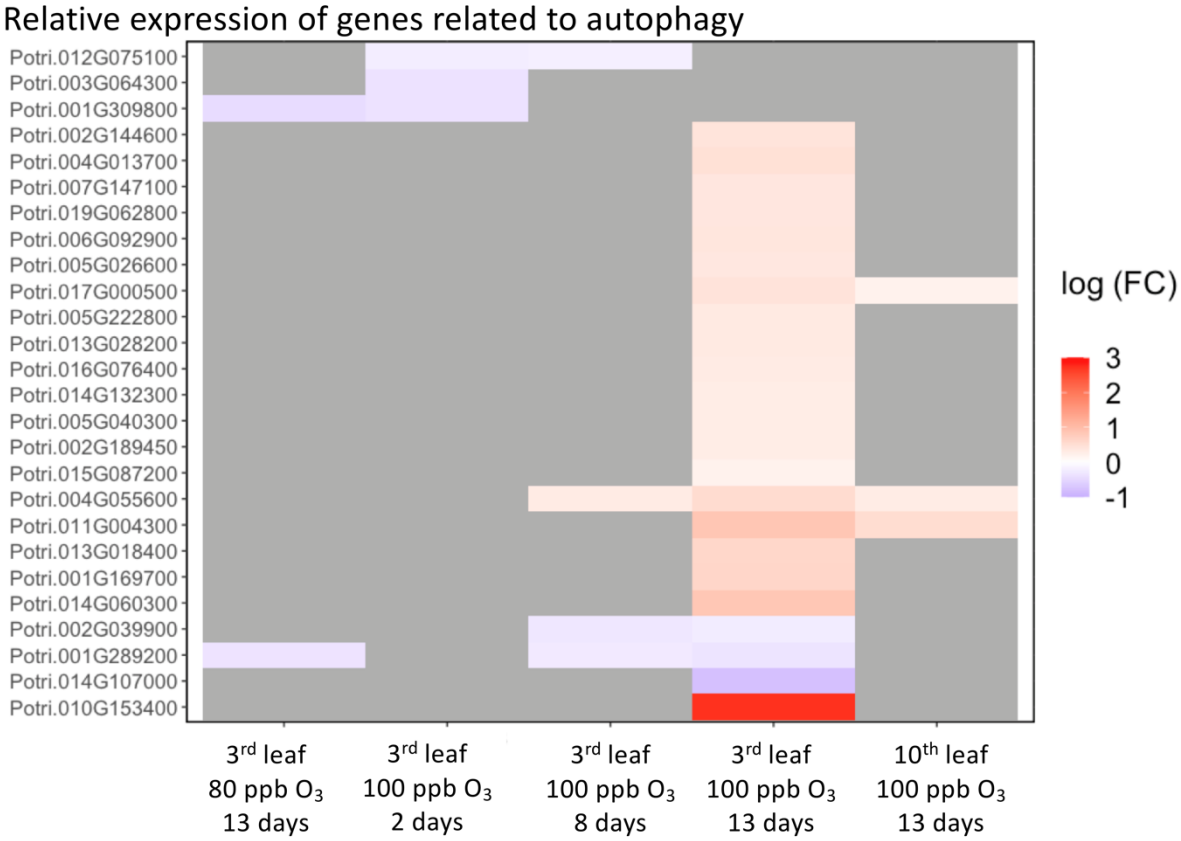

Figure S5. Heatmap showing relative expression of genes related to autophagy (according to (Han et al., 2011)) at the third and tenth leaf position of hybrid poplars exposed to O_3 treatments (80 and 100 ppb).

Table S3. List of GO enrichment of WGCNA modules

Tags	GO ID	GO Name	GO Category	Modules	FDR	P-Value
[OVER]	GO:0006464	cellular protein modification process	BIOLOGICAL_PROCESS	1	1.99E-88	5.38E-90
[OVER]	GO:0006950	response to stress	BIOLOGICAL_PROCESS	1	1.74E-57	7.52E-59
[OVER]	GO:0009607	response to biotic stimulus	BIOLOGICAL_PROCESS	1	5.92E-53	3.84E-54
[OVER]	GO:0007165	signal transduction	BIOLOGICAL_PROCESS	1	1.07E-40	1.57E-41
[OVER]	GO:0042221	response to chemical	BIOLOGICAL_PROCESS	1	3.74E-36	6.66E-37
[OVER]	GO:0009719	response to endogenous stimulus	BIOLOGICAL_PROCESS	1	4.32E-22	1.24E-22
[OVER]	GO:0009856	pollination	BIOLOGICAL_PROCESS	1	9.44E-17	3.01E-17
[OVER]	GO:0009056	catabolic process	BIOLOGICAL_PROCESS	1	3.02E-14	1.01E-14
[OVER]	GO:0006810	transport	BIOLOGICAL_PROCESS	1	3.42E-12	1.35E-12
[OVER]	GO:0008219	cell death	BIOLOGICAL_PROCESS	1	6.03E-10	2.61E-10
[OVER]	GO:0009628	response to abiotic stimulus	BIOLOGICAL_PROCESS	1	2.42E-09	1.06E-09
[OVER]	GO:0065009	regulation of molecular function	BIOLOGICAL_PROCESS	1	8.17E-05	4.73E-05
[OVER]	GO:0019725	cellular homeostasis	BIOLOGICAL_PROCESS	1	0.024631423	0.017042282
[OVER]	GO:0005886	plasma membrane	CELLULAR_COMPONENT	1	1.35E-20	4.01E-21
[OVER]	GO:0005768	endosome	CELLULAR_COMPONENT	1	2.05E-12	7.76E-13
[OVER]	GO:0005783	endoplasmic reticulum	CELLULAR_COMPONENT	1	3.25E-08	1.44E-08
[OVER]	GO:0005777	peroxisome	CELLULAR_COMPONENT	1	1.31E-07	6.29E-08
[OVER]	GO:0005829	cytosol	CELLULAR_COMPONENT	1	1.72E-06	9.32E-07
[OVER]	GO:0005773	vacuole	CELLULAR_COMPONENT	1	3.76E-04	2.21E-04
[OVER]	GO:0005794	Golgi apparatus	CELLULAR_COMPONENT	1	0.0072766	0.004798623
[OVER]	GO:0005654	nucleoplasm	CELLULAR_COMPONENT	1	0.00760299	0.005054961
[OVER]	GO:0000166	nucleotide binding	MOLECULAR_FUNCTION	1	1.32E-48	1.29E-49
[OVER]	GO:0016301	kinase activity	MOLECULAR_FUNCTION	1	9.04E-46	1.03E-46
[OVER]	GO:0005515	protein binding	MOLECULAR_FUNCTION	1	1.95E-34	3.58E-35
[OVER]	GO:0030246	carbohydrate binding	MOLECULAR_FUNCTION	1	3.42E-27	8.68E-28
[OVER]	GO:0003700	DNA-binding transcription factor activity	MOLECULAR_FUNCTION	1	3.30E-05	1.86E-05
[OVER]	GO:0008289	lipid binding	MOLECULAR_FUNCTION	1	0.001210287	7.47E-04
[OVER]	GO:0003682	chromatin binding	MOLECULAR_FUNCTION	1	0.013849967	0.009358086
[OVER]	GO:0003677	DNA binding	MOLECULAR_FUNCTION	1	0.047819333	0.034636706
[OVER]	GO:0007049	cell cycle	BIOLOGICAL_PROCESS	2	3.88E-29	2.52E-30
[OVER]	GO:0016043	cellular component organization	BIOLOGICAL_PROCESS	2	1.09E-23	8.80E-25
[OVER]	GO:0015979	photosynthesis	BIOLOGICAL_PROCESS	2	2.92E-23	2.52E-24
[OVER]	GO:0006091	generation of precursor metabolites and energy	BIOLOGICAL_PROCESS	2	1.75E-14	2.28E-15
[OVER]	GO:0005975	carbohydrate metabolic process	BIOLOGICAL_PROCESS	2	2.86E-14	3.86E-15
[OVER]	GO:0006259	DNA metabolic process	BIOLOGICAL_PROCESS	2	1.43E-09	2.40E-10
[OVER]	GO:0009606	tropism	BIOLOGICAL_PROCESS	2	1.10E-04	2.80E-05
[OVER]	GO:0009058	biosynthetic process	BIOLOGICAL_PROCESS	2	4.83E-04	1.54E-04
[OVER]	GO:0006629	lipid metabolic process	BIOLOGICAL_PROCESS	2	7.86E-04	2.73E-04
[OVER]	GO:0009790	embryo development	BIOLOGICAL_PROCESS	2	0.00252785	9.70E-04
[OVER]	GO:0016049	cell growth	BIOLOGICAL_PROCESS	2	0.003844295	0.001620838
[OVER]	GO:0009416	response to light stimulus	BIOLOGICAL_PROCESS	2	0.017431446	0.008385939
[OVER]	GO:0030154	cell differentiation	BIOLOGICAL_PROCESS	2	0.039796738	0.021726868
[OVER]	GO:0009507	chloroplast	CELLULAR_COMPONENT	2	5.32E-199	2.88E-201
[OVER]	GO:0009579	thylakoid	CELLULAR_COMPONENT	2	5.37E-78	8.71E-80
[OVER]	GO:0005856	cytoskeleton	CELLULAR_COMPONENT	2	4.78E-29	3.36E-30
[OVER]	GO:0005739	mitochondrion	CELLULAR_COMPONENT	2	1.19E-06	2.77E-07
[OVER]	GO:0005576	extracellular region	CELLULAR_COMPONENT	2	5.85E-06	1.42E-06
[OVER]	GO:0005886	plasma membrane	CELLULAR_COMPONENT	2	0.015033369	0.006907224
[OVER]	GO:0005618	cell wall	CELLULAR_COMPONENT	2	0.017431446	0.0083368
[OVER]	GO:0003774	motor activity	MOLECULAR_FUNCTION	2	4.35E-16	5.41E-17
[OVER]	GO:0016740	transferase activity	MOLECULAR_FUNCTION	2	8.65E-04	3.09E-04
[OVER]	GO:0004518	nuclease activity	MOLECULAR_FUNCTION	2	0.028027064	0.014089281
[OVER]	GO:0015979	photosynthesis	BIOLOGICAL_PROCESS	4	1.65E-12	2.68E-14
[OVER]	GO:0006091	generation of precursor metabolites and energy	BIOLOGICAL_PROCESS	4	5.95E-06	6.25E-07
[OVER]	GO:0007623	circadian rhythm	BIOLOGICAL_PROCESS	4	5.95E-06	7.53E-07
[OVER]	GO:0009416	response to light stimulus	BIOLOGICAL_PROCESS	4	1.52E-04	3.29E-05
[OVER]	GO:0005975	carbohydrate metabolic process	BIOLOGICAL_PROCESS	4	2.13E-04	4.71E-05
[OVER]	GO:0019725	cellular homeostasis	BIOLOGICAL_PROCESS	4	2.39E-04	5.68E-05
[OVER]	GO:0019748	secondary metabolic process	BIOLOGICAL_PROCESS	4	0.046434264	0.015310757
[OVER]	GO:0009507	chloroplast	CELLULAR_COMPONENT	4	4.06E-25	2.20E-27
[OVER]	GO:0009579	thylakoid	CELLULAR_COMPONENT	4	9.96E-11	2.15E-12
[OVER]	GO:0016020	membrane	CELLULAR_COMPONENT	4	1.06E-06	6.87E-08
[OVER]	GO:0005215	transporter activity	MOLECULAR_FUNCTION	4	0.009593335	0.002644649
[OVER]	GO:0003824	catalytic activity	MOLECULAR_FUNCTION	4	0.011803625	0.003381579
[OVER]	GO:0003700	DNA-binding transcription factor activity	MOLECULAR_FUNCTION	4	0.029284857	0.009022902
[OVER]	GO:0019538	protein metabolic process	BIOLOGICAL_PROCESS	7	0.005318114	5.75E-04
[OVER]	GO:0005783	endoplasmic reticulum	CELLULAR_COMPONENT	7	5.99E-30	3.24E-32
[OVER]	GO:0005794	Golgi apparatus	CELLULAR_COMPONENT	7	1.86E-12	6.02E-14
[OVER]	GO:0005773	vacuole	CELLULAR_COMPONENT	7	1.40E-09	6.83E-11
[OVER]	GO:0005886	plasma membrane	CELLULAR_COMPONENT	7	3.22E-06	2.43E-07
[OVER]	GO:0005829	cytosol	CELLULAR_COMPONENT	7	7.96E-06	6.88E-07
[OVER]	GO:0005618	cell wall	CELLULAR_COMPONENT	7	0.014979612	0.002510097
[OVER]	GO:0016787	hydrolase activity	MOLECULAR_FUNCTION	7	0.006024197	6.84E-04
[OVER]	GO:0016740	transferase activity	MOLECULAR_FUNCTION	7	0.017677365	0.003057706
[OVER]	GO:0006259	DNA metabolic process	BIOLOGICAL_PROCESS	9	1.39E-05	3.76E-07
[OVER]	GO:0007049	cell cycle	BIOLOGICAL_PROCESS	9	9.29E-04	5.02E-05
[OVER]	GO:0030154	cell differentiation	BIOLOGICAL_PROCESS	9	9.59E-04	6.74E-05
[OVER]	GO:0007275	multicellular organism development	BIOLOGICAL_PROCESS	9	0.018824514	0.00345964
[OVER]	GO:0016043	cellular component organization	BIOLOGICAL_PROCESS	9	0.020361075	0.004292335
[OVER]	GO:0005634	nucleus	CELLULAR_COMPONENT	9	3.76E-06	4.07E-08
[OVER]	GO:0005576	extracellular region	CELLULAR_COMPONENT	9	0.028530709	0.006631462
[OVER]	GO:0003677	DNA binding	MOLECULAR_FUNCTION	9	8.60E-10	4.65E-12
[OVER]	GO:0003700	DNA-binding transcription factor activity	MOLECULAR_FUNCTION	9	0.0137785	0.002085395
[OVER]	GO:0005975	carbohydrate metabolic process	BIOLOGICAL_PROCESS	11	5.69E-04	8.23E-06
[OVER]	GO:0016043	cellular component organization	BIOLOGICAL_PROCESS	11	6.99E-04	2.65E-05
[OVER]	GO:0019748	secondary metabolic process	BIOLOGICAL_PROCESS	11	0.03992895	0.003237482
[OVER]	GO:0005856	cytoskeleton	CELLULAR_COMPONENT	11	2.08E-08	1.12E-10
[OVER]	GO:0005576	extracellular region	CELLULAR_COMPONENT	11	6.99E-04	2.60E-05
[OVER]	GO:0071944	cell periphery	CELLULAR_COMPONENT	11	0.031567323	0.001945858
[OVER]	GO:0016020	membrane	CELLULAR_COMPONENT	11	0.03992895	0.00312252

Table S4. List of core genes of WGCNA modules

Genes	kWithin	Modules	annotAll
Potri.004G036600	1867.63562	1	secretory carrier 3
Potri.003G129900	1808.38936	1	RING/U-box superfamily protein
Potri.012G011500	1806.75641	1	RING/U-box superfamily protein
Potri.014G111900	1805.98592	1	WRKY family transcription factor
Potri.018G006400	1791.7149	1	Protein of unknown function (DUF1644)
Potri.014G041300	1785.37297	1	NAC domain containing protein 28
Potri.001G273400	1785.17022	1	pyrimidine 2
Potri.010G212200	1781.86487	1	alpha/beta-Hydrolases superfamily protein
Potri.015G058200	1770.31343	1	exocyst subunit exo70 family protein E2
Potri.002G154600	1992.11208	2	Ribosomal L5P family protein
Potri.014G096500	1970.97712	2	thylakoid rhodanese-like
Potri.006G221100	1963.86822	2	ribosomal protein L4
Potri.003G167700	1951.35122	2	cyclophilin 20-2
Potri.006G228200	1946.92905	2	Fatty acid/sphingolipid desaturase
Potri.005G052000	1938.18653	2	Ribose 5-phosphate isomerase, type A protein
Potri.001G200300	1933.62901	2	Ribonuclease III family protein
Potri.001G404700	1924.80755	2	Cyclophilin-like peptidyl-prolyl cis-trans isomerase family protein
Potri.009G081200	1923.02742	2	pyrophosphorylase 6
Potri.009G049400	1920.8924	2	ALBINA 1
Potri.019G043300	213.559098	4	sigma factor A
Potri.003G119200	212.872469	4	PGR5-LIKE A
Potri.013G148900	205.155822	4	photosynthetic electron transfer C
Potri.014G092200	201.691952	4	Uncharacterized conserved protein (DUF2358)
Potri.017G090100	199.463836	4	(1 of 1) PF14234 - Domain of unknown function (DUF4336) (DUF4336)
Potri.009G043800	197.327539	4	-
Potri.016G115200	196.461189	4	light harvesting complex photosystem II
Potri.001G201500	194.291582	4	alpha/beta-Hydrolases superfamily protein
Potri.008G128900	194.133751	4	quinolinate phoshoribosyltransferase
Potri.005G083200	193.173183	4	ABC2 homolog 13
Potri.014G026800	59.7588624	7	(1 of 2) PTHR31852:SF44 - EMB
Potri.004G117100	52.3373145	7	COBRA-like protein 1 precursor
Potri.009G139600	50.295337	7	geranylgeranyl reductase
Potri.016G109700	49.0765826	7	O-fucosyltransferase family protein
Potri.011G169700	48.1186818	7	Ribonuclease E inhibitor RraA/Dimethylmenaquinone methyltransferase
Potri.003G174200	47.4941749	7	Serinc-domain containing serine and sphingolipid biosynthesis protein
Potri.006G186600	47.4379213	7	LJRHL1-like 1
Potri.008G053300	47.2833267	7	Oligosaccaryltransferase
Potri.005G063700	47.078679	7	plant U-box 25
Potri.006G189600	46.8869695	7	(1 of 1) PTHR35121:SF2 - GB
Potri.003G164200	27.4912976	11	kinase interacting (KIP1-like) family protein
Potri.011G120200	26.4800132	11	laccase 17
Potri.009G042500	25.5204492	11	Laccase/Diphenol oxidase family protein
Potri.011G096500	25.4046407	11	IQ-domain 10
Potri.011G120300	25.2656279	11	laccase 17
Potri.002G111900	24.890208	11	tubulin alpha-2 chain
Potri.006G177600	24.0386329	11	nodulin MtN21 /EamA-like transporter family protein
Potri.007G047500	23.6572462	11	Nucleotide-diphospho-sugar transferases superfamily protein
Potri.015G129400	23.5858415	11	FASCICLIN-like arabinogalactan-protein 11
Potri.012G127900	23.2925965	11	FASCICLIN-like arabinogalactan-protein 11

Table S5. List of genes highly correlated with leaf percentage area showing HR-like lesion.

Genes	R^2 coeficient	Slope of regression line	Annotation
Potri.001G374600	0.815	38.33	glutamate receptor 2.7
Potri.004G027400	0.814	72.08	S-locus lectin protein kinase family protein
Potri.001G302400	0.809	49.6	UDP-glycosyltransferase 73B4
Potri.001G374700	0.807	38.96	glutamate receptor 2.7
Potri.003G099000	0.791	35.85	NB-ARC domain-containing disease resistance protein
Potri.004G076200	0.767	55.81	Class I glutamine amidotransferase-like superfamily protein
Potri.010G232700	0.759	72.14	glycosyltransferase family protein 47
Potri.009G140800	0.745	74.34	Transmembrane amino acid transporter family protein
Potri.007G125800	0.738	151.29	Protein kinase superfamily protein
Potri.010G097600	0.735	69.34	glutaredoxin-related
Potri.003G181400	0.733	570.39	cinnamoyl coa reductase 1
Potri.017G076800	0.731	1244.64	Major facilitator superfamily protein
Potri.007G125200	0.729	130.47	suppressor of npr1-1 constitutive 4
Potri.006G048500	0.727	99.45	Glycosyltransferase family 61 protein
Potri.001G317001	0.726	39.59	-
Potri.001G131500	0.722	149.87	-
Potri.003G152400	0.722	64.14	-
Potri.003G149700	0.72	87.24	NAC domain containing protein 42
Potri.006G209200	0.716	150.66	NAC domain containing protein 90
Potri.007G125450	0.716	263.32	suppressor of npr1-1 constitutive 4
Potri.016G123300	0.716	64.81	lectin receptor kinase
Potri.001G038525	0.713	143.06	Wall-associated kinase family protein
Potri.005G188300	0.713	135.14	pathogenesis-related family protein
Potri.001G040500	0.709	37.04	Wall-associated kinase family protein
Potri.001G040628	0.705	30.31	Wall-associated kinase family protein
Potri.008G175100	0.703	203.94	glutathione S-transferase tau 7
Potri.016G122650	0.703	45.15	lectin receptor kinase

REFERENCES

Bagard, M., Jolivet, Y., Hasenfratz-Sauder, M.P., Gerard, J., Dizengremel, P., and Le Thiec, D. (2015). Ozone exposure and flux-based response functions for photosynthetic traits in wheat, maize and poplar. *Environ Pollut* 206**,** 411-420.

Bagard, M., Le Thiec, D., Delacote, E., Hasenfratz-Sauder, M.P., Banvoy, J., Gerard, J., Dizengremel, P., and Jolivet, Y. (2008). Ozone-induced changes in photosynthesis and photorespiration of hybrid poplar in relation to the developmental stage of the leaves. *Physiol Plant* 134**,** 559-574.

Bellini, E., and De Tullio, M.C. (2019). Ascorbic acid and ozone: Novel perspectives to explain an elusive relationship. *Plants* 8.

Bhattacharjee, S. (2005). Reactive oxygen species and oxidative burst: Roles in stress, senescence and signal transduction in plants. *Curr. Sci.* 89**,** 1113-1121.

Büker, P., Feng, Z., Uddling, J., Briolat, A., Alonso, R., Braun, S., Elvira, S., Gerosa, G., Karlsson, P.E., Le Thiec, D., Marzuoli, R., Mills, G., Oksanen, E., Wieser, G., Wilkinson, M., and Emberson, L.D. (2015). New flux based dose-response relationships for ozone for European forest tree species. *Environ Pollut* 206**,** 163-174.

Cho, K., Shibato, J., Kubo, A., Kohno, Y., Satoh, K., Kikuchi, S., Sarkar, A., Agrawal, G.K., and Rakwal, R. (2013). Comparative analysis of seed transcriptomes of ambient ozone-fumigated 2 different rice cultivars. *Plant Signal Behav* 8**,** e26300.

Coleman, J.S. (1986). Leaf development and leaf stress: increased susceptibility associated with sink-source transition. *Tree Physiol.* 2**,** 289-299.

Conesa, A., Gotz, S., Garcia-Gomez, J.M., Terol, J., Talon, M., and Robles, M. (2005). Blast2GO: a universal tool for annotation, visualization and analysis in functional genomics research. *Bioinformatics* 21**,** 3674-3676.

Del Fabbro, C., Scalabrin, S., Morgante, M., and Giorgi, F.M. (2013). An Extensive Evaluation of Read Trimming Effects on Illumina NGS Data Analysis. *Plos One* 8.

Dizengremel, P., Jolivet, Y., Tuzet, A., Ranieri, A., and Le Thiec, D. (2013). "Integrative leaf-level phytotoxic ozone dose assessment for forest risk modelling," in *Climate Change, Air Pollution and Global Challenges: Understanding and Perspectives from Forest Research,* eds. R. Matyssek, N. Clarke, P. Cudlin, T.N. Mikkelsen, J.P. Tuovinen, G. Wieser *&* E. Paoletti. (Netherlands: Elsevier), 267-288.

Faoro, F., and Iriti, M. (2009). Plant cell death and cellular alterations induced by ozone: key studies in Mediterranean conditions. *Environ Pollut* 157**,** 1470-1477.

Fu, T.M., and Tian, H. (2019). Climate change penalty to ozone air quality: Review of current understandings and knowledge gaps. *Curr. Pollut. Rep.* 5**,** 159-171.

Goodstein, D.M., Shu, S.Q., Howson, R., Neupane, R., Hayes, R.D., Fazo, J., Mitros, T., Dirks, W., Hellsten, U., Putnam, N., and Rokhsar, D.S. (2012). Phytozome: a comparative platform for green plant genomics. *Nucleic Acids Research* 40**,** D1178-D1186.

Günthardt-Goerg, M.S., and Vollenweider, P. (2007). Linking stress with macroscopic and microscopic leaf response in trees: new diagnostic perspectives. *Environ Pollut* 147**,** 467-488.

Han, S.J., Yu, B.J., Wang, Y., and Liu, Y.L. (2011). Role of plant autophagy in stress response. *Protein & Cell* 2**,** 784-791.
Jolivet, Y., Bagard, M., Cabane, M., Vaultier, M.N., Gandin, A., Afif, D., Dizengremel, P., and Le Thiec, D. (2016). Deciphering the ozone-induced changes in cellular processes: a prerequisite for ozone risk assessment at the tree and forest levels. *Ann. For. Sci.* 73**,** 923-943.
Joo, J.H., Wang, S., Chen, J.G., Jones, A.M., and Fedoroff, N.V. (2005). Different signaling and cell death roles of heterotrimeric G protein alpha and beta subunits in the Arabidopsis oxidative stress response to ozone. *Plant Cell* 17**,** 957-970.
Jwa, N.S., and Hwang, B.K. (2017). Convergent Evolution of Pathogen Effectors toward Reactive Oxygen Species Signaling Networks in Plants. *Frontiers in Plant Science* 8.
Kangasjarvi, J., Jaspers, P., and Kollist, H. (2005). Signalling and cell death in ozone-exposed plants. *Plant Cell & Environ.* 28**,** 1021-1036.
Karlsson, P., Braun, S., Broadmeadow, M., Elvira, S., Emberson, L., Gimeno, B.S., Le Thiec, D., Novak, K., Oksanen, E., Schaub, M., Uddling, J., and Wilkinson, M. (2007). Risk assessments for forest trees: The performance of the ozone flux versus the AOT concepts. *Environ Pollut* 146**,** 608-616.
Kim, D., Pertea, G., Trapnell, C., Pimentel, H., Kelley, R., and Salzberg, S.L. (2013). TopHat2: accurate alignment of transcriptomes in the presence of insertions, deletions and gene fusions. *Genome Biology* 14.
Knox, J.P. (2008). Revealing the structural and functional diversity of plant cell walls. *Current Opinion in Plant Biology* 11**,** 308-313.
Langfelder, P., and Horvath, S. (2008). WGCNA: an R package for weighted correlation network analysis. *Bmc Bioinformatics* 9.
Li, F., Wang, J., Ma, C.L., Zhao, Y.X., Wang, Y.C., Hasi, A., and Qi, Z. (2013). Glutamate Receptor-Like Channel3.3 Is Involved in Mediating Glutathione-Triggered Cytosolic Calcium Transients, Transcriptional Changes, and Innate Immunity Responses in Arabidopsis. *Plant Physiology* 162**,** 1497-1509.
Liao, Y., Smyth, G.K., and Shi, W. (2014). featureCounts: an efficient general purpose program for assigning sequence reads to genomic features. *Bioinformatics* 30**,** 923-930.
Lichtenthaler (1987). ChlorolShylls and Carotenoids: Pigments of Photosynthetic Biomembranes. *METHODS IN ENZYMOLOGY* 148.
Loraine, A.E., Mccormick, S., Estrada, A., Patel, K., and Qin, P. (2013). RNA-Seq of Arabidopsis Pollen Uncovers Novel Transcription and Alternative Splicing. *Plant Physiology* 162**,** 1092-1109.
Love, M.I., Huber, W., and Anders, S. (2014). Moderated estimation of fold change and dispersion for RNA-seq data with DESeq2. *Genome Biology* 15.
Lu, H.W., Gordon, M.I., Amarasinghe, V., and Strauss, S.H. (2020). Extensive transcriptome changes during seasonal leaf senescence in field-grown black cottonwood (Populus trichocarpa Nisqually-1). *Scientific Reports* 10.
Maas, R., and Grennfelt, P. (2016). Towards cleaner air. Scientific assessment report. Emep steering body and working group on effects of the convention on long-range transboundary air pollution, Oslo. 12-16.
Manzoor, H., Kelloniemi, J., Chiltz, A., Wendehenne, D., Pugin, A., Poinssot, B., and Garcia-Brugger, A. (2013). Involvement of the glutamate receptor AtGLR3.3 in plant defense signaling and resistance to Hyaloperonospora arabidopsidis. *Plant Journal* 76**,** 466-480.

Marchica, A., Lorenzini, G., Papini, R., Bernardi, R., Nali, C., and Pellegrini, E. (2019). Signalling molecules responsive to ozone-induced oxidative stress in *Salvia officinalis*. *Sci Total Environ* 657**,** 568-576.
Mayta, M.L., Hajirezaei, M.R., Carrillo, N., and Lodeyro, A.F. (2019). Leaf Senescence: The Chloroplast Connection Comes of Age. *Plants-Basel* 8.
Mills, G., Pleijel, H., Braun, S., Buker, P., Bermejo, V., Calvo, E., Danielsson, H., Emberson, L., Fernandez, I.G., Grunhage, L., Harmens, H., Hayes, F., Karlsson, P.E., and Simpson, D. (2011). New stomatal flux-based critical levels for ozone effects on vegetation. *Atmos. Environ.* 45**,** 5064-5068.
Moura, B.B., Alves, E.S., Marabesi, M.A., De Souza, S.R., Schaub, M., and Vollenweider, P. (2018). Ozone affects leaf physiology and causes injury to foliage of native tree species from the tropical Atlantic Forest of southern Brazil. *Sci Total Environ* 610**,** 912-925.
Natali, L., Vangelisti, A., Guidi, L., Remorini, D., Cotrozzi, L., Lorenzini, G., Nali, C., Pellegrini, E., Trivellini, A., Vernieri, P., Landi, M., Cavallini, A., and Giordani, T. (2018). How Quercus ilex L. saplings face combined salt and ozone stress: a transcriptome analysis. *Bmc Genomics* 19.
Nosenko, T., Hanke-Uhe, M., Heine, P.A., Shahid, A., Dubel, S., Rennenberg, H., Schumacher, J., Winkler, J.B., Schnitzler, J.P., Hansch, R., and Kaufholdt, D. (2021). Plant Defense Proteins as Potential Markers for Early Detection of Forest Damage and Diseases. *Frontiers in Forests and Global Change* 4.
Pasqualini, S., Piccioni, C., Reale, L., Ederli, L., Della Torre, G., and Ferranti, F. (2003). Ozone-induced cell death in tobacco cultivar Bel W3 plants. The role of programmed cell death in lesion formation. *Plant Physiol* 133**,** 1122-1134.
Pell, E.J., Sinn, J.P., Brendley, B.W., Samuelson, L., Vinten-Johansen, C., Tien, M., and Skillman, J. (1999). Differential response of four tree species to ozone-induced acceleration of foliar senescence. *Plant Cell & Environ.* 22**,** 779-790.
Proietti, C., Anav, A., De Marco, A., Sicard, P., and Vitale, M. (2016). A multi-sites analysis on the ozone effects on gross primary production of european forests. *Sci Total Environ* 556**,** 1-11.
Qiu, X.M., Sun, Y.Y., Ye, X.Y., and Li, Z.G. (2020). Signaling Role of Glutamate in Plants. *Frontiers in Plant Science* 10.
R Development Core Team (2017). "R: A language and environment for statistical computing". (Vienna, Austria: R Foundation for Statistical Computing).
Reich, P.B. (1983). Effects of low concentrations of O3 on net photosynthesis, dark respiration, and chlorophyll contents in aging hybrid poplar leaves. *Plant Physiol* 73**,** 291-296.
Revell, L.E., Tummon, F., Stenke, A., Sukhodolov, T., Coulon, A., Rozanov, E., Garny, H., Grewe, V., and Peter, T. (2015). Drivers of the tropospheric ozone budget throughout the 21st century under the medium-high climate scenario RCP 6.0. *Atmospheric Chem. Phys.* 15**,** 5887-5902.
Richet, N., Tozo, K., Afif, D., Banvoy, J., Legay, S., Dizengremel, P., and Cabane, M. (2012). The response to daylight or continuous ozone of phenylpropanoid and lignin biosynthesis pathways in poplar differs between leaves and wood. *Planta* 236**,** 727-737.
Schindelin, J., Arganda-Carreras, I., Frise, E., Kaynig, V., Longair, M., Pietzsch, T., Preibisch, S., Rueden, C., Saalfeld, S., Schmid, B., Tinevez, J.Y., White, D.J., Hartenstein, V., Eliceiri, K., Tomancak, P., and Cardona, A. (2012). Fiji: an open-source platform for biological-image analysis. *Nat. Methods* 9**,** 676-682.

Schraudner, M., Moeder, W., Wiese, C., Van Camp, W., Inze, D., Langebartels, C., and Sandermann, H. (1998). Ozone-induced oxidative burst in the ozone biomonitor plant, tobacco Bel W3. *Plant Journal* 16**,** 235-245.

Singh, P., and Zimmerli, L. (2013). Lectin receptor kinases in plant innate immunity. *Frontiers in Plant Science* 4.

Soltani, N., Best, T., Grace, D., Nelms, C., Shumaker, K., Romero-Severson, J., Moses, D., Schuster, S., Staton, M., Carlson, J., and Gwinn, K. (2020). Transcriptome profiles of Quercus rubra responding to increased O-3 stress. *Bmc Genomics* 21.

Street, N.R., James, T.M., James, T., Mikael, B., Jaakko, K., Mark, B., and Taylor, G. (2011). The physiological, transcriptional and genetic responses of an ozone-sensitive and an ozone tolerant poplar and selected extremes of their F2 progeny. *Environ Pollut* 159**,** 45-54.

Strohm, M., Eiblmeier, M., Langebartels, C., Jouanin, L., Polle, A., Sandermann, H., and Rennenberg, H. (1999). Responses of transgenic poplar (*Populus tremula* x *P-alba*) overexpressing glutathione synthetase or glutathione reductase to acute ozone stress: visible injury and leaf gas exchange. *J Exp Bot* 50**,** 365-374.

Strohm, M., Eiblmeier, M., Langebartels, C., Jouanin, L., Polle, A., Sandermann, H., and Rennenberg, H. (2002). Responses of antioxidative systems to acute ozone stress in transgenic poplar (*Populus tremula* x *P-alba*) over-expressing glutathione synthetase or glutathione reductase. *Trees-Struct Funct.* 16**,** 262-273.

Takken, F.L.W., Albrecht, M., and Tameling, W.I.L. (2006). Resistance proteins: molecular switches of plant defence. *Current Opinion in Plant Biology* 9**,** 383-390.

Trapnell, C., Pachter, L., and Salzberg, S.L. (2009). TopHat: discovering splice junctions with RNA-Seq. *Bioinformatics* 25**,** 1105-1111.

Turc, B., Vollenweider, P., Le Thiec, D., Gandin, A., Schaub, M., Cabane, M., and Jolivet, Y. (2021). Dynamics of Foliar Responses to O-3 Stress as a Function of Phytotoxic O-3 Dose in Hybrid Poplar. *Frontiers in Plant Science* 12.

Tuskan, G.A., Difazio, S., Jansson, S., Bohlmann, J., Grigoriev, I., Hellsten, U., Putnam, N., Ralph, S., Rombauts, S., Salamov, A., Schein, J., Sterck, L., Aerts, A., Bhalerao, R.R., Bhalerao, R.P., Blaudez, D., Boerjan, W., Brun, A., Brunner, A., Busov, V., Campbell, M., Carlson, J., Chalot, M., Chapman, J., Chen, G.L., Cooper, D., Coutinho, P.M., Couturier, J., Covert, S., Cronk, Q., Cunningham, R., Davis, J., Degroeve, S., Dejardin, A., Depamphilis, C., Detter, J., Dirks, B., Dubchak, I., Duplessis, S., Ehlting, J., Ellis, B., Gendler, K., Goodstein, D., Gribskov, M., Grimwood, J., Groover, A., Gunter, L., Hamberger, B., Heinze, B., Helariutta, Y., Henrissat, B., Holligan, D., Holt, R., Huang, W., Islam-Faridi, N., Jones, S., Jones-Rhoades, M., Jorgensen, R., Joshi, C., Kangasjarvi, J., Karlsson, J., Kelleher, C., Kirkpatrick, R., Kirst, M., Kohler, A., Kalluri, U., Larimer, F., Leebens-Mack, J., Leple, J.C., Locascio, P., Lou, Y., Lucas, S., Martin, F., Montanini, B., Napoli, C., Nelson, D.R., Nelson, C., Nieminen, K., Nilsson, O., Pereda, V., Peter, G., Philippe, R., Pilate, G., Poliakov, A., Razumovskaya, J., Richardson, P., Rinaldi, C., Ritland, K., Rouze, P., Ryaboy, D., Schmutz, J., Schrader, J., Segerman, B., Shin, H., Siddiqui, A., Sterky, F., Terry, A., Tsai, C.J., Uberbacher, E., Unneberg, P., et al. (2006). The genome of black cottonwood, Populus trichocarpa (Torr. & Gray). *Science* 313**,** 1596-1604.

Vollenweider, P., Günthardt-Goerg, M.S., Menard, T., Baumgarten, M., Matyssek, R., and Schaub, M. (2019). Macro- and microscopic leaf injury triggered by ozone stress in beech foliage (*Fagus sylvatica* L.). *Ann. For. Sci.* 76**,** 71.
Vollenweider, P., Ottiger, M., and Günthardt-Goerg, M.S. (2002). Validation of leaf ozone symptoms in natural vegetation using microscopical methods. *Environ Pollut* 124**,** 101-118.
Waldeck, N., Burkey, K., Carter, T., Dickey, D., Song, Q.J., and Taliercio, E. (2017). RNA-Seq study reveals genetic responses of diverse wild soybean accessions to increased ozone levels. *Bmc Genomics* 18.
Whaley, A., Sheridan, J., Safari, S., Burton, A., Burkey, K., and Schlueter, J. (2015). RNA-seq analysis reveals genetic response and tolerance mechanisms to ozone exposure in soybean. *Bmc Genomics* 16.
Wittig, V.E., Ainsworth, E.A., Naidu, S.L., Karnosky, D.F., and Long, S.P. (2009). Quantifying the impact of current and future tropospheric ozone on tree biomass, growth, physiology and biochemistry: a quantitative meta-analysis. *Glob. Change Biol.* 15**,** 396-424.
Xu, E.J., Vaahtera, L., Horak, H., Hincha, D.K., Heyer, A.G., and Brosche, M. (2015). Quantitative trait loci mapping and transcriptome analysis reveal candidate genes regulating the response to ozone in Arabidopsis thaliana. *Plant Cell and Environment* 38**,** 1418-1433.
Yendrek, C.R., Koester, R.P., and Ainsworth, E.A. (2015). A comparative analysis of transcriptomic, biochemical, and physiological responses to elevated ozone identifies species-specific mechanisms of resilience in legume crops. *J Exp Bot* 66**,** 7101-7112.
Zhang, J., Schaub, M., Ferdinand, J.A., Skelly, J.M., Steiner, K.C., and Savage, J.E. (2010). Leaf age affects the responses of foliar injury and gas exchange to tropospheric ozone in *Prunus serotina* seedlings. *Environ Pollut* 158**,** 2627-2634.
Zhang, J.F., Wei, Y.J., and Fang, Z.F. (2019). Ozone Pollution: A Major Health Hazard Worldwide. *Frontiers in Immunology* 10.

Chapitre 5

SYNTHESE GENERALE

Chapitre 5 : Synthèse générale

Le travail réalisé dans le cadre de cette thèse avait pour objectif principal de **relier le développement spatio-temporel des changements structuraux et ultrastructuraux avec les réponses cellulaires en relation avec la dose d'O_3 effective.** La démarche expérimentale de notre étude consistait à soumettre de jeunes peupliers (2,5 mois) à des niveaux réalistes d'O_3 (80 et 100 ppb) en conditions contrôlées afin d'étudier la dynamique des réponses cellulaires et structurales en fonction du POD et de l'âge de la feuille. L'utilisation de deux concentrations d'O_3 et le suivi des effets sur deux niveaux de feuilles ont permis d'obtenir des dynamiques de réponses différentes en fonction du POD, et ainsi de mieux comprendre leurs mécanismes. Grâce au recours de différentes techniques d'analyses (physiologique, cellulaire, structurale et transcriptomique) les dynamiques de réponse cellulaires en réponse à l'O_3 ont pu être caractérisées.

1. Deux dynamiques de réponses bien distinctes

Au cours des expérimentations, les dynamiques de réponses physiologiques, structurales et transcriptomiques se sont développées bien en amont de l'émergence de symptômes visibles ou de la perte de feuilles, et aucune réduction de biomasse n'a été observé.

1.1 Dynamique de la sénescence

Dans nos expérimentations, l'accélération de la sénescence (ACS) a été premièrement suivie par la diminution de l'assimilation nette de CO_2 et la dégradation des chlorophylles. Tout d'abord, l'O_3 a accéléré le déclin ontologique de A_{net}, ce qui est bien documentées dans le cas de diverses espèces, y compris les peupliers (Pell et al., 1992; Bagard et al., 2015; Dusart et al., 2019b). Cette diminution de l'assimilation nette de CO_2 pourrait résulter d'une conductance stomatique plus faible, limitant l'entrée de l'O_3 mais aussi du CO_2. En effet, ce n'est pas étonnant au vu des effets de l'O_3 sur les stomates qui va d'une part induire leurs fermetures et d'autre part ralentir les mouvements des cellules de gardes, désigné sous le terme de « *stomatal*

sluggishness ». (Kangasjarvi et al., 2005; Paoletti and Grulke, 2010; Dumont et al., 2013; Dusart et al., 2019b). Un autre paramètre pouvant expliquer cette réduction d'assimilation nette de CO_2, et dont la diminution ontologique est également accélérée par l'O_3, est la conductance mésophyllienne (Xu et al., 2019). La diminution de l'assimilation nette de CO_2 a précédé la réduction de la teneur en chlorophylles des feuilles, une autre réponse physiologique foliaire observée en réponse à l'O_3 (Reich, 1983; Bagard et al., 2015; Dusart et al., 2019b) et indicative de l'ACS. La réduction progressive des paramètres physiologiques en réponse à l'O_3 à mesure que le POD augmente, souligne donc une dynamique monotone et plutôt linéaire de l'ACS.

Cette dynamique monotone a également été observé d'un point de vue structural. En effet, d'une manière générale, l'apparition et l'intensité des changements structuraux reliés à l'ACS, comme une augmentation de la taille de la vacuole, une activité nucléique plus faible et une dégradation des chloroplastes (Mikkelsen and HeideJorgensen, 1996; Günthardt-Goerg and Vollenweider, 2007; Moura et al., 2018), ont été fortement liés au traitement O_3 et au POD. Etant donné les liens évidents existant entre l'assimilation nette de CO_2, la concentration en chlorophylles et les chloroplastes, une attention particulière a été portée à leur égard. La quantification de leurs traits structuraux a en effet montré une relation étroite avec le traitement O_3 et le POD, en particulier l'augmentation en nombre et en taille des plastoglobules et le changement de forme des chloroplastes, probablement expliqués par la dégradation des thylakoïdes (Lichtenthaler, 2013).

Toujours en accord avec cette dynamique progressive et monotone de l'ACS, l'étude transcriptomique a montré une accélération de l'expression ontologique de gènes co-exprimés (module WGCNA 1 et 2). Dans le module 1, on retrouvait beaucoup de gènes impliqués dans la réponse au stress, la mort cellulaire et la dégradation de protéines, dont l'expression qui augmentait avec le développement ontologique, a été accéléré par l'O_3. Le module 2 montrait un profil inversé à celui du module 1, c'est à dire que l'expression des gènes qu'il regroupait a diminué avec le développement ontologique de la feuille, ce qui a été accéléré par l'O_3. Ce module regroupait beaucoup de gènes impliqués dans la photosynthèse dont la photochimie, le métabolisme des carbohydrates et la croissance cellulaire. De plus, une étude récente (Lu et al., 2020) a caractérisé les changements d'expression de gènes survenant pendant la sénescence automnal chez le peuplier. La comparaison de leurs résultats avec les nôtres a révélé que des gènes régulés (sur- et sous-exprimés) avec

la mise en place de la sénescence automnal l'étaient aussi en réponse à l'O_3 après seulement 2 jours d'exposition, indiquant déjà que les changements d'expression de gènes surviennent bien avant ceux structuraux ou physiologiques (les 2 derniers survenant à peu près en même temps). De plus, le nombre de gènes régulés communs à la sénescence automnale et à l'O_3 a augmenté de façon linéaire (500, 1000, 2000 après 2, 8 et 13 jours de traitement), ce qui est très cohérent avec le profile monotone de la dynamique de l'ACS.

Lors de la sénescence automnale, le chloroplaste occupe une place centrale puisqu'une diminution de sa capacité antioxydante entraîne une augmentation des ROS induits par la photosynthèse qui déclenche le processus de sénescence par signalisation jusqu'au noyau (Lee et al., 2007; Mayta et al., 2019). Par conséquent, les ROS induits par l'O_3 peuvent contribuer à accélérer la sénescence cellulaire en augmentant le stress oxydant dans le chloroplaste, libérant ainsi des ROS qui vont déclencher les processus de sénescence par signalisation au noyau.

1.2 Dynamique de la réponse HR-like

La dynamique des lésions microscopiques résultant d'une réaction HR-like a été suivi grâce à la coloration au bleu trypan, et quantifiée ensuite par analyse d'image assistée par ordinateur. Des marqueurs structuraux typiques de HR-like ont été détectés dans les cellules mortes colorées par le bleu trypan (Paoletti et al., 2009; Vollenweider et al., 2013; Feng et al., 2016; Vollenweider et al., 2019) pour assurer qu'elles découlaient bien d'une réaction HR-like. Ce nouveau test de nécrose cellulaire a fourni une capacité sans précédent d'évaluation quantitative des réactions de mort cellulaire dans des conditions expérimentales, en surmontant les limitations et les incertitudes liées à l'observation des seules lésions visibles.

La dynamique d'émergence des lésions HR-like de type sigmoïde observée dans les feuilles matures est en accord avec les éléments moléculaires et structuraux déjà existant sur les processus de HR-like. Il est considéré que la forte augmentation de la surface des lésions en pourcentage reflète l'achèvement rapide de la mort cellulaire une fois que la PCD a commencé (Overmyer et al., 2005; Günthardt-Goerg and Vollenweider, 2007). Enfin, le plateau atteint indique la restriction des lésions (probablement par l'intermédiaire de JA), bloquant leurs propagations ultérieures (Overmyer et al., 2003; Kangasjarvi et al., 2005; Marchica et al., 2019). Dans les

feuilles plus jeunes, l'expérimentation a été interrompue avant qu'un plateau ait pu être atteint. Supportant cette dynamique de type sigmoïde, un nombre beaucoup plus important de gènes exprimés régulés par l'O_3 a été détecté lorsque des lésions HR-like ont été observées, ce qui s'explique probablement par la régulation de la mort cellulaire impliquant plusieurs voies dont les mécanismes se chevauchent (Kangasjarvi et al., 2005; Xu et al., 2015). Néanmoins, malgré une corrélation élevée avec les lésions HR-like avec les modules WGCNA 1 et 7, aucun n'a montré un profil similaire à celui de la dynamique des HR-like. Toutefois, le module 1 regroupait des gènes impliqués dans la réponse au stress biotique (et dans une moindre mesure abiotique), dans la mort cellulaire alors que le module 7 comprenait des gènes impliqués dans le modelage de la paroi cellulaire. Cela indique une relation étroite entre la réponse à l'O_3 et (i) la mort cellulaire survenant en cas de stress biotique et (ii) le métabolisme de la paroi cellulaire.

Lors d'un stress biotique, une première accumulation apoplastique de ROS a lieu par l'intermédiaire de la NADPH oxydase après reconnaissance du pathogène, ce qui induit une réponse hypersensible (HR) dans la cellule (Jwa and Hwang, 2017). Étant donné les similitudes étroites déjà observées entre HR et HR-like (Vollenweider et al., 2002; Bhattacharjee, 2005; Günthardt-Goerg and Vollenweider, 2007; Moura et al., 2018), nos résultats peuvent suggérer un effet similaire avec une accumulation apoplastique de ROS induite par l'O_3 qui pourrait mimer celle induite sous le contrôle de la NADPH oxydase sous stress biotique, et déclencher la réaction HR-like. De plus, un dépôt de callose entre la membrane plasmique et la paroi cellulaire a été observé dans les cellules saines adjacentes aux lésions HR-like, comme cela est généralement observé en cas d'intrusion d'un agent pathogène (Wang et al., 2021). Lors de l'attaque d'un pathogène, le dépôt de callose a plusieurs rôles, notamment celui de renforcer la paroi cellulaire et de restreindre l'entrée des enzymes de dégradation de la paroi sécrétées par les pathogènes, afin de limiter la propagation des dommages. Le dépôt de callose suite à une exposition à l'O_3 a été largement documenté (Vollenweider et al., 2002; Paoletti et al., 2009; Feng et al., 2016), cependant, selon nos connaissances, c'est la première fois que le dépôt de callose a été clairement observé entre la membrane plasmique et la paroi cellulaire d'une cellule adjacente saine. Il est bien connu que l'acide salicylique (SA) et l'acide jasmonique (JA) favorisent et limitent respectivement la mort cellulaire (Kangasjarvi et al., 2005). Puisque le dépôt de callose est augmenté par SA et supprimé par JA en réponse au stress biotique (Yi et al., 2014),

nos résultats suggèrent que le dépôt de callose en réponse à l'O_3 est une conséquence de la propagation des lésions HR-like par l'intermédiaire de SA, et que JA pourrait limiter ce dépôt de callose autour des sites nécrotiques.

L'analyse d'image avec le logiciel WinCELL est basée sur la classification des couleurs en deux catégories, ce qui nous a permis de quantifier les lésions non oxydées et oxydées (les lésions oxydées étant beaucoup plus sombres). Les changements REDOX pendant le stress oxydatif et la mort cellulaire constituent un processus important de la physiologie cellulaire (Foyer and Noctor, 2005) qui est bien documenté dans le cas du stress O_3 (Ranieri et al., 2000; Baier et al., 2005; Chen and Gallie, 2005; Bellini and De Tullio, 2019) et détectable avec différents marqueurs structuraux et ultra-structuraux (Moura et al., 2018; Vollenweider et al., 2019). Les lésions oxydées et totales de type HR ont montré une dynamique similaire à l'augmentation du POD. Les principales différences entre les lésions oxydées et les lésions non oxydées étaient un pourcentage de surface plus faible, un retard dans le développement et une sévérité plus élevée (une perturbation du contenu cellulaire plus forte). Bien que les lésions non oxydées et oxydées puissent correspondre à deux types de lésion HR-like, il est plus probable qu'elles correspondent à deux stades différents de la lésion, ce qui a été confirmé par l'étude des changements structuraux et ultra-structuraux. En effet, l'observation des lésions HR-like sous microscope électronique a révélé une évolution post-mortem du contenu cellulaire, confirmant que les lésions non-oxydées et oxydées correspondent à deux étapes de la réaction HR-like. La surface plus petite de lésions oxydées vs non-oxydées ainsi que l'état final du matériel cellulaire dégradé (homogène et dense) supporte cette idée. Enfin, l'évolution post-mortem du contenu cellulaire suggère que ce processus n'était pas sous contrôle biologique, mais plus la conséquence de processus physico-chimique.

Etant donné la relation étroite entre l'ACS et les HR-like avec les ROS, la dynamique opposée des changements transcriptomiques des 2 processus est probablement la conséquence d'une signalisation différente qui pourrait être induite par une origine spatiale distincte de la source des ROS.

1.3 Une forte dépendance des dynamiques aux conditions environnementales

Une première évidence de la dépendance des réponses HR-like et ACS avec les conditions expérimentales a été l'observation des lésions HR-like dans la couche du parenchyme palissadique inférieur. En effet, en conditions naturelles les lésions HR-like sont observées dans la couche du parenchyme palissadique supérieur. Dans ces conditions, un gradient de sévérité des lésions est observé de la face adaxiale vers la face abaxiale de la feuille (Günthardt-Goerg and Vollenweider, 2007; Moura et al., 2018). De plus, dans nos conditions expérimentales, la HR-like a été observée bien avant l'ACS, ce qui contraste également avec les données de terrain (Vollenweider et al., 2019).

Ces différences avec les conditions de terrain indiquent de faibles niveaux de stress photo-oxydant dans nos conditions contrôlées (Foyer et al., 1994; Günthardt-Goerg and Vollenweider, 2007; Guerrero et al., 2013). Compte tenu d'un PAR maximal supérieur à 2000 µmol m^{-2} s^{-1} en condition de lumière élevée sur le terrain (Ritchie, 2010; Poorter et al., 2019) contre 350 µmol m^{-2} s^{-1} dans nos chambres de fumigation, les particularités de réaction HR-like - ainsi que l'apparition tardive de l'ACS - peuvent être attribuées aux spécificités de nos conditions environnementales, notamment en ce qui concerne l'apport de PAR. Ce résultat fournit donc une confirmation supplémentaire de la dépendance étroite entre l'expression des symptômes de l'O_3 dans le feuillage et les conditions environnementales d'exposition (Paoletti et al., 2009; Moura et al., 2018; Vollenweider et al., 2019).

2. L'importance du stade de développement foliaire dans la réponse à l'O_3

Les changements d'expression de gènes, les réductions des échanges gazeux foliaires et de contenu en chlorophylle, le développement de lésions HR-like et de changement structuraux relié à l'ACS, ainsi que l'émergence symptômes visibles se sont produits plus tard et pour des PODs plus importants dans la jeune feuille, en comparaison à la feuille mature. Étant donné la conductance stomatique et le POD plus élevés chez les jeunes feuilles, une plus grande tolérance à l'O_3 par une fermeture

des stomates, et donc un flux d'O_3 plus faible, peut être exclue. De plus, vu que l'enrichissement fonctionnel des gènes exprimés de manière différentielle en réponse à l'O_3 est similaire dans les deux positions de feuille, la régulation d'une voie spécifique en réponse à l'O_3 expliquant les différences de sensibilité entre les feuilles est à priori exclue. Cette moindre sensibilité des feuilles en expansion a été confirmée par de précédentes études (Reich, 1983; Paakkonen et al., 1996; Strohm et al., 2002; Bagard et al., 2008; Zhang et al., 2010; Guerrero et al., 2013).

Les modules de co-expression englobant les gènes différentiellement exprimés (M1, M2, M7, M4 et M11) ont montré des profils dépendant fortement de l'ontologie de la feuille, et l'effet de l'O_3 sur les changements transcriptomiques s'est produit une fois que l'expansion de la feuille a été réalisée, comme précédemment observé au moins pour le soja (Waldeck et al., 2017). Cependant, contrairement aux modules 1 et 2, les gènes des modules 4, 7, 11 ont montré une régulation différente de leur expression une fois que la feuille était complètement étendue. Le module 4 contenait des gènes liés à la photosynthèse, et la forte corrélation entre son profil et l'assimilation nette de CO_2 suggère un impact de l'O_3 sur la fixation du CO_2 une fois que l'appareil photosynthétique est pleinement fonctionnel. Le module 11 englobait des gènes liés à la paroi et à la structure cellulaire pendant l'expansion de la feuille. Leur expression pendant la croissance cellulaire peut contribuer à retarder les effets négatifs de l'O_3 sur la structure de la cellule, permettant ainsi une préservation de l'intégrité et une viabilité plus longue. Le module 7 était intéressant car l'expression de ses gènes diminuait avec le développement des feuilles, puis augmentait à nouveau en réponse à l'exposition à l'O_3 une fois la feuille étendue. Ces gènes sont impliqués dans des processus métaboliques protéiques partiellement localisés dans la paroi cellulaire. Bien qu'elle ait été observée aux deux positions de feuille, l'activité d'épaississement de la paroi cellulaire était plus élevée dans les feuilles jeunes, comparé aux feuilles matures, ce qui s'explique principalement par les différences d'ontologie de la feuille. En effet, au cours de l'expansion des feuilles et de la croissance cellulaire des jeunes feuillages, la paroi cellulaire est étroitement modelée par des protéines pariétales pour permettre l'expansion des cellules et contribuer à leur adaptation à un environnement changeant (Knox, 2008). De plus, l'expansion cellulaire implique une régulation transcriptionnelle fine de l'homéostasie des ROS (Mangano et al., 2016; Schmidt et al., 2016), ce qui permet de faire face à la diffusion des ROS induit par l'O_3, au moins pendant la croissance cellulaire.

L'effet de l'O_3 observé une fois l'expansion cellulaire réalisée est cohérente avec l'augmentation générale de la sensibilité au stress des feuilles après la transition puits-source (Coleman, 1986). Cependant, nos résultats nous amènent à considérer que la meilleure tolérance des jeunes feuilles de peuplier est plus probablement due à un remodelage plus actif de la paroi cellulaire (M7), à une intégrité plus facile à maintenir (M11), et à un appareil photosynthétique moins sensible parce qu'il n'est pas encore totalement fonctionnel (M4) qu'à une augmentation des teneurs en composés phénoliques ou de l'activité antioxydante comme cela a été proposé précédemment (Strohm et al., 2002; Bellini and De Tullio, 2019; Turc et al., 2021). Néanmoins il n'est pas exclu qu'un niveau constitutif plus élevé d'antioxydant soit présent dans les jeunes feuilles.

3. Seuils de risques

Au cours de nos expériences, le seuil critique (CL) actuel (POD_1 pour le hêtre et le bouleau = 5,2 mmol O_3 m^{-2} ; (Mills G. et al., 2017)) était équivalent à un POD_0 de 5,7 mmol O_3 m^{-2}. Ce CL a été systématiquement dépassé dans les feuilles matures (environ 1.3 fois) et jeunes (environ 2.2 fois). Si aucune altération de la morphologie et de la biomasse des arbres ne fut constatée, des réductions des échanges gazeux foliaires, le développement de lésions microscopiques et l'apparition de symptômes visibles ont déjà été observés sur les feuilles matures pour un flux d'O_3 entrant s'élevant respectivement à 0.8, 0.7 et 1.46 fois le CL actuel. Dans les feuilles jeunes, ces réponses ont été détectées pour une dose d'O_3 au minimum 1.8 fois au-dessus du CL actuel. Dans les forêts, la recherche de marqueurs microscopiques (structurales et ultra-structurales) de stress de l'O_3 peuvent être utiles pour déterminer les effets néfastes de l'O_3 sur le feuillage, et peuvent être liées à la dose d'O_3 subie (Vollenweider et al., 2019).

Dans notre étude, les lésions HR-like ont été détectées dans deux états d'oxydation différents (non-oxydé vs oxydé) et ce changement d'état d'oxydation contribue à l'apparition de lésions visibles. En effet, elles apparaissent lorsque les lésions oxydées sont suffisamment fréquentes pour être détectées à l'œil nu à l'échelle de la feuille alors que les lésions non oxydées (même en grand groupe) sont invisibles à l'échelle de la feuille (Turc et al., 2021). Par conséquent, l'étude des blessures visibles résultant d'une réaction de type HR afin d'évaluer le stress dû à l'O_3 en forêt

est une bonne chose car elle est spécifique à la réponse à l'O_3, mais elle manque manifestement de sensibilité, ce qui conduit à une sous-estimation de l'effet négatif de l'O_3 sur le feuillage. Bien que typiques du stress dû à l'O_3, les changements liés à l'ACS ne sont pas utilisés dans l'évaluation des risques, principalement en raison de leur manque de spécificité à la réponse à l'O_3, ce qui rend leur utilisation plus compliquée dans la végétation naturelle ou semi-naturelle. Cependant, dans notre étude la dynamique des changements liés à l'ACS était étroitement liée au POD, la diminution de la taille des chloroplastes se produisant avec l'entrée de l'O_3 dans la feuille mais avant l'augmentation en taille et nombre des plastoglobules et le changement de forme des chloroplastes qui s'ensuit. Par conséquent, l'évaluation du stress lié à l'O_3 à l'aide de la validation microscopique peut considérer les changements liés aux chloroplastes comme une indication de l'absorption de l'O_3 par la feuille. Néanmoins, étant donné la synergie entre le stress photooxydant et oxydant, une attention particulière doit être accordée aux conditions d'illumination du feuillage.

Les premiers changements transcriptomiques ont été détectés pour une dose d'O_3 s'élevant à 0.35 et 1.57 fois le CL dans les feuilles matures et jeunes respectivement. Cependant, la dose cumulée d'O_3 dans les feuilles n'était pas suffisante pour les expliquer vu que beaucoup plus de gènes exprimés différemment ont été détectés dans le traitement à 100 vs 80 ppb d'O_3, malgré des niveaux de POD_0 similaires. Ainsi, nous avons proposé une liste de gènes hautement exprimés et corrélés avec les lésions de type HR en réponse à l'O_3 (Tableau S4), qui peut être une liste initiale pour déterminer les marqueurs moléculaires de l'O_3 pour le diagnostic de la santé des forêts, comme récemment proposé par (Nosenko et al., 2021) dans le cas des pathogènes. Parmi les cinq gènes les plus corrélés avec les lésions de type HR, quatre codent pour des gènes impliqués dans la réponse au stress biotique et/ou abiotique et comprennent deux récepteurs du glutamate (GLR), une protéine kinase de la lectine du locus S et une protéine de résistance aux maladies contenant le domaine NB-ARC. Chez les plantes, il a été récemment montré que le glutamate (Glu) possède des propriétés de signalisation impliquées dans de nombreux processus physiologiques, notamment la croissance, la germination, l'architecture des racines, la résistance aux agents pathogènes et la réponse au stress abiotique (Qiu et al., 2020). Le Glu exerce sa fonction de signalisation par le biais du récepteur du glutamate (GLR), qui est partiellement responsable de l'augmentation cytosolique du Ca^{2+} induisant l'expression de gènes liés à la défense (métacaspase) après une infection

par un pathogène (Li et al., 2013; Manzoor et al., 2013). Les kinases des récepteurs de lectine sont impliquées dans la reconnaissance des pathogènes et l'activation ultérieure des gènes liés à la défense (Singh and Zimmerli, 2013) et la protéine contenant le domaine NB-ARC est impliquée dans la défense contre les pathogènes (Takken et al., 2006). Par conséquent, les gènes corrélés aux lésions de type HR ont une fonction dans la réponse au stress biotique, ce qui rend difficile la recherche de marqueurs moléculaires spécifiques du stress O_3.

Dans tous les cas, ces résultats soulignent la forte dépendance des évaluations de sensibilité aux paramètres sélectionnés et à l'échelle d'observation. Ils soulignent également la difficulté d'appréhender la réponse à l'ensemble du houppier compte tenu de la différence de sensibilité entre feuillage mature et jeune ce qui, par conséquent, complique l'évaluation du risque. Ils indiquent enfin qu'en dessous du CL, on peut s'attendre à des effets significatifs sur le feuillage des arbres, tels que des changements d'expression gène, l'altération de la physiologie des feuilles et le développement de nécroses microscopiques dans des parties étendues du mésophylle. Néanmoins ces modifications n'ont pas encore d'impact sur la croissance.

Conclusions & perspectives

Les travaux menés dans le cadre de cette thèse ont permis d'approfondir les connaissances sur les dynamiques des réponses cellulaires (physiologique, microscopique et transcriptomique) en réponse à une exposition à l'O_3. Les dynamiques des réponse ACS et HR-like observées sont très contrastées (monotone vs sigmoïdal) indépendamment de la position des feuilles, avant tout symptôme visible et tout effet sur la morphologie des arbres. Ces différences ont aussi été observées d'un point de vue structural puisque la réaction HR-like démarre par la mort de la cellule, alors que dans le cas de l'ACS la mort de la cellule est la fin du processus. Néanmoins, les dynamiques de réponses sont fortement liées à l'âge de la feuille en fonction du temps ou du POD_0, conduisant à un décalage dans les feuilles en expansion. En ce sens, les résultats de l'étude transcriptomique suggèrent fortement que l'expression des gènes impliqués dans le développement lors de l'expansion des feuilles pourrait conférer à la plante une plus grande tolérance au stress O_3 (figure 13).

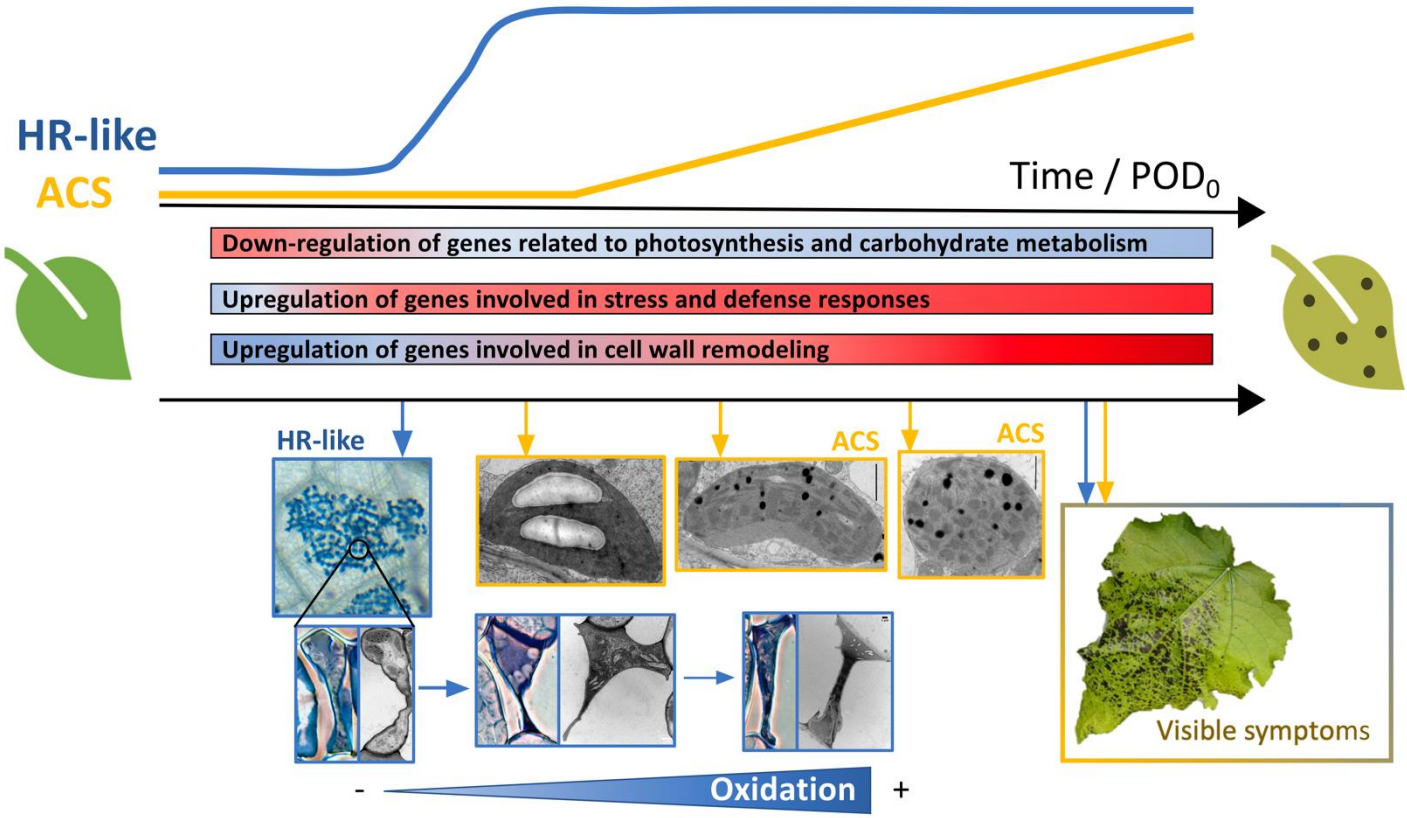

Figure 13. Schéma de synthèse de la dynamique des réponses cellulaires dans les feuilles de peuplier (*Populus tremula x alba*) en réponse à l'O_3.

Plusieurs perspectives se présentent à l'issu de ce travail :

- Le dosage de la capacité antioxydante (ascorbate/glutathion) des feuilles matures et jeunes. En effet, l'étude transcriptomique n'a révélé aucune indication de la stimulation des voies de biosynthèses de l'ascorbate et du glutathion. Cependant, la piste d'un niveau constitutif plus élevé dans les jeunes *vs* vieilles feuilles reste à explorer.
- La validation des gènes marqueurs de stress O_3 reste également à approfondir dans d'autres espèces et dans des conditions environnementales variées.
- De nombreuses analogies ont déjà été faites entre la réponse à l'O_3 (HR-like) et aux pathogènes (HR), et les résultats présentés dans l'étude transcriptomique vont également dans ce sens au vu de l'implication des gènes corrélés avec le niveau de HR-like dans la réponse au stress biotique. Il serait intéressant de comparer ces deux réponses dans le même système, et avec des techniques similaires, afin de bien caractériser les processus de signalisation et les mécanismes de mort cellulaire induit pendant les deux stress, et ainsi apporter des détails sur les ressemblances et différences qu'il peut y avoir entre ces deux réponses.

REFERENCES

Ahmad, R., Zuily-Fodil, Y., Passaquet, C., Bethenod, O., Roche, R., and Repellin, A. (2012). Ozone and aging up-regulate type II metacaspase gene expression and global metacaspase activity in the leaves of field-grown maize (Zea mays L.) plants. *Chemosphere* 87**,** 789-795.

Bagard, M., Jolivet, Y., Hasenfratz-Sauder, M.P., Gerard, J., Dizengremel, P., and Le Thiec, D. (2015). Ozone exposure and flux-based response functions for photosynthetic traits in wheat, maize and poplar. *Environ Pollut* 206**,** 411-420.

Bagard, M., Le Thiec, D., Delacote, E., Hasenfratz-Sauder, M.P., Banvoy, J., Gerard, J., Dizengremel, P., and Jolivet, Y. (2008). Ozone-induced changes in photosynthesis and photorespiration of hybrid poplar in relation to the developmental stage of the leaves. *Physiol Plant* 134**,** 559-574.

Baier, M., Kandlbinder, A., Golldack, D., and Dietz, K.J. (2005). Oxidative stress and ozone: perception, signalling and response. *Plant Cell & Environ.* 28**,** 1012-1020.

Bartoli, G., Forino, L.M.C., Tagliaferri, A., Bernardi, R., and Durante, M. (2010). Ozone damage and tolerance in leaves of two poplar genotypes. *Caryologia*.

Bartoli, G., Forino, L.M.C., Tagliasacchi, A.M., and Durante, M. (2013). Cell death induced by ozone stress in the leaves of Populus deltoides x maximowiczii. *Biologia Plantarum* 57**,** 514-524.

Bellini, E., and De Tullio, M.C. (2019). Ascorbic acid and ozone: Novel perspectives to explain an elusive relationship. *Plants* 8.

Bhalerao, R., Keskitalo, J., Sterky, F., Erlandsson, R., Bjorkbacka, H., Birve, S.J., Karlsson, J., Gardestrom, P., Gustafsson, P., Lundeberg, J., and Jansson, S. (2003). Gene expression in autumn leaves. *Plant Physiology* 131**,** 430-442.

Bhattacharjee, S. (2005). Reactive oxygen species and oxidative burst: Roles in stress, senescence and signal transduction in plants. *Curr. Sci.* 89**,** 1113-1121.

Blokhina, O., and Fagerstedt, K. (2006). *Oxidative stress and antioxidant defenses in plants.* Imperial Coll Press.

Booker, F.L., Reid, C.D., Brunschonharti, S., Fiscus, E.L., and Miller, J.E. (1997). Photosynthesis and photorespiration in soybean [Glycine max (L.) Merr.] chronically exposed to elevated carbon dioxide and ozone. *Journal of Experimental Botany* 48**,** 1843-1852.

Brehelin, C., Kessler, F., and Van Wijk, K.J. (2007). Plastoglobules: versatile lipoprotein particles in plastids. *Trends in Plant Science* 12**,** 260-266.

Büker, P., Feng, Z., Uddling, J., Briolat, A., Alonso, R., Braun, S., Elvira, S., Gerosa, G., Karlsson, P.E., Le Thiec, D., Marzuoli, R., Mills, G., Oksanen, E., Wieser, G., Wilkinson, M., and Emberson, L.D. (2015). New flux based dose-response relationships for ozone for European forest tree species. *Environ Pollut* 206**,** 163-174.

Bussotti, F., Agati, G., Desotgiu, R., Matteini, P., and Tani, C. (2005). Ozone foliar symptoms in woody plant species assessed with ultrastructural and fluorescence analysis. *New Phytologist* 166**,** 941-955.

Cabane, M., Pireaux, J.C., Leger, E., Weber, E., Dizengremel, P., Pollet, B., and Lapierre, C. (2004). Condensed lignins are synthesized in poplar leaves exposed to ozone. *Plant Physiol.* 134**,** 586-594.

Calatayud, A., Iglesias, D.J., Talon, M., and Barreno, E. (2004). Response of spinach leaves (*Spinacia oleracea* L.) to ozone measured by gas exchange, chlorophyll a fluorescence, antioxidant systems, and lipid peroxidation. *Photosynthetica* 42**,** 23-29.

Carter, C., Pan, S.Q., Zouhar, J., Avila, E.L., Girke, T., and Raikhel, N.V. (2004). The vegetative vacuole proteorne of Arabidopsis thaliana reveals predicted and unexpected proteins. *Plant Cell* 16**,** 3285-3303.

Castagna, A., and Ranieri, A. (2009). Detoxification and repair process of ozone injury: from O3 uptake to gene expression adjustment. *Environ Pollut* 157**,** 1461-1469.

Chaerle, L., Hagenbeek, D., Vanrobaeys, X., and Van Der Straeten, D. (2007). Early detection of nutrient and biotic stress in Phaseolus vulgaris. *International Journal of Remote Sensing* 28**,** 3479-3492.

Chang, K.L., Petropavlovskikh, I., Cooper, O.R., Schultz, M.G., and Wang, T. (2017). Regional trend analysis of surface ozone observations from monitoring networks in eastern North America, Europe and East Asia. *Elementa-Science of the Anthropocene* 5.

Chanin, M., Clerbaux, C., and Godin-Beekmann, S. (2015). Evolution de l'ozone troposphérique : le point en 2015.

Chen, Z., and Gallie, D.R. (2005). Increasing tolerance to ozone by elevating foliar ascorbic acid confers greater protection against ozone than increasing avoidance. *Plant Physiol.* 138**,** 1673-1689.

Cho, K., Shibato, J., Kubo, A., Kohno, Y., Satoh, K., Kikuchi, S., Sarkar, A., Agrawal, G.K., and Rakwal, R. (2013). Comparative analysis of seed transcriptomes of ambient ozone-fumigated 2 different rice cultivars. *Plant Signal Behav* 8**,** e26300.

Chrobok, D., Law, S.R., Brouwer, B., Linden, P., Ziolkowska, A., Liebsch, D., Narsai, R., Szal, B., Moritz, T., Rouhier, N., Whelan, J., Gardestrom, P., and Keech, O. (2016). Dissecting the Metabolic Role of Mitochondria during Developmental Leaf Senescence. *Plant Physiology* 172**,** 2132-2153.

Citepa, R. (2019). Inventaires des émissions de polluants atmosphériques et de gaz à effet de serre en France - Format Secten.

Coleman, J.S. (1986). Leaf development and leaf stress: increased susceptibility associated with sink-source transition. *Tree Physiol.* 2**,** 289-299.

Conklin, P.L., and Last, R.L. (1995). Differential Accumulation of Antioxidant Messenger-Rnas in Arabidopsis-Thaliana Exposed to Ozone. *Plant Physiology* 109**,** 203-212.

Cooper, O.R., Parrish, D.D., Ziemke, J., Balashov, N.V., Cupeiro, M., Galbally, I.E., Gilge, S., Horowitz, L., Jensen, N.R., Lamarque, J.F., Naik, V., Oltmans, S.J., Schwab, J., Shindell, D.T., Thompson, A.M., Thouret, V., Wang, Y., and Zbinden, R.M. (2014). Global distribution and trends of tropospheric ozone: An observation-based review. *Elementa: Science of the Anthropocene* 2**,** 000029.

D'haese, D., Horemans, N., De Coen, W., and Guisez, Y. (2006). Identification of late O3-responsive genes in Arabidopsis thaliana by cDNA microarray analysis. *Physiologia Plantarum* 128**,** 70-79.

Dghim, A.A., Dumont, J., Hasenfratz-Sauder, M.P., Dizengremel, P., Le Thiec, D., and Jolivet, Y. (2013). Capacity for NADPH regeneration in the leaves of two poplar genotypes differing in ozone sensitivity. *Physiol Plant* 148**,** 36-50.

Diara, C., Castagna, A., Baldan, B., Mensuali-Sodi, A., Sahr, T., Langebartels, C., Sebastiani, L., and Ranieri, A. (2005). Differences in the kinetics and scale of signalling molecule production modulate the ozone sensitivity of hybrid poplar clones: the roles of H2O2, ethylene and salicylic acid. *New Phytologist* 168**,** 351-364.

Dixon, R.A., Achnine, L., Kota, P., Liu, C.J., Reddy, M.S.S., and Wang, L.J. (2002). The phenylpropanoid pathway and plant defence - a genomics perspective. *Molecular Plant Pathology* 3**,** 371-390.

Dizengremel, P. (2001). Effects of ozone on the carbon metabolism of forest trees. *Plant Physiology and Biochemistry* 39**,** 729-742.

Dizengremel, P., Le Thiec, D., Bagard, M., and Jolivet, Y. (2008). Ozone risk assessment for plants: central role of metabolism-dependent changes in reducing power. *Environ Pollut* 156**,** 11-15.

Dizengremel, P., Le Thiec, D., Hasenfratz-Sauder, M.P., Vaultier, M.N., Bagard, M., and Jolivet, Y. (2009). Metabolic-dependent changes in plant cell redox power after ozone exposure. *Plant Biology* 11**,** 35-42.

Dumont, J., Keski-Saari, S., Keinanen, M., Cohen, D., Ningre, N., Kontunen-Soppela, S., Baldet, P., Gibon, Y., Dizengremel, P., Vaultier, M.N., Jolivet, Y., Oksanen, E., and Le Thiec, D. (2014). Ozone affects ascorbate and glutathione biosynthesis as well as amino acid contents in three Euramerican poplar genotypes. *Tree Physiol* 34**,** 253-266.

Dumont, J., Spicher, F., Montpied, P., Dizengremel, P., Jolivet, Y., and Le Thiec, D. (2013). Effects of ozone on stomatal responses to environmental parameters (blue light, red light, CO2 and vapour pressure deficit) in three *Populus deltoides* x *Populus nigra* genotypes. *Environ Pollut* 173**,** 85-96.

Dusart, N., Gerard, J., Le Thiec, D., Collignon, C., Jolivet, Y., and Vaultier, M.N. (2019a). Integrated analysis of the detoxification responses of two Euramerican poplar genotypes exposed to ozone and water deficit: Focus on the ascorbate-glutathione cycle. *Sci Total Environ* 651**,** 2365-2379.

Dusart, N., Vaultier, M.N., Olry, J.C., Bure, C., Gerard, J., Jolivet, Y., and Le Thiec, D. (2019b). Altered stomatal dynamics of two Euramerican poplar genotypes submitted to successive ozone exposure and water deficit. *Environ Pollut* 252**,** 1687-1697.

Emberson, L.D., Wieser, G., and Ashmore, M.R. (2000). Modelling of stomatal conductance and ozone flux of Norway spruce: comparison with field data. *Environmental Pollution* 109**,** 393-402.

Fagundes, D., Bohn, B., Cabreira, C., Leipelt, F., Dias, N., Bodanese-Zanettini, M.H., and Cagliari, A. (2015). Caspases in plants: metacaspase gene family in plant stress responses. *Functional & Integrative Genomics* 15**,** 639-649.

Feng, G., Calatayud, V., García-Breijo, F., Reig-Armiñana, J., and Feng, Z. (2016). Effects of elevated ozone on physiological, anatomical and ultrastructural characteristics of four common urban tree species in China. *Ecol. Indic.* 67**,** 367-379.

Feng, Z.Z., and Kobayashi, K. (2009). Assessing the impacts of current and future concentrations of surface ozone on crop yield with meta-analysis. *Atmospheric Environment* 43**,** 1510-1519.

Fontaine, V., Cabane, M., and Dizengremel, P. (2003). Regulation of phosphoenolpyruvate carboxylase in Pinus halepensis needles submitted to ozone and water stress. *Physiologia Plantarum* 117**,** 445-452.

Fontaine, V., Pelloux, J., Podor, M., Afif, D., Gerant, D., Grieu, P., and Dizengremel, P. (1999). Carbon fixation in Pinus halepensis submitted to ozone. Opposite response of ribulose-1,5-bisphosphate carboxylase/oxygenase and phosphoenolpyruvate carboxylase. *Physiologia Plantarum* 105**,** 187-192.

Foyer, C.H., Lelandais, M., and Kunert, K.J. (1994). Photooxidative stress in plants. *Physiol Plant* 92**,** 696-717.

Foyer, C.H., and Noctor, G. (2005). Redox homeostasis and antioxidant signaling: A metabolic interface between stress perception and physiological responses. *Plant Cell* 17**,** 1866-1875.

Fuhrer, J., Skarby, L., and Ashmore, M.R. (1997). Critical levels for ozone effects on vegetation in Europe. *Environ Pollut* 97**,** 91-106.

Gaudel, A., Cooper, O.R., Ancellet, G., Barret, B., Boynard, A., Burrows, J.P., Clerbaux, C., Coheur, P.F., Cuesta, J., Cuevas, E., Doniki, S., Dufour, G., Ebojie, F., Foret, G., Garcia, O., Granados-Munoz, M.J., Hannigan, J.W., Hase, F., Hassler, B., Huang, G., Hurtmans, D., Jaffe, D., Jones, N., Kalabokas, P., Kerridge, B., Kulawik, S., Latter, B., Leblanc, T., Le Flochmoen, E., Lin, W., Liu, J., Liu, X., Mahieu, E., Mcclure-Begley, A., Neu, J.L., Osman, M., Palm, M., Petetin, H., Petropavlovskikh, I., Querel, R., Rahpoe, N., Rozanov, A., Schultz, M.G., Schwab, J., Siddans, R., Smale, D., Steinbacher, M., Tanimoto, H., Tarasick, D.W., Thouret, V., Thompson, A.M., Trickl, T., Weatherhead, E., Wespes, C., Worden, H.M., Vigouroux, C., Xu, X., Zeng, G., and Ziemke, J. (2018). Tropospheric Ozone Assessment Report: Present-day distribution and trends of tropospheric ozone relevant to climate and global atmospheric chemistry model evaluation. *Elementa-Science of the Anthropocene* 6.

Gerosa, G., Marzuoli, R., Desotgiu, R., Bussotti, F., and Ballarin-Denti, A. (2008). Visible leaf injury in young trees of Fagus sylvatica L. and Quercus robur L. in relation to ozone uptake and ozone exposure. An Open-Top Chambers experiment in South Alpine environmental conditions. *Environ Pollut* 152**,** 274-284.

Gorai, A.K., Tchounwou, P.B., and Mitra, G. (2017). Spatial Variation of Ground Level Ozone Concentrations and its Health Impacts in an Urban Area in India. *Aerosol and Air Quality Research* 17**,** 951-964.

Gottardini, E., Cristofori, A., Pellegrini, E., La Porta, N., Nali, C., Baldi, P., and Sablok, G. (2016). Suppression Substractive Hybridization and NGS Reveal Differential Transcriptome Expression Profiles in Wayfaring Tree (Viburnum lantana L.) Treated with Ozone. *Frontiers in Plant Science* 7.

Guerrero, C.C., Gunthardt-Goerg, M.S., and Vollenweider, P. (2013). Foliar symptoms triggered by ozone stress in irrigated holm oaks from the city of madrid, spain. *Plos One* 8.

Günthardt-Goerg, M.S. (1996). Different response to ozone of tobacco, poplar, birch and alder.

Gunthardt-Goerg, M.S., Mcquattie, C.J., Maurer, S., and Frey, B. (2000). Visible and microscopic injury in leaves of five deciduous tree species related to current critical ozone levels. *Environmental Pollution* 109**,** 489-500.

Gunthardt-Goerg, M.S., Mcquattie, C.J., Scheidegger, C., Rhiner, C., and Matyssek, R. (1997). Ozone-induced cytochemical and ultrastructural changes in leaf mesophyll cell walls. *Canadian Journal of Forest Research* 27**,** 453-463.

Günthardt-Goerg, M.S., and Vollenweider, P. (2007). Linking stress with macroscopic and microscopic leaf response in trees: new diagnostic perspectives. *Environ Pollut* 147**,** 467-488.

Gupta, P., Duplessis, S., White, H., Karnosky, D.F., Martin, F., and Podila, G.K. (2005). Gene expression patterns of trembling aspen trees following long-term exposure to interacting elevated CO2 and tropospheric O3. *New Phytol* 167**,** 129-141.

Han, H., Liu, J., Yuan, H.L., Zhuang, B.L., Zhu, Y., Wu, Y., Yan, Y.H., and Ding, A.J. (2018). Characteristics of intercontinental transport of tropospheric ozone from Africa to Asia. *Atmospheric Chemistry and Physics* 18**,** 4251-4276.

He, R., Drury, G.E., Rotari, V.I., Gordon, A., Willer, M., Farzaneh, T., Woltering, E.J., and Gallois, P. (2008). Metacaspase-8 modulates programmed cell death induced by ultraviolet light and H2O2 in Arabidopsis. *Journal of Biological Chemistry* 283**,** 774-783.

Heggestad, H.E., and Middleton, J.T. (1959). Ozone in High Concentrations as Cause of Tobacco Leaf Injury. *Science* 129**,** 208-210.

Janda, M., and Ruelland, E. (2015). Magical mystery tour: Salicylic acid signalling. *Environmental and Experimental Botany* 114**,** 117-128.

Jiang, J.H., Aksoyoglu, S., Ciarelli, G., Baltensperger, U., and Prevot, A.S.H. (2020). Changes in ozone and PM2.5 in Europe during the period of 1990-2030: Role of reductions in land and ship emissions. *Science of the Total Environment* 741.

Jones, A.M. (2001). Programmed cell death in development and defense. *Plant Physiology* 125**,** 94-97.

Jwa, N.S., and Hwang, B.K. (2017). Convergent Evolution of Pathogen Effectors toward Reactive Oxygen Species Signaling Networks in Plants. *Frontiers in Plant Science* 8.

Kangasjarvi, J., Jaspers, P., and Kollist, H. (2005). Signalling and cell death in ozone-exposed plants. *Plant Cell & Environ.* 28**,** 1021-1036.

Karlsson, P., Braun, S., Broadmeadow, M., Elvira, S., Emberson, L., Gimeno, B.S., Le Thiec, D., Novak, K., Oksanen, E., Schaub, M., Uddling, J., and Wilkinson, M. (2007). Risk assessments for forest trees: The performance of the ozone flux versus the AOT concepts. *Environ Pollut* 146**,** 608-616.

Karlsson, P.E., Klingberg, J., Engardt, M., Andersson, C., Langner, J., Karlsson, G.P., and Pleijel, H. (2017). Past, present and future concentrations of ground-level ozone and potential impacts on ecosystems and human health in northern Europe. *Sci Total Environ* 576**,** 22-35.

Keating, T., Zuber, A., Denter, F., Seddon, J., Travnikov, O., Gusev, A., Carmichael, G., Parrish, D., and Grano, D. (2010). Hemispheric Transport of Air Pollution

Kefauver, S.C., Penuelas, J., Ribas, A., Diaz-De-Quijano, M., and Ustin, S. (2014). Using Pinus uncinata to monitor tropospheric ozone in the Pyrenees. *Ecological Indicators* 36**,** 262-271.

Kerstiens, G., and Lendzian, K.J. (1989). Interactions between Ozone and Plant Cuticles .1. Ozone Deposition and Permeability. *New Phytologist* 112**,** 13-19.

Koch, J.R., Scherzer, A.J., Eshita, S.M., and Davis, K.R. (1998). Ozone sensitivity in hybrid poplar is correlated with a lack of defense-gene activation. *Plant Physiology* 118**,** 1243-1252.

Krupa, S., Mcgrath, M.T., Andersen, C.P., Booker, F.L., Burkey, K.O., Chappelka, A.H., Chevone, B.I., Pell, E.J., and Zilinskas, B.A. (2001). Ambient ozone and plant health. *Plant Disease* 85**,** 4-12.

Laisk, A., Kull, O., and Moldau, H. (1989). Ozone Concentration in Leaf Intercellular Air Spaces Is Close to Zero. *Plant Physiology* 90**,** 1163-1167.

Lam, E. (2004). Controlled cell death, plant survival and development. *Nature Reviews Molecular Cell Biology* 5**,** 305-315.

Lee, K.P., Kim, C., Landgraf, F., and Apel, K. (2007). EXECUTER1- and EXECUTER2-dependent transfer of stress-related signals from the plastid to the nucleus of Arabidopsis

thaliana. *Proceedings of the National Academy of Sciences of the United States of America* 104**,** 10270-10275.

Li, F., Wang, J., Ma, C.L., Zhao, Y.X., Wang, Y.C., Hasi, A., and Qi, Z. (2013). Glutamate Receptor-Like Channel3.3 Is Involved in Mediating Glutathione-Triggered Cytosolic Calcium Transients, Transcriptional Changes, and Innate Immunity Responses in Arabidopsis. *Plant Physiology* 162**,** 1497-1509.

Li, P., Feng, Z.Z., Catalayud, V., Yuan, X.Y., Xu, Y.S., and Paoletti, E. (2017). A meta-analysis on growth, physiological, and biochemical responses of woody species to ground-level ozone highlights the role of plant functional types. *Plant Cell & Environ.* 40**,** 2369-2380.

Lichtenthaler, H. (2013). "Plastoglobuli, Thylakoids, Chloroplast Structure and Development of Plastids," in *Plastid Development in Leaves during Growth and Senescence,* eds. B. Biswal, K. Krupinska & U. Biswal. Springer), 337-361.

Locato, V., and De Gara, L. (2018). - Programmed Cell Death in Plants: An Overview. - *Methods Mol Biol. 2018;1743:1-8. doi: 10.1007/978-1-4939-7668-3_1.***,** T - ppublish.

Lu, H.W., Gordon, M.I., Amarasinghe, V., and Strauss, S.H. (2020). Extensive transcriptome changes during seasonal leaf senescence in field-grown black cottonwood (Populus trichocarpa Nisqually-1). *Scientific Reports* 10.

Maas, R., and Grennfelt, P. (2016). Towards cleaner air. Scientific assessment report. Emep steering body and working group on effects of the convention on long-range transboundary air pollution, Oslo. 12-16.

Mangano, S., Juarez, S.P.D., and Estevez, J.M. (2016). ROS Regulation of Polar Growth in Plant Cells. *Plant Physiology* 171**,** 1593-1605.

Manzoor, H., Kelloniemi, J., Chiltz, A., Wendehenne, D., Pugin, A., Poinssot, B., and Garcia-Brugger, A. (2013). Involvement of the glutamate receptor AtGLR3.3 in plant defense signaling and resistance to Hyaloperonospora arabidopsidis. *Plant Journal* 76**,** 466-480.

Marchica, A., Lorenzini, G., Papini, R., Bernardi, R., Nali, C., and Pellegrini, E. (2019). Signalling molecules responsive to ozone-induced oxidative stress in *Salvia officinalis*. *Sci Total Environ* 657**,** 568-576.

Marzuoli, R., Gerosa, G., Bussotti, F., and Pollastrini, M. (2019). Assessing the Impact of Ozone on Forest Trees in An Integrative Perspective: Are Foliar Visible Symptoms Suitable Predictors for Growth Reduction? A Critical Review. *Forests* 10.

Marzuoli, R., Gerosa, G., Desotgiu, R., Bussotti, F., and Ballarin-Denti, A. (2009). Ozone fluxes and foliar injury development in the ozone-sensitive poplar clone Oxford (Populus maximowiczii x Populus berolinensis): a dose-response analysis. *Tree Physiol* 29**,** 67-76.

Mayta, M.L., Hajirezaei, M.R., Carrillo, N., and Lodeyro, A.F. (2019). Leaf Senescence: The Chloroplast Connection Comes of Age. *Plants-Basel* 8.

Mcadam, E.L., Brodribb, T.J., and Mcadam, S.a.M. (2017). Does ozone increase ABA levels by non-enzymatic synthesis causing stomata to close? *Plant Cell and Environment* 40**,** 741-747.

Mierziak, J., Kostyn, K., and Kulma, A. (2014). Flavonoids as Important Molecules of Plant Interactions with the Environment. *Molecules* 19**,** 16240-16265.

Mikkelsen, T.N., and Heidejorgensen, H.S. (1996). Acceleration of leaf senescence in *Fagus sylvatica* L by low levels of tropospheric ozone demonstrated by leaf colour,

chlorophyll fluorescence and chloroplast ultrastructure. *Trees-Struct Funct.* 10**,** 145-156.

Miller, J.D., Arteca, R.N., and Pell, E.J. (1999). Senescence-associated gene expression during ozone-induced leaf senescence in Arabidopsis. *Plant Physiology* 120**,** 1015-1023.

Mills, G., Pleijel, H., Braun, S., Buker, P., Bermejo, V., Calvo, E., Danielsson, H., Emberson, L., Fernandez, I.G., Grunhage, L., Harmens, H., Hayes, F., Karlsson, P.E., and Simpson, D. (2011). New stomatal flux-based critical levels for ozone effects on vegetation. *Atmos. Environ.* 45**,** 5064-5068.

Mills, G., Sharps, K., Simpson, D., Pleijel, H., Broberg, M., Uddling, J., Jaramillo, F., Davies, W.J., Dentener, F., Van Den Berg, M., Agrawal, M., Agrawal, S.B., Ainsworth, E.A., Buker, P., Emberson, L., Feng, Z.Z., Harmens, H., Hayes, F., Kobayashi, K., Paoletti, E., and Van Dingenen, R. (2018). Ozone pollution will compromise efforts to increase global wheat production. *Global Change Biology* 24**,** 3560-3574.

Mills G., Harmens H., Hayes F., Pleijel H., Buker P., and I., G. (2017). Mapping critical levels for vegetation. Manual on methodologies and criteria for Modelling and mapping critical loads and levels and air pollution effects, Risks and Trends. *International Cooperative Programme on Effects of Air Pollution on Natural Vegetation and Crops***,** 1-66.

Mittler, R. (2017). ROS Are Good. *Trends in Plant Science* 22**,** 11-19.

Monks, P.S., Archibald, A.T., Colette, A., Cooper, O., Coyle, M., Derwent, R., Fowler, D., Granier, C., Law, K.S., Mills, G.E., Stevenson, D.S., Tarasova, O., Thouret, V., Von Schneidemesser, E., Sommariva, R., Wild, O., and Williams, M.L. (2015). Tropospheric ozone and its precursors from the urban to the global scale from air quality to short-lived climate forcer. *Atmospheric Chemistry and Physics* 15**,** 8889-8973.

Moura, B.B., Alves, E.S., Marabesi, M.A., De Souza, S.R., Schaub, M., and Vollenweider, P. (2018). Ozone affects leaf physiology and causes injury to foliage of native tree species from the tropical Atlantic Forest of southern Brazil. *Sci Total Environ* 610**,** 912-925.

Moura, B.B., De Souza, S.R., and Alves, E.S. (2014). Response of Brazilian native trees to acute ozone dose. *Environmental Science and Pollution Research* 21**,** 4220-4227.

Muller, R. (2009). A brief history of stratospheric ozone research. *Meteorologische Zeitschrift* 18**,** 3-24.

Musselman, R.C., Lefohn, A.S., Massman, W.J., and Heath, R.L. (2006). A critical review and analysis of the use of exposure- and flux-based ozone indices for predicting vegetation effects. *Atmos. Environ.* 40**,** 1869-1888.

Natali, L., Vangelisti, A., Guidi, L., Remorini, D., Cotrozzi, L., Lorenzini, G., Nali, C., Pellegrini, E., Trivellini, A., Vernieri, P., Landi, M., Cavallini, A., and Giordani, T. (2018). How Quercus ilex L. saplings face combined salt and ozone stress: a transcriptome analysis. *Bmc Genomics* 19.

Nooden, L.D., Guiamet, J.J., and John, I. (1997). Senescence mechanisms. *Physiologia Plantarum* 101**,** 746-753.

Nosenko, T., Hanke-Uhe, M., Heine, P.A., Shahid, A., Dubel, S., Rennenberg, H., Schumacher, J., Winkler, J.B., Schnitzler, J.P., Hansch, R., and Kaufholdt, D. (2021). Plant Defense Proteins as Potential Markers for Early Detection of Forest Damage and Diseases. *Frontiers in Forests and Global Change* 4.

Ogawa, D., Nakajima, N., Tamaoki, M., Aono, M., Kubo, A., Kamada, H., and Saji, H. (2007). The isochorismate pathway is negatively regulated by salicylic acid signaling in O-3-exposed Arabidopsis. *Planta* 226**,** 1277-1285.

Overmyer, K., Brosche, M., and Kangasjarvi, J. (2003). Reactive oxygen species and hormonal control of cell death. *Trends Plant Sci* 8**,** 335-342.

Overmyer, K., Brosche, M., Pellinen, R., Kuittinen, T., Tuominen, H., Ahlfors, R., Keinanen, M., Saarma, M., Scheel, D., and Kangasjarvi, J. (2005). Ozone-induced programmed cell death in the *Arabidopsis* radical-induced cell death1 mutant. *Plant Physiol* 137**,** 1092-1104.

Overmyer, K., Tuominen, H., Kettunen, R., Betz, C., Langebartels, C., Sandermann, H., and Kangasjarvi, J. (2000). Ozone-sensitive Arabidopsis rcd1 mutant reveals opposite roles for ethylene and jasmonate signaling pathways in regulating superoxide-dependent cell death. *Plant Cell* 12**,** 1849-1862.

Paakkonen, E., Metsarinne, S., Holopainen, T., and Karenlampi, L. (1996). The ozone sensitivity of birch (*Betula pendula*) in relation to the developmental stage of leaves. *New Phytol.* 132**,** 145-154.

Paoletti, E., Contran, N., Bernasconi, P., Gunthardt-Goerg, M.S., and Vollenweider, P. (2009). Structural and physiological responses to ozone in Manna ash (Fraxinus ornus L.) leaves of seedlings and mature trees under controlled and ambient conditions. *Science of the Total Environment* 407**,** 1631-1643.

Paoletti, E., and Grulke, N.E. (2010). Ozone exposure and stomatal sluggishness in different plant physiognomic classes. *Environ Pollut* 158**,** 2664-2671.

Papazian, S., Khaling, E., Bonnet, C., Lassueur, S., Reymond, P., Moritz, T., Blande, J.D., and Albrectsen, B.R. (2016). Central Metabolic Responses to Ozone and Herbivory Affect Photosynthesis and Stomatal Closure. *Plant Physiology* 172**,** 2057-2078.

Pasqualini, S., Piccioni, C., Reale, L., Ederli, L., Della Torre, G., and Ferranti, F. (2003). Ozone-induced cell death in tobacco cultivar Bel W3 plants. The role of programmed cell death in lesion formation. *Plant Physiol* 133**,** 1122-1134.

Pell, E.J., Eckardt, N., and Enyedi, A.J. (1992). Timing of ozone stress and resulting status of ribulose bisphosphate carboxylase oxygenase and associated net photosynthesis. *New Phytol* 120**,** 397-405.

Pellegrini, E., Trivellini, A., Campanella, A., Francini, A., Lorenzini, G., Nali, C., and Vernieri, P. (2013). Signaling molecules and cell death in Melissa officinalis plants exposed to ozone. *Plant Cell Reports* 32**,** 1965-1980.

Pellegrini, E., Trivellini, A., Cotrozzi, L., Vernieri, P., and Nali, C. (2016). Involvement of Phytohormones in Plant Responses to Ozone. - 245.

Pelloux, J., Jolivet, Y., Fontaine, V., Banvoy, J., and Dizengremel, P. (2001). Changes in Rubisco and Rubisco activase gene expression and polypeptide content in Pinus halepensis M. subjected to ozone and drought. *Plant Cell and Environment* 24**,** 123-131.

Pleijel, H., Broberg, M.C., Uddling, J., and Mills, G. (2018). Current surface ozone concentrations significantly decrease wheat growth, yield and quality. *Science of the Total Environment* 613**,** 687-692.

Poorter, H., Niinemets, U., Ntagkas, N., Siebenkas, A., Maenpaa, M., Matsubara, S., and Pons, T. (2019). A meta-analysis of plant responses to light intensity for 70 traits ranging from molecules to whole plant performance. *New Phytol* 223**,** 1073-1105.

Proietti, C., Anav, A., De Marco, A., Sicard, P., and Vitale, M. (2016). A multi-sites analysis on the ozone effects on gross primary production of european forests. *Sci Total Environ* 556**,** 1-11.

Ranieri, A., Serini, R., Castagna, A., Nali, C., Baldan, B., Lorenzini, G., and Soldatini, G., F. (2000). Differential sensitivity to ozone in two poplar clones. *Physiologia Plantarum*.

Rao, M.V., Lee, H., Creelman, R.A., Mullet, J.E., and Davis, K.R. (2000). Jasmonic acid signaling modulates ozone-induced hypersensitive cell death. *Plant Cell* 12**,** 1633-1646.

Reich, P.B. (1983). Effects of low concentrations of O3 on net photosynthesis, dark respiration, and chlorophyll contents in aging hybrid poplar leaves. *Plant Physiol* 73**,** 291-296.

Revell, L.E., Tummon, F., Stenke, A., Sukhodolov, T., Coulon, A., Rozanov, E., Garny, H., Grewe, V., and Peter, T. (2015). Drivers of the tropospheric ozone budget throughout the 21st century under the medium-high climate scenario RCP 6.0. *Atmospheric Chem. Phys.* 15**,** 5887-5902.

Richet, N., Tozo, K., Afif, D., Banvoy, J., Legay, S., Dizengremel, P., and Cabane, M. (2012). The response to daylight or continuous ozone of phenylpropanoid and lignin biosynthesis pathways in poplar differs between leaves and wood. *Planta* 236**,** 727-737.

Ritchie, R.J. (2010). Modelling photosynthetic photon flux density and maximum potential gross photosynthesis. *Photosynthetica* 48**,** 596-609.

Rocha, G.L. (2017). *Programmed Cell Death-Related Proteases in Plants.* IntechOpen.

Rogers, H.J. (2005). "Cell death and organ development in plants," in *Current Topics in Developmental Biology, Vol 71*.), 225-+.

Rowland, F.S. (2009). "Stratospheric Ozone Depletion," in *Twenty Years of Ozone Decline*.), 23-66.

Rubin, M.B. (2003). The history of ozone - part III) - C.D. Harries and the introduction of ozone into organic chemistry. *Helvetica Chimica Acta* 86**,** 930-940.

Sacchelli, S., Carrari, E., Paoletti, E., Anav, A., Hoshika, Y., Sicard, P., Screpanti, A., Chirici, G., Cocozza, C., and De Marco, A. (2021). Economic impacts of ambient ozone pollution on wood production in Italy. *Scientific Reports* 11.

Sandermann, H., Ernst, D., Heller, W., and Langebartels, C. (1998). Ozone an abiotic elicitor of plant defense reactions. *Trends Plant Sci*.

Schmidt, R., Kunkowska, A.B., and Schippers, J.H.M. (2016). Role of Reactive Oxygen Species during Cell Expansion in Leaves. *Plant Physiology* 172**,** 2098-2106.

Schraudner, M., Moeder, W., Wiese, C., Van Camp, W., Inze, D., Langebartels, C., and Sandermann, H. (1998). Ozone-induced oxidative burst in the ozone biomonitor plant, tobacco Bel W3. *Plant Journal* 16**,** 235-245.

Sharma, A., Shahzad, B., Rehman, A., Bhardwaj, R., Landi, M., and Zheng, B.S. (2019). Response of Phenylpropanoid Pathway and the Role of Polyphenols in Plants under Abiotic Stress. *Molecules* 24.

Sicard, P., Dalstein-Richier, L., and Vas, N. (2011). Annual and seasonal trends of ambient ozone concentration and its impact on forest vegetation in Mercantour National Park (South-eastern France) over the 2000-2008 period. *Environmental Pollution* 159**,** 351-362.

Sicard, P., De Marco, A., Dalstein-Richier, L., Tagliaferro, F., Renou, C., and Paoletti, E. (2016). An epidemiological assessment of stomatal ozone flux-based critical levels for visible

ozone injury in Southern European forests. *Science of the Total Environment* 541**,** 729-741.
Sicard, P., De Marco, A., Troussier, F., Renou, C., Vas, N., and Paoletti, E. (2013). Decrease in surface ozone concentrations at Mediterranean remote sites and increase in the cities. *Atmospheric Environment* 79**,** 705-715.
Sicard, P., Hoshika, Y., Carrari, E., De Marco, A., and Paoletti, E. (2021). Testing visible ozone injury within a Light Exposed Sampling Site as a proxy for ozone risk assessment for European forests. *Journal of Forestry Research* 32**,** 1351-1359.
Sillman, S. (1999). The relation between ozone, NOx and hydrocarbons in urban and polluted rural environments. *Atmospheric Environment* 33**,** 1821-1845.
Simon, H., Reff, A., Wells, B., Xing, J., and Frank, N. (2015). Ozone Trends Across the United States over a Period of Decreasing NOx and VOC Emissions. *Environmental Science & Technology* 49**,** 186-195.
Singh, P., and Zimmerli, L. (2013). Lectin receptor kinases in plant innate immunity. *Frontiers in Plant Science* 4.
Sitch, S., Cox, P.M., Collins, W.J., and Huntingford, C. (2007). Indirect radiative forcing of climate change through ozone effects on the land-carbon sink. *Nature* 448**,** 791-794.
Soltani, N., Best, T., Grace, D., Nelms, C., Shumaker, K., Romero-Severson, J., Moses, D., Schuster, S., Staton, M., Carlson, J., and Gwinn, K. (2020). Transcriptome profiles of Quercus rubra responding to increased O-3 stress. *Bmc Genomics* 21.
Staehelin, J., Harris, N.R.P., Appenzeller, C., and Eberhard, J. (2001). Ozone trends: A review. *Reviews of Geophysics* 39**,** 231-290.
Street, N.R., James, T.M., James, T., Mikael, B., Jaakko, K., Mark, B., and Taylor, G. (2011a). The physiological, transcriptional and genetic responses of an ozone-sensitive and an ozone tolerant poplar and selected extremes of their F2 progeny. *Environ Pollut* 159**,** 45-54.
Street, N.R., Tallis, M.J., Tucker, J., Brosche, M., Kangasjarvi, J., Broadmeadow, M., and Taylor, G. (2011b). The physiological, transcriptional and genetic responses of an ozone- sensitive and an ozone tolerant poplar and selected extremes of their F-2 progeny. *Environmental Pollution* 159**,** 45-54.
Strohm, M., Eiblmeier, M., Langebartels, C., Jouanin, L., Polle, A., Sandermann, H., and Rennenberg, H. (2002). Responses of antioxidative systems to acute ozone stress in transgenic poplar (*Populus tremula* x *P-alba*) over-expressing glutathione synthetase or glutathione reductase. *Trees-Struct Funct.* 16**,** 262-273.
Takken, F.L.W., Albrecht, M., and Tameling, W.I.L. (2006). Resistance proteins: molecular switches of plant defence. *Current Opinion in Plant Biology* 9**,** 383-390.
Tamaoki, M., Matsuyama, T., Kanna, M., Nakajima, N., Kubo, A., Aono, M., and Saji, H. (2003). Differential ozone sensitivity among Arabidopsis accessions and its relevance to ethylene synthesis. *Planta* 216**,** 552-560.
Turc, B., Vollenweider, P., Le Thiec, D., Gandin, A., Schaub, M., Cabane, M., and Jolivet, Y. (2021). Dynamics of Foliar Responses to O3 Stress as a Function of Phytotoxic O-3 Dose in Hybrid Poplar. *Frontiers in Plant Science* 12.
Tuzet, A., Perrier, A., Loubet, B., and Cellier, P. (2011). Modelling ozone deposition fluxes: The relative roles of deposition and detoxification processes. *Agricultural and Forest Meteorology* 151**,** 480-492.
Van Wijk, K.J., and Kessler, F. (2017). "Plastoglobuli: Plastid Microcompartments with Integrated Functions in Metabolism, Plastid Developmental Transitions, and

Environmental Adaptation," in *Annual Review of Plant Biology, Vol 68*. (Palo Alto: Annual Reviews), 253-289.

Vingarzan, R. (2004). A review of surface ozone background levels and trends. *Atmospheric Environment* 38**,** 3431-3442.

Vollenweider, P., Fenn, M.E., Menard, T., Günthardt-Goerg, M., and Bytnerowicz, A. (2013). Structural injury underlying mottling in ponderosa pine needles exposed to ambient ozone concentrations in the San Bernardino Mountains near Los Angeles, California. *Trees* 27**,** 895-911.

Vollenweider, P., Günthardt-Goerg, M.S., Menard, T., Baumgarten, M., Matyssek, R., and Schaub, M. (2019). Macro- and microscopic leaf injury triggered by ozone stress in beech foliage (*Fagus sylvatica* L.). *Ann. For. Sci.* 76**,** 71.

Vollenweider, P., Menard, T., Arend, M., Kuster, T.M., and Gunthardt-Goerg, M.S. (2016). Structural changes associated with drought stress symptoms in foliage of Central European oaks. *Trees-Struct Funct.* 30**,** 883-900.

Vollenweider, P., Ottiger, M., and Günthardt-Goerg, M.S. (2002). Validation of leaf ozone symptoms in natural vegetation using microscopical methods. *Environ Pollut* 124**,** 101-118.

Waldeck, N., Burkey, K., Carter, T., Dickey, D., Song, Q.J., and Taliercio, E. (2017). RNA-Seq study reveals genetic responses of diverse wild soybean accessions to increased ozone levels. *Bmc Genomics* 18.

Wang, Y., Li, X.F., Fan, B.F., Zhu, C., and Chen, Z.X. (2021). Regulation and Function of Defense-Related Callose Deposition in Plants. *International Journal of Molecular Sciences* 22.

Whaley, A., Sheridan, J., Safari, S., Burton, A., Burkey, K., and Schlueter, J. (2015). RNA-seq analysis reveals genetic response and tolerance mechanisms to ozone exposure in soybean. *Bmc Genomics* 16.

Wittig, V.E., Ainsworth, E.A., Naidu, S.L., Karnosky, D.F., and Long, S.P. (2009). Quantifying the impact of current and future tropospheric ozone on tree biomass, growth, physiology and biochemistry: a quantitative meta-analysis. *Glob. Change Biol.* 15**,** 396-424.

Xu, E.J., Vaahtera, L., and Brosche, M. (2015). Roles of Defense Hormones in the Regulation of Ozone-Induced Changes in Gene Expression and Cell Death. *Molecular Plant* 8**,** 1776-1794.

Xu, Y.S., Feng, Z.Z., Shang, B., Dai, L.L., Uddling, J., and Tarvainen, L. (2019). Mesophyll conductance limitation of photosynthesis in poplar under elevated ozone. *Sci Total Environ* 657**,** 136-145.

Yendrek, C.R., Koester, R.P., and Ainsworth, E.A. (2015). A comparative analysis of transcriptomic, biochemical, and physiological responses to elevated ozone identifies species-specific mechanisms of resilience in legume crops. *J Exp Bot* 66**,** 7101-7112.

Yi, S.Y., Shirasu, K., Moon, J.S., Lee, S.G., and Kwon, S.Y. (2014). The Activated SA and JA Signaling Pathways Have an Influence on flg22-Triggered Oxidative Burst and Callose Deposition. *Plos One* 9.

Zhang, J., Gao, F., Jia, H., Hu, J., and Feng, Z. (2019). Molecular response of poplar to single and combined ozone and drought. *Sci Total Environ* 655**,** 1364-1375.

Zhang, J., Schaub, M., Ferdinand, J.A., Skelly, J.M., Steiner, K.C., and Savage, J.E. (2010). Leaf age affects the responses of foliar injury and gas exchange to tropospheric ozone in *Prunus serotina* seedlings. *Environ Pollut* 158**,** 2627-2634.

Zhang, L., Xiao, S., Chen, Y.J., Xu, H., Li, Y.G., Zhang, Y.W., and Luan, F.S. (2017). Ozone sensitivity of four Pakchoi cultivars with different leaf colors: physiological and biochemical mechanisms. *Photosynthetica* 55**,** 478-490.

Zhang, Y.Q., Cooper, O.R., Gaudel, A., Thompson, A.M., Nedelec, P., Ogino, S.Y., and West, J.J. (2016). Tropospheric ozone change from 1980 to 2010 dominated by equatorward redistribution of emissions. *Nature Geoscience* 9**,** 875-+.

Zhao, H., Zheng, Y.F., Li, T., Wei, L., and Guan, Q. (2018). Temporal and Spatial Variation in, and Population Exposure to, Summertime Ground-Level Ozone in Beijing. *International Journal of Environmental Research and Public Health* 15.

Zimmermann, P., and Zentgraf, U. (2005). The correlation between oxidative stress and leaf senescence during plant development. *Cellular & Molecular Biology Letters* 10**,** 515-534.

Abstract: With background concentrations having reached phytotoxic levels during the last century, tropospheric ozone (O_3) has become a key climate change agent, counteracting carbon sequestration by forest ecosystems. Impacts on vegetation includes physiological alteration, structural and ultrastructural changes and transcriptomic deregulation leading to plant growth inhibition (and yield loss). However, few studies have investigated the link between the dynamics of these events. Considering that one of the main gap for implementing the recent O_3 flux-based critical levels (CL) concerns the quantification of plant capacity to neutralize a portion of the O_3 entering the leaf, a better understanding of cellular response dynamics to O_3 is required. In this context, young poplar (*Populus tremula x alba*, 717-1b4 INRAE clone) were exposed to 80 or 100 ppb O_3 in fully controlled conditions during 30 days. All analysis were performed on two leaves differing by their developmental stage (fully expanded vs in expansion). After a latency period driven by foliar development, net CO_2 assimilation and stomatal conductance decreased in response to O_3. Hypersensitive response-like appeared early during exposure, and showed sigmoidal-like dynamic, varying according to leaf age. Ontological evolution of HR-like lesion showed post-mortem evolution cellular material. Genes whose expression was highly correlated with HR-like were all involved in response to biotic stress, and can constitute a starting list of investigation to determine O_3 stress molecular markers. Accelerated Cell Senescence (ACS), followed through chlorophyll content, was later induced and showed monotonic dynamic. Senescence related genes were regulated early during O_3 exposure and dynamics of ACS-related microscopic changes were depending on O_3 treatments, leaf position and POD_0. Hence, this work demonstrates the development of a complex syndrome of early reactions to O_3 stress in leaves, with distinct dynamics and mechanisms of the HR-like and ACS processes. These processes could result from distinct spatial accumulation of O_3-induced ROS. Finally, this study also suggested that expression of genes involved in development during leaf expansion could confer higher tolerance to O_3 stress.

Résumé : Les concentrations de fond ayant atteint des niveaux phytotoxiques au cours du siècle dernier, l'ozone troposphérique (O_3) est devenu un agent clé du changement climatique, contrecarrant le piégeage du carbone par les écosystèmes forestiers. L'impact sur la végétation comprend des altérations physiologiques, des changements structuraux et ultrastructuraux, ainsi qu'une dérégulation transcriptomique qui conduisent à une inhibition de croissance (et une baisse de rendement) pour les plantes. Cependant, peu d'études ont examiné le lien entre les dynamiques de ces différents évènements. Considérant que l'une des principales lacunes pour la mise en œuvre des récents niveaux critiques (CL) basés sur les flux d'O_3 concerne la quantification de la capacité des plantes à neutraliser une partie de l'O_3 entrant dans la feuille, une meilleure compréhension de la dynamique de la réponse cellulaire à l'O_3 est requise. Dans ce contexte, de jeunes peupliers (*Populus tremula x alba*, clone INRAE 717-1b4) ont été exposés à 80 ou 100 ppb O_3 dans des conditions entièrement contrôlées et pendant 30 jours. Toutes les analyses ont été effectuées sur deux feuilles différant par leur stade de développement (pleinement développé vs en expansion). Après une période de latence due au développement foliaire, l'assimilation nette de CO_2 et la conductance stomatique diminuent en réponse à l'O_3. La réponse de type hypersensible apparaît tôt pendant l'exposition, suivant une dynamique de type sigmoïde, variant selon l'âge de la feuille. La lésion de type HR présente alors une évolution post-mortem du matériel cellulaire. Les gènes dont l'expression était fortement corrélée avec la HR-like sont tous impliqués dans la réponse au stress biotique, et peuvent constituer une liste préliminaire pour la détermination de marqueurs moléculaires du stress O_3. La sénescence cellulaire accélérée (ACS), suivie par la teneur en chlorophylles, est induite plus tardivement et suit une dynamique monotone. Par contre, les gènes liés à la sénescence sont régulés assez tôt et la dynamique des changements microscopiques liés à l'ACS varie en fonction du traitements O_3, de la position des feuilles et du POD_0. En conséquence, ce travail démontre le développement d'un syndrome complexe de réactions précoces au stress O_3 dans les feuilles, avec des dynamiques et des mécanismes distincts du HR-like et de l'ACS. Le développement de ces deux processus pourrait résulter d'une accumulation spatiale distincte des ROS induits par l'O_3. Enfin, cette étude suggère également que l'expression des gènes impliqués dans le développement lors de l'expansion des feuilles pourrait conférer à la plante une plus grande tolérance au stress O_3.

Abstract: With background concentrations having reached phytotoxic levels during the last century, tropospheric ozone (O_3) has become a key climate change agent, counteracting carbon sequestration by forest ecosystems. Impacts on vegetation includes physiological alteration, structural and ultrastructural changes and transcriptomic deregulation leading to plant growth inhibition (and yield loss). However, few studies have investigated the link between the dynamics of these events. Considering that one of the main gap for implementing the recent O_3 flux-based critical levels (CL) concerns the quantification of plant capacity to neutralize a portion of the O_3 entering the leaf, a better understanding of cellular response dynamics to O_3 is required. In this context, young poplar (*Populus tremula x alba*, 717-1b4 INRAE clone) were exposed to 80 or 100 ppb O_3 in fully controlled conditions during 30 days. All analysis were performed on two leaves differing by their developmental stage (fully expanded vs in expansion). After a latency period driven by foliar development, net CO_2 assimilation and stomatal conductance decreased in response to O_3. Hypersensitive response-like appeared early during exposure, and showed sigmoidal-like dynamic, varying according to leaf age. Ontological evolution of HR-like lesion showed post-mortem evolution cellular material. Genes whose expression was highly correlated with HR-like were all involved in response to biotic stress, and can constitute a starting list of investigation to determine O_3 stress molecular markers. Accelerated Cell Senescence (ACS), followed through chlorophyll content, was later induced and showed monotonic dynamic. Senescence related genes were regulated early during O_3 exposure and dynamics of ACS-related microscopic changes were depending on O_3 treatments, leaf position and POD_0. Hence, this work demonstrates the development of a complex syndrome of early reactions to O_3 stress in leaves, with distinct dynamics and mechanisms of the HR-like and ACS processes. These processes could result from distinct spatial accumulation of O_3-induced ROS. Finally, this study also suggested that expression of genes involved in development during leaf expansion could confer higher tolerance to O_3 stress.

Résumé : Les concentrations de fond ayant atteint des niveaux phytotoxiques au cours du siècle dernier, l'ozone troposphérique (O_3) est devenu un agent clé du changement climatique, contrecarrant le piégeage du carbone par les écosystèmes forestiers. L'impact sur la végétation comprend des altérations physiologiques, des changements structuraux et ultrastructuraux, ainsi qu'une dérégulation transcriptomique qui conduisent à une inhibition de croissance (et une baisse de rendement) pour les plantes. Cependant, peu d'études ont examiné le lien entre les dynamiques de ces différents évènements. Considérant que l'une des principales lacunes pour la mise en œuvre des récents niveaux critiques (CL) basés sur les flux d'O_3 concerne la quantification de la capacité des plantes à neutraliser une partie de l'O_3 entrant dans la feuille, une meilleure compréhension de la dynamique de la réponse cellulaire à l'O_3 est requise. Dans ce contexte, de jeunes peupliers (*Populus tremula x alba*, clone INRAE 717-1b4) ont été exposés à 80 ou 100 ppb O_3 dans des conditions entièrement contrôlées et pendant 30 jours. Toutes les analyses ont été effectuées sur deux feuilles différant par leur stade de développement (pleinement développé vs en expansion). Après une période de latence due au développement foliaire, l'assimilation nette de CO_2 et la conductance stomatique diminuent en réponse à l'O_3. La réponse de type hypersensible apparaît tôt pendant l'exposition, suivant une dynamique de type sigmoïde, variant selon l'âge de la feuille. La lésion de type HR présente alors une évolution post-mortem du matériel cellulaire. Les gènes dont l'expression était fortement corrélée avec la HR-like sont tous impliqués dans la réponse au stress biotique, et peuvent constituer une liste préliminaire pour la détermination de marqueurs moléculaires du stress O_3. La sénescence cellulaire accélérée (ACS), suivie par la teneur en chlorophylles, est induite plus tardivement et suit une dynamique monotone. Par contre, les gènes liés à la sénescence sont régulés assez tôt et la dynamique des changements microscopiques liés à l'ACS varie en fonction du traitements O_3, de la position des feuilles et du POD_0. En conséquence, ce travail démontre le développement d'un syndrome complexe de réactions précoces au stress O_3 dans les feuilles, avec des dynamiques et des mécanismes distincts du HR-like et de l'ACS. Le développement de ces deux processus pourrait résulter d'une accumulation spatiale distincte des ROS induits par l'O_3. Enfin, cette étude suggère également que l'expression des gènes impliqués dans le développement lors de l'expansion des feuilles pourrait conférer à la plante une plus grande tolérance au stress O_3.